THE ECO-HYDROLOGY OF GLACIER SURFACES

Ian Thomas Stevens

Vadrec del Forno, Switzerland in July 2016

Department of Geography and Earth Science
Aberystwyth University

June 2019
Thesis submitted for the degree of Doctor of Philosophy

Declarations and Statements

Word count of thesis:	47.458
DECLERATION: This work has not previously been accepted in substance for any degree and is not concurrently submitted in candidature for any degree.	
Candidate Name:	Ian Thomas Stevens
Signature:	
Date:	07/06/2019

Statement 1:

This thesis is the result of my own investigations, except where otherwise stated. Where **correction services*** have been used, the extent and nature of the correction is clearly marked in a footnote(s).

Other sources are acknowledged by footnotes giving explicit references. A bibliography is appended.

Signature:	
Date:	07/06/2019

[*this refers to the extent to which the text has been corrected by others]

Statement 2

I hereby give consent for my thesis, if accepted, to be available for photocopying and for inter-library loan, and for the title and summary to be made available to outside organisations.

Signature:	
Date:	07/06/2019

Abstract

Recent work has highlighted the importance of the so-called "weathering crust" as a microbially and hydrologically active layer on glacier surfaces. However, this layer is yet to undergo investigation, with no estimates of water, microbial or nutrient fluxes through it to downstream freshwater and marine ecosystems. The mechanics of the weathering crust, and its role in transport and/or retention of particulate impurities at the glacier surface presents a research imperative. To investigate the eco-hydrology of glacier surfaces, this thesis presents a dataset collected at eleven sites in the Northern Hemisphere from the Canadian Arctic to the European Alps, collected between 2014 and 2016. To interrogate this dataset, the study develops and tests a novel logging piezometer which is used to calculate mean weathering crust hydraulic conductivity at all locations of 0.184 m d^{-1}, equivalent to a sandstone, and meltwater velocities of 10^{-1} m d^{-1}. This hydrologically poor aquifer, causes the storage of water at the surface for tens of day, providing an ideal medium for biogeochemical cycling. For microbial cell enumeration, a flow cytometry protocol is presented which is suitable for glacial environments providing accurate, reliable cell counts. Across the eleven sites, mean microbial cell concentration in weathering crust meltwater was revealed to be $\approx 10^4$ cells mL^{-1}. It was unclear what controls exist upon cell concentrations in the weathering crust, however no links between weathering crust hydraulic conductivity, electrical conductivity or water temperature and cell concentrations were observed. Cellular particulate organic carbon flux (POC) form this active environment contributes a minimum of 1.1 Tg of cellular carbon per year to downstream freshwater and marine environments per year.

Acknowledgements

Throughout my PhD I have received help, support and motivation from many individuals and bodies both academic and personally. Firstly, I wish to extend thanks to my supervisors Tris Irvine-Fynn, Arwyn Edwards and Andy Mitchell, whom without this PhD project would never have initially got off the ground. Especial thanks go to Tris, who has had the misfortune to supervise all of my major projects throughout my academic career to date and is probably glad that he won't get a huge pile of work to deal with in very little time again (at least from me) for a while. I'd also like to thank him for making some great trips viable for me, such as tagging along to Svalbard, returning to New Zealand and attending the AGU (although perhaps some stories about the latter should remain in San Francisco…). Throughout the last four years all three of my supervisors they have provided extensive support, encouragement and criticism in my development as an interdisciplinary researcher. Further thanks are given to my two examiners, Jonathan Bridge and Nozomu Takeuchi, whose comments have vastly improved the final thesis.

A large amount of field data was collected from a raft of locations for the completion of this study, and without the assistance of many others this would have been an unfeasibly large and lonely task. As such, I wish to thank (in no particular order) Stephen Brough, Mike Stuart and Jayne Kamintzis, for the Arolla trip in which Tris had a close shave; Phil Porter, Andy Hodson and all the other members of the windswept Svalbard campaign in which we nearly lost a boat; and Tom Holt, Jayne (again) and Martin Smart for joining me in practising for roles as porters at Vadrec del Forno. Thanks for the latter field campaign are also extended to Beat, Aleana and Kornelius who welcomed me with open arms and made the Fornohütte feel like my second home for a month. I also wish to thank the proper biologists for letting me into the lab with them and showing me the ropes, particularly Jerry Gokul, Ottavia Cavalli and Susan Girwood, thanks for your help in completing simple tasks and, mainly, finding things. Without your collective inputs I'd probably still be sitting in front of a flow cytometer.

Without funding supplied by many bodies, the field campaigns, laboratory equipment and consumables required for this PhD would have been in short supply. As such, the following bodies are thanked for their financial and/or logistical support: Aberystwyth University (Department of Geography and Earth Sciences); The Gilchrist Educational Trust; The Scottish Arctic Club; The Royal Geographical Society (with IBG); UNIS; EU F7 INTERACT (grant: SCARFACE to Tristram Irvine-Fynn and Arwyn Edwards); The Royal Society (grant: RG130314 to AE and TI-F); The Polar Continental Shelf Program (PSCP) and National Sciences and Research Council (NSERC) (to Brian Moorman); the Climate Change Consortium for Wales (C3W grant: Proof of

Concept to TI-F); The Dark Snow Project (especially Karen Cameron and Jason Box for their support for TI-F in Greenland); and the National Research Network for Low Carbon Energy and Environment (NRN-LCEE) funded by the Welsh Government and the Higher Education Funding Council for Wales (HEFCW) (to Andrew Mitchell). The AGU and BSG are also acknowledged for supporting my attendance to the Fall Meeting in 2016, enabling the further development of Chapter 3 and the associated publication.

On a more personal note, I'd like that thank everyone that I've climbed, run, walked, cycled or trained with over the past four years for providing me with some respite from working and ensuring that this thesis stayed unfinished right until the deadline. Whilst this is far from a complete list, special mentions go to Arthur, Richard (aka Alex), Joe, Emily, Adam, Tom, Ed, Matt, James and (another) Joe. I'd also like to thank Neil for distracting me with coffee and non-work-related chat, and Jayne for providing me with support once she decided I was bearable. Finally, and most importantly I wish to thank my parents, for financial support throughout (although whether you got better value for these 40,000 words or by helping my brother buy a house is a decision I'll leave to you) but mostly for the unquestioning encouragement and support throughout this entire process.

Table of Contents

List of Figures

List of Tables

1. Introduction

1.1 Background and context

Glacier surfaces are changing on a global scale as a response to ongoing climatic change (Ming et al., 2012; Oerlemans et al., 2009; Tao et al., 2013) with increased rates of mass loss observed globally since the 19th century across small mountain glaciers (Dyurgerov and Meier, 2000) and the Greenland and Antarctic Ice Sheets (Rignot et al., 2011). Melt processes, occurring in the ablation zone, release stored "impurities" (Dancer et al., 1997), incorporated into glacial ice via snow deposition and firnification in the accumulation zone (Bøggild et al., 2010). These so-called impurities include clastic sediment "dusts", black carbon, persistent organic pollutants, anthropogenic and natural radionuclides, and microorganisms including single and multi-celled eukaryotes, archaea and bacteria (Baccolo et al., 2017; Edwards, 2015; Hodson, 2014; Lehmann et al., 2016; Łokas et al., 2016; Łokas et al., 2018; Segawa et al., 2013), which are supplemented with locally derived material deposited by aeolian processes (Fischer et al., 2007; Ruth et al., 2003; Tedstone et al., 2017; Wientjes et al., 2017). However, there is a lack of understanding of the provenance, fate and impacts of these impurities upon melt processes and biogeochemical cycling on the ice surface itself and within the proglacial environments to which they are exported.

Presence of dusts and the accumulation and growth of distributed microbial communities and their humic by-products (Stibal et al., 2010) on glacier surfaces have been linked with albedo reduction (Musilova et al., 2016), further exacerbating the effect of increasing global temperatures upon glacial melt rates. The most pertinent class of impurities are distributed microbial communities, with recent work demonstrating that 73 % of spatial variability in the dark zone of the Greenland Ice Sheet can be explained by the presence of such microorganisms (Ryan et al., 2018). The ongoing emergence and dispersal of such impurities plays a key role in the future darkening and spatial expansion of both the Greenland dark zone and in the ablation zones ice masses around the globe, and is best exemplified by recently identified decadal-scale darkening trends in Greenland (Tedstone et al., 2017) and the European Alps, specifically Switzerland (Naegeli et al., 2019). However, there is currently limited understanding of the mechanics underlying the redistribution of impurities that have been liberated from melting ice. Determining the process(es) relating to the transport and residence time of dust and microbial cells across ice surfaces represents a critical research gap, essential to accurately constrain spatio-temporal patterns of albedo across ablation zones.

A hypothesised transport pathway for the redistribution of surface impurities is the weathering crust (Yang et al., 2018a), a near-surface porous aquifer up to 2 m thick (Irvine-Fynn et al., 2011), commonly found on ablating glacier surfaces. Acknowledgement of the weathering crust has challenged the hitherto commonly held assumption that meltwater and impurities are transferred virtually instantaneously from the point of production to supraglacial channels (Fountain and Walder, 1998), where they are rapidly advected from the ice surface. Transport of microbial cells through the weathering crust is thought to be size-selective (Irvine-Fynn et al., 2012), linked with cross-sectional pore area between weathered ice crystals. This system demonstrates potential to both transfer and retain impurities, darkening ice surfaces by acting as a mechanical filter and influencing surface albedo due to the translucent nature of ice above it. Despite the recent surge in interest in supraglacial hydrology evident in the literature, (e.g. Gleason et al., 2016; Karlstrom et al., 2013; Karlstrom et al., 2014; Mantelli et al., 2015; McGrath et al., 2011; Rippin et al., 2015; Smith et al., 2015; Smith et al., 2017; St. Germain and Moorman, 2016; Yang and Smith, 2013; Yang et al., 2018b) a detailed understanding of the fundamental metrics of the weathering crust, and their variation in space and time is still lacking (Irvine-Fynn et al., 2011). Whilst recent work has been undertaken examining these variables and the potential short-term water storage capacity of the weathering crust (e.g. Cook et al., 2015; Cooper et al., 2018), there remains a scarcity of porous media measurements, such as hydraulic conductivity, across a spectrum of thermal regimes and glaciated regions.

Glacial environments have traditionally been considered too harsh for significant microbial life to occur. It has been considered that any such life was either dormant or functioning sub-optimally; given that to survive, organisms have to be at least tolerant to extreme cold, low nutrient availability, and seasonally variable UV radiation levels (Cameron et al., 2012; Goordial et al., 2013; Harding et al., 2011; Larose et al., 2013). However, the presence of microbes in such environments is now well established (e.g. Anesio et al., 2017; Hodson et al., 2008; Larose et al., 2010; Laybourn-Parry et al., 2012), with glacier surfaces worldwide containing an estimated 10^{25} to 10^{29} microorganisms (Irvine-Fynn and Edwards, 2014; Priscu and Christner, 2004), an equivalent order of magnitude to tropical rainforest soils (Whitman et al., 1998). Despite such enumerative estimates, there is, to date, no widely accepted standard enumeration protocol for supraglacial samples (Miteva, 2008), fundamental for robust and reliable enumeration measurements to define how supraglacial microbes, interact with their surrounding environment and to examine microbial fluxes (Fredrickson and Balkwill, 1998).

The albedo-reducing potential of the microbes found on glacier surfaces is best exemplified by consideration of the direct effects, due to the production of pigments in response to high levels of UV irradiance and/or nutrient limitation (Cook et al., 2017). Pigment change to an existing surface population, the exposure (via melt-out) of a previously buried community, and the proliferation of cells as a result of biological growth all result in darker surfaces. Filamentous organisms, such as cyanobacteria, interact with sediment particles and ice crystals increasing the residence time of the former on the ice surface via the formation of cryoconite holes (Langford et al., 2010). Transient water storage within the weathering crust provides prolonged opportunities for biological processes including replication and biogeochemical cycling, but residence times of microbes within the weathering crust remain unexplored.

As well as acting as a key control upon albedo, ice-surface microbial communities play vital roles in carbon and nitrogen cycling (Cook et al., 2010; Hodson et al., 2007; Telling et al., 2012a; Telling et al., 2012b), transforming labile inorganic nutrients, such as ammonium and phosphate, into organic forms (Anesio et al., 2009). On a global scale, glacier surfaces represent a poorly understood carbon (Hood et al., 2015) and nutrient reservoir. Due to the availability of liquid meltwater, photosynthetically available radiation, and relatively high concentrations of nutrients (Cook et al., 2016), ablation zones represent a glacial biodiversity hotspot supporting active phototrophic and heterotrophic (Christner et al., 2018) metabolism. At a regional scale, changes in glacier run-off may represent an important flux of labile, ecosystem-fertilising organic carbon to the supra-, en-, sub- and stream and marine pro-glacial environments (Musilova et al., 2017). Therefore, glaciers represent a key link between terrestrial and aquatic carbon fluxes. Whilst this proportion is small in the context of global carbon fluxes, glacier derived DOC is highly biologically available in contrast to other sources (such as vascular plants and marine algae), with 25-95 % metabolised in laboratory assays of microbial heterotrophs (Hood et al., 2009; Singer et al., 2012). Establishing microbial delivery rates from the weathering crust to the efficient, channelised drainage pathway to proglacial environments requires greater understanding of microbial transfers across the ice-sheet surface where microbial cells are metabolically and reproductively active.

Ultimately, the weathering crust will modulate meltwater and impurity fluxes to downstream environments from ablating glaciers and ice sheets. Widely assumed to be an important element of the biogeochemical budget (Cook et al., 2015; Irvine-Fynn et al., 2012; Rassner et al., 2016; Stevens et al., 2018), few datasets examine microbial abundance, activity or transfers within the weathering crust.

Therefore, to characterise these surface changes and extraglacial nutrient fluxes, it is necessary to understand the changing input from glaciers, including how cells are stored, transported and exported through and across the supraglacial hydrological system.

1.2 Research aim and objectives

This thesis aims to examine the eco-hydrology of glacier surfaces, quantifying and exploring mechanisms and environmental variables controlling transport of water and microbial cells through the weathering crust found at the near-surface of ablating glaciers and ice sheets, and estimate the downstream delivery of carbon in the form of microbial cells to downstream environments from non-Antarctic glaciers. To achieve this aim, five key objectives are defined:

1. Develop and establish a protocol and instrument suitable for the calculation of hydraulic conductivity of the near surface weathering crust, applying existing groundwater knowledge and techniques.
2. Characterise weathering crust hydraulic conductivity across a range of glaciers in a variety of climatic, latitudinal and geographic settings.
3. Optimise the high-throughput method of flow cytometry (FCM) to ensure accurate and reliable cell counting in supraglacial environments, assessing uncertainties due to the influence of cell and sediment type and concentration.
4. Quantify microbial cell concentration in weathering crust meltwater across an assortment of Northern Hemisphere glaciers using FCM and establish glacier-scale differences in cell concentration, highlighting potential controls upon it.
5. Examine links between hydraulic factors and microbial cell concentrations to assess the extent to which the former influence the latter in time and space at Vadrec del Forno, a typical Alpine valley glacier located in the Swiss Alps.

1.3 Thesis structure

Chapter 2 reviews existing literature pertaining to the weathering crust, including its formation, hydrology and context within the wider supraglacial system in addition to consideration of fluid flow mechanics of porous media in terrestrial environments. The flourishing field of supraglacial microbiology is outlined, with the biogeochemical role of these microorganisms highlighted. Finally,

the established body of knowledge of microbial transfers and dynamics in terrestrial media is described.

Chapter 3 was originally published in Hydrological Processes in 2018 (Stevens et al., 2018). This chapter describes the development and application of a novel piezometric probe to calculate hydraulic conductivity of the weathering crust at 10 ice masses across the Northern Hemisphere.

Chapter 4 evaluates the application of flow cytometry to the supraglacial environment, using samples developed from laboratory cultures of cryospheric bacteria. An array of cell types, abiotic particle types, and concentrations of each are considered to establish criteria for which FCM provides an acceptable level of accuracy for cell enumerations in the weathering crust.

Chapter 5 expands on the dataset presented in Chapter 3, by considering linkages between weathering crust hydraulics and microbial cell concentrations of the waters within it. The global dataset of microbial cell concentrations is substantially expanded, and carbon exports from the supraglacial environment is estimated to the year 2099.

Chapter 6 considers the variables examined above at local scale, examining a micro-catchment at Vadrec del Forno, a Swiss Alpine glacier.

Chapter 7 provides a discussion and summary of the key findings of the four experimental chapters (3-6), exploring the dynamics and implications of microbial cell transfer though the weathering crust.

Appendix 1 presents exemplar data from Chapter 3 (Stevens et al., 2018).

Appendix 2 was originally published in Frontiers in Microbiology in 2015 (Stibal et al., 2015). It is included within this thesis due to the contribution of the author regarding cell count method testing and can be considered a pre-cursor to Chapter 4 (evaluation and optimisation of flow cytometry for glacial samples).

1.4 Author contributions to published and collaborative work

Several chapters demonstrate contributions from a team of academic colleagues, which are outlined below. All initials refer to titled authors in the original manuscript(s), otherwise names and

affiliations are provided; for chapters which are not explicitly described usual supervisory contributions were provided by Tristram D.L. Irvine-Fynn (TDI), Andrew C. Mitchell (ACM) and Arwyn Edwards (AE) (all Aberystwyth University).

Chapter 3: IS wrote the manuscript, with input from TDI, Phil Porter (PP, University of Hertfordshire), Joe Cook (JC; University of Sheffield) and ACM. All analyses and data processing were undertaken by IS. Fieldwork was undertaken by TDI, JC, AE, Martin Smart (MSm, University of Hertfordshire), and Brian J. Moorman (BJM, University of Calgary) in 2014; and IS, TDI, PP, and Andy J. Hodson (AJH, UNIS) in 2015. The study and equipment design were originally conceptualised by TDI, building on the original study of JC. Piezometers were constructed by Steve Norburn (University of Sheffield) and Dave Kelly (AU).

Chapter 4: All laboratory work, analyses and data processing were undertaken by IS. Fieldwork was undertaken by TDI, JC, AE, MSm and BJM in 2014; IS, TI-F, PP, and AJH in 2015; and IS and MSm in 2016.

Chapter 5: Fieldwork was undertaken by TDI, JC, AE, MSm, BJM, PP and AJH, as per Chapter 3. All laboratory analyses and writing were undertaken by the author.

Chapter 6: Data collection, processing and laboratory analysis was carried out by IS, excluding the remotely sensed imagery. Orthoimagery was collected and supplied by Thomas Holt (AU) and Morgan J. Gibson (AU). The DEM was supplied by Edward A. Roberts (previously AU) who undertook all data collection and processing, with support from Alun Hubbard (AU).

2. A Review of Supraglacial Hydrology and Microbial Ecology

Supraglacial hydrology directly connects melt processes on the glacier surface to those of meltwater delivery to downstream systems, hence it is imperative to characterise this system to understand the response of glaciers and ice sheets within the context of changing global climate (IPCC, 2013). Current knowledge and models (e.g. Bougamont and Bamber, 2005) assume that friction limited surface flow determines the rate of transport of meltwater across the glacier surface. Comprehensive reviews of temperate (e.g. Fountain and Walder, 1998; Hubbard and Nienow, 1997) and non-temperate (e.g. Irvine-Fynn et al., 2011c) glacier hydrology, including en- and subglacial systems, incorporate this simple, rapid-response run-off model. However, a porous surface layer, the so-called "weathering crust" (Müller and Keeler, 1969), develops on the surface of ablating ice masses and complicates this simple model (Figure 2.1). In addition to flow across and through the surface and near-surface, supraglacial water may be temporarily stored within components of this system (Jansson et al., 2003), including in the seasonal or perennial snow pack, within firn (e.g. Forster et al., 2014; Munro, 2011), the ablating ice surface (i.e. the weathering crust) (e.g. Cooper et al., 2018; Smith et al., 2017b), or surface meltwater ponds (e.g. Das et al., 2008). How meltwater drains through glaciers is critical to ice dynamics, runoff characteristics and water quality in glacially-fed catchments (Milner et al., 2017), especially given the melt-out of organic (e.g. Battin et al., 2016; Hood et al., 2015; Singer et al., 2012; Wilhelm et al., 2013) and inorganic particulates deposited on ice masses since ~1850 by anthropogenic pollution (e.g. Bettinetti et al., 2016), which are ultimately transported into downstream freshwater catchments and marine ecosystems.

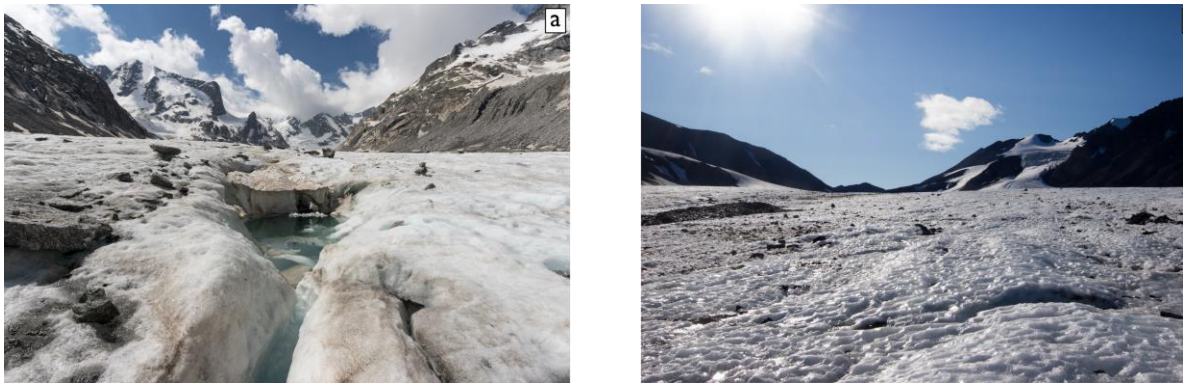

Figure 2.1 a) A weathered ice surface at Vadrec del Forno (Switzerland) in July 2016, typical of a glacier surface which has been exposed to a period of clear-sky conditions. In contrast, panel b shows the smooth, "glassy" unweathered surface of Protektorbreen (Svalbard) in August 2015 following a four-day period of cloud cover, wind and heavy rain.

This chapter will review the hydrology and microbiology of glacier surfaces, providing an outlook on contemporary knowledge pertaining to these interlinked systems. Initially, the roles of glacier thermal regime and melt processes shall be considered, which are both factors in weathering crust formation, development and degradation. Given the nature of the investigative techniques used to quantify weathering crust hydrology, the fundamental laws of porous media hydraulics determined in terrestrial media such as soils and rocks will be presented. The flourishing field of supraglacial microbiology will then be outlined, and comparisons drawn with similar terrestrial systems. The chapter will conclude with a hypothesised conceptual model based upon current knowledge of terrestrial systems and establish the research questions that will be investigated within this thesis.

2.1 Thermal regime

Thermal regime directly influences glacier hydrology, acting as a controlling factor upon the transfer of meltwater between the supra-, en-, and subglacial systems and the characteristics of the near-surface. A full review of the role of thermal regime upon supraglacial hydrology is beyond the scope of this thesis, with information herein linked solely with supraglacial processes. A full review can be found within Irvine-Fynn et al. (2011c).

The key distinction between temperate and non-temperate (polythermal) glaciers is that the entirety of a temperate glacier is above the pressure melting point (PMP), whereas non-temperate glaciers contain ice both above and below this temperature in a multitude of spatial arrangements (Irvine-Fynn et al., 2011c; Pettersson et al., 2004). Regardless of large-scale thermal regime, a transient thermal layer is observed in the ablation zone, which varies in temperature seasonally. The transient thermal layer acts as a substrate for supraglacial hydrology and thus heavily influences its characteristics. During the winter, a cold wave penetrates down from the surface due to air temperatures consistently < 0 °C (Blatter and Hutter, 1991; Cuffey and Paterson, 2010). At this time, this layer is typically snow-covered, and as such is considered inactive in terms of ice hydrology, although may be subject to hydrological processes within the snowpack (see Bales and Harrington, 1995; Jansson et al., 2003). Higher (i.e. > 0 °C) air temperatures in the spring and summer drive ablation and increase the temperature of this layer to the PMP (Cuffey and Paterson, 2010). For non-temperate glaciers, this layer is typically in the order of metres thick (e.g. Sobota, 2009), bound at depth by "cold" ice below the PMP.

In contrast to cold ice, which does not contain any interstitial liquid and is effectively impermeable, temperate ice has an interstitial liquid content of ~ 9% (Pettersson et al., 2004). The polycrystalline structure of glacial ice facilitates vein development (Hambrey et al., 2004; Mader, 1992; Nye and Frank, 1973; Nye, 1989) when above the PMP, forming void spaces and providing temperate ice with primary permeability (i.e. water flow between the crystal matrix) similar to that of granite (Jordan and Stark, 2001). Hence throughout the depth profile of a temperate ice mass, interstitial water is present.

A non-temperate thermal regime generally results in less dynamic ice masses when contrasted to temperate ice masses. This is largely due to the prevailing climatic conditions which tend to be cold and dry, hindering the formation of surface structures such as crevasses and moulins. Coupled with typically lower ablation rates than their temperate counterparts, more pervasive and extensive channelised supraglacial drainage networks (Irvine-Fynn et al., 2011c; Rippin et al., 2015) are often evident on non-temperate ice masses.

2.2 Surface energy balance and darkening

2.2.1 An overview of melt processes

Melt processes occurring in the transient temperate layer provide water to the glacial hydrological system and as such control the storage and discharge of glacial meltwaters (Jansson et al., 2003). Furthermore, it is important to consider the role of melt processes as they provide a proposed mechanism for the formation of the weathering crust (Müller and Keeler, 1969). An overview of surface energy balance is beyond the scope of this thesis, and for further detail Benn and Evans, (2010), Cuffey and Paterson (2010) and Hock (2005) should be referred to. Surface meltwater production is controlled by energy balance (Equation 2.1), where Q_M is energy available to melt ice, α is ice surface albedo ($0 \leq \alpha \leq 1$), SWR_{in} is incoming shortwave radiation, LWR_{in} is incoming longwave radiation, LWR_{out} is outgoing longwave radiation, Q_H is sensible heat flux, Q_L is the latent heat flux, Q_R is the heat flux from rainfall and Q_G is the energy required to raise the temperature of the ice to melting point. By convention, energy inputs to the glacier surface are positive and outputs are negative. SWR_{in}, LWR_{in} and LWR_{out} are referred to as the radiative components, whilst the remaining components, excluding Q_M and Q_G, are referred to as the turbulent components.

$$Q_M = (1 - \alpha)SWR_{in} + LWR_{in} + LWR_{out} + Q_H + Q_L + Q_R + Q_G \quad \text{[Equation 2.1]}$$

Typically, most energy supplied to a glacier surface is in the form of radiation (≈ 77 % globally), although climate, location and meteorological conditions influence this balance (Willis et al., 2002). Net radiation is considered as two separate components, defined by wavelength: shortwave radiation (SWR), originating from the sun, and longwave radiation (LWR), which is thermal radiation of terrestrial or atmospheric origin. Albedo, or surface reflectivity, ranges from 0.1 for debris-covered ice to 0.9 for fresh dry snow (Cuffey and Paterson, 2010), and acts as a significant control upon SWR receipt at the glacier surface. For an ablating ice surface albedo is typically ≈ 0.30, (Cuffey and Paterson, 2010), meaning that ≈ 70% of incident SWR energy provides energy for melt. At a local, catchment scale albedo can be highly variable due to debris cover, presence of cryoconite or surface meltwater, or ice crystal colour, size and structure and may locally enhance melting and affect drainage pathways (e.g. Adhikary et al., 2000; Rippin et al., 2015; Takeuchi et al., 2001a).

Most melt models (conceptual or numerical) assume that all shortwave radiation is absorbed at the surface, simply ignoring the component of subsurface melt and its additional complexities. In part, this is because limited agreement exists regarding the portioning of SWR receipt between the surface plane and subsurface zone. Greuell and Oerlemans (1989) suggest that 36 % of shortwave radiation energy penetrates the near-surface, and using mean radiative: turbulent energy input ratios suggested by (Willis et al., 2002), it can be estimated that 19% and 28% of total melt energy is received beneath the ice surface in maritime and continental environment, respectively, driving weathering crust formation.

Turbulent fluxes supply the remainder of energy for surface melt and are directly influenced by conditions within the ice-air boundary layer, ≤ 2 m above the glacier surface (Cuffey and Paterson, 2010). The temperature and humidity gradient between the ablating ice surface and this layer acts as a control upon the turbulent fluxes, as does the nature of the flow of air, its turbulence being determined by the wind speed, atmospheric stability and ice surface roughness. The latter of these factors further links directly with the channelised hydrology network, with rill and channel development promoting surface roughness in addition to micro-scale topography (Rippin et al., 2015).

2.2.2 Albedo

An understanding of albedo feedback processes is essential when considering and modelling ice melt and describing the climate of ice-covered regions. During the last 20 years, surface albedo of glaciers and ice sheets around the world has demonstrated a net-negative trend (e.g. Naegeli et al., 2019; Painter et al., 2013; Paul and Kääb, 2005; Paul et al., 2007; Tedesco et al., 2016). The most important factors controlling albedo is that of debris cover (Brock, 2004; Brock et al., 2000; Klok et al., 2003). Surface debris is incorporated to the ice surface from continental-scale atmospheric sources, often in snow and rainfall in addition to direct deposition (e.g. (Koch and Hansen, 2005; Paul et al., 2005; Zappa and Kan, 2007)); local-scale dust accumulations from valley sides exposed due to retreat and down wasting (Oerlemans et al., 2009); and melting of outcropping, debris-rich ice (e.g. Wientjes et al., 2011). Microbial activity on snow and ice surfaces can also contribute to albedo reduction, termed "bioalbedo" (Cook et al., 2017; Ryan et al., 2018; Tedstone et al., 2018; Williamson et al., 2019). For ice with debris cover ≤ 10 %, microscale inhomogeneities in ice crystal structure act as the fundamental control of albedo (Azzoni et al., 2016).

Seasonal debris cover change can be exemplified on the Forni Glacier (Italy). In 2013, debris deposition upon the debris-free surface was ~6 g m^{-2} day^{-1} during the ablation season (Azzoni et al., 2016). Similar darkening processes have been observed as a result of deposition of black carbon and dust in the snowpack in accumulation areas accelerating snow melt at high-elevation Asian glaciers (Brun et al., 2015; Flanner et al., 2009; Ginot et al., 2014; Yasunari et al., 2010); on the Greenland Ice Sheet (GrIS) (Dumont et al., 2014; Stibal et al., 2017; Tedesco et al., 2016; Tedstone et al., 2017); and in the Canadian Arctic (Mortimer and Sharp, 2018).

Surface water, either from melt or precipitation, can directly or indirectly influence debris cover and distribution and therefore albedo. A decrease in albedo increases SWR receipt and hence melt rate, acting to provide greater meltwater volumes to the surface which then mobilise debris and can act to reduce surface albedo. However liberated debris is added to this system from ablating ice crystals, and ablating ice surfaces generally darken throughout the melt season (e.g. Adhikary et al., 2000; Brock, 2004; Klok et al., 2003). However, albedo is increased after rainfall events during which debris is removed from the surface, whilst reduced melt rates associated with rainfall lower debris input from ice liberation. For example, an albedo increase of 0.2 following rainfall has been observed in the European Alps, with albedo restored to its pre-storm values 1 - 4 days following

the rainfall event (Azzoni et al., 2016). Despite this understanding, the role of the weathering crust in the redistribution of debris and microbial cells across and through glacier surfaces remains unconsidered.

2.2.3 Formation of the weathering crust

The weathering crust forms because of sub-surface internal ice melt at as short-wave radiative energy penetrates the translucent ice surface (Figure 2.2). The attenuation of the penetration of shortwave radiation imposes a depth limit upon internal melting, forming a "photic zone" (Irvine-Fynn and Edwards, 2014) in the order of 10s cm thick. Hypothetically, this layer could extend in depth to an order of meters for optically clear blue ice as defined by Beer's Law, which describes radiation decay as a function of depth (Oke, 1987). Radiation decay occurs because of reflection and refraction of radiation from ice crystals, microstructures and liquid water within veins between crystals (Hodson et al., 2013; McIntyre, 1984). Melt occurs preferentially along crystal boundaries (Nye, 1991) enlarging interstitial spaces and reducing bulk ice density (LaChapelle, 1959). Heat flow in unsaturated air spaces between crystals further reduces crystal cohesion (Nye and Frank, 1973; Nye, 1991). In the weathering crust, bulk density increases non-linearly with depth depending on time-of-day (Schuster, 2001) and antecedent meteorological conditions (e.g. Müller and Keeler, 1969). A depth threshold occurs at which ice is essentially impermeable (Irvine-Fynn and Edwards, 2014), and as such the weathering crust can be considered a perched aquifer. In non-temperate ice masses, this threshold is linked with the transient thermal layer, and the aquiclude is due to ice below the PMP with no interstitial melt water. For temperate glaciers, the aquiclude is comprised of essentially impermeable unweathered ice, which, despite the presence of interstitial meltwater, has a hydraulic conductivity equivalent to a granite (Jordan and Stark, 2001) and is therefore effectively impermeable.

Maximal rates of weathering crust formation occur under clear-sky conditions, when SWR receipt is at its highest, whilst degradation occurs during periods of high cloud cover and rainfall (Müller and Keeler, 1969). Cloudy, wet conditions reduce or even eliminate sub-surface melting in-line with SWR receipt reduction and promote refreezing of meltwater within pore spaces while simultaneously enhancing ablation of low-density ice via turbulent melt processes (Schuster, 2001).

Whilst this thesis focusses on Arctic, sub-Arctic and Alpine settings, it is important to outline the different processes driving weathering crust formation in Antarctica. Here, low air

temperatures limit surface melting, with internal near-surface melting driven by the generation of a "solid state greenhouse effect" powered by SWR penetration (Brandt and Warren, 1993; Liston et al., 1999) resulting in solar heating of the near-surface. The disconnected supraglacial hydrology of

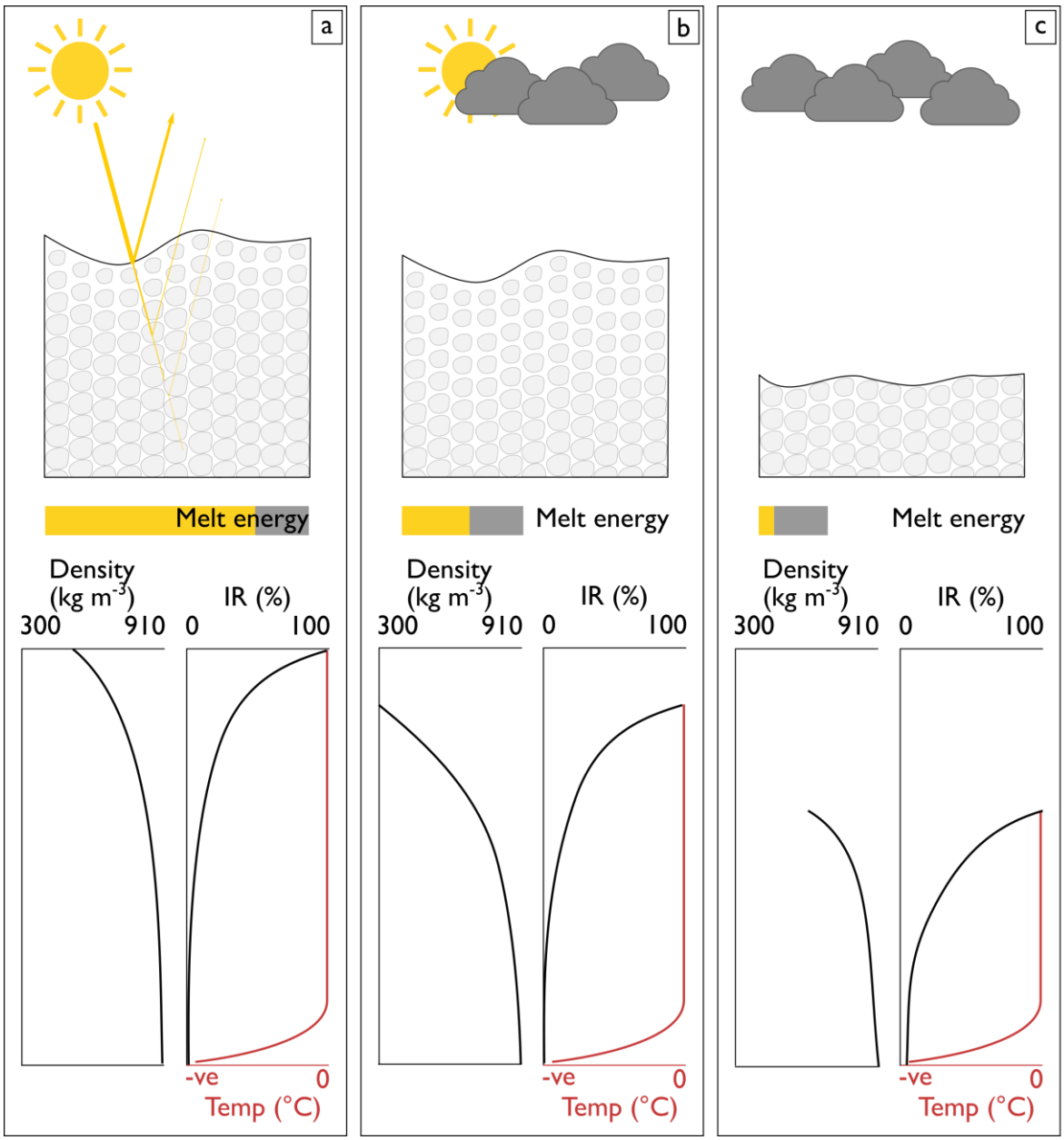

Figure 2.2 A schematic diagram showing the development and degradation of the weathering crust in clear sky and cloudy conditions respectively. In panel i, clear sky conditions dominate and SWR receipt is high (as indicated by the yellow component of the melt energy bar, relative units). SWR penetrates the surface, causing melt of ice crystals at depth along the crystal boundaries. Due to attenuation and reflection of SWR at depth, melt rates decrease and a distinct depth-density relationship develops. In panel ii, the period of clear sky conditions in panel i has caused extensive sub-surface melting and a fully formed weathering crust. However, an increase in cloud cover decreases radiative energy flux and therefore total melt energy. By panel iii, cloud cover dominates, and SWR flux is reduced to nearly zero; turbulent fluxes dominate the energy available for melting. As a result, ice crystal size is not reduced like in panel i, and the weathered ice is stripped from the surface by melt, leaving a hard, glassy surface and ice of a greater density at the surface of the glacier.

Antarctica (e.g. Fountain et al., 2004; Hodson et al., 2013) prevents drainage of this meltwater which simply refreezes *in situ* (Hoffman et al., 2016; Hoffman et al., 2014) and has little impact on ablation.

2.3 Supraglacial hydrology: an overview

Water flow over exposed glacier surfaces and through the near surface can be considered as a function of ice permeability at two scales: primary permeability, which is water flow through intact ice and snow; and secondary permeability via channels, fractures and other passageways (Fountain and Walder, 1998). Intergranular ice drainage from the glacier surface to the bed was proposed by Shreve, (1972) and Röthlisberger (1972) and further developed by Nye and Frank (1973). However, veins between unweathered ice crystals are small, ≤ 0.7 mm (Nye, 1991), may be blocked by air bubbles (Lliboutry, 1996) and can close due to ice deformation and recrystallisation (Lliboutry, 1971). Morphologies of inter-crystalline spaces are veins at triple junctions, which intersect to form veins, and lenses between crystals (Mader, 1992; Nye, 1989). There is debate as to the volume of water this network is able to transport (see Lliboutry, 1996; Nye, 1997), however, for unweathered, englacial ice a permeability in the order of 10^{-18} m^2, equivalent to granite, is suggested by with throughflow rates of 10^{-8} – 10^{-13} m s^{-1} (Jordan and Stark, 2001; Raymond and Harrison, 1975), implying a very small rate of inter-crystalline water flow. As such, intact ice can be considered essentially impermeable, meaning that water will flow across the surface of it. Intergranular drainage and thus primary permeability of ice masses on a glacier-scale can be considered negligible.

2.3.1 Channelised flow

As non-weathered glacier ice is essentially impermeable, meltwater flows across the surface of ice masses due to secondary permeability in the form of channelised flow (Ferguson, 1973). Glacial hydrological systems are highly variable in space and time, depending on climate, thermal regime, and glacier geometry. They develop throughout the ablation season, transitioning from rills on the winter snowpack to a fully developed dendritic surface drainage system (Kostrzewski and Zwolinski, 1995). At the start of the melt season a proportion of meltwater frozen at the base of the snowpack forms superimposed ice (Müller, 1962) which can provide a significant contribution to the annual accumulation budget on Arctic glaciers (Wadham and Nuttall, 2002). This accentuates reduced permeability of non-temperate glaciers resulting in the accumulation of meltwater upon the surface during the early ablation season with snowmelt lakes representing a significant delay in seasonal runoff (Hodgkins, 2001).

The contrasting permeabilities of snow and ice mean that supraglacial drainage systems of each surface have significantly different characteristics. On wet snow surfaces, meltwater percolates down through the snowpack (Benson, 1996) and refreezing of this meltwater releases latent heat to the snowpack, accelerating its melt and removal from the glacier surface. Drainage of water through the snowpack develops into the formation of rills and subsequently channels as the melt season progresses and as water content increases, with discharge becoming more efficient over time (Jansson et al., 2003). Firn aquifers, observed in Greenland (e.g. Miller et al., 2017) and sub-Arctic locations (e.g. Schneider, 1999) also act to dampen runoff from the glacier surface by several days or weeks, storing water in a layer than can be several metres thick (Jansson et al., 2003; Schneider, 2001).

In the supraglacial ablation zone, regular spatial organisation of channels is common (e.g. Karlstrom et al., 2014; Knighton, 1985, 1981; Marston, 1983), as it is in terrestrial environments. In such environments, rill spacing is determined by the turbulent flow of open-channel hydraulics rather than the evolution of the erodible bed (Izumi and Parker, 1995). This is demonstrated in supraglacial channel spacing, which is inversely proportional to slope and friction (Mantelli et al., 2015) with the dependency on slope a result of the reduction of bed-induced crossflow pressure gradient as slope steepens. When slope remains constant a greater coefficient of friction results in an enhanced response of the flow field to perturbations in the bed resulting from ice roughness. As such slope, meltwater depth and surface roughness are considered the primary controls upon supraglacial channel spacing (Mantelli et al., 2015).

Theakstone and Knudsen (1981) suggest that the formation of glacial rills and channels provides further evidence that ice permeabilities are low and that an insignificant volume of meltwater is transmitted between ice crystals. However, Mantelli et al. (2015) argue that a weathering crust would not prevent the initiation of rills, rather that it would only occur once the weathering crust exceeds its transport capacity, resulting in surface flow of excess water. Similar processes are present in the model of stream formation for hillslopes; once the porous surface media (typically soil) becomes saturated or water input is greater than infiltration rates overland flow occurs, and sheet flow organises into rills (Lu and Godt, 2013).

Supraglacial channel spacing is in the order of several metres on both non-temperate and temperate ice masses (see Karlstrom et al., 2014; Mantelli et al., 2015). The relevance of stream spacing to the hydraulic transmissivity of the weathering crust is that it governs the distance of

travel of a water molecule from the point of melt to the channelised system. Coupled with velocity of water transfer, distance from a point to the stream network defines the storage period of water within the weathering crust (Cooper et al, 2018; Smith et al., 2017; Smith et al., 2015).

2.3.2 The role of the weathering crust

To date, there is limited acknowledgement of the importance of the weathering crust as a mechanism through which meltwater may be transported {Derikx, 1973 #62;Wakahama, 1973 #270;Larson, 1977 #146;Larson, 1978 #147;Irvine-Fynn, 2011 #122;Cook, 2015 #536;Munro, 2011 #185}(Smith et al., 2017b). However, water retention within the weathering crust dampens the runoff response (Jansson et al., 2003; Munro, 2011; Shea et al., 2005), contrasting with the traditional view that surface runoff over glaciers is an efficient process (e.g. Fountain and Walder, 1998). For example, Munro (2011) suggests delays of 1 – 2 h between peak melt and peak stream discharge for a catchment with high stream density, and 7.5 – 12 hr for a catchment with one distinct channel. In contrast, Willis et al. (2002) report a ≤ 1 hr lag time, although throughout this study period rainfall and cloud cover were common, with associated low SWR receipt and as such the weathering crust was likely poorly developed.

Meltwater transport velocities of 6.0×10^{-8} to 7.0×10^{-4} m s^{-1} (2.2×10^{-4} to 2.5 m hr^{-1}) are suggested within the weathering crust by (Wakahama et al., 1973), measured using dye tracing techniques. The velocities reported, when considered with a channel spacing in the order of metres, align strongly with the longer response times suggested by (Munro, 2011). However, at shorter response times and/or slower velocities, it is unfeasible that the pulse of meltwater resulting in peak stream discharge is directly supplied from meltwater produced on the same day, implying piston flow and a short-term multiday storage of water within the weathering crust. For example, a water molecule transported at the lower quartile of the (Wakahama et al., 1973) velocities (i.e. 0.6 m hr^{-1}) would take 16 hours to flow 10 m, excluding the time taken for meltwater to infiltrate into the weathering crust.

This behaviour is similar from a hydrological perspective, to seasonal snow and firn, which are perched, unconfined aquifers that drain to otherwise impermeable ice (Fountain and Walder, 1998). Snow and firn (densities of 200 – 300 kg m^{-3} and 400 – 830 kg m^{-3} respectively (Cuffey and Paterson, 2010)) have relatively large, well connected spaces between crystals. Snow has a permeability of 10^{-5} – 10^{-9} m^2 (Albert and Perron, 2000; Thompson et al., 2016), whilst denser firn

is less permeable, 10^{-12} – 10^{-10} m^2 (Forster et al., 2014; Koenig et al., 2014; Miller et al., 2017). Work undertaken in the snowpack, suggests highly heterogeneous percolation rates of meltwater (Campbell et al., 2006; Gerdel, 1954; Schneider and Jansson, 2004), which aligns well with the spatial and temporal heterogeneity observed by Cook et al. (2015b) in the weathering crust.

Despite its role within the supraglacial system, the hydrological dynamics of the weathering crust remain poorly defined. Despite this, limited research efforts have been concentrated on near surface water flow, although more recent work has begun to focus on the weathering crust (Cook et al., 2015b; Cooper et al., 2018; Hoffman et al., 2014; Yang et al., 2018b).

2.4 Fundamentals of groundwater hydrology

It has been suggested by Campbell and Rasmussen (1973), Derikx (1973) and Sharp et al. (1998) that groundwater techniques are applied to examine water transfer through the weathering crust. However, despite this repeated call, there has been limited consideration of the wreathing crust using these methods. Therefore, with the aim of applying this body of knowledge to establish the fluid and impurity transport dynamics of the weathering crust, a brief review of the fundamentals of groundwater hydrology will be given herein.

The precise route that water will take over or through a porous medium depends on the balance between the forces that drive water flow; and resistance to flow. Water flow is, at the fundamental level, defined by the hydraulic head (h) governed by gravity (g) and elevation head (z), occurring perpendicularly to lines of equal head. In a saturated groundwater system water pressure (P) and fluid density (ρ_w) must also be considered (Equation 2.2).

$$h = z + \frac{P}{\rho_w g} \qquad \text{[Equation 2.2]}$$

Resistance to flow within porous media is measured using either hydraulic conductivity (K) or intrinsic permeability (κ), both of which decrease with increasing resistance to flow. Intrinsic permeability is a measure of the ability of a porous material to allow a fluid to pass through it, independent of the fluid, and is related to total porosity, defined as the ratio of void volume to total volume of a medium. Controls upon total porosity include the shape and size distribution of particles; in poorly sorted media, small particles can occupy void spaces between larger particles,

resulting in lower total porosity than would be observed for a well sorted medium (Brutsaert, 2005). However, not all pores meaningfully contribute to water transfer, and may be disconnected "dead ends" or be blocked by particulate impurities. Effective porosity can be an order of magnitude lower than total porosity in sedimentary rocks (Croff et al., 1985).

Hydraulic conductivity additionally considers the degree of saturation, density and viscosity of the fluid flowing through the media. Typically, in the terrestrial environment, in saturated conditions hydraulic conductivity is proportional to intrinsic permeability. However, in the glacial environment water temperatures are close to 0 °C (Isenko et al., 2005), and given the inverse non-linear relationship between water viscosity and temperature (Kestin et al., 1978) it is important to look beyond intrinsic permeability when considering water flux through the weathering crust. In a medium of equal intrinsic permeability, fluids of greater viscosity have lower hydraulic conductivity values, and *vice versa* (Freeze and Cherry, 1979). Hydraulic conductivity can be highly variable beyond levels common for other physical properties; it is known to vary over 13 orders of magnitude (10^{-8} to 10^{5} m d^{-1}; Freeze and Cherry, 1979). Variations of several orders of magnitude are common in single aquifers (Lu et al., 2002), or even within single boreholes and hence in practice quantification of hydraulic conductivity to within an order of magnitude is typically acceptable (Younger, 2009).

2.4.1 Darcy's Law

Hydraulic conductivity, despite having the same units as velocity, does not directly represent the flow rate of water through the porous medium, but rather is a coefficient of proportionality linking cross-sectional area (A), of the media, flow rate (Q) and hydraulic gradient, (i), and is described in Darcy's Law (Darcy, 1856; Equation 2.3). Darcy's Law assumes that a medium is saturated, and that fluid flow is laminar requiring suitably slow flow rates; in the presence of large conduits and steep hydraulic gradients this assumption may be violated (Younger, 2009). The presence of bubbles and varying water heads (and subsequently hydraulic potential) across capillary and vein networks in the weathering crust brings the use of Darcy's Law into question (Lliboutry, 1996), and hence evaluation of its application is necessary. However, Darcy's Law is considered valid for unconfined, saturated media which exhibit these phenomena (Buckingham, 1907).

$$Q = KiA \quad \text{[Equation 2.3]}$$

The assumptions of Darcy's Law are also violated at low flow rates ($\leq 10^{-4}$ m d^{-1}) and permeabilities (Miller and Low, 1963; Swartzendruber, 1968). For example, at pore diameters ≤ 10 μm the movement of water under the impulse of i is so slow that molecular diffusion becomes the more rapid and hence dominant flow mechanism (Younger, 2009). Other driving factors may also contribute significantly to flow at these low flow rates, including thermal, osmotic and electrical effects (Brutsaert, 2005; Cahill and Parlange, 1998). There is no accepted universal theory given the complexity of controls of slow-flowing water within a porous medium, and as such it is pragmatically preferable to accept Darcy's Law when hydraulic conductivity is within typical magnitudes (Brutsaert, 2005) and assume that in these cases hydraulic head is the substantial driving force of water transport (Milly, 1984).

When considering the transport of impurities, it should be noted that the velocity of a fluid within pores (pore velocity, v) of medium is not equal to the Darcy velocity, which assumes flow over the entire area of the porous medium. Clearly, fluid only flows in the pore spaces of the medium and the velocity within pores is therefore greater than the Darcy velocity, inversely proportional to proportion of the medium occupied by connected voids; i.e. the effective porosity, n_e (Equation 2.4; Schwartz and Zhang, 2004). Hence when considering the transport of cells through the weathering crust, both hydraulic conductivity and effective porosity need to be considered.

$$v = \frac{Q}{n_e} \qquad \text{[Equation 2.4]}$$

2.4.2 Fracture flow: a question of scale?

In rocks, structural features such as fractures exert a major influence on groundwater flow at micro, macro and regional scales (e.g. Whitehead, 1996). Presence of fractures does not necessarily mean that a pathway for fluid flow exists, fractures must be connected and free of blockages. However, in media with interconnected fracture networks, fractures often provide the main pathway for fluid flow. Porosity (and therefore intrinsic permeability) of fracture networks is directly proportional to fracture aperture and inversely proportional to fracture spacing (Romm, 1966). For a single uniform fracture, hydraulic conductivity is proportional to the fluid properties (viscosity and density), gravity and the fracture aperture (b) (Equation 2.5).

$$K = \frac{\rho_w g b^2}{12\mu} \qquad \text{[Equation 2.5]}$$

Fractures are rarely uniform, in which case Equation 2.5 is modified to incorporate a roughness parameter in the divisor as an increase in roughness of the fracture walls decreases its hydraulic conductivity. Furthermore, single fractures are rare within media, and fracture network flow usually requires a modelling approach to resolve. Practically, it is often not possible to consider flow through individual fractures or simple sets of fractures. If a medium is significantly fractured and considered from a great enough distance, the medium appears to be a porous medium. This "continuum approach" identifies that a clear threshold cannot be drawn between media which are "fractured" and "unfractured", and as such it most practical to consider the medium at a scale at which a Darcian approach is suitable when large, single fractures are not identified (Schwartz and Zhang, 2004).

2.4.3 Infiltration and unsaturated flows

Infiltration is the process of downwards entry of water into porous media through the unsaturated zone to the saturated zone. In terrestrial systems, this is typically in the form of precipitation, but can also be comprised of snowmelt. Infiltration rate is sensitive to the rate of water addition to the surface, near-surface conditions and antecedent water content of the porous media, decreasing inversely with time during a water input event (Horton, 1933). Once the rate of the addition of water exceeds the infiltration rate, water will pond on the surface, initially in depressions, allowing overland flow to occur. Surface connected pores move water downwards, forming a "wetting front" in the unsaturated (vadose) zone of the medium, moving downwards at a rate determined by the hydraulic head, tension head and unsaturated hydraulic conductivity. Once the wetting front reaches the water table, water then joins the saturated zone and active flow system.

In the unsaturated zone, defined as the zone in which the volume of liquid is less than the volume of void space, flow mechanics are complicated by the presence of two fluid phases (usually air and water). In a similar manner to the saturated zone, the unsaturated zone can be characterised in terms of hydraulic head (h), defined by the elevation head (z) and pressure head (ψ) (Equation 2.6). Pressure head is negative in the unsaturated zone ($\psi < 0$, i.e. less than atmospheric pressure) positive in the saturated zone ($\psi > 0$), and zero at the water table. For this reason, the pressure head in the unsaturated zone is also referred to as the tension head, acknowledging the capillary

forces which bind water to solids and prevent water in partially saturated soils from flowing into a borehole (Schwartz and Zhang, 2004).

$$h = z + \psi \qquad \text{[Equation 2.6]}$$

Hydraulic conductivity in unsaturated media is strongly dependent on the degree of saturation, the pressure head and capillary pressure. A medium with low water content (i.e. a mostly air-filled system) has a strongly negative pressure head, a large resistance to flow and therefore low hydraulic conductivity. Conversely, a medium near to saturation (ψ close to 0), hydraulic conductivity takes its maximum value. Water content is defined by the difference between the inflow and outflow rates of water. Changes in water content via the processes of wetting and drying is characterised by a hysteric, non-linear relationship between pressure head and volumetric water content. At both large and small water contents, small changes in water content are linked with relatively large changes in pressure head, reflecting the fact that, at low water content, soils do not lose all their water (termed the residual water content). As volumetric water content approaches the residual water content, the water phase may be discontinuous through the media, and hydraulic conductivity will be virtually zero. Flow in this zone can be considered using a modified Darcy equation (Equation 2.7), using the Richards equation with appropriate conditions to give a field of pressure head (not shown; see Richards, 1931). Solutions to the Richard's equation are modelled, a task for which many models exist such as HYDRUS 1D (Šimůnek et al., 1998; Vogel et al., 1996), 2D and 3D (Šimůnek et al., 2008), TOUGH (Finsterle et al., 2012; Jung et al., 2017) and VS2DI (Healy, 2008), amongst others.

$$Q = -K\psi iA \qquad \text{[Equation 2.7]}$$

The direction of flow in unsaturated hillslopes is generally not well understood, in contrast to saturated, isotropic, homogenous hillslopes. In saturated conditions, flow is generally laterally downslope under the driving forces of gravity and constant pressure, which are governed by hillslope geometry, water input characteristics and hydrologic properties of the hillslope media. However, in unsaturated conditions the gradient of moisture content and therefore pressure potential plays a significant role, yielding spatially and temporally complex flow patterns. These patterns can include upslope lateral flow in addition to downslope flow, and downward vertical flow through the medium (Sinai and Dirksen, 2006). For flow patterns to be defined in the unsaturated zone of an isotropic and homogenous hillslope, the history of moisture content (i.e.

from field measurements) and recent rainfall intensity must be known (Lu et al., 2011), and is further complicated by anisotropy and/or heterogeneity.

2.4.4 Capillary rise and vapour flow

Capillary rise refers to the upward movement above the water table under the driving force of capillarity, which will cease at a certain height (h_c), above which pore water exists in a continuous form. This upwards movement of water acts to resist infiltration. The height of capillary rise is directly rated to the suction at which a porous medium reaches the residual water content; those with fine particles have the highest capillary rise (clay soils in the order of decametres, silty soils the order of metres and sandy soils centimetres to decimetres (Lu and Godt, 2013)). As such, the height of capillary rise (mm) can be empirically linked with the particle size of the media at the 10 % and finer (D_{10}) fraction (mm) (Lu and Likos, 2004; Equation 2.8).

$$h_c = -990 \ln(D_{10}) - 1540 \qquad \text{[Equation 2.8]}$$

When considering a moist medium subject to a sustained humidity gradient at the ground surface, the rate, as well as the height, of rise becomes of practical importance; the humidity gradient acts as the main control and the rate of capillary rise can be estimated using the vapour flow theory. Fick's law (Equation 2.9) can be used to describe vapour flow within a porous media or at the atmosphere subsurface interface, where vapour flow velocity (q_v) is described as the product of the density of water vapour (ρ_v) and a vapour diffusion coefficient (D_v) of the media. The vapour diffusion coefficient can be estimated (Equation 2.10) using the air-filled porosity (n_a) and vapour-free diffusion coefficient (D_0), which ranges between 10^{-9} to 10^{-6} $m^2 s^{-1}$ for pure air.

$$q_v = -D_v \nabla \rho_v \qquad \text{[Equation 2.9]}$$

$$D_v = \frac{2}{3} n_a D_0 \qquad \text{[Equation 2.10]}$$

Water vapour density can be quantified using the ideal gas law (Equation 2.11), in which ω_w is the molecular mass of water, R the universal gas constant, T temperature and u_v vapour pressure, itself described for saturated conditions in Equation 2.12 (Tetens, 1930). Therefore, water flux through vapour near the surface of a saturated porous media can be given in Equation 2.13 (Lu and Likos, 2004), where λ is the latent heat of vaporisation (≈ 2.48 kJ g^{-1} at 10 °C).

$$\rho_v = \frac{\omega_w}{RT} u_v \qquad \text{[Equation 2.11]}$$

$$u_v = 0.611\, e^{\left(17.27\frac{T-273.2}{T-36}\right)} \qquad \text{[Equation 2.12]}$$

$$q_v = D_v \rho_v \left(-\frac{\nabla RH}{RH} + \frac{\nabla T}{T} - \frac{\lambda \omega_w \nabla T}{RT^2}\right) \qquad \text{[Equation 2.13]}$$

Equation 2.13 demonstrates that vapour flows from areas of high humidity to low humidity, and from regions of high temperature to low temperature, with a counteracting flux to compensate for the contraction of and consequent increased vapour density in relatively low temperature air.

2.4.5 Surface water interaction

The process by which water leaves the ground flow system and returns to the surface is termed discharge. This includes outflow to rivers and lakes as seepage through the channel walls, and flow to surface springs, although a layer of relatively low hydraulic conductivity at channel walls or lake margins can complicate this process (Peterson and Wilson, 1988). Furthermore, streams and lakes can also contribute to groundwater recharge as well as discharge, and lakes can contribute to both groundwater discharge and recharge simultaneously, allowing for throughflow of groundwater (Winter, 1999; Figure 2.3). In the terrestrial environment, evapotranspiration is a key process in the loss of water from aquifers, but the lack of vascular plants in the supraglacial environment precludes water loss via transpiration.

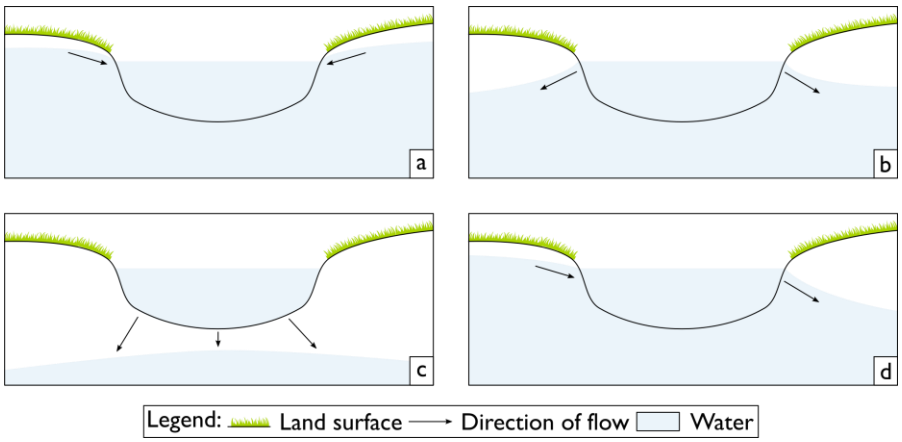

Figure 2.3 Summary of aquifer and stream/lake interactions. a) a gaining stream (i.e. water is moved from the groundwater system to the stream, discharging groundwater); b) a connected losing stream (recharging groundwater); c) a disconnected losing stream; and d) a throughflow lake, both discharging and recharging

2.4.6 Non-fluid mass transfer in groundwater

Non-fluid mass, such as sediment, cells or solutes can be transported through the groundwater system by advection, diffusion or dispersion, with the potential for modification of solutes by biogeochemical cycling or sorbtion onto the porous medium or sediment transported within the groundwater. In the case of advection (mass transport due to the flow of water) the direction and rate of transport coincides with the flow of groundwater; hence knowledge of the groundwater flow pattern implies knowledge about advective transport. For most practical problems, non-fluid mass will be transported at the pore water velocity (Equation 2.4). Diffusion (mixing caused by random motions in the solute) is incredibly slow as a mass transport process and is typically unimportant if water is flowing and is further hindered by collisions with the solid phase of porous media. Dispersion is the mixing of two fluids of differing compositions, spreading non-fluid mass beyond the region it would normally occupy by advection alone. It is driven by local differences around the mean flow velocity, driven by local scale inhomogeneities and consequent hydraulic conductivities in the media.

2.5 Microbiology of glacier surfaces

Historically, a purely physical approach was applied to the study of glaciers despite the acknowledgement of glacier surface biota from expeditions dating back to the 1890s (Hodson et al., 2015). Snow and ice environments were considered irrelevant in terms of microbiology due to their low temperatures, high UV irradiation, low nutrients and low water availability (Maccario et al., 2015). However, a long overdue shift in perceptions has recently occurred. Rather than being considered as lifeless, ice is now considered to be "Earth's largest freshwater ecosystem" (Edwards et al., 2014) and distinct biome (Anesio and Laybourn-Parry, 2012; Hodson et al., 2008). The influence of microbial processes within the terrestrial, aquatic and marine biospheres in shaping their habitats and influencing landscape scale processes is well recognised but has seen limited exploration within glacial systems (Cook et al., 2015a). Processes range from the biocatalysis of ice crystal formation (Georlette et al., 2004), albedo reduction at the ice-atmosphere interface (e.g. Takeuchi et al., 2001a), microbe-mediated subglacial weathering (e.g. Mitchell et al., 2013) and biogeochemical cycling (e.g. Cameron et al., 2012; Lutz et al., 2016) including the fixation of atmospheric carbon (e.g. Cook et al., 2016b; Koziol et al., 2018).

The extent of the microbial glacial biome remains poorly defined, but estimates suggest a range of 4×10^{25} to 7×10^{29} non-eukaryotic (i.e. bacteria and archaea) cells are contained within glacial systems (Anesio and Laybourn-Parry, 2012). Cells are concentrated within interstitial meltwater at the near-surface ($> 10^6$ cells mL^{-1} in contrast to 10^2 - 10^3 cells mL^{-1} in glacial ice (Mader et al., 2006)), with $\geq 10^{26}$ globally (Irvine-Fynn and Edwards, 2014). This estimated cellular abundance is comparable with rainforest soils (10^{27}) or the global oceanic photic zone (10^{25}) (Falkowski et al., 2008). However, the knowledge of microbial abundance within glacial systems is only based on a low number of samples from easily accessible sites, and hence is less robust than those from other ecosystems (e.g. Whitman et al., 1998). This estimate is further complicated by the challenges presented by glacier samples with regards to the enumeration of microbes within them: glacier ice tends to have low microbial abundance and additionally includes mineral particles, to which cells may be attached. At present, epifluorescence microscopy (EFM) is suggested as the most reliable technique to overcome these issues and provide reliable estimates of microbial abundance (Stibal et al., 2015); however, this technique remains far from perfect with accuracies of <50% for samples with less than 10^3 cells mL.

2.5.1 Sources of glacial microbes

Microbial inoculation occurs from the release of microbes stored within ice as a product of ablation (Dancer et al., 1997), at an estimated rate of $10^{17\text{-}21}$ a^{-1} globally (Rogers et al., 2004). The initial source of microbial cells is within snow deposited in the accumulation season, with microbial cells retained during the process of firnification, ultimately becoming incorporated into the ice (Edwards et al., 2014), prior to this liberation. It is unknown whether such microbes are biogeochemically active, becoming re-animated after a period of dormancy, or are dead, and simply particulate organic carbon within the supraglacial system. Specifically considering the weathering crust, the redistribution of material in, mixing of/in and collapse of cryoconite holes can directly deliver cells and sediments. (Hodson et al., 2007; Irvine-Fynn et al., 2011b; Mindl et al., 2007; Stibal et al., 2012b). Hole collapse does not imply the immediate removal of material from the glacier surface as dispersed granules can a) initiate the formation of new holes (Takeuchi et al., 2001b) and/or could be retained within the weathering crust (Irvine-Fynn et al., 2011a; Irvine-Fynn et al., 2012).

Furthermore, aeolian transfer from ice-marginal habitats inoculates glacier surfaces with bacteria as glaciers are typically surrounded by debris sources which are fine enough to be deposited across the entire ice surface (e.g. moraine; Segawa et al., 2014). Significant inputs of this nature have been observed in Svalbard (Edwards et al., 2013b); which presents a similar glacial architecture (i.e. valley glaciers in surrounds with limited vegetation development) to Arctic Sweden. Similar delivery of microbiota to glacier surfaces is observed within the European Alps (Franzetti et al., 2017) and Greenland (Cameron et al., 2015; Musilova et al., 2015; Šantl-Temkiv et al., 2018).

2.5.2 Stream and weathering crust meltwaters

Within the weathering crust, the microbial community survive within a photic zone due to the genesis of meltwater and provision of photosynthetically available radiation (Edwards et al., 2014; Irvine-Fynn and Edwards, 2014). As water mobility is limited within unweathered, ice so is cellular mobility (Price, 2007). The porous nature of the weathering crust potential facilities the translocation of cells, clastic sediment and solutes which may act as biological nutrients (Christner et al., 2018; Cook et al., 2015b) or as components of biogeochemical cycles either within the glacial or proglacial environments. However, the photic zone/weathering crust appears to represent somewhat of a logical paradox, as an ice mass ablates microbial biomass accumulates, rather than being eluted by meltwater (Irvine-Fynn et al., 2012). As such, glacier surface transport processes mediating the delivery of cells, biotic and abiotic material to downstream glacial, terrestrial and aquatic habitats are likely incredibly complex. Within streams, microbes are active, demonstrating nutrient retention and turnover (Scott et al., 2010).

2.5.3 Cryoconite holes

The most visually apparent microbial community upon the ice surface is cryoconite; microbe-mineral aggregates formed via mechanical and biochemical flocculation and found within small melt ponds ≤ 50 cm diameter (Cook et al., 2016a; Hodson et al., 2008). Cyanobacterial filaments and extra-cellular polymeric substances (EPS) bind granules, which have diameters ≤ 100 μm (Langford et al., 2010). As relatively stable, nutrient-rich and well-illuminated environments they are areas of high microbial biodiversity upon the glacier surface (Cook et al., 2010; Edwards et al., 2013a; Hodson et al., 2008; McIntyre, 1984; Wharton et al., 1985). Hole morphologies and biochemistry typically undergo constant evolution, only reaching a steady-state

equilibrium when sediment flux is zero, the substrate is uniform and radiation flux constant (Cook et al., 2015a).

Aggregate motion within holes is controlled by local hydrological conditions (Irvine-Fynn et al., 2011b) and thermodynamic processes which maximize ecosystem productivity (Cook et al., 2010). However, granule and cell motion between holes via the weathering crust remains unknown. The fate of cryoconite holes remains undetermined. They may "melt out" (i.e. ablation results in a re-equalisation of the surface with the hole base) or become disaggregated and collapse due to the encroachment of the active supraglacial hydrological system (Takeuchi et al., 2000) causing downstream redistribution of material (Irvine-Fynn et al., 2011b).

It is important to note that these observations are skewed towards northern hemisphere systems which are exposed to the environment, allowing for influx of material, rather than the permanently lidded systems common in Antarctica (e.g. Fountain et al., 2004). In contrast to those of other ice masses, Antarctic cryoconite holes often feature perennial ice lids, isolating them from gaseous, hydrological, microbiological and sedimentological exchanges with the environment, and interact with each other hydrologically through the frozen, permeable near-surface layer (MacDonell and Fitzsimons, 2008; MacDonell and Fitzsimons, 2012; MacDonell et al., 2016).

2.5.4 Biogeochemical cycling and fluxes

A microbiological approach compliments contemporary glaciological investigation strategies as the "poorly catalogued" (Rinke et al., 2013) microbiological population of glacial surfaces drives many biogeochemical cycles (Falkowski et al., 2008) in both glacial and non-glacial environments. Those processes which occur on glacier surfaces remain poorly characterised, despite an increasing recognition of their importance within biogeochemical cycling on a global scale (e.g. Anesio et al., 2009; Cameron et al., 2012; Hodson et al., 2007; Hodson et al., 2005; Hood et al., 2015; Wadham et al., 2013).

Ice-surface bacterial communities play vital roles in carbon and nitrogen cycling (Cook et al., 2010; Hodson et al., 2007; Segawa et al., 2014; Telling et al., 2012a; Telling et al., 2012b) transforming labile inorganic nutrients, such as ammonium and phosphate, into organic forms (Anesio et al., 2009) that ultimately contribute to the pool of ice-locked organic matter. For example,

in Arctic environments, prolonged residence times of cryoconite are associated with enhanced stability and periods of net carbon fixation (Cook et al., 2012; Hodson et al., 2007).

On a global scale, such organic matter represents a poorly understood carbon reservoir (Hood et al., 2015). At a regional scale, climate-driven changes in glacier run-off may represent an important global flux of organic carbon, and glaciers represent a key link between terrestrial and aquatic carbon. For example, the Greenland Ice Sheet and mountain glaciers are major sources of particulate and dissolved organic carbon (POC and DOC respectively), exporting 1.97 and 1.04 TgC a^{-1} (Hood et al., 2015), accumulated from primary production and aeolian deposition (Hood et al., 2009; Singer et al., 2012; Stibal et al., 2012a). In Greenland, half of glacially exported nitrogen is sourced from microbial activity within glacial sediment at the surface and the bed of the ice (Boyd et al., 2011; Telling et al., 2012b; Wadham et al., 2016) with similar processes also observed on valley glaciers (Hodson et al., 2008; Telling et al., 2011). Climate change contributes to these fluxes; approximately 13 % of annual DOC flux from glaciers to proglacial marine and terrestrial environments is a result of mass loss which is expected to accelerate over the next century (Bliss et al., 2014; Radić et al., 2014). Whilst this proportion is small in the context of global carbon fluxes, glacier derived DOC is highly biologically available in contrast to other sources, with ≤ 95 % metabolised in laboratory assays of microbial heterotrophs (Hood et al., 2009; Singer et al., 2012).

Annual global downstream transport of glacial cells is 3.15×10^{21} cells yr^{-1} (Irvine-Fynn and Edwards, 2014), which, whilst insignificant in terms of global cell flux (≤ 0.1%) may be important on a local scale. Traditionally, deglaciating catchments are viewed as a classic example of primary succession (e.g. Chapin et al., 1994) which is likely to be challenged with increasing awareness of transport processes of biological material and cells from glaciers within glaciated catchments. Increased emphasis is being placed upon microbial processes within glacial forefields (Bradley et al., 2014; Schutte et al., 2009; Zumsteg et al., 2011) complementing the classical consideration of succession. The transport of active microorganisms from the glacier surface may impact the cycling on and quantities of carbon discharged from glaciers to proglacial environments, depending on their functional diversity (Anesio et al., 2009; Cook et al., 2012) and may affect dissolved organic matter (DOM) delivery to and microbial ecosystem structure of downstream environments (e.g. (Bhatia et al., 2013; Lawson et al., 2014; Musilova et al., 2017; Smith et al., 2017a)).

The scale of worldwide ice loss creates a need to evaluate spectrum of these downstream effects on freshwater rivers (Hotaling et al., 2017), lakes and near-shore marine ecosystems. For

example, Hood et al. (2015) and Milner et al. (2017) call for a global census and continuous monitoring of key biogeochemical variables, adopting standard techniques to provide greater understanding of current and future regulating services of glacier-fed rivers. Microbial biodiversity and function in alpine headwaters have been largely unexplored, despite the between stream microbial communities and their general importance to biodiversity, ecosystem processes and biogeochemistry (Battin et al., 2016; Zeglin, 2015).

The weathering crust and supraglacial streams are crucial transport pathways in glacial ecosystems, yet their role in the moderation of cell, particulate and solute fluxes remain unclear. To characterise these surface changes and nutrient fluxes, it is necessary to understand the changing input from glaciers, including how cells are stored, transported and exported through and across the supraglacial hydrological system.

2.6 Eco-hydrology of non-glacial environments

Eco-hydrology is defined as the interaction between hydrological and ecological sciences, and the impact of each system upon the other (Hannah et al., 2004). Microbial communities in non-glacial environments are examined briefly herein as they present potential analogues with which to study glacial eco-hydrology. In the freshwater environment, water is important as both a major internal constituent of biota and as the environmental matrix. This is the case for the glacial system, but more conventionally studied analogous freshwater ecosystems include, rivers, terrestrial aquifers, snowfields, and seasonal lacustrine ice. The microbial ecology of seasonal and perennial sea ice is also examined, with potential analogues considered due to the low temperatures which exist. Many organisms can grow in extreme environments (Seckbach, 2000), with those that favour cold conditions termed "psychrophiles".

Limitations in the external concentrations of inorganic nutrients such as nitrogen and phosphorous, and organic carbon, occur widely in freshwater environments, especially in snow and groundwater aquifers, restricting growth of hetero- and autotrophic microorganisms. In the water column of most lakes and rivers, most bacteria are in a starvation-induced state of dormancy (Jones, 1971). Freshwater bacteria have evolved a range of molecular and physiological mechanisms to survive under low nutrient conditions, blooming when nutrient availability increases (Menzel and Ryther, 1970; Morita, 1997). Temperature is another important factor that determines growth and survival of microorganism, and each organism has a characteristic range of temperatures which it

can inhabit with microorganisms found in environments from ≤ 0 °C to ≤ 100 °C (Willey et al., 2008).

2.6.1 Rivers

The aquatic environment of both streams and rivers is dominated by continuous unidirectional flow with low retention time and no thermal or chemical stratification due to the turbulence associated with water flow. This limits development of the planktonic community which is rapidly advected downstream (Sigee, 2005). Hence, benthic algal and bacterial biofilms are particularly important, with filamentous green and blue-green algae important primary producers, responding rapidly to changes in water quality (Biggs, 1996), although such organisms can also be dispersed if entrained in the water flow., with an inverse relationship between velocity of river flow and immigration of organisms into benthic communities (McCormick and Stevenson, 1991), linked with a reduction in the rate of cell delivery as cells remain in suspension. Water velocity also acts as a determinant in nutrient supply to the benthic ecosystem (Biggs et al., 1998).

2.6.2 Soil and rock aquifers

Soils, and water enclosed in soil and bedrock aquifers represent extensive microbial habitats with bacterial concentrations in groundwater in the range 10^2 to 10^8 cells mL^{-1} (Madigan et al., 2015). Both media are similarly lacking in sunlight and are periodically or permanently anoxic.

Soil is one of the diverse habitats known for microorganisms, with thousands of different prokaryotic species per gram (Torsvik et al., 1990). Despite substantial species variation dominant phyla are relatively constant (Madigan et al., 2015). Understanding of major controls of microbial community composition is soils has yet to be achieved, which can feed back into changes in soil and ecosystem processes (Schimel, 1995; Waldrop et al., 2000). Potential contributing factors driving differences in soil microbial communities include types and amounts of organic carbon and water (Sylvia et al., 2005), which are highly correlated with observed differences in community composition (Drenovsky et al., 2004). Organic carbon limits microbial communities in most soils (Aldén et al., 2001) and additions of labile organic material rapidly alter microbial communities by selecting for populations that are most competitive in terms of growth rates and ability to absorb nutrients. Water content influences communities both directly and indirectly through impacts on oxygen concentrations and nutrient availability (Bossio and Scow, 1998). In soils, microorganisms

can act to block pore spaces, reducing hydraulic conductivity and decreasing water infiltration rate (Seki et al., 1998).

Microbial communities in subterranean systems are found at depths ≤ 200 m and demonstrate considerable physical diversity (Madigan et al., 2015). In groundwater, microorganisms can be motile (i.e. flagellated) by are more commonly present in biofilms bound to solid surfaces, including both litho- and heterotrophic organisms (Fredrickson et al., 1989). When concentrations of organic compounds are low, immotile bacteria have a competitive advantage (e.g. Kelly et al., 1988), with the converse situation also the case; a greater proportion of motile bacteria are observed in highly contaminated systems (Ghiorse and Wilson, 1988). Predominant microorganisms are thought to be aerobic heterotrophs of the genus *Pseudomonas*, adapted to survive a range of adverse conditions including low nutrient concentrations, and are adapted to grow and survive at the extremes of organic carbon availability, with total bacterial counts in pristine aquifers directly correlated with organic carbon levels (Kazumi and Capone, 1994).

Significant correlation has been observed between bacterial abundance and hydraulic conductivity (Levine and Ghiorse, 1990), with bacteria found to be more abundant in sand sediments than clayey sediment. This correlation may reflect the difficulty in colonisation of finer-grained sediments, which mechanically filter finely grained organisms. Furthermore, media with greater hydraulic conductivity have larger fluxes of water, delivering nutrients and DOM to bacterial cells.

2.6.3 Snow

The snow surface presents challenging conditions for organisms living upon it; levels of irradiance, including the UV element of the spectra are high, nutrient concentration and temperatures are low, and periods of desiccation are common. Hence active phases are restricted to periods with water availability, with cells mainly dormant during an annual cycle. The most visually apparent form of microorganism in snow is coloured, so-called "snow algae", which are in fact flagellated protozoa (belonging to the Phytomastigophora) and can reach concentrations of $\leq 8.6 \times 10^5$ cells mL^{-1} (snow water equivalent) (Jones et al., 2001). Bacteria are also observed, even in the most extreme environments such as Antarctica where annual temperature ranges are -85 to -13 °C, exhibiting growth in temperatures above -17 °C (Carpenter et al., 2000). Abundances range

between 600 (e.g. Liu et al., 2009) and 2×10^5 cells mL^{-1} (e.g. Amato et al., 2007), with deposition of cells connected to aeolian particulates (Chuvochina et al., 2011).

Snowpacks can act as control upon subglacial biogeochemical processes, with links drawn between recession of seasonal snow, subglacial drainage and the aeration of subglacial sediments driving a redox environment characterising subglacial microbiology and delivering nutrients and organic matter to the bed (Hodson et al., 2008; Tranter et al., 2005). Whilst such processes remain poorly defined for the supraglacial environment, with research focus on non-glacial snowpacks, it seems reasonable to consider that the melting seasonal snowpack may exert a similar influence at the beginning of the melt season. Despite limited liquid meltwater, nitrogen cycling during the spring melt period has been identified (Larose et al., 2013). Clay particles and dust are an important component of this biogeochemical cycle (Amoroso et al., 2009) acting to reduce the photolytic losses to the atmosphere (Björkman et al., 2014) enhancing the assimilation of nitrate into cryospheric ecosystems.

Algal taxa within the perennial snowpack differ from those within seasonal snow found in the ablation area (Takeuchi, 2013). This is significant in terms of glacial melt processes due to differing controls upon algal blooms in each community and the influence of such algae upon albedo; this is especially of interest upon the Greenland Ice Sheet (Cook et al., 2012; Lutz et al., 2014; Uetake et al., 2010; Wientjes et al., 2011; Yallop et al., 2012). It was suggested by (Takeuchi et al., 2015) that algal albedo reduction increased the melting rate of Glacier 31, Suntar-Khayata Mountain Range, Siberia by a factor if 1.6 - 2.6 when compared with clean ice.

2.6.4 Lake ice

Bacteria of diverse morphology, including filamentous forms ≤ 100 μm long, are found in seasonal ice on the surface of alpine lakes in abundances ≤ 1.6×10^6 cells mL^{-1} (Felip et al., 1995). The bulk of microbial activity is observed within surface slush layers, which was greater than that observed in the underlying lake waters. However, chlorophyll-α levels in the slush layer where five orders of magnitude lower than sea ice; between 0.22 and 0.50 μg L^{-1}, indicative of an oligotrophic environment, highlighting the importance of allochthonous carbon and nitrogen to sustain net heterotrophy. Bacteria in the slush layer were mainly larger than 2.6 μm, whilst those in the lake water were small ≤ 1 μm (Alfreider et al., 1996).

2.6.5 Sea ice

Sea ice covers approximately 7 % of the Earth's ocean surface at its maximum extent (Vaughan et al., 2013) and hence represents a major microbiological ecosystem. Bacterial abundance can reach 2.0×10^6 cells m^{-2} (Laurion et al., 1995). Little is known about viruses in sea ice, except that most are bacteriophages (Gowing, 2003). The ice itself is a porous medium, with a permeability between 10^{-11} to 10^{-9} m^2 (Eicken et al., 2002), equivalent to that of the weathering crust (Karlstrom et al., 2014). These pore spaces provide a habitat for a range of microorganisms (algae, bacteria, protozoans and viruses) which occupy ≤ 41 % of the surface area of brine-filled internal channels at 2 °C (Krembs et al., 2000). Channel morphology has major implications for food-web relationships within the ice, over half of the channels have a diameter ≤ 200 μm (≈ 50 % ≤ 41 μm), allowing microorganisms resident within them to escape grazing from larger predators, such as ciliated protozoans. However, these narrow channels are unfavourable for the transport of molecules vital for sustaining physiological function.

In sea ice, chlorophyll-α concentrations (a widely applied estimate of biomass of photosynthetic communities) are ≤ 1000 μg L^{-1}, supporting high level of photosynthesis and primary production. Low light is typically the limiting factor for photosynthesis, rather than nutrient availability. Furthermore, sea ice algae are adapted to deal with low-light conditions, which prevail during periods of snow cover; photosynthesis has been observed at irradiances of 1 μmol photons m^{-2} s^{-1} (McMinn et al., 2007).

2.7 The weathering crust: a conceptual model

Despite some examination estimating bulk rates of meltwater transfer through the weathering crust, limited work has yet taken place to assess values of and controls upon crust hydraulic conductivity and permeability. The weathering crust is a potential location for the short-term storage of meltwater (Irvine-Fynn et al., 2006; Larson, 1977, 1978) and acts as a control upon near-surface drainage velocities (Munro, 2011; Schuster, 2001; Shea et al., 2005; Wakahama, 1978; Wakahama et al., 1973) providing a substrate vulnerable to rill initiation and development of channelised flow (Mantelli et al., 2015). Microscale weathering crust processes are linked with the development of macroscale supraglacial flow features (Karlstrom et al., 2014), indicating the requirement to further understand near-surface flow dynamics.

Flow through the weathering crust may act as a medium through which microbial cells, abiotic particulates and chemical species may be exported from storage in glacial ice via melt processes (Irvine-Fynn et al., 2012), subsequently influencing downstream catchments, seeding them with cells, organic material and nutrients such as carbon, nitrogen and phosphorus (Bagshaw et al., 2013; Hood et al., 2015; Milner et al., 2017; Singer et al., 2012; Wilhelm et al., 2013). Additionally, hydrological perturbance within the weathering crust influences *in situ* microbial communities (Edwards et al., 2011), and acts as a substrate for the development of cryoconite holes (Irvine-Fynn and Edwards, 2014), which are connected hydrologically with the weathering crust (Cook et al., 2015b). Whilst there is some understanding of water transport rates through the weathering crust, colloid and contaminant transfers remain unexplored. The following conceptual model will be used as a basis for examination of the eco-hydrology of this unexplored component of the glacial hydrological system.

2.7.1 Formation, degradation and regional-scale variation

The processes of formation and degradation of the weathering crust are intrinsically linked with its capacity to store and transfer water, cells, sediment and solutes within and through the supraglacial hydrological system. Formation processes are summarised in Figure 2.2, with melt at depth driving density and pore size changes. In clear-sky conditions, radiative fluxes provide the majority of energy for melt (≈ 70 %), 36 % of which penetrates the ice surface causing sub-surface melting (Greuell and Oerlemans, 1989). Weathering crust thickness increases to a maximal depth throughout the ablation season in at highly variable rates depending on synoptic conditions (Cook et al., 2015b). Considering a starting point where ice is unweathered (and has a density of ≈ 917 kg m^{-3}), ice crystals melt at their boundaries, decreasing crystal size and bulk density, conversely increasing pore size. Due to the non-linear extinction of SWR at depth in the weathering crust, this density-depth curve would also be expected to be non-linear (Figure 2.2). Throughout this formation processes, surface lowering will also occur, however at a lesser rate than suggested by traditional melt models which do not account for sub-surface melt. If synoptic patterns remain constant (i.e. clear, sunny conditions prevail), this system will reach an equilibrium state, where the weathering crust reaches a minimum bulk density and maximum thickness, where surface lowering rate is equal to that of the depth penetration of the base of the weathering crust.

Conversely, a cloudy and/or rainy period of weather, where radiative fluxes are proportionally reduced in comparison to turbulent fluxes, will cause degradation of the weathering crust. Low density near-surface ice can be easily ablated, whilst the downwards penetration of the weathering crust base ceases due to a lack of SWR receipt. This will increase the bulk density and decrease the thickness of the weathering crust. Furthermore, cooler air temperatures are commonly associated with such synoptic conditions, and if ≤ 0 °C have potential to promote refreezing of interstitial meltwater. In addition to synoptic-scale formation and degradation processes diurnal patterns in SWR receipt, linked with daylight hours, can be expected to drive weathering crust development on a shorter time scale. Using bulk weathering crust density as measure of the degree of weathering of near surface ice, this is demonstrated in Figure 2.4.

On a regional to global scale, differing climatic settings would be expected to determine the rate of weathering crust development; demonstrating similar spatial patterns to those which govern SWR receipt, as this is key component which drives weathering crust formation. Firstly, continental environments, such as the European Alps, derive a greater proportion of melt energy from radiative fluxes than their maritime (such as Scandinavia) equivalents (Willis et al., 2002); as cloudy conditions are more common in the latter environments. Similar variation would be expected related to annual variations in synoptic conditions, such as summer with above average cloud cover. Therefore, in continental regions, weathering crust development would be expected to occur at a faster rate than maritime regions as more energy is available for melt at depth. Furthermore, the latitude of the glacier would be expected to influence weathering crust development, also as a function of both radiation receipt (Figure 2.5). In the mid-latitudes, such as the European Alps, greater diurnal fluctuation in weathering crust

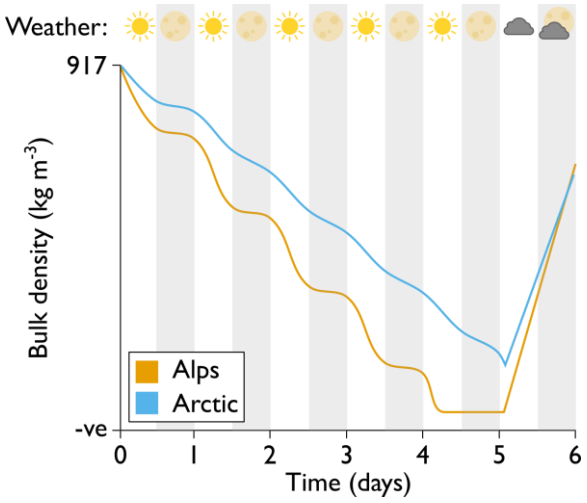

Figure 2.4 Conceptual development of the weathering crust measured using the proxy of bulk density, of the weathering crust over a period of six days in the Arctic and European Alps. In the European alps, higher SWR receipt during daylight hours causes the weathering crust to develop more quickly than in the Arctic, whilst the converse is true overnight (where Alpine SWR receipt is zero). On day 4, the Alpine weathering crust reaches an equilibrium of maximal development (note that this is an indicative example only, not an empirical hypothesis). On day 5, a period of cloudy weather results in degradation of the weathering crust. Due to higher air temperatures, and therefore turbulent fluxes in the Alps degradation occurs at a faster rate than in the Arctic.

formation and degradation would be expected than at high latitudes (such as Svalbard) but greater average receipt of radiation at the high latitudes would be expected to correlate with faster weathering crust development, reaching the equilibrium phase more quickly. To a lesser degree, aspect may also play a role; in the northern hemisphere radiation receipt is reduced on north facing glaciers when contrasted with south facing glaciers, and as such weathering crust development would be slower.

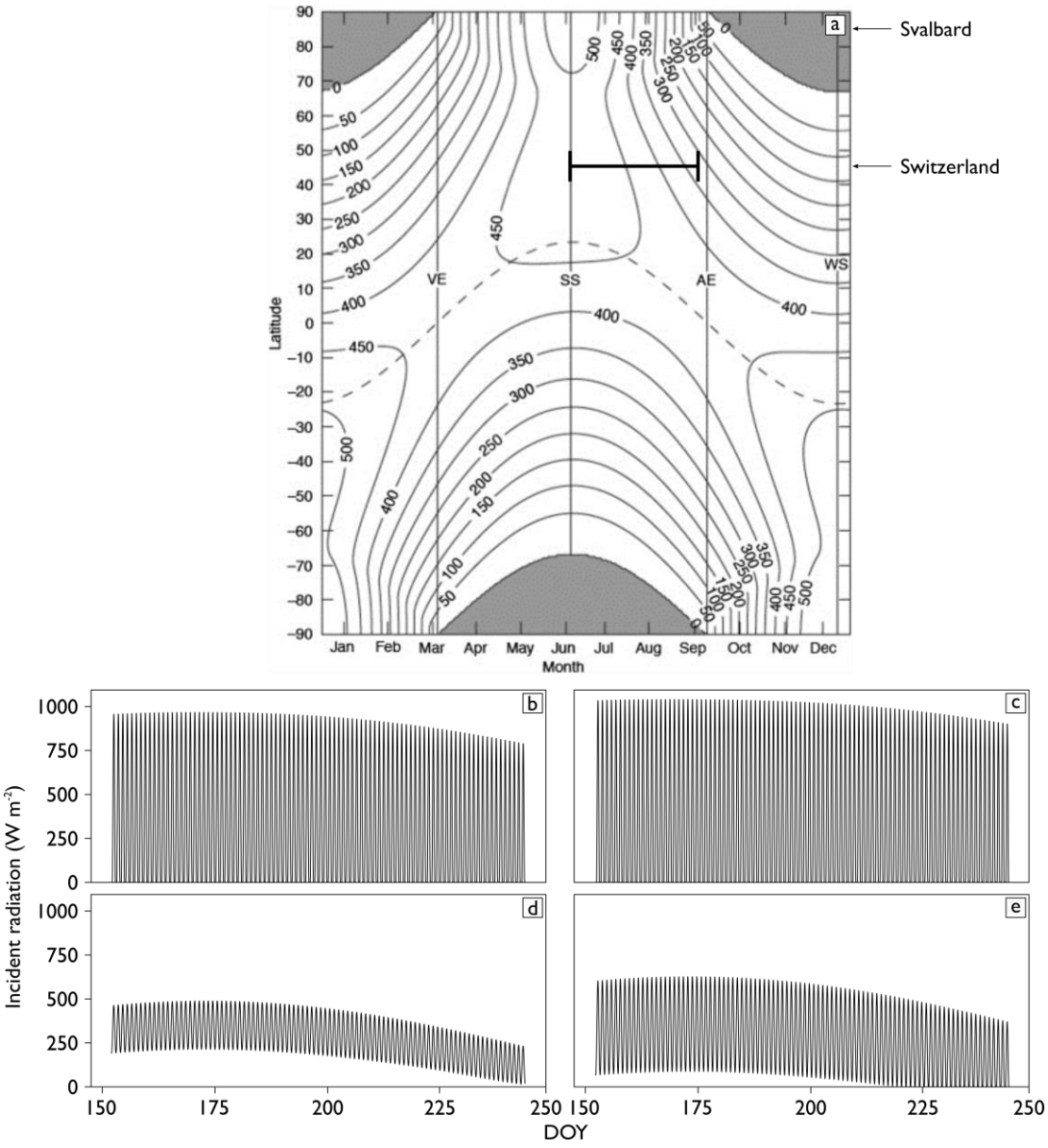

Figure 2.5 a) Daily average insolation at the top of atmosphere as a function of season and latitude (Fu et al., 2015), with the two example locations and period of interest indicated. b-e) modelled incident radiation for hypothetical north and south facing glaciers in the Swiss Alps (2000 m asl) and Svalbard (100 m asl) (both 5 ° slope) using the model described in {Irvine-Fynn, 2014 #120} between the 1st June and 31st August (b = Switzerland; north facing, c = Switzerland; south facing, d= Svalbard; north facing, e= Svalbard; south facing).

2.7.2 Weathering crust hydrology

Acknowledgement of the WCA has challenged the hitherto commonly held assumption that meltwater is transferred virtually instantaneously from the point of production to supraglacial channels (Fountain and Walder, 1998). Comparing flow velocities in the weathering crust (10^{-8} to 10^{-4} m s^{-1} Wakahama et al., 1973), to supraglacial stream velocities that typically range from 10^{-2} to

With the clear controls that local energy receipt, subsurface melt rates and disaggregation, and ice structure and crystal size have on the bulk and vein network density of the weathering crust, the flow of water is equally spatially and temporally varied.

However, it should be noted that during periods of high meltwater input, the weathering crust itself will be subject to melting, changing its hydraulic conductivity. Cook et al. (2015b) reported water levels varied on synoptic and daily time scales, with water table height falling as SWR receipt increased and the weathering crust's interstitial space enlarged, increasing hydraulic conductivity. Here, the assumption is that despite the increase in melt, driving water production at the surface, the relative magnitude of subsurface melting and increase in water transport capacity of the weathering crust offset the increasing water volume delivered to it. In this study, the water table returned towards the ice surface as reductions in SWR and meltwater heat flux cause the contraction of the pore spaces in the weathering crust via interstitial freezing of meltwater. However, given the latent heat released during the refreezing of interstitial meltwater (see Paterson, 1994), a period of freezing air temperature for hours or even days is unlikely to result in complete re-freezing of the liquid component of the weathering crust, but may cause the overnight reduction of hydraulic conductivity on a diurnal scale.

Discharge occurs from the weathering crust primarily via the transfer of meltwater to supraglacial streams, from where it is rapidly advected from the glacier surface to the en-, sub- and ultimately proglacial systems. Given the expected depths of the water table from the ice surface and the typical water levels in supraglacial streams, it is hypothesised that such streams will be of the gaining type (Figure 2.3). Regarding cryoconite holes, Cook et al. (2015b) assert that the water level in such holes is equal to the weathering crust, making them comparable to throughflow-type lakes. This presumes that the walls of the cryoconite hole are of equal hydraulic conductivity to the weathering crust surrounding it. Cryoconite holes may also be perched above the water table given their top-down formation (Gribbon, 1979) in a disconnected losing architecture. Such a hydrological arrangement would most likely occur during the process of cryoconite hole formation, when holes are shallow (i.e. ≤ 10 cm) and therefore above the water table. In which case, water fluctuation within cryoconite holes would not be representative of water table fluctuation, rather input of meltwater, downwards drainage and evaporation within the hole. It should be noted that this arrangement is compatible with the fall in water levels during periods of peak melt observed by Cook et al. (2015b), increase in hydraulic conductivity would enhance the rate of water drainage through the weathering

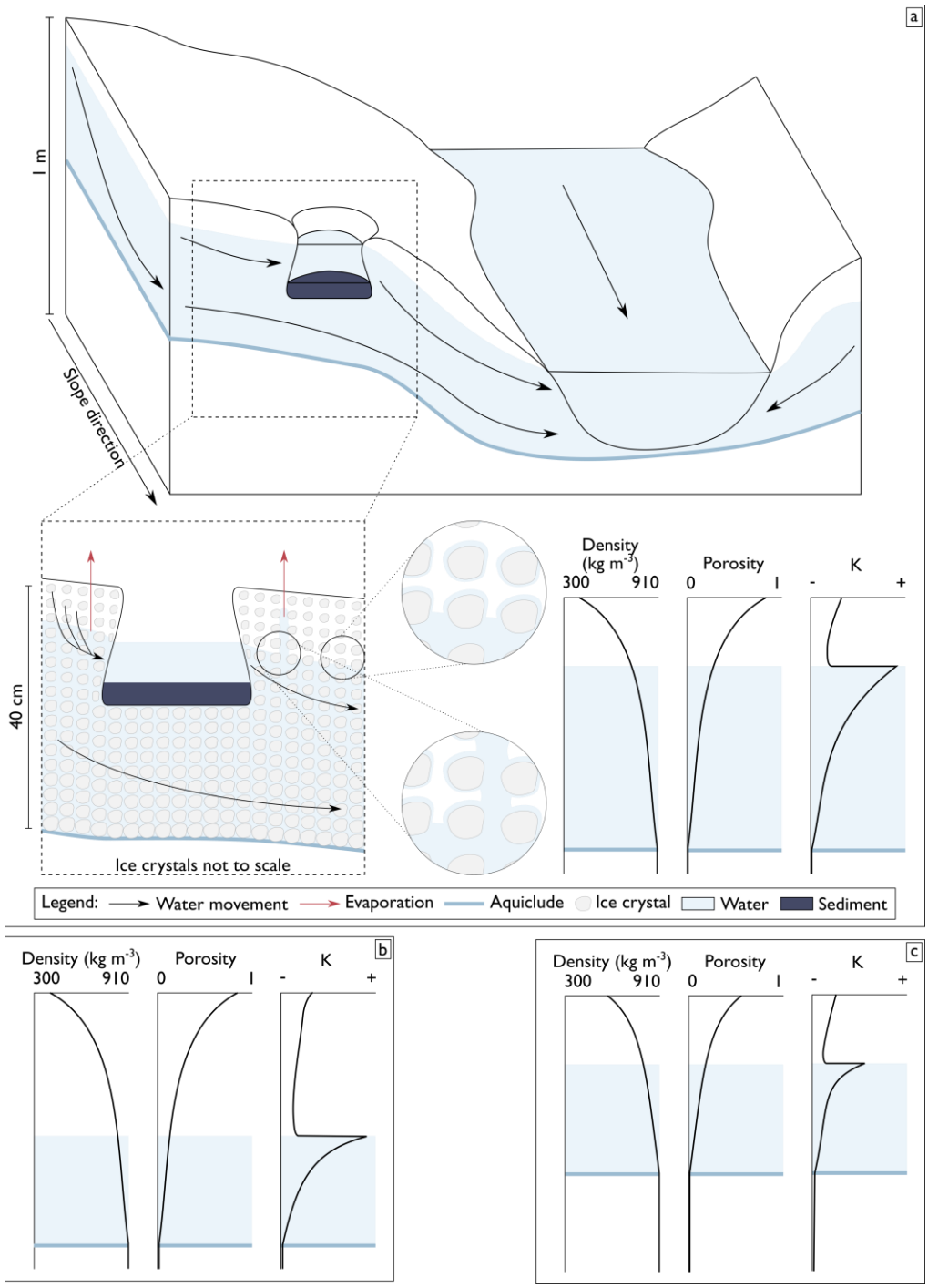

Figure 2.6 A conceptual model of water flow through the weathering crust. a) catchment-scale water flow, ultimately into supraglacial streams in topographic lows, where water is rapidly advected from the surface. Water is lost from the weathering crust via evaporation, with capillary action drawing water upwards in the unsaturated zone, and meltwater from the surface and subsurface infiltrates through the unsaturated zone to the water table, which fluctuates with recharge and discharge. The inset indicates a fully developed weathering crust, comparable with Figure 2.3b. In this example, a cryoconite hole acts as a throughflow, gaining and losing water. Depending on the position of the water table, cryoconite holes may also gain or lose water to the weathering crust. Hypothesised density, porosity and hydraulic conductivity profiles are indicated; in the unsaturated zone water content controls hydraulic conductivity, and in the saturated zone, porosity is the key control. b) and c) indicate these profiles under different conditions: panel b a low water table in a developed weathering crust, and panel c a shallow, poorly developed weathering crust.

crust, and relatively high midday temperatures promoting evaporation from holes causing the water level to drop. Evaporative losses of water to the surface boundary layer, can also be expected, driven by a humidity gradient from the unsaturated zone of the weathering crust. Water drawn upwards by capillary rise is likely most susceptible to this process.

Above the water table, the weathering crust will be analogous to the vadose or unsaturated zone observed in soils and groundwater systems. Meltwater, not only from the surface but throughout the depth profile of the ablating weathering crust, will either a) be added from melting ice in the saturated zone directly to the meltwater within the saturated zone, or b) undergo gravity-driven infiltration through the unsaturated zone to the saturated zone.

In the unsaturated zone, water migrates through water films surrounding ice crystals, and as a result of sensible and latent heat transfer associated with melting and refreezing at the crystal scale, driven by gravity and water surface tension. In this zone, hydraulic conductivity is driven by water content, which is highest at the surface, where the energy available for melt is at its greatest, and just above the water table where water is drawn upwards via capillary action. At the surface, unsaturated hydraulic conductivity is therefore driven by melt rate, positively correlating with water content, and at the water table by humidity and temperature gradients between the weathering crust and the ice surface. Hence, unsaturated hydraulic conductivity will be highest during periods of peak melt. Infiltrating meltwater travels downwards, driven by gravity, through this system until it reaches the saturated zone, described above.

The lower vertical limit of the weathering crust is defined by an aquiclude which varies across a range of environmental settings. In Arctic environments, the hydrologically active zone is thermally defined by the transient thermal layer. At the base of this, ice is below the PMP and is essentially impermeable. In contrast, all ice in temperate glaciers is above the PMP. Without the presence of an extensive cold-ice layer, an aquiclude is generated via water pressure in saturated veins and lenses located upon grain boundaries (Lliboutry, 1996). This aquiclude is likely to respond to synoptic variation in pressure gradients, capillary forces and evaporation.

2.7.3 Eco-hydrology of the weathering crust

Microbial cells can be expected to be found in a multitude of habitats within the weathering crust (Figure 2.7). A depth gradient is observed with a dominance of phototrophic bacteria, algae

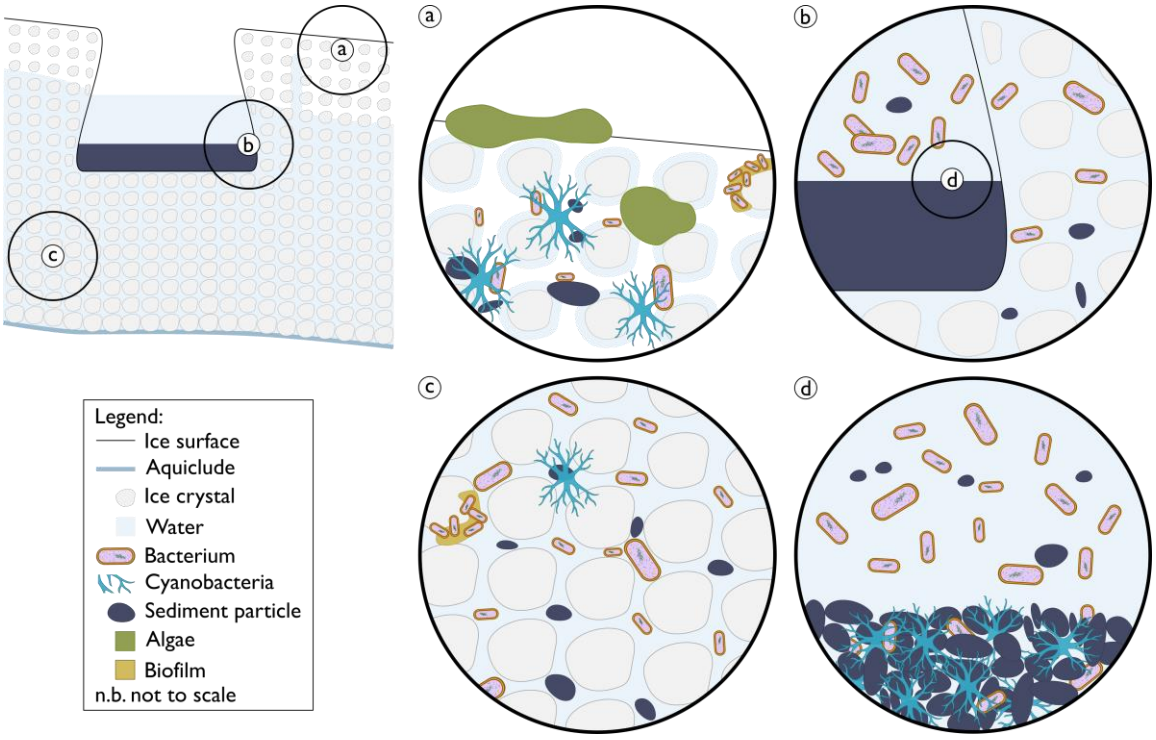

Figure 2.7 Microbial habitats within the weathering crust. a) The surface and immediate surface within it, including surface algae, cyanobacteria in addition to cells in water films on ice crystals and those which have formed biofilms around ice crystals. b) the margin of a cryoconite hole, where pelagic microbes (primarily bacteria) can transfer through the hole walls with water movements. c) Deeper in the weathering crust, reduced radiation receipt is aligned with fewer phototrophic microbes. At depth, vein sizes between ice crystals are smaller, and microbes are mechanically filtered. d) The sediment layer of a cryoconite hole, bound by cyanobacteria with embedded bacterial cells. Phototrophs are found at the surface of this layer, where radiation receipt is greatest. Connections between microbes in the sediment and water phase of holes remain unclear.

and cyanobacteria near the ice surface, where radiation receipt is highest. In contrast, reduced radiation receipt at depth would be expected to correlate with a dominance of heterotrophs. Controls on microbial concentrations can be expected to be availability of nutrients and water, replication rate and residence time, removal of cells via advective transport in meltwaters and viral controls. Previous work (e.g. Mader et al., 2006) report cell concentrations in interstitial melt water of $\leq 10^6$ cells mL^{-1}, and as such similar concentrations can be expected to be observed in weathering crust meltwater. Despite existing estimates, there is a lack of a single efficient, robust and repeatable counting technique for enumeration of cells in supraglacial environments.

Advective cell transport and nutrient availability are hypothesised to correlate with hydraulic conductivity. Higher hydraulic conductivities are associated with greater pore water velocities, delivering water and nutrients to cells which are bound to ice crystals, either mechanically or in biofilms. In contrast, higher pore water velocities will be associated with increased transport rates

of planktonic cells, particulate impurities and aggregates of these, transporting them through the weathering crust to the supraglacial stream network. A size-selective control will occur on the transport of pelagic cells, related to pore size; cells which are larger than the pores through which their transport path leads will become trapped, blocking the pore (reducing effective porosity) and darkening the near-surface of the ice. This is expected to be more common near the base of the weathering crust, where pore sizes are smaller than near the surface due to lesser radiation receipt and melting. Modal cell size observed in supraglacial streams is ≤ 2 μm (Irvine-Fynn et al., 2012), and as these cells are hypothesised to have been transported through the weathering crust, it would be expected that cell size distributions in the latter environment will be similar. Motile bacterial types are uncommon in the weathering crust (Christner et al., 2018), and active cellular movement is hence thought to be uncommon at best.

Interaction between the planktonic cells and particulates of the weathering crust and cryoconite holes is unclear. Export of cells from cryoconite aggregates is more likely than sediment due to the critical competence required for their entrainment and the role of the weathering crust as a mechanical filter; large cryoconite floccules (≥ 100 μm; Langford et al., 2010) are unlikely to pass through the weathering crust, even if entrained. However, if water is free the move between cryoconite holes and the weathering crust unimpeded (as implied by Cook et al. (2015b), it would be expected that planktonic cells can be transported between the two, subject to the filtering conditions hypothesised above. Given that cryoconite holes are "hotspots" of microbial activity on glacier surfaces, it is expected that interaction between the sediment phase and water phase of the hole will result in an increased concentration of nutrients and planktonic cells in cryoconite waters when contrasted with the weathering crust. As such, plumes of enhanced concentrations of both would be expected downflow from cryoconite holes.

Residence time within the weathering crust of planktonic cells is linked with the rates at which cells are transported through the system, and, when considering concentrations, with replication rate. Typical doubling rates of microbes observed in the weathering crust are the order of days (Anesio et al., 2010), and as such microbes which take this time to be transported through the weathering crust can be expected to replicate. Bioavailable nutrient inputs are intrinsically linked with cell replication rates as the former enables the latter and it is widely accepted that aquatic bacterioplankton growth is determined by the trophic state of the system (Pinhassi and Berman, 2003). Glacier surfaces are nutrient-limited environments (Irvine-Fynn et al., 2012), and despite

phototrophic activity within the weathering crust (generating carbon and oxygen to drive heterotrophic metabolisms) (Säwström et al., 2002; Telling et al., 2010) consumers must acquire other vital nutrients released from melting surface ice and delivered by percolating meltwater. In nutrient limited Arctic freshwaters, nutrient-addition has been demonstrated to stimulate bacterial growth and doubling times, as has temperature (Säwström et al., 2007b). Therefore, in addition to residence time ample nutrients must be available for cells to replicate. If doubling does occur, cell concentration would be inversely proportional to distance from a sample point to a stream, as longer residence time would allow the time required for replication to occur if nutrient supply was not a limiting factor. This hypothesis is however complicated by the presence of bacteriophage viruses within the weathering crust (e.g. Bellas et al., 2013; Rassner et al., 2016; Säwström et al., 2007a; Säwström et al., 2007b), which may also act to limit cell concentration.

2.8 Research gaps and study direction

Supraglacial hydrology is undergoing somewhat of a resurgence, based upon a re-emerging research interest in supraglacial melt processes, and technological advances such as the use of UAVs, improved remote sensing platforms and computer processing power. Coupled with the developing focus on supraglacial microbiology and transport of cells and impurities through and from glacier surfaces, and associated downstream impacts of this hitherto poorly considered carbon flux, this chapter highlights the following research gaps which will be addressed in this thesis:

1. Whilst there are estimates of weathering crust hydraulic conductivities, little is known regarding the controls upon this beyond the theorised principles of radiation receipt as a driver for intercrystalline melt, density reduction and an associated increase in porosity and hydraulic conductivity. Furthermore, investigation needs to be undertaken to determine if the use of Darcy's Law is the most appropriate technique in which to examine this layer. Therefore, Chapter 3 will develop and test a logging piezometer for the quantification of hydraulic conductivity within the weathering crust.
2. It is hypothesised and seems reasonable that the hydraulic conductivity of the weathering crust is highly variable in both time and space. However, no studies have yet aimed to characterise the spatio-temporal variability of this layer, and role of ice mass characteristics and thermal regime upon it. Chapter 3 will investigate regional-scale variation in hydraulic conductivity of the weathering crust at a multitude of sites and climatic settings across the

northern hemisphere. Temporal and local-scale spatial fluctuations will be examined at one site, Vadrec del Forno (Switzerland) in Chapter 6.

3. Transport of cells, particulate impurities, and solutes through the weathering crust from allo- and autochthonous sources remains poorly understood. Within the context of global climatic change and associated predicted melt rate increases of global glaciers, many contaminants archived within glacial ice are expected to "melt out" and become mobile. Understanding the transport mechanisms of these impurities is critical to ascertain their potential influence upon a) glacial biogeochemical cycles and microbial ecology and b) downstream interactions with proglacial and oceanic environments. Chapter 4 will develop a robust, accurate and repeatable technique for enumeration of cells in weathering crust meltwaters. Chapter 5 will apply this technique using samples at a multitude of sites and climatic settings across the northern hemisphere and aim to establish broad links between hydraulic conductivity of the weathering crust and planktonic cell concentrations, assessing the flux of cells and mass of cellular carbon from glacier surfaces. Chapter 6 will examine local-scale spatial and temporal trends in a supraglacial catchment on Vadrec del Forno (Switzerland).

The near-surface weathering crust remains poorly understood despite the role it clearly plays within the transport of meltwater, biotic and abiotic particles within the supraglacial environment. It acts as a control upon microbial communities, biogeochemical cycling and surface albedo, yet many questions remain as to its role and controls upon these key variables which influence glacial melt, and down-catchment hydrochemistry and biology. Surface meltwater is the key vector for understanding the transfer of nutrients, cells and organic matter are transported through glaciers and establishing how they will respond to climate change. This thesis will begin to elucidate the role of the weathering crust and the supraglacial ecosystem.

3. Near-surface Hydraulic Conductivity of Northern Hemisphere Glaciers

Ian T. Stevens[1], Tristram D.L. Irvine-Fynn[1]*, Philip R. Porter[2], Joseph M. Cook[3], Arwyn Edwards[1,4], Martin Smart[2], Brian J. Moorman[5], Andy J. Hodson[3,6], Andrew C. Mitchell[1]

[1]Centre for Glaciology, Aberystwyth University, Aberystwyth, UK; [2]Geography and Environmental Science, University of Hertfordshire, Hatfield, UK; [3]Department of Geography, University of Sheffield, Sheffield, UK; [4]Institute of Biology Environment Rural Science, Aberystwyth University, Aberystwyth, UK; [5]Department of Geography, University of Calgary, Alberta, Canada; [6]UNIS, Longyearbyen, Norway

3.1 Publication history

This chapter was originally published in Hydrological Processes in 2018, following a poster presentation at AGU in 2016, and is reproduced here without addition or subtraction of material. Note that figure, table and equation nomenclature has been adjusted from the paper to ensure consistency throughout the thesis document. Author contributions to this paper are outlined in section 1.4, and supplementary data in Appendix 1.

3.2 Abstract

The hydrology of near-surface glacier ice remains neglected aspect of glacier hydrology despite its role in modulating meltwater delivery to downstream environments. To elucidate the hydrological characteristics of this near-surface glacial "weathering crust", we describe the design and operation of a bespoke capacitance-based piezometer that enables rapid, economical deployment across multiple sites and provides an accurate, high resolution record of near-surface water level fluctuations. Piezometer tests were conducted on the surface of ten northern hemisphere glaciers. Through application of standard terrestrial hydrology bail-recharge techniques, we derive hydraulic conductivity (K) values from 0.003 to 3.519 m d^{-1}, with a mean of 0.185 ± 0.019 m d^{-1}. These results are comparable to those obtained in other discrete studies of glacier near-surface ice, and for firn, and indicate that the weathering crust represents a hydrologically inefficient, aquifer. Hydraulic conductivity was positively correlated with water table height but negatively correlated with both altitude and cumulative short-

wave radiation since the last synoptic period either of negative air temperatures or dominated by turbulent energy fluxes. The large range of *K* observed suggests complex interactions between meteorological influences and differences arising from variability in ice structure and crystallography. Our data demonstrate a greater complexity of near-surface ice hydrology than hitherto appreciated and support the notion that the weathering crust can regulate the supraglacial discharge response to melt production. The conductivities reported here, coupled with typical supraglacial channel spacing, suggest that meltwater can be retained within the weathering crust for at least several days. This has implications not only for the accuracy of predictive meltwater runoff models, but we also argue for biogeochemical processes and transfers that are strongly conditioned by water residence time and the efficacy of the cascade of sediments, contaminants, microbes and nutrients to downstream ecosystems. Since continued atmospheric warming will incur rising snowline elevations and glacier thinning, the supraglacial hydrological system may assume greater importance in many mountainous regions and, consequently, detailing weathering crust hydraulics represents a research priority since the flow-path it represents remains poorly constrained.

3.3 Introduction

Most glacial runoff occurs during the summer melt season and typically fluctuates according to diurnal energy balance oscillations (Hock et al., 2005). It has often been assumed that the snow-free glacier surface imparts minimal delay between meltwater generation and its delivery to englacial, subglacial and proglacial environments (Fountain and Walder, 1998). However, meltwater storage at an ablating glacier surface has been inferred from geophysical data (e.g. Irvine-Fynn et al., 2006; Moore et al., 1999) and meltwater budgets (e.g. Irvine-Fynn, 2008; Larson, 1978). Discrepancies in the timing and volume of modelled ablation and observed meltwater discharge have also been observed for snow-free supraglacial catchments in alpine (e.g. Munro, 2011) and ice sheet (e.g. McGrath et al., 2011; Rennermalm et al., 2013) settings. Consequently, there has been a growing recognition of the glacial "weathering crust" (Müller and Keeler, 1969): the shallow (typically 0.01 - 2 m) layer of porous ice which typifies ablating glacier surfaces, which has been referred to as "honeycomb" or "coral" ice (e.g. Cutler and Munro, 1996; Zeng et al., 1984). Despite the recent surge in interest in supraglacial hydrology evident in the literature, (e.g. Gleason et al., 2016; Karlstrom et al., 2013; Karlstrom et al., 2014; Mantelli et al., 2015; McGrath et al., 2011; Rippin et al., 2015; Smith et al., 2015; St. Germain and Moorman, 2016; Yang et al., 2016; Yang and Smith, 2013), a detailed understanding of the

hydraulic conductivity (K) and permeability ($\varkappa$) of the weathering crust, and their variation in space and time is still lacking (Cook et al., 2015; Irvine-Fynn et al., 2011b; Karlstrom and Yang, 2016).

The porous weathering crust ice layer develops as a function of three primary drivers: (i) subsurface melt caused by incident solar radiation (Müller and Keeler, 1969; Munro, 1990); (ii) heat flow within interstitial spaces that further contributes to declining ice crystal cohesion (Hoffman et al., 2014; Mader, 1992; Nye, 1991), and (iii) kinetic energy and frictional heat transfers from water flow through interstitial flowpaths (Koizumi and Naruse, 1994). The depth of the weathering crust that develops during synoptic clear sky conditions is related to Beer's Law (Cook et al., 2015; Oke, 1987), which defines an exponential increase in bulk ice density with depth (LaChapelle, 1959) from ~300-400 kg m^{-3} to 870-917 kg m^{-3} over length scales between a few centimetres to several decimetres or more (Brandt and Warren, 1993; Müller and Keeler, 1969; Schuster, 2001; Shumskii, 1964). Factors controlling the depth of weathering crust development include the coefficient of extinction of shortwave radiation (SWR_{in}), itself governed by ice type, crystal size, impurity and air bubble content and their emergence rates, and the zenith angle, intensity and duration of solar radiation receipt. Clear skies lead to glacier surface energy balance dominated by radiative fluxes, which promote weathering crust growth, in some cases of stagnating ice to a depth in excess of 2 m (Fountain and Walder, 1998; Larson, 1977). Reduced incident radiation (e.g. due to cloud cover) and high precipitation cause turbulent energy to dominate the glacier surface energy balance, promoting surface lowering which reduces the thickness of the weathering crust (Müller and Keeler, 1969; Shumskii, 1964). Variations in the thickness and porosity of the weathering crust at synoptic and seasonal time-scales likely results lead to temporal and spatial variability in supraglacial hydraulic permeability, conductivity and meltwater storage potential. The dynamic properties of this near-surface porous media likely influence meltwater transfer, modulating the lag time between *in situ* meltwater production and associated runoff signals (Karlstrom et al., 2014; Munro, 2011).

Hydraulic conductivities between 10^{-2} and 10^{-6} m s^{-1} (10^{3} and 10^{-2} m d^{-1}) for differing depths, sample times and general surface topographies have previously been measured for glaciers in Alaska and Norway (Larson, 1977; Theakstone and Knudsen, 1981; Wakahama, 1978; Wakahama et al., 1973). In contrast, theoretical estimates based on assumed values for near-surface ice properties suggest a permeability of ~10^{-10} m^2 for the Llewellyn Glacier, Juneau Ice Field, Canada (Karlstrom et al., 2014). However, as (Theakstone and Knudsen, 1981) cautioned, rigorous comparisons of these types of data should not be made, due to marked contrasts in geographical location, climatic setting, glacier

morphology, and experimental methods. Rather, these limited observations emphasise the need to use a standardised approach to characterising glacier surface hydraulic conductivity across a range of study areas to understand the processes controlling shallow-subsurface glacier hydrology.

In addition to controlling and modulating meltwater fluxes, the importance of weathering crust hydrology is of primary concern for understanding ice surface nutrient and sediment fluxes and supraglacial microbial ecology. Redistribution of fine supraglacial debris and dust across an ablating ice surface is commonly described (e.g. Adhikary et al., 2000; Hodson et al., 2007; Irvine-Fynn et al., 2011a; Oerlemans et al., 2009; Porter et al., 2010), while hydrological flowpaths in the glacier near-surface control the export of microbes and associated nutrients to extraglacial environments (Cook et al., 2015; Hotaling et al., 2017; Irvine-Fynn et al., 2012). The weathering crust is now recognised as an ecosystem in its own right (e.g. Cook et al., 2016; Cook et al., 2015; Hodson et al., 2008; Irvine-Fynn and Edwards, 2014; Stibal et al., 2012). The hydrological characteristics of the weathering crust influence microbial activity in cryoconite (Edwards et al., 2011; Hodson et al., 2007) and the increased residence time afforded by percolation within the interstitial voids of the weathering crust affords microbiota, fine inorganic and organic particles, dissolved nutrients and viruses opportunities for interaction and turnover in spite of the low growth rates and metabolic activities associated with cold environments (Rassner et al., 2016). Furthermore, legacy contaminant and particulate impurity transport through glacier systems (Bogdal et al., 2009; Hodson, 2014; Łokas et al., 2016) and their accumulation in down-stream environments (e.g. Bettinetti et al., 2016; Bizzotto et al., 2009; Bogdal et al., 2010) must be influenced by hydrological flow through the porous near-surface ice – a process which remains a contemporary research imperative (Grannas et al., 2013). For these reasons, with recognition of understanding the hydraulic conductivity of the weathering crust assumes significance in the hydrology, biogeochemistry, ecotoxicology and ecology of supraglacial systems.

Therefore, to address the critical research gap weathering crust hydrological characteristics represent, we undertook the first multi-site study to assess hydraulic conductivity using a consistent methodology adapted from terrestrial hydrology. Traditional terrestrial hydrological techniques developed for groundwater investigations can be applied to glacial environments (e.g. Derikx, 1973; Sharp et al., 1998). Soil and bedrock aquifers are porous media with a depth-limited storage capacity, making their measurement techniques transferable to the analogous supraglacial weathering crust (Hodgkins, 1997; Irvine-Fynn and Edwards, 2014; Lliboutry, 1996; Nye, 1991). A novel electronic piezometer was used to monitor water levels and recharge rates in auger holes at high temporal

resolution to derive hydraulic conductivity (*K*) values. We describe the findings from eight valley glaciers distributed across the Northern Hemisphere, and two sites at the western margin of the Greenland Ice Sheet and elucidate potential drivers of weathering crust development and hydraulic properties.

3.4 Materials and Methods

To examine the hydraulic conductivity, *K*, of the glacial weathering crust we employed piezometer-based techniques adapted from those used to measure groundwater transfers (Amoozegar and Warrick, 1986; Freeze and Cherry, 1979). Recently, a similar approach has been used to examine the firn aquifer on the Greenland Ice Sheet (see Miller et al., 2017).

3.4.1 Electronic piezometer design

Capacitance piezometers have been well-described in the literature (e.g. Baxter, 1996; Reverter et al., 2007; Ross, 1983; Wilner, 1960). Here, a complementary metal-oxide semiconductor (CMOS) device (e.g. Texas Instruments, USA item TLC555CP) was configured in a circuit that acts as an oscillator with an output frequency determined by the capacitance of capacitor C1 and the resistance of resistor R2 (Figure 3.1a, Figure 3.1c). The capacitor was created using a 0.6 m length of 50 mm polypropylene tubing inside which was placed a 50 cm length of 1 mm aluminium angle and a looped 0.25 mm (30 AWG) Kynar insulated silver-plated copper wire (Figure 3.1b). The Kynar wire is kept taut by anchoring the wire with a 3 mm nylon bolt at the top of the aluminium angle, and with a 25 mm × 4 mm stainless steel extension spring secured with a nylon bolt at the base of the aluminim angle (see also Ross, 1983). Regular holes are drilled around the circumference of the tube along its length, to allow uninterupted ingress and egress of water. The frequency of the output signal scales in proportion to capacitance; as the water level rises capacitance is reduced, output frequency increases and *vice versa*. To reduce heat transfer between the device and ice surface, tubes are coated in adhesive silver foil. This foil cover was found to reduce the exposed tube temperatures by 0.5 °C when subjected to typical mountain environment conditions. The addition of a frequency to voltage convertor (e.g. Texas Instruments, USA LM2907N) produces a single-ended voltage output of between 1.0 and 2.8 V which, here, is logged using a battery-powered USB 'Track-it' Data Logger (Monarch Instruments, USA). The circuitry and battery are housed at the top of the piezometer within the plastic tube and require minimal weatherproofing. The design of the circuit means that output frequency is independent

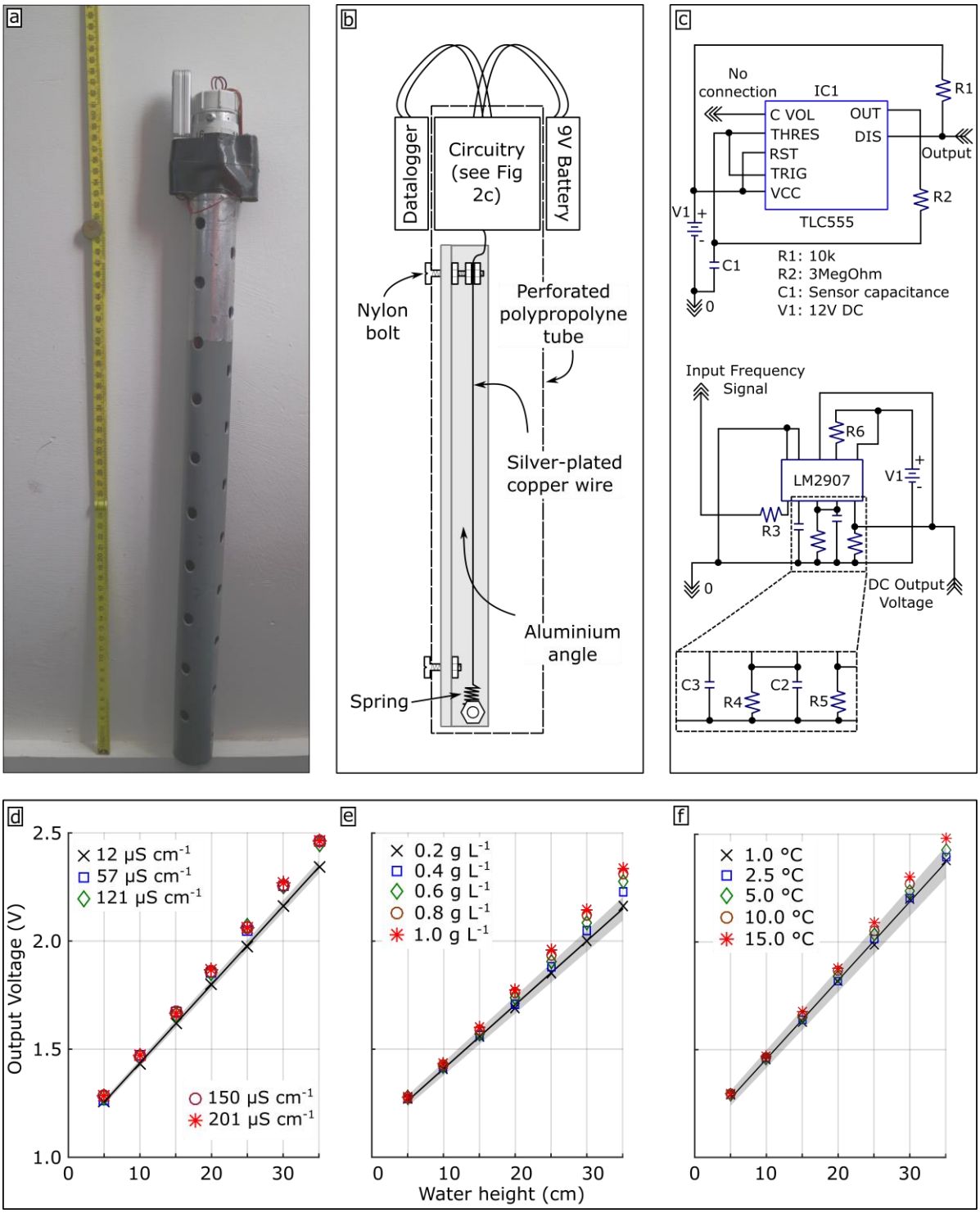

Figure 3.1 Probe design and calibration. a) An image of a water-level probe including a centimetre scale. b) A cartoon schematic of the probe design. c) The wiring diagram for the probe circuitry, as indicated in Figure 3.1b. Probe voltage outputs at given water levels under specific water conditions, with the black line indicating a linear regression (r2 > 0.99) and the grey area a 95% confidence bound, for the typical supraglacial conditions (X) and for other variable conditions of electrical conductivity (d), suspended sediment load (e) and temperature (f).

of supply voltage, therefore there is negligible variation to the output signal due to battery depletion,

making the sensors well suited to deployment in remote environments where regular battery changes may not be possible. Piezometer output is close to linear (Figure 3.1d-f) and is not influenced by electrical conducitivity (EC), suspended sediment concentration (SSC) or temperature levels within the limits commonly observed in supraglacial environments. Calibration of individual piezeometers is simply a matter of recording voltage at a variety of known, incremental water levels and applying a linear function to the resultant datesets.

3.4.2 Electronic piezometers: data processing

Aquifer hydraulic conductivity (*K*) is commonly assessed using piezometer tests, which quantify the nature of hydrological recovery of an auger hole following a disturbance to the water level, either where auger holes are emptied (bail test) or artificially overfilled (slug test) (Amoozegar and Warrick, 1986; Freeze and Cherry, 1979; Moore, 2002). A notable issue with the application of slug testing in the glacial environment is caused by the low permeability (e.g. (Lliboutry, 1971; Lliboutry, 1996; Nye, 1991) and density gradient (e.g. Müller and Keeler, 1969) of ice when compared with a soil aquifer for which the test was designed. By introducing additional water to an auger-hole, the water table would artificially rise, and water would flow through the unsaturated, higher porosity weathering crust, and likely result in an overestimation of *in situ K*. The bail-recharge method was considered more appropriate for use in the supraglacial environment, although water flow into the auger-hole occurs isotropically from three-dimensions as a 'false' water head is generated by the empty hole (Figure 3.2; Moore, 2002). However, by considering the rate of water level rise, this phenomenon can be eliminated mathematically with several solutions proposed, including the formulation by (Bouwer and Rice, 1976):

$$K = \frac{Q \cdot \ln(\frac{R_e}{r_w})}{2\pi \cdot L \cdot y} \qquad \text{[Equation 3.1]}$$

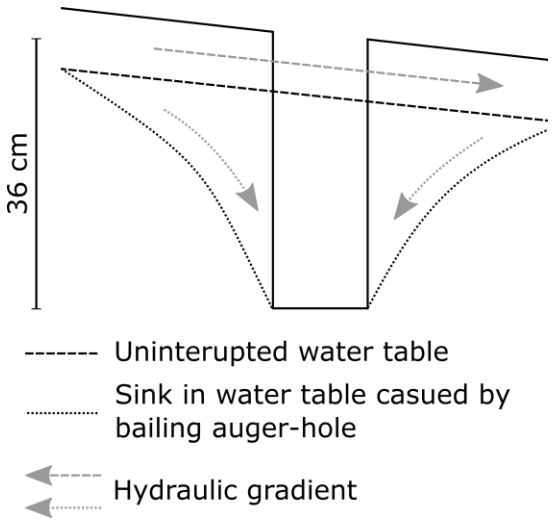

Figure 3.2 The role of auger-hole drilling on the water table and idealised hydraulic head. The drilling and bailing of an auger hole causes a localised drop in the water table (with radius up to 2m) altering the hydraulic gradient indicated by the grey arrows. Note that the hydraulic gradient indicated by these arrows corresponds with the water table of the same line style, i.e. the dashed grey arrows represent the hydraulic gradient of the uninterrupted water table whilst the dotted arrows correspond with the modified water table.

where Q is the water flow into the auger-hole ($cm^3\ s^{-1}$), and the remaining length terms (all in cm) include L, the height of the well through which water enters, y is the vertical distance between the water surface in the auger hole and the equilibrium water table, R_e is the effective radius over which *y* is dissipated, and r_w is the radius of the auger-hole. For the equation to be valid, a single auger-hole is required, and it is specifically applicable to partially penetrating, unsealed wells in unconfined aquifers, such as the weathering crust. Q can be defined through knowledge of the auger-hole dimensions and the recharge rate detailed in the output from the piezometer as the water level recovers. Whilst R_e can be determined empirically using axisymmetric node networks (Bouwer and Rice, 1976), the term $\ln(R_e/r_w)$ can be determined using an approximation given as:

$$\ln\left(\frac{R_e}{r_w}\right) = \left[\frac{1.1}{\ln(\frac{h}{r_w})} + \frac{A + B \cdot \ln[(D-h)/r_w]}{L/r_w}\right]^{-1} \qquad \text{[Equation 3.2]}$$

for which D is the distance between the water table in the aquifer and the impermeable ice representing the base of the aquifer, and h the depth of the water in the auger hole (both in cm). A and B are dimensionless constants, determined using the ratio L/r_w (see (Bouwer and Rice, 1976). One condition of the empirical approximation presented in Equation 4.2 is that $0 < (D\text{-}h)/r_w \leq 6$; if these conditions are not met, $(D\text{-}h)/r_w$ is adjusted to equal 6.

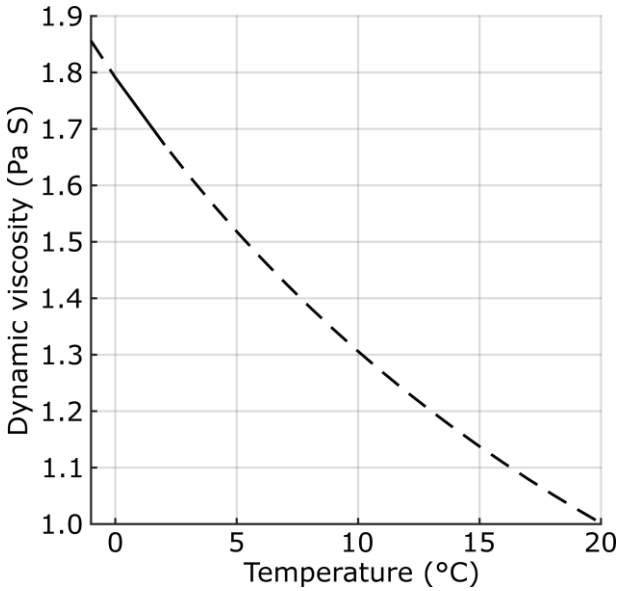

Figure 3.3 Dynamic viscosity, μ, of water as controlled by temperature in the range -1 °C ≥ t ≥ 20 °C (after Kestin, 1978). Note, the area of interest, 0.1 °C ≥ t ≥ 2 °C, aligning with observed auger-hole temperatures, is highlighted with a solid line.

Following the derivation of *K*, primary ice permeability (κ) can be calculated, after Bear (1972):

$$\kappa = K\frac{\mu}{\rho_w g} \qquad \text{[Equation 3.3]}$$

where ρ_w is the density of water (taken as 1000 kg m^{-3}), g is acceleration due to gravity (0.981 m s^{-2}) and μ is the dynamic viscosity of water (in Pa S). Water viscosity is temperature dependent (Figure 3.3) and, in the range of interest characteristic for supraglacial water

temperatures (< 2 °C; Isenko et al., 2005) it is useful to note that viscosities are 1.4 to 1.8 times that at 20 °C.

3.4.3 Hydrological data collection

Bail-recharge tests were conducted at ten sites across the northern hemisphere cryosphere bridging a range of latitudes and climatic settings (Table 3.1; Figure 3.4). At Haut Glacier d'Arolla, Switzerland, and Fountain Glacier Bylot Island (HACH and FGBI, respectively), holes were drilled at strategic locations along transects or semi-randomised grids within a defined supraglacial micro-catchment, whilst on the K-Transect of western Greenland (GRDS), nine holes were distributed across a 30 × 30 m grid. At other sites including those in Sweden (SGSE, RGSE), Austria (RMOS, GBOS), at the Greenland Ice Sheet margin (GRKM) and Svalbard (PBSV, FFSV) experiments were conducted opportunistically using glacier-wide randomised grid sampling or short transects over smaller, hydrologically active areas.

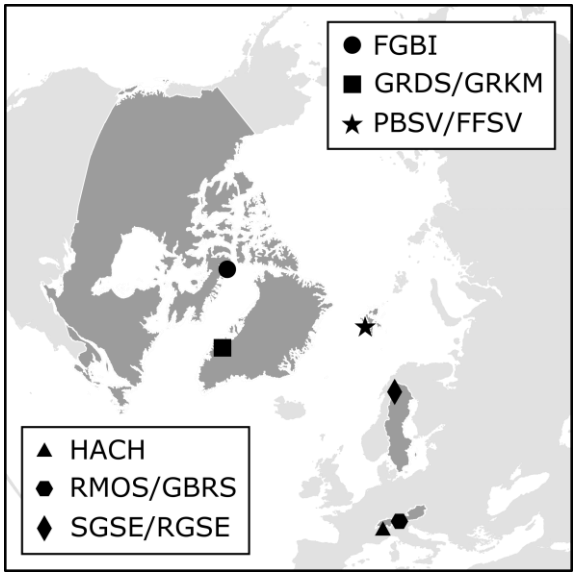

Figure 3.4 A hemispheric location map of glaciers sampled within this study. Letter codes are identified within Table 3.1.

At all sites, 36 cm deep auger-holes were drilled using a 5 cm diameter Kovacs drill. The auger-hole depth enabled the upper 30 cm of the weathering crust to be examined, since there is a 6 cm 'dead space' at the base of the piezometer. Auger-holes were emptied using a biOrb™ manual syphon with a 5 cm nozzle head. The piezometer was inserted immediately, and recharge monitored at 2 s intervals. In cases where auger-holes were reused during a single day, ablation resulted in some widening of the uppermost 5 cm of auger-hole, but this had negligible influence upon the bail-recharge experiments due to the water table typically found ~14 cm from the glacier surface. The representativeness of the 36 cm deep auger-holes is assessed in Section 3.1.

Time-series of auger-hole water column height were converted to recharge water volume and corrected to account for water displacement arising from piezometer installation. Recharge curves were manually examined and divided into three distinct stages (Figure 3.5): (i) Stage 1 is a linear stage which

Table 3.1 Summary of glacier sites sampled within the study.

Glacier Name	Country	Fieldwork Period	Glacier Code	Latitude (°N)	Area (km^2)	Elevation (m asl)	Daylight hours (decimal)	Max daily solar zenith (°)	Climate and thermal regime	Further reference
Protektorbreen	Svalbard, Norway	13/08/15 to 17/08/15	PBSV	78.24	7.60	5 – 700	24	25.2 – 26.5	Polar maritime Cold	Hagen et al., 1993; Hodson and Irvine-Fynn, unpublished data
Foxfonna	Svalbard, Norway	08/08/15	FFSV	78.12	3.95	675 – 950	24	28.0	Polar maritime Cold	Hagen et al., 1993; Liestøl, 1967; Rutter et al., 2011
Fountain Glacier	Bylot Island, Canada	07/07/14 to 23/07/14	FGBI	72.95	72.0	330 – 1100	24	37.2 – 39.5	Polar continental Non-temperate polythermal	St. Germain and Moorman, 2016; Wainstein et al., 2014; Whitehead et al., 2013; Whitehead et al., 2014
Rabots Glaciär	Sweden	22/08/14	RGSE	67.91	3.70	1070 – 1640	16.4	33.8	Polar maritime Non-temperate polythermal	Björnsson, 1981; Brugger, 2007; Brugger et al., 2005
Storglaciären	Sweden	24/08/14	SGSE	67.90	3.10	1120 – 1730	16.1	33.1	Polar maritime Non-temperate polythermal	Björnsson, 1981; Brugger, 2007; Hock and Holmgren, 2005; Holmlund and Eriksson, 1989; Jansson, 1995
Greenland Ice Sheet (Point 660)	Greenland	06/08/14 to 07/08/14	GRKM	67.16	-	≈ 630	18.2 – 18.3	39.6 – 39.9	Polar maritime Non-temperate	Smith et al., 2015; van de Wal et al., 2008; van de Wal et al., 2005; Yang et al., 2016

Table 3.1 (continued).

Glacier Name	Country	Fieldwork Period	Glacier Code	Latitude (°N)	Area (km^2)	Elevation (m asl)	Daylight hours (decimal)	Max daily solar zenith (°)	Climate and thermal regime	Further reference
Greenland Ice Sheet (S6)	Greenland	22/07/14 to 29/07/14	GRDS	67.08	NA	≈ 1100	19.5 – 20.6	41.9 – 43.4	Polar maritime Non-temperate	Smith et al., 2015; van de Wal et al., 2008; van de Wal et al., 2005; Yang et al., 2016
Gaisbergferner	Austria	08/09/14	GBOS	46.83	1.03	2460 - 3390	12.9	48.8	Alpine continental Temperate	Abermann et al., 2009; Fischer, 2010
Rotmoosferner	Austria	11/09/14	RMOS	46.82	3.17	2450 - 3000	12.9	47.6	Alpine continental Temperate	Abermann et al., 2009; Anesio et al., 2010; Edwards et al., 2013
Haut Glacier d'Arolla	Switzerland	19/07/15 to 28/07/15	HACH	45.98	6.30	2550 – 3500	14.9 – 15.3	63.0 – 64.5	Alpine continental Temperate	Brock et al., 2000; Mitchell et al., 2001; Pellicciotti et al., 2005; Willis et al., 2002

represents pressure driven recharge as a result of the artificial water head generated by the presence of the bailed auger-hole within the weathering crust; (ii) Stage 2 is a non-linear decreasing stage (i.e., recharge rate falls with time/rise in auger-hole water level), identified as representing a reduction in the influence of pressure-driven flow from three dimensions, and representing the flow of water through an undisturbed weathering crust (i.e., the idealised water table in Figure 3.2). Stage 3 is a linear stage with a gradient of 0, at which point water in the auger-hole is equilibrated with the level of the water table in the surrounding weathering crust (Figure 3.5).

Hydraulic conductivity, *K*, was calculated using Equations 3.1 and 3.2, where recharge rate derived from Stage 2 defines **Q**, and the stable water level at Stage 3 substituted for **y**. To ensure $y \neq 0$, the Stage 3 auger-hole recharge data was filtered and limited to 0.01 V below the voltage observed for the static equilibrium water table water depth. In the discrete cases where the auger-hole exhibited 'incomplete recharge', either **y** was defined using a repeat or proximal measurement within 10 minutes of the curtailed measurement, or a mean water table depth for the specific glacier was used.

In the absence of detailed weathering crust density profiles with depth, we parameterised **D** (Equation 3.2) to be 40 cm which ensured the ratio L/R_w equalled 14.4; consequently, following

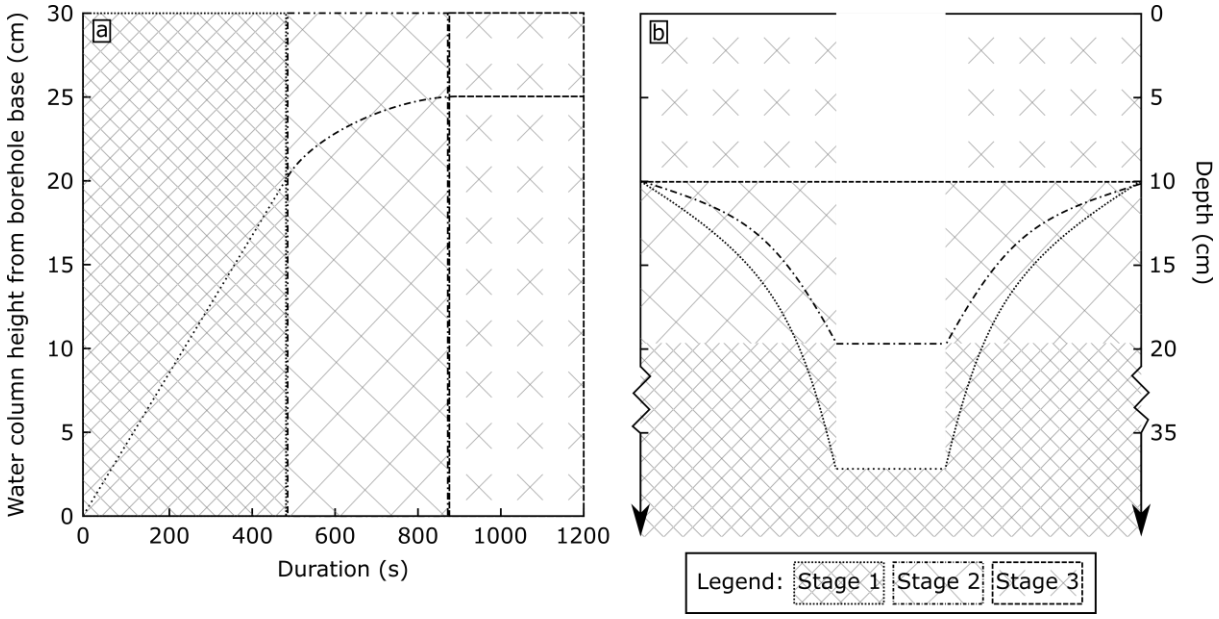

Figure 3.5 a) An idealised recharge curve. In panel b), each dashed line indicates the position of an idealised water table; during stage 1, anisotropic, pressure driven flow dominates due to the large hydraulic head generated by the presence of an auger-hole (in black) generated sink in the water table. Through stage 2, this influence is reduced (although still prevalent) but influence of this false water head decreases as the hole fills (aligning with the non-linear stage in panel i). At stage 3, the water level in the borehole is equilibrated with the surrounding water table and recharge stops as the auger-hole becomes equilibrated with the surrounding weathering crust water table.

Bouwer and Rice (1976)'s condition that for $7 < L/r_w < 16$, constants A and B (Equation 3.2) are defined as 2 and 0.25, respectively. The uncertainty related to this assumption was negligible: in cases where D exceeds 40 cm, there is no change in the estimated *K*, while if D-h was reduced to the smallest possible value within the piezometer's measurement capabilities, there is an underestimate in *K* of only 6.5%. To quantify the uncertainties that resulted from the manual definition of Stage 2 in the recharge curve, a subsample of 25 recharge curves were selected randomly, covering all glaciers and a representative range of recharge rates. By identifying potential errors in the location of the transition between Stages 1 and 2 in this subsample, uncertainty in the calculated *K* was estimated as ± 4.8 %, and again considered negligible.

3.4.4 Ancillary data collection

Automated weather stations (AWSs) were installed locally at all sites apart from GBOS and RMOS. In a few cases missing data was interpolated using data from the nearest alternative weather station. Where SWR_{in} data was unavailable it was modelled (Irvine-Fynn et al., 2014) and a cloud cover correction applied using observations from local weather stations (see Greuell et al., 1997). Modelled data correlated well with measured values during the period for which directly measured SWR_{in} was available ($r^2 = 0.81$). Using these data, cumulative energy input (MJ m^{-2}) from SWR_{in} since the last freeze event (i.e. temperature < 0 °C) was calculated to explore the qualitative observations of Muller and Keeler (1969) regarding weathering crust development processes. For glaciers with full meteorological data, meltwater production (M) was modelled using a point-based energy balance model (Brock and Arnold, 2000) at all auger-hole sites for each glacier, with a modification applied to arctic glaciers to account for the high solar azimuth (Irvine-Fynn et al., 2014).

3.5 Results

3.5.1 Piezometer evaluation

Firstly, to assess the representativeness of the 36 cm auger-holes, comparisons were made with proximate holes with depths of 16 and 26 cm at FGBI and GRDS, with additional 46 cm deep auger holes at the former site (Figure 3.6). Auger-holes were located within ~0.5 m of each other over a visually similar ice type, to minimise the influence of hole-to-hole disturbance and mitigate spatial variations in ice structure. Shapiro-Wilk tests highlighted the hydraulic conductivity data were not

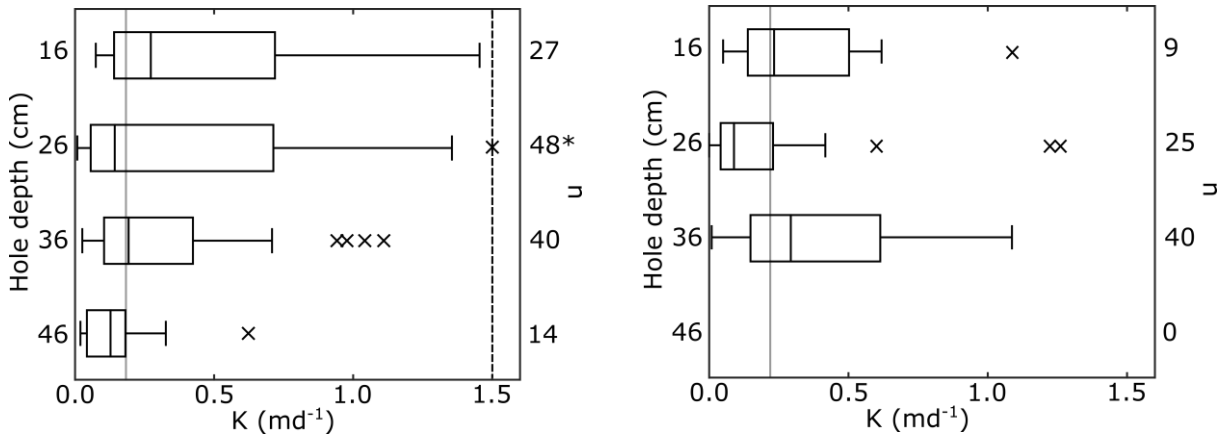

Figure 3.6 Change in K with auger-hole depth for a; left) FGBI and b; right) GRDS, indicating median for each site (solid vertical line) of 0.183 and 0.220 m d^{-1}, respectively. Sample sizes (n) are noted on the right of the diagram. *Note one outlying data point ≥ 1.5 m d^{-1}.

normally distributed at either site. For FGBI, an independent samples median test highlighted no significant difference in median values of K between different hole depths ($p < 0.05$). However, a Kruskall-Wallis test indicated a difference in distribution of K values across the four-contrasting auger-hole depth groups ($p < 0.05$), with the bounds of total ranges and interquartile ranges decreasing with an increase in auger-hole depth. Dunn's post-hoc testing indicated that only the 46 cm and 16 cm groups were significantly differently distributed from each other ($p < 0.05$). Similarly, or GRDS, an independent samples median test indicated that median K was significantly different between the three groups ($p < 0.05$). A Kruskall-Wallis test indicated that distribution of K across the three depth groups was significantly different ($p < 0.05$), with Dunn's post hoc testing indicating the presence of a pairwise significant difference in data distribution only between the 26 cm and 36 cm groups ($p < 0.05$). However, there is no significant difference between any of the depth groups and the overall median for GRDS.

As there is no systematic significant difference between medians for auger-holes of 16, 26, 36 and 46 cm in depth, any of these depths could have likely been selected as a methodological optimum. A shallow hole would require a smaller volume of water to fill and would enable a greater frequency of measurements to be recorded in a fixed period and may increase clarity of temporal trends, especially over a diurnal timescale. However, when the water table is low, shallow holes may be unsuitable as they may be perched above the water table, resulting in an inability to assess hydraulic conductivity. Conversely, a deeper auger-hole (e.g. 46 cm) would be unlikely to have such an issue but would take longer to fill reducing the frequency of *K* measurements. As such we recommend and adopted 36 cm

as an optimum auger-hole depth as a compromise to maximise the frequency of data collection for assessment of weathering crust hydraulic parameters.

To ascertain the repeatability of the bail-recharge method, rapid (< 15 minutes) repeat measurements were undertaken at four sites (PBSV, SGSE, GRKM and GRDS). All repeat measurements were recorded within a maximum 30-minute window to minimise any temporal variations in *K*. During these repeats, a constant equilibrium water table depth was assumed (range within ± 5 % of the mean) to prevent undesirable influence of a falling water table due to aquifer drainage upon *K*. Relative standard deviation (n = 19) across the four sites was 40.9%. Of note, the contrast in medians reported for varied auger-hole depths also all fell within this error associated with repeatability. Whilst this may appear initially to represent a high level of uncertainty in our estimates of *K*, typical ranges of *K* in groundwater studies cover a range of thirteen magnitudes (Freeze and Cherry 1979) and quantification of *K* to within one order of magnitude is usually sufficiently precise for most analyses (Younger, 2009). Our calculated relative standard deviation falls within this acceptable range, and as such, we are confident that our single-measure method provided suitably reliable and precise estimates of *K* within the weathering crust.

3.5.2 Quantification of and controls upon *K*

A total of 280 successful recharge experiments were conducted on 10 northern hemisphere glacier ablation zones. Twenty-five 'unsuccessful' experiments were reported in which holes were not refilled to > 6 cm depth; these were typically associated with cloudy and/or rainy conditions but had no clearly systematic cause and occurred randomly across all glacier sites. Mean *K* across the eight field sites was 0.185 ± 0.019 m d^{-1} (SD = 0.310 m d^{-1}, range = 0.003 – 3.519 m d^{-1}). Mean permeability was 0.384 ± 0.060 m^2 (with a range from 0.018 – 3.451 m d^{-1}). Neither hydraulic conductivity nor permeability data were normally distributed (Shapiro-Wilk, n = 280 and 111, respectively, $p < 0.05$). Ranges and medians of *K* at each glacier plotted with site latitude as a variable (Figure 3.7) highlighted a potential relationship between latitude and *K*: a statistically significant, weak positive correlation existed between the variables (Spearman's $r = 0.140$, $p < 0.05$, n = 280).

To interrogate the environmental factors that may define *K*, specifically examining differing stages of weathering crust development, further non-parametric correlations were undertaken between *K* and potential explanatory variables. Such variables included water table height, as measured from the base of the 36 cm auger-holes according to the Stage 3 piezometer recharge records. The potential

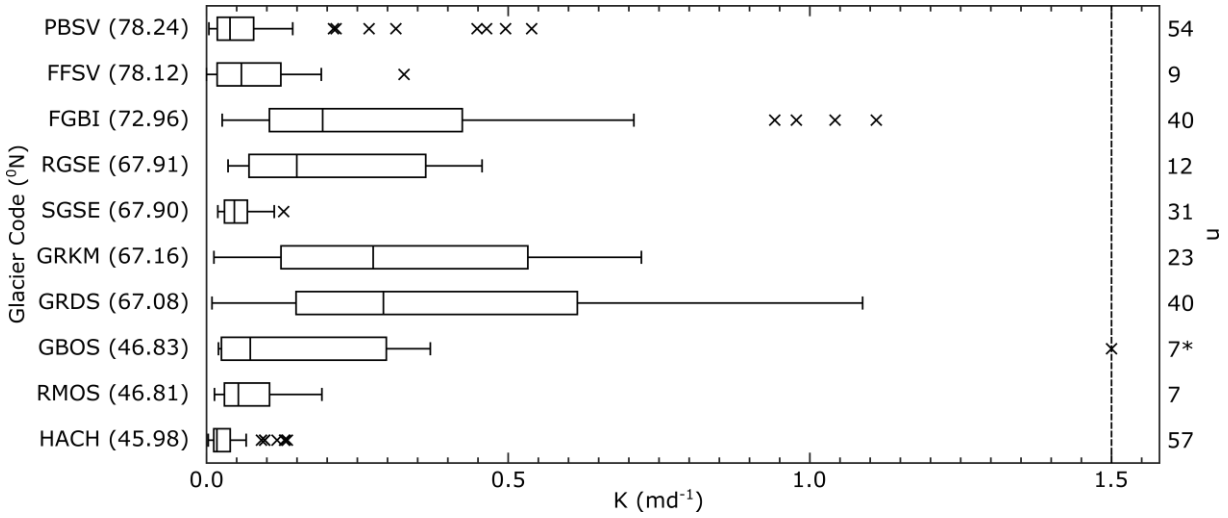

Figure 3.7 Hydraulic conductivity of holes of 36 cm depth across all glaciers within the sample set, with latitudes displayed in degrees North of the equator. Sample sizes (n) are noted on the right of the diagram. * Note, the x axis is limited to 1.5 m d^{-1}, with one outlying point above this limit at GBOS, with a value of 3.519 m d^{-1}.

for the water table to be influenced by the melt rate and ingress of surface water into the weathering crust was further considered by using site altitude and the energy balance model melt output (M) for the 1-hour time period preceding the observation of *K* as explanatory variables. Further, based on Müller and Keeler's (1969) conceptual model of weathering crust development, cumulative SWR_{in} receipt since (i) freezing, (ii) the previous rainfall event, and (iii) the period of dominant turbulent fluxes were calculated as variables.

Freezing of interstitial meltwater is may reduce interstitial pore size and decrease the hydraulic conductivity of the weathering crust. However, given the latent heat released during the refreezing of interstitial meltwater (see Paterson, 1994), a period of freezing air temperature for hours or even days is unlikely to result in complete re-freezing of the liquid component of the weathering crust. However, it is important to note that such a cold wave propagates downwards (Irvine-Fynn et al., 2011b; Paterson, 1994), so any refreezing will occur in the less dense, more porous upper weathering crust and hence may have a greater influence on *K* than would be expected. Rainfall events and cloudy periods, where turbulent fluxes dominate the energy balance equation (see Hock, 2005) are identified as crucial for "resetting" of the weathering crust surface (Müller and Keeler, 1969). Observations of summer rainfall are limited within our dataset, however we assume that precipitation, as measured at local AWSs, is in the form of rain either supported by *in situ* observations or as defined by air temperatures in excess of 4 °C. For the available data, two periods of rainfall were identified, one at HACH, comprising a 10-hour period of overnight rainfall (17 mm total) and another at SGSE/RGSE,

where 2.4 mm of rain fell in eight hours. Melt modelling data are used to determine the ratio of SWR_{in}:turbulent fluxes at each glacier site, with a period of dominant turbulent energy flux (DTEF) defined as when > 50 % of energy for melt is supplied by turbulent fluxes for a duration of at least three hours. This duration is selected to ensure that the predominant weather pattern is that of a cloudy sky, rather than a low sun angle and high air temperatures which can occur during sunrise and sunset. Available meteorological data allowed for determination of this variable at GRDS, & SGSE/RGSE. For GRDS, two DTEF periods were observed, both between midnight (00:00) and 07:00 when the solar azimuth was low: total melt during the two periods was 1.71 and 0.57 mm water equivalent (w.e.). A more marked period of DTEF was observed at RGSE and SGSE, with a 37 and 39-hour DTEF period with 27.06 and 25.03 mm w.e. of melt respectively. With freezing, rainfall and DTEF periods being indicative of (at least partial) resetting of the weathering crust, cumulative SWR_{in} should identify the subsequent increase in near-surface ablation, the disaggregation of ice crystals and increasing porosity and hydraulic conductivity.

The following significant ($p < 0.01$) monotonic correlations are highlighted between *K* and the following independent variables (Table 3.2): a) negative correlation with cumulative SWR_{in} since freezing; b) strong negative correlation with cumulative SWR_{in} since previous DTEF period; iii) weakly negative correlation with altitude, c) strongly positive correlation with water table height.

Table 3.2 Correlation matrix highlighting monotonic relationships with hypothesised controls upon hydraulic conductivity (*K*) of the weathering crust.

Glacier	n	Cumulative SWR_{in} 0 °C	Cumulative SWR_{in} precipitation	Cumulative SWR_{in} DTEF	Elevation	Water table	Melt
PBSV	54	0.398**	-	-	-0.321*	0.547**	0.520**
FFSV	9	-	-	-	-	0.786*	-
FGBI	40	0.281	-	-	0.173	0.375*	-
RGSE	12	0.272	0.272	0.272	0.203	0.835**	-0.488
SGSE	31	-0.050	-0.050	-0.050	0.428*	0.249	0.212
GRDS	40[a]	0.209	-	-0.133 (30)	0.123	0.639**	0.225
GRKM	23	-	-	-	-	0.352	-
GBOS	7	-	-	-	-0.40	0.809*	-
RMOS	7	-	-	-	-0.378	-0.204	-
HACH	57[a]	0.098	0.112 (19)	-	0.168	0.306*	-0.253
All	280[a]	-0.404** (234)	0.134 (62)	-0.658** (73)	-0.256**	0.710**	-0.52 (129)

[a] With missing cases or lacking data, in these cases n is noted in brackets.
Values shown are Spearman's r with significant values (two-tailed) marked. * $p < 0.05$; ** $p < 0.01$.

Similar analysis was undertaken for permeability (κ; Table 3.3) for PBSV and HACH located at each extreme of the latitudinal range of field sites within this study. Mean auger-hole water temperatures of 0.57 ± 0.02 °C and 0.17 ± 0.01 °C, and ranges of 0.20 – 0.90 and 0.10 – 0.40 °C,

Table 3.3 Correlation matrix highlighting monotonic relationships with hypothesised controls upon permeability (κ) of the weathering crust.

Glacier	n	Cumulative SWR_{in} 0 °C	Elevation	Water Table	Melt
PBSV	54	0.398**	-0.321*	0.548*	0.519**
HACH	57	0.093	0.171	0.304*	-0.272
All	111	-0.165	-0.291**	0.574**	0.415**

n.b. Latitude and elevation are not considered as independent variables due to a lack of data.
Values shown are Spearman's r with significant values (two-tailed) marked. * $p < 0.05$; ** $p < 0.01$.

respectively. This yielded permeability values ranging over 3 orders of magnitude from 0.018 and 3.45 m^2. However, with auger-hole water temperature data only available for two glaciers, our interpretations are limited. By estimating a mean water temperature for all other glaciers, any correlations with environmental variables would simple mirror those reported for *K* (see Equation 3.3 and Figure 3.3).

3.6 Discussion

Ablating glacier surfaces are characterised by a porous ice weathering crust which may influence meltwater, sediment, microbial cell and nutrient storage and transport (Edwards et al., 2011; Hodson et al., 2007; Irvine-Fynn et al., 2012; Stibal et al., 2012). Here, we have presented data from a low-cost capacitance piezometer which, to our knowledge, is the first comprehensive set of measurements across multiple glacier sites using a standardised methodology to describe *K* for weathering crust ice.

3.6.1 Application of piezometers and Darcian flow model to the weathering crust

The piezometer described provides high-resolution water level data. The application of the piezometer in supraglacial environments enabled quantification of the hydraulic properties of the weathering crust and was used to test the applicability of Darcy's Law to the weathering crust. Darcy's Law describes diffuse water flow through a homogenous porous media and is therefore not applicable where flow is confined to discrete conduits thought so-called 'karstic flow' (Moore, 2002). Karstic flow would cause the recharge curves to show step-changes where water suddenly enters a conduit (Hartmann et al., 2014). This characteristic or phenomenon in the recharge curves was not observed, indicating that flow through the weathering crust is effectively homogenous at the synoptic scale and that Darcy's Law can be applied with confidence to weathering crust hydrology.

3.6.2 Hydraulic conductivity of the weathering crust

At the ten sites examined across the northern hemisphere, mean weathering crust *K* was 0.185 ± 0.019 m d^{-1}. This value is equivalent to those reported for sandstone (10^{-1} – 10^{1} m d^{-1}), or stratified clay soil (10^{-1} – 10^{2} m d^{-1}) (Bear, 1972) and hence, hydrologically, the glacial weathering crust can be considered as a poor, impervious aquifer. This also compares well, albeit an order of magnitude lower, to the recent 10^{0} – 10^{2} m d^{-1} estimates for the hydraulic conductivity of firn on alpine glaciers (e.g. Fountain, 1989; Schneider, 1999) and the Greenland Ice Sheet (Miller et al., 2017). Our *K* values are the same order of magnitude as those reported for ablating glacier ice by (Cook et al., 2015), and similar to the lower-order estimates given by previous site-specific studies (Karlstrom et al., 2014; Larson, 1977; Theakstone and Knudsen, 1981; Wakahama, 1978; Wakahama et al., 1973). Our estimated ranges of weathering crust hydraulic conductivity still encompassed the values derived from Medenhall and Llewellyn Glaciers (Juneau Icefield, Alaska/British Columbia) despite the absence of such a maritime environment in the study sites reported here.

The estimates of *K* in the weathering crust approaching that of sandstone or clay would see surprising given the degrading near-surface ice surface would suggest a higher porosity and potentially an increased hydraulic conductivity. However, hydraulic permeability and conductivity are also governed by the scale of and linkage between void spaces in a porous medium (Bear, 1972). Both the angularity of ice crystals and the immobile viscous water layers that surround them (Nye, 1991) reduce the hydraulic conductivity through, respectively, increasing micro-scale flowpath tortuosity and reducing permeability. Water movement in the uppermost 2 m of a glacier is typically driven upward due to the near-surface water pressure gradient (Lliboutry, 1996) that can be influenced by meteorological conditions and is complicated further by the capillary force that retains and restricts water flow (Bear, 1972), allowing flow in opposition to the gravity- and slope-driven directions. Moreover, observations of local water tables identified in open cryoconite holes suggests that the water table is commonly several centimetres to three decimetres below the ice surface (Cook et al., 2016; Cook et al., 2015), and so *K* is retrieved for depths below the most porous surface ice. Combined with the near-surface density gradient, these mechanical conditions may in part explain the low K identified for the apparently porous weathering crust. Studies conducted in the 1970s and 1980s used contrasting methods, including dyes such as ink (Wakahama et al., 1973) and fluorescein (Theakstone and Knudsen, 1981). Ink and tracer dyes such as fluorescein and rhodamine are highly dispersive within water (Smart and Laidlaw, 1977); therefore, the use of dyes may result in an overestimation of *K,* as

the tracer will likely have dispersed through the sub-surface water column rather than acting conservatively and matching the water flow rate. (Theakstone and Knudsen, 1981) work focused on the quantification of meltwater flow rates through the supraglacial drainage network, and they only estimated the delay to flow caused by the weathering crust as a component of this. Despite this difference in emphasis, our upper estimates for *K* coincide with Theakstone and Knudsen's median estimates, while difference compared to the *K* value reported for Medenhall Glacier (Karlstrom et al., 2014) may simply be due to the particular environmental and climatic setting, solar radiation receipt and synoptic progress through individual melt seasons.

One issue arising with the use of pumped wells (e.g. Larson, 1977) for the estimation of *K* in glaciological environments is that the technique requires the addition of water, which causes a local increase in water table height. As SWR_{in} receipt decreases with depth in the near surface (Cook et al., 2015) it is expected that pore size, permeability and *K* will also decrease. The inverse is also true, so by introducing a false rise in the water table, *K* is measured through more porous ice which is typically above the equilibrium water table and hence not necessarily describing *K* for the true transmission of meltwater at a given point in time and generating artificially elevated estimates of its value. To emphasise this assertion, our data show that an increase in water table height correlates with an increase in *K* and highlight the need to consider methods of describing hydraulic conductivity cautiously.

3.6.3 Controls upon hydraulic conductivity of the weathering crust

In the weathering crust, the mechanism for pore enlargement is hypothesised as the cumulative receipt of subsurface SWR_{in} and internal melt of ice (Cook et al., 2015; Hoffman et al., 2014; Müller and Keeler, 1969). This is evidenced by the lower bulk density and greater intergranular pore space of the weathering crust when contrasted with un-weathered glacier ice (LaChapelle, 1959; Nye, 1991). This enlargement of inter-crystalline pores would result in an increase in hydraulic conductivities. Latitude is weakly positively correlated with *K*, Figure 3.7 indicates that the highest *K* values are observed in the 67 – 72 °N latitude band. The energy available for weathering crust development is constrained by latitude, typically with more intense SW_{in} and higher summer season air temperature even at elevation in lower latitudes. However, this contradicts our findings, which suggest glacier ice dynamics and net ablation may also affect the formation of a weathering crust: glaciers exhibiting higher ice emergence rates may offset the evolution of a deeper porous surface layer, while enhanced rates of ablation and runoff may lead to an enhanced abundance of rills and streams which through

energy transfers and forming topographic variability can degrade the weathering crust and slow the vertical evolution and spatial extent of the weathering crust. Such hydrological disturbance may also be affected by glacier surface slope (e.g. Hodson et al., 2007; Mantelli et al., 2015; Rippin et al., 2015). However, these relationships are further complicated by regional climatology, synoptic meteorology and local altitude and topography (Barry, 2008). For example, summer cloud cover and precipitation are common in both the Alps (e.g. Rudolph et al., 2011) and Svalbard (e.g. Førland and Hanssen-Bauer, 2000), and these conditions are known to reduce or minimise weathering crust development (Müller and Keeler, 1969). Shading by surrounding terrain will dictate SWR_{in} receipt and influence the formation of a porous ice layer, while particularly in mid- and high-latitudes, as a consequence of solar geometry, glacier orientation and surface slope may become more influential. This further level of quantification is necessary to better constrain the supraglacial environment as a modulator of meltwater discharge both at the (sub)catchment scale and glacier scale.

The analyses seeking to identify additional potential controlling factors on *K* in terms of cumulative SWR_{in} receipt since any partial or complete 'resetting' of the weathering crust resulted in less intuitive conclusions. The negative correlations between *K* and SWR_{in} since last freezing and DTEF periods indicated that as the weathering crust developed, there was a reduction in the hydraulic permeability. This was unexpected as low radiative and high turbulent energy transfers, such as cloudy periods, often including rainfall, have been anecdotally linked with weathering crust removal (Müller and Keeler, 1969) and hence such synoptic conditions were expected to be associated with lowered *K* as was evident from the 'failed' recharge experiments. Here, we suggest that the development and rise of a water table does not necessarily occur coincidentally with progressive ice crystal disaggregation; the rise in the water table may lag behind the creation of intergranular void space implying a low water table is associated with low *K* values. To support this argument is the observation that *K* is not correlated solely with melt which might be expected to increase the water table height and hence hydraulic conductivity. This implies that additional processes are occurring, which preclude any direct relationship between melt rate and *K*: for example, there could be refreezing at depth within the weathering crust and reduction of liquid water volume, or the low transmission rates incur delay as pore spaces are filled. Here, there may be analogies with the progress of the wetting front in a snowpack (e.g. Marsh and Woo, 1984) or infiltration to frozen soil (e.g. Gray et al., 2001), but to develop this level of process understanding would require further investigation.

The additional complexity hydrology itself may impact on defining *K* is best evidenced by the positive relationship between *K* and water table height. Observations from cryoconite holes suggests there is a variable water table height within the weathering crust both at sub-diurnal and synoptic time-scales (Cook et al., 2015). These variations may arise from the bulk density increase with depth within the weathering crust, or because of a changing local base-level. Once the ability of the weathering crust to transport water is exceeded by the melt input the water table will rise into the increasingly more porous near-surface ice, and the piezometer derived *K* value increases. Hydraulic conductivity may, in this scenario, also rise if the base-level for the drainage pathway remains broadly the same due to the dampened response of the supraglacial stream network to peak melt (e.g. Munro, 2011; Smith et al., 2015) and the hydraulic gradient increases. However, as weathering crust is drained as melt rates and associated water inputs reduce overnight, and the supraglacial stream base level drops, the water table and pressure head falls, hence *K* is reduced. Our feedback loop between meltwater input, water table height and *K* would explain why *K* and melt do not directly correlate as a response time is required, dependant on infiltration rate, for the water table level to rise.

Our data from 10 glacier sites shows that *K* exhibited values over a range of four magnitudes (relative standard deviation of ~180%) and even upon individual glaciers there is a high local-scale variability (Figure 3.7). While the relationships described above provide some indications of conceivable causes in the variability in *K* values, there are clearly complex interactions between potential driving meteorological variables, which are problematic to disentangle without further study. However, one further aspect which influences the fabric of the weathering crust and hence the nature of the pores within is the microscale ice-structure, which is difficult to characterise and quantify and is not included within this dataset. Ice structure and fabric will directly condition pore size and shape, interstitial connectedness and tortuosity, and therefore likely influence the hydraulic behaviour of the weathering crust. Ice structure and fabric can vary across a range of length scales (see Hambrey and Lawson, 2000; Hudleston, 2015). Consequently, crystal size, packing and orientation may play an important role in defining the rate and location at which water is transferred through the weathering crust, by controlling potential pore size, shape and geometry once crystal boundaries are preferentially melted to form pores. Consequently, from the above discussion, the implication is that more surveys of *K* under variable but constrained environmental parameters, and over extended time-frames, are required to better define the primary drivers and rates of weathering crust development and its spatial and vertical extent.

3.6.4 Hydrological role of the weathering crust and relevance to impurity transport

This study highlights a typically overlooked component of the supraglacial hydrological system: with near-surface glacier ice traditionally considered as essentially impermeable (e.g. Hodgkins, 1997) with an immediate hydrological response time (e.g. Fountain and Walder, 1998); our data emphasises the weathering crust as a hitherto neglected yet important aspect of supraglacial hydrology. The presence of a water table at depth below the ice surface emphasises the potential for short-term meltwater storage, retention and delay in runoff. We propose that as surface ice ablates during the ablation season, under clear sky conditions, the weathering crust develops (Müller and Keeler, 1969) and meltwater is routed through this near-surface layer. As our data show, meltwater flow through the weathering crust can be relatively slow, yet supraglacial stream discharge response to peak melt typically occurs within < 12 hours (Munro, 2011). The hydraulic conductivities calculated here, coupled with typical < 10 m channel spacing upon glacier surfaces (e.g. Karlstrom et al., 2014), imply that a parcel of meltwater could remain within the weathering crust for a minimum of 68 hours.

At synoptic and diurnal time-scales, we hypothesise that in response to the energy balance, additional 'new' meltwater enters the weathering crust causing the water table to rise, which positively influences *K*, and either overrides or displaces 'old' stored or retained meltwater. This type of water turnover is common for rainfall events in terrestrial environments (e.g. Brutsaert, 2005; Lu and Godt, 2013). When melt production exceeds the infiltration rate of the weathering crust, or the water table rises to the surface, it would be expected that saturated sheet flow might occur over the surface; however, due to the complex nature of glacier surfaces, sheet flow is uncommon and was not observed during our observation periods, and drainage via rills and small streams evolves quickly (e.g. Mantelli et al., 2015). However, the observation of *K* being dependent on water table elevation suggests the hydraulic properties exhibit a gradient with depth in the near surface and also spatially and temporally variable. Consequently, the proportions of meltwater that may be delayed at a variety of time-scales in their delivery to supraglacial rill and stream networks remain undefined.

The presence of a near-surface aquifer on ablating glacier surfaces with a low hydraulic conductivity may also have significant implications for the transfer of impurities across exposed ice and affect biogeochemical cycling. Here, we argue that based on contemporary understanding there is a need for future research to explore a range of these potential affects. Considering the characteristic

and ubiquitous presence of fine inorganic dust (e.g. Oerlemans et al., 2009), microbes (e.g. Edwards et al., 2014; Hodson et al., 2008; Stibal et al., 2012) and other particulate impurities and contaminants (e.g. Hodson, 2014) on glacier surfaces, the poor hydraulic conductivity of the weathering crust may have important implications on the transport rate of such particulates. To date, there has been no clear or detailed assessment of the rates at which impurities are transferred over ablating ice surfaces. (Irvine-Fynn et al., 2012) reported inefficient transport processes through and storage of microbial cells within the near-surface of an Arctic glaciers. Here, the low *K* values align well with such an assertion of inefficient water transfer. However, the relationship between impurity transport and *K* is unlikely to be a simple linear function due to the potential of the weathering crust to act as mechanical filter, preventing transfer of particles with diameters in excess of pore sizes, or bio- and physio-chemical processes resisting or accentuating impurity transport (e.g. Dolev et al., 2016; Jepsen et al., 2006; Jepsen et al., 2010; Mader et al., 2006). Therefore, fluctuations in the water table and of varied hydraulic conductivity at diurnal or synoptic time-scales, or over space, may be crucial in defining the character of impurities transported through or from a glacier's surface. Indeed, recent work has suggested that water flux and the hydraulic delivery of dissolved nutrients within meltwater to surface microbial habitats may be a crucial influence for microbial community structure and activity (e.g. Dubnick et al., 2017; Edwards et al., 2011), and controls downstream ecology and characteristics (e.g. Singer et al., 2012; Wilhelm et al., 2013). Furthermore, when combined with typical *in situ* doubling times of the water-borne cryospheric microbial communities of < 60 days, and in some instances < 5 days (Anesio et al., 2010), and clear evidence of their capacity to influence nutrient cycling (Scott et al., 2010), the potential for the supraglacial weathering crust as a microbial habitat (Irvine-Fynn and Edwards, 2014) merits further investigation. Specifically, the retention of mineral dust and microbes within the weathering crust holds the potential to contribute to supraglacial biogeochemical cycles. For example, increased residence time within the weathering crust permits greater interactions between dust, dilute nutrients, low-density bacterial hosts and their viral parasites (Rassner et al., 2016). The hydraulics of the weathering crust, and the recognition of 'old' and 'new' meltwaters, may hold potential influence on the transfer rates for solutes and dissolved organic compounds or contaminants within the glacier system. However, the *in-situ* fate of supraglacial solutes, organic compounds and contaminants during the ablation season still remains poorly characterised.

As both Grannas et al. (2013) and Hotaling et al. (2017) concluded, there remains a pressing need to better constrain the nature and variability of supraglacial hydrological flowpaths particularly to define their impact on contaminant and impurity transfer, microbial communities and biogeochemical

function both for glacier surfaces and glacier-fed ecosystems. This is particularly significant under the spectre of projected future changes to glacier and ice sheet runoff regimes (e.g. Bliss et al., 2014; Franco et al., 2013). In many glacierised regions, atmospheric warming, rising snowlines and expanding ablation areas may result in extensive supraglacial hydrology even as total glacier areas decline. Similarly, glacier thinning and cooling in higher latitudes (e.g. Delcourt et al., 2013; Irvine-Fynn et al., 2011b) may also promote an increasing dominance of supraglacial hydrology. Consequently, understanding the influence that the weathering crust has on modulating supraglacial runoff and its characteristics is important to improve predictive hydrological models. This assessment of weathering crust hydrology presents a first step to better characterising this commonly overlooked supraglacial flowpath and exploring the controls that dictate spatial and temporal variation in hydraulic conductivity of near-surface glacier ice.

3.7 Conclusions

We present a robust but simple piezometer probe design that permits low-cost, high-resolution, repeatable water level monitoring. The economical nature of the piezometer design, combined with its limited power requirements, make it ideally suited to spatially widespread deployment in remote locations and for hydrological applications beyond those described here. We describe a field methodology that allows spatially widespread monitoring of glacier weathering crust water level fluctuations at multiple sites. Data collected from a spatially extensive suite of field sites allows examination of weathering crust *K*, and we quantify a mean *K* of 0.185 m d^{-1} which is an equivalent value to sandstone and firn and therefore leads us to regard the weathering crust as a hydrologically poor, impervious aquifer that can delay water transfer through the supraglacial hydrological system and acting as a transient, multi-day storage reservoir within this network. This role as a regulator of meltwater egress has the potential to impact upon supraglacial sediment, impurity and biological budgets and associated basin-scale exports at a range of spatial and temporal scales. Such fluxes have consequent impacts upon the supraglacial ecosystem, through influencing the storage and transport of microbes, fine mineral grains, and associated nutrients or contaminants. However, our analysis demonstrates that the precise nature of the controls that drive the hydrological characteristics of the weathering crust are clearly complex and multi-faceted and, although water table height clearly exerts a fundamental control, investigation of the role of hyper-local ice structure and crystallography and consequent impacts on near-surface sedimentary- and eco- systems likely represents a fruitful avenue for further investigation.

3.8 Acknowledgements

Financial support for this work was gratefully received from: Aberystwyth University (Department of Geography and Earth Sciences), Gilchrist Educational Trust, EU F7 INTERACT (grant: SCARFACE to TDI and AE), Royal Geographical Society (Fieldwork grant: to ITS), Royal Society (grant: RG130314 to AE and TDI), Scottish Arctic Club (grant: to ITS), PSCP and NSERC (for support on Bylot Island: to BJM), and the Climate Change Consortium for Wales (C3W grant: Proof of Concept to TDI). JMC acknowledges the Rolex Awards for Enterprise. TDI and JMC also acknowledge NERC Consortium Grant 'Black and Bloom'. The Dark Snow Project, and Karen Cameron and Jason Box, are thanked for the support in Greenland. The authors wish to thank Stephen Jennings, Ottavia Cavalli, Stephen Brough, Sarah St Germain, Michael Hambrey and Jayne Kamintizis for invaluable assistance throughout various field campaigns. Andy Porter provided generous guidance with regards to the electronics and drawing the circuit diagrams in Figure 3.2. Dave Kelly (Aberystwyth) is thanked for refinement and construction of the piezometer probes, developing prototypes built by Stephen Norburn (Sheffield).

4. Evaluation and Optimisation of Flow Cytometry for Glacial Meltwater Samples

4.1. Introduction

Enumeration measurements are fundamental to studying the microbiology of any environment and the interaction of microorganisms within and with it, providing the necessary basis for interpreting microbiological activity (Fredrickson and Balkwill, 1998). However, accurate and reproducible application of these techniques to the glacial environment remains challenging due to the presence of cell fragments (e.g. Irvine-Fynn et al., 2012), viruses (e.g. Rassner et al., 2016), clastic sediment particles, and microbe-clast aggregates within meltwaters, alongside the requirement to store and transport samples from remote environments to a suitable laboratory (e.g. Barnett et al., 2016). The recent works of Stibal et al. (2015) and Santibanez et al. (2016) have sought to evaluate the application of existing cell enumeration techniques (including Epifluorescence Microscopy (EFM), Flow Cytometry (FCM) and quantitative Polymerase Chain Reaction (qPCR)) in the glacial environment, estimating accuracy of artificial samples comprised of known concentrations of cultured bacterial cells and clastic sediments, the outputs of which are summarised in Figure 4.1.

Despite this work, there remains no widely-accepted standard enumeration protocol for such samples (Miteva, 2008), given that these evaluative studies do not present a protocol suited to the enumeration of cells found in glacial meltwaters from the sub- or supraglacial environments, including streams, cryoconite waters or the water found in the weathering crust. This is either due to: a) a limited scope of concentrations tested in the case of Santibanez et al. (2016) (who did not test samples containing $\geq 10^6$ cells mL^{-1}, or with clastic sediment loads aside from 10^{-1} g L^{-1}); or b) due to unsatisfactory performance of the protocol in the case of (Stibal et al., 2015).

Notably, the work of (Stibal et al., 2015) assessed three commonly applied techniques for environmental and laboratory microbial cell enumeration: epifluorescence microscopy (EFM) (e.g. Karl et al., 1999; Priscu et al., 1999; Säwström et al., 2002); quantitative polymerase chain reaction (qPCR) (e.g. Hamilton et al., 2013; Zarsky et al., 2013); and flow cytometry (FCM) (e.g. Irvine-Fynn et al., 2012; Liu et al., 2006; Miteva et al., 2009; Miteva and Brenchley, 2005; Miteva et al., 2004; Santibanez et al., 2016; Yao et al., 2008).

Imaging techniques such as EFM (alongside light and electron microscopy) allows for direct visualisation of cells and aggregates in either two or three dimensions, and has been applied

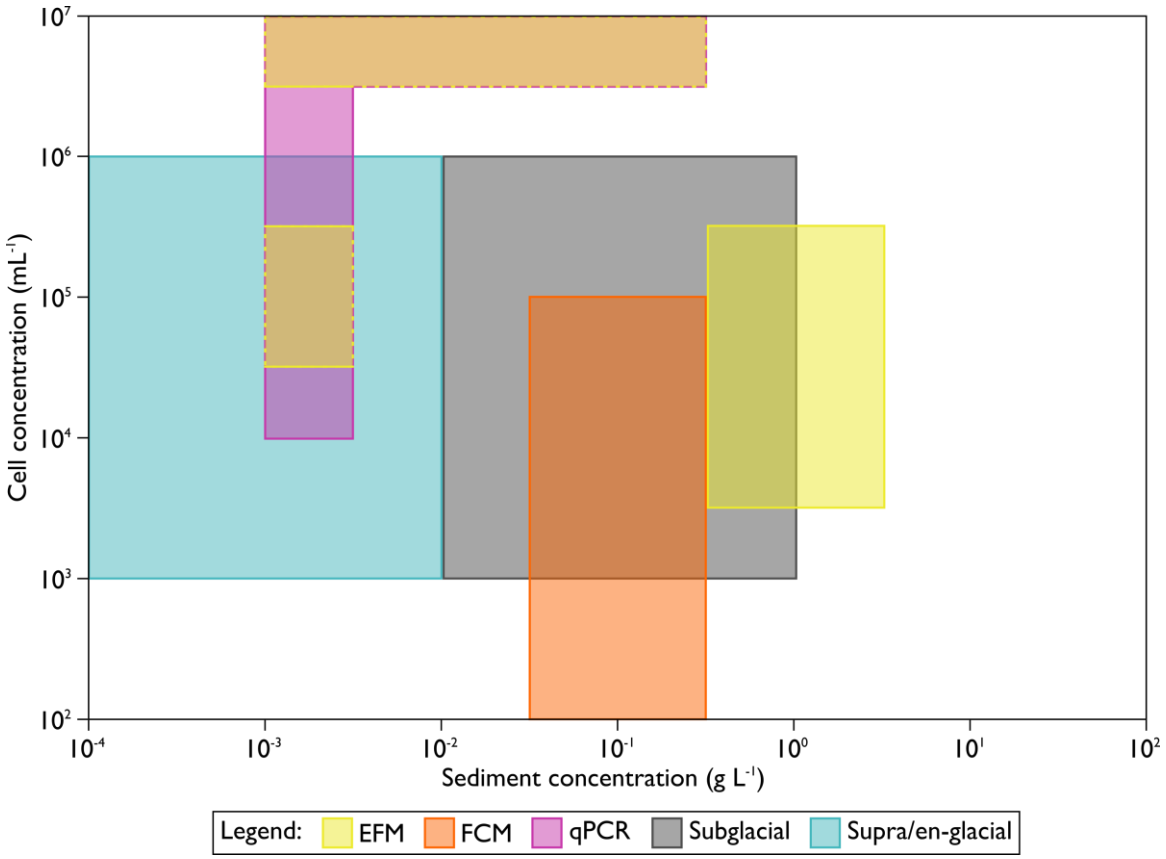

Figure 4.1 Ranges of cell and sediment concentrations for which EFM, FCM and qPCR exhibit acceptable accuracy (100 ± 25 %) and precision (≤ 20 % relative standard deviation) for the enumeration of glacial samples. Typical concentrations of cells and sediments in different glacial hydrological environments are highlighted; the supra-glacial hydrological environment category incorporates supraglacial streams, cryoconite waters and surface ice and ice cores. Shaded areas with dashed borders indicate that two enumeration techniques are suitably accurate and precise. Data compiled from: Amato et al., 2007; Anesio et al., 2010; Bartholomew et al., 2011; Bøggild et al., 2010; Collins, 1979; Foreman et al., 2007; Hodson et al., 2013; Irvine-Fynn et al., 2012; Karl et al., 1999; Mindl et al., 2007; Miteva et al., 2009; Priscu et al., 1999; Santibanez et al., 2016; Säwström et al., 2002; Skidmore et al., 2000; Stibal et al., 2015; Svensson et al., 2000.

extensively for cell size, morphology and enumeration (e.g. Felip et al., 2007), but typically use small sample volumes (often as low as 0.1 µL), increasing uncertainty, are time-consuming and labour intensive, and are prone to operator error such as mis-counting. qPCR offers a faster, DNA based quantification method using fluorescence probes (Madigan et al., 2015). However, qPCR does not enable any examination of cell size or morphology, and inherently incorporates bias associated with all PCR-based methods and hence may not necessarily reflect the entire microbial ecosystem. Whilst conventional plating is an important detection method for microbial cells, it has been estimated that ≤ 1 % of microorganisms present can be detected using this method (Allen et al., 2004).

Considering the limitations of the above enumeration techniques, FCM demonstrates potential for the enumeration of microbial cells in glacial hydrological systems as a high throughput, robust enumeration technique (Irvine-Fynn and Edwards, 2014), but despite its potential has seen

limited application to supraglacial samples. However, data from FCM can be ambiguous due to lack of guidelines, controls and the subjective nature of gating strategies, especially when considering small cells near to the detection limits (Nebe-von-Caron, 2009) such as glacial prokaryotes prevalent in glacial environments (e.g. Franzetti et al., 2013; Musilova et al., 2015; Christner et al., 2018) which can exhibit diameters ≤ 1 μm (Irvine-Fynn et al., 2012). Therefore, this chapter develops an accurate and repeatable protocol with a functional range suited to enumeration microbial cells within supraglacial meltwaters (Figure 4.1), whilst quantifying the influence of compounding factors such as cell genus, sediment mineralogy and the type of fixative used, none of which are formally considered in previous work.

4.2. Materials and methods

4.2.1 Preparation of artificial samples

To examine the accuracy of FCM as a microbial cell enumeration method for glacial meltwaters, artificial samples of known clastic sediment and bacterial concentrations were created. Two genera of psychrophilic β-proteobacteria, a subphylum typically prevalent in glacial samples (e.g. Cameron et al., 2012; Cameron et al., 2016; Edwards et al., 2014; Musilova et al., 2015), *Polaromonas sp.* and *Janthinobacterium sp.* were cultured in 0.5 × R2A (Reasoner and Geldreich, 1985) at 13 °C for a minimum of 10 days. *Polaromonas sp.* is a genus distributed globally across glacial and high-altitude environments including Antarctica, Greenland, the Himalaya, and European Alps (Ambrosini et al., 2016; Margesin et al., 2012) and it has been suggested that the genus is the dominant bacteria of glacial ice and sediment (Darcy et al., 2011). *Janthinobacterium sp.* has been observed in soils in maritime Antarctica and the Antarctic peninsula (Shivaji et al., 1991), as well as glacial sediments in the Karakoram (Rafiq et al., 2017). To extract cells from the growth media, isolates of each culture were centrifuged at 4000 G for 15 minutes and suspended in Type I Ultrapure water (Elga, UK). Isolates were subsequently enumerated using a Sony SH-800EC Cell Sorter (Sony Biotechnology, Japan) to establish concentration prior to dilution. Whilst this may generate issues of bias, for cell-only suspensions FCM is highly suitable for enumeration studies (Shapiro, 2003), including in aquatic samples (Wang et al., 2010).

The clastic sediment component was comprised of multitude of different clast types, including a) supraglacial sediment from Robertson Glacier (Canada) and Haut Glacier d'Arolla (Switzerland); b) a non-location specific granitic rock sample and; c) single-mineral samples of quartz, calcite and olivine. To ensure size equivalence with typical particulates found in supraglacial meltwater (Chikita et al., 2001) and prevent blockage of the cell sorter (nozzle size: 100 μm), all

sediment was dry-sieved to ensure a maximum clast diameter of 63 μm. Clasts were furnaced at 550 °C for 5 hours to combust all organic material (Mook and Hoskin, 1982) and then suspended in Type I Ultrapure water (Elga, UK) at the desired concentration(s). Clast suspensions were subsequently checked for cells using light microscopy after staining with SYBR Gold (Invitrogen, USA) (1 × final concentration) DNA stain to prevent contamination.

These biotic and abiotic isolates were combined at a range of cell and clast concentrations designed to mimic those of glacial meltwaters (Table 4.1; Figure 4.1). All samples were left for ~24 hours to allow for bacterial interaction with clasts as would occur in natural samples. To further examine the role of fixative type upon enumeration accuracy and reproducibility, a pilot study was conducted on 10 samples per cell-type using no fixative, glutaraldehyde and Sodium Azide, in addition to formaldehyde, before creation of the entire sample set. For this pilot study, sediment from Haut Glacier d'Arolla was used throughout. Concentrations ranged from 3.0×10^3 to 1.3×10^5 cells mL^{-1} and 10^{-4} to 10^0 g L^{-1} respectively, with each sample produced in triplicate. Considering the outcomes of this preliminary study, remaining samples were fixed with paraformaldehyde (2 % w/v final concentration) and frozen at -20 °C for a minimum period of five days.

Table 4.1 Isolate-particle matrix listing concentrations, sediment types and bacterial genera of artificial samples under examination.

		Clastic Sediment Concentration (g L^{-1})									
		0		0.001		0.01		0.1		1.0	
Cell Concentration (cells mL^{-1})	0.0	None	None	None	HACH	None	HACH	None	All	None	All
	3.0×10^3	Pol.	None	Pol.	HACH	Pol.	HACH	-	-	-	-
	4.3×10^3	Pol.	None	Pol.	HACH	Pol.	HACH	-	-	-	-
	4.1×10^3	Pol.	None	Pol.	HACH	Pol.	HACH	-	-	-	-
	5.9×10^3	Jan.	None	Jan.	HACH	Jan.	HACH	Jan.	All	Jan.	All
	7.2×10^3	Jan.	None	Jan.	HACH	Jan.	HACH	-	-	-	-
	1.0×10^4	Jan.	None	-	-	-	-	Jan.	All	Jan.	All
	1.2×10^4	Jan.	None	Jan.	HACH	Jan.	HACH	-	-	-	-
	1.8×10^4	Pol.	None	-	-	-	-	Pol.	All	Pol.	All
	2.7×10^4	Both	None	-	-	-	-	Both	All	Both	All
	2.9×10^4	Jan.	None	-	-	-	-	Jan.	All	Jan.	All
	8.2×10^4	Pol.	None	-	-	-	-	Pol.	All	Pol.	All
	8.4×10^4	Pol.	None	Pol.	HACH	Pol.	HACH	-	-	-	-
	1.2×10^5	Pol.	None	-	-	-	-	Pol.	All	Pol.	All
	1.3×10^5	Jan.	None	Jan.	HACH	Jan.	HACH	-	-	-	-

Genus abbreviations: Both = *Polaromonas* and *Janthinobacterium*; Pol. = *Polaromonas*; and Jan. = *Janthinobacterium*.
Sediment abbreviations: All = all sediment types or HACH = Haut Glacier d'Arolla only.

4.2.2 Cytometric Protocol

4.2.2.1 Flow cytometer and settings

FCM measurements were undertaken using a Sony SH-800EC cell sorter (Sony Bioscience, Japan), configured with three excitation lasers (405, 488 and 638 nm), and eight detectors, incorporating six fluorescence detectors, forward scatter (FSC) and back scatter (BSC, equivalent to side scatter, SSC, on other instruments). The wavelengths for the six fluorescence detectors are determined by the optical filter pattern (OFP) of the instrument, for this study the default pattern, OFP1, was used (Table 4.2). The instrument employs a disposable "Sorting Chip" with an optional nozzle diameter of either 100 or 130 μm, which influences the flow core size and flow rate, the latter also taking into consideration user-selectable "sample pressure". This study used the 488 nm laser and a 100 μm sorting chip, enabling flow rates of 6 – 89 μL min^{-1}; Sony do not provide data on flow core sizes. Sample acquisition and data analyses were performed using the proprietary Sony Cell Sorter Software, digitising scatter (height, width and area) and fluorescence (area only) parameters over a six-decade logarithmic scale (Figure 4.2). Notable contrasts between the instrument and more commonly used cytometers (such as the BD Biosciences Accuri C6 (BD Biosciences, UK) and derivates) is the reduced data collection scale, use of BSC instead of SSC and the existence of a sorting chip within the instrument rather than a flow cell which requires periodic cleaning. The sorting chip was replaced, auto-aligned and calibrated daily, using 8-peak reference beads (Sony Biotechnology, Japan) as per the manufacturer's instructions.

Table 4.2 Fluorescence detectors for the Sony SH-800EC configured using Optical Filter Pattern 1.

Detector	Wavelength (nm)
FL1	525 ± 50
FL2	585 ± 30
FL3	617 ± 30
FL4	665 ± 30
FL5	720 ± 60
FL6	785 ± 60
FSC	488 ± 17
BSC	488 ± 17

Instrumental threshold settings are applied to allow for the removal background noise, comprised of low-level signals that occur within the electronics and stray light collected by the optics. Noise can also occur from the liquid phase of the sample under test and is inherent to all samples and cytometry as a technique (Shapiro, 2003). Once an event results in a signal above the threshold, an "event" is recorded (Figure 4.2). Setting of thresholds was undertaken for the FSC channel, with thresholds being instrument, environment, and sample-type specific, and were established using 1 μm size-calibration beads (Molecular Probes, USA) suspended in Ultrapure Water (Elga) ensuring enumeration of small particles whilst the threshold remained above the "noise floor". Thresholding was undertaken in the FSC channel, set at 0.05 % with a gain setting

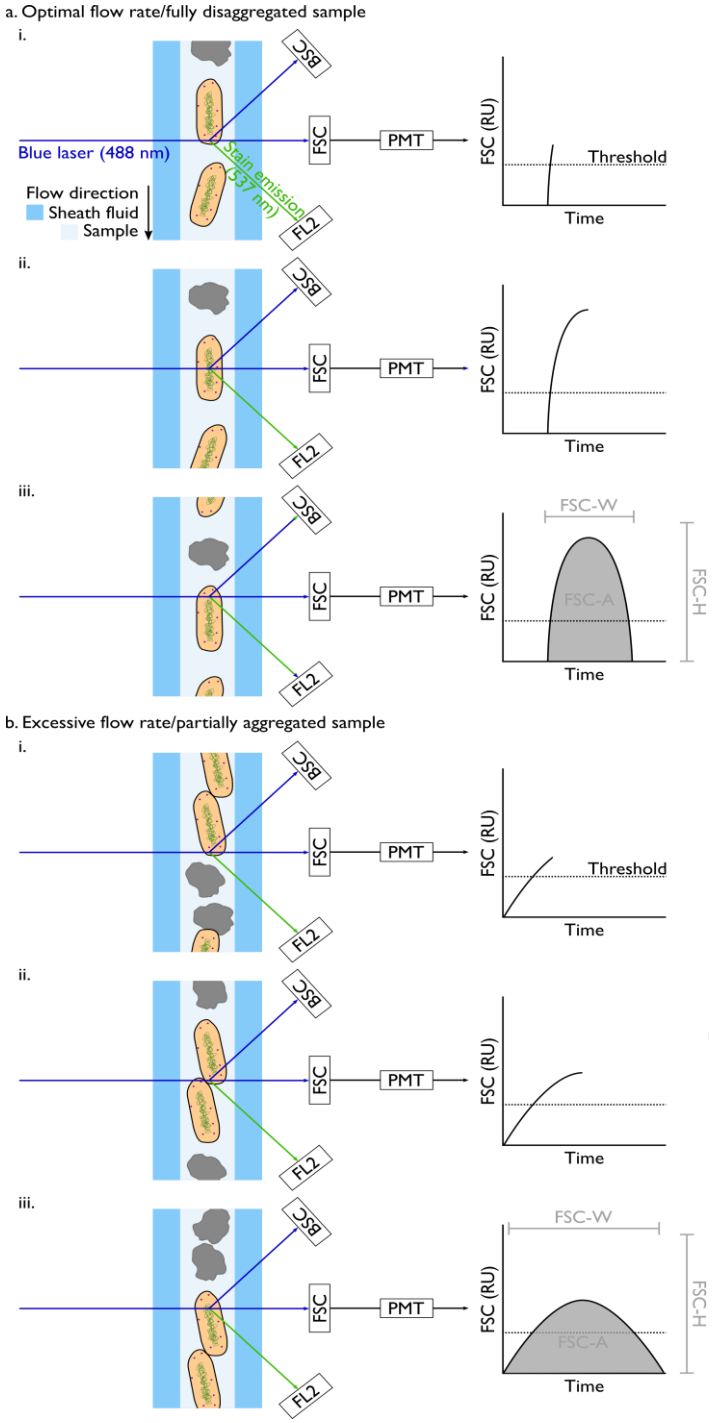

Figure 4.2 Schematic demonstrating the automated process of "event" measurement using flow cytometry. In 4.2a·i-iii, a single microbial cell, contained within the sample medium (dark blue; usually water) is entrained within the "flow core" and hydrodynamically focussed by the sheath fluid (light blue). Between i – iii, the cell passes the laser, which is either scattered at a small angle (typically 0.5 – 2.0 °); FSC, or an orthogonal (90 °) angle; BSC (aka SSC), which are crudely proportional to cell size (Mullaney et al., 1969) and internal cell complexity (Salzman et al., 1975) respectively. In this example, nucleic acids are stained using SYBR Gold, which is maximally excited at a wavelength of 498 nm and emits maximally at 537 nm, measured in FL2 for the SH-800EC using OFP1 (Table 4.2). Other stains will have different emission and excitation wavelengths. Signals are amplified by a photomultiplier tube (PMT), the sensitivity of which can be adjusted in the instrument settings. When intensity of the signal crosses the set threshold, an event is recorded. In this experimental set-up, FSC was used as the "trigger channel", which means that once the threshold is crossed in this channel all parameters (FSC, BSC, FL2) of an event are recorded. 4.2b·i-iii demonstrates the effects of a sample which is not fully disaggregated, are above the optimal detection concentration, or for which the flow rate is set above the optimal rate. "Clumped" particles (either cell-cell, as in this example, or cell-clast/clast-clast or multiples thereof) occur in these situations and can be identified using the FSC-A and FSC-H signals (compare the signal graphs 4.2a·iii and 4.2b·iii; see Figure 4.4a). To reduce the number of clumped particles, further disaggregation, dilution or reduction of the flow rate can be undertaken. However, cells which are aggressively disaggregated may lyse, over-diluted samples may fall below the detection rate of the instrument being used, and low flow rates increase the time taken to measure an appropriate sample volume (400 - 1500 µL).

of 1. Once established, thresholds were re-examined twice daily to account for instrumental drift; however, no adjustments were deemed necessary during sample analysis.

4.2.2.2 Stain selection

The nucleic acid stain used was SYBR Gold (Invitrogen, USA) at 1 × final concentration. SYBR Gold is an unsymmetrical cyanine dye, exhibiting > 1000 × signal enhancement when bound with nucleic acids, increasing the signal to background ratio enhancing the ability to discriminate between stained and unstained particles. When bound to double- or single-strand DNA, or to RNA, the quantum yield is ~0.6 (Tuma et al., 1999), comparing favourably to SYTOX green (~0.53) (Roth et al., 1997), used by Santibanez et al. (2016). In contrast, SYBR Green I, a monomeric unsymmetrical cyanine dye which has been widely used for microbial enumeration in aquatic ecosystems (e.g. Gasol and Del Giorgio, 2000), has a higher quantum yield for double-strand DNA (~0.8), but lower for single-strand DNA and RNA (~0.4). (Invitrogen). Despite this apparent favourability of SYBR Green I, SYBR Gold is recommended as the most sensitive DNA stain for detection of small masses of DNA by the manufacturer, hence its application herein.

4.2.2.3 Sample pre-treatment and analysis protocol

The analysis protocol is summarised in Figure 4.3. Samples were defrosted at room temperature (see Santibanez et al., 2016) for further consideration of sample defrosting procedures) and vortexed for ≥ 30 seconds to disaggregate cell-cell and cell-clast agglomerations. Two 1 mL aliquots of each sample were taken in a sterile flow hood, with one of these samples stained within 5 minutes using SYBR Gold (1 × final concentration). Both experimental aliquots were stored in the dark at 20 °C for a between minimum of twenty minutes and a maximum of four hours prior to enumeration to allow for complete staining and to prevent bleaching of the photosensitive stain.

Experimental aliquots were analysed using the Sony SH-800EC described in section 4.2.2.1, using the 488 nm blue laser for sample excitation, with measurement in the FSC-A, FSC-H, FSC-W, BSC-A and FL2 channels (Table 4.2). Unstained and stained experimental aliquots were measured in batches of four to prevent cross-over of stain with blank samples of Ultrapure water examined between batches to monitor cytometer cleanliness and background drift. An automated cleaning procedure was carried out between measurement of each experimental aliquot. Immediately prior to measurement, all experimental aliquots were vortexed for ≥ 30 seconds to ensure disaggregation of particles and even dispersal of cells throughout the suspension.

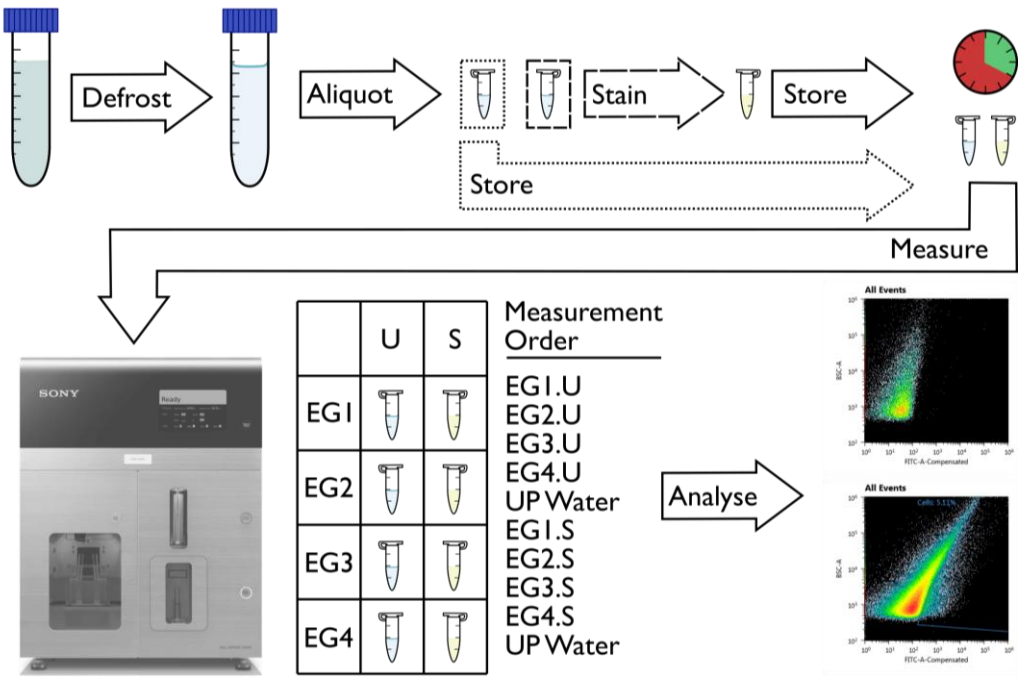

Figure 4.3 Flow chart indicating sample analyses procedures, from a frozen sample to in-software analysis. 1) Samples are defrosted at room temperature in the dark. 2) 2 × 1 mL aliquots of sample are taken in a sterile flow hood. 3) One aliquot is stained using SYBR Gold (1 × final conc.). 4) Experimental aliquots are stored in the dark at room temperature for up to 4 hours prior to measurement. 5) Measurement is undertaken in the order outlined using the Sony SH800-EC. 6) Data is analysed using the proprietary Sony software. Prior to stage 2 and 5, sample sand experimental aliquots were vortexed for a minimum of 30 seconds.

A minimum volume of 400 µL of sample was analysed at a flow rate which represented a compromise between short duration and ensuring the event rate remained within detection limits of < 20,000 events per second (eps), and ideally beneath the "optimal rate" of 10,000 eps. Low flow rates are typically used for dense cell samples to reduce co-incident events (Figure 4.2b) which are associated with under-enumeration of microbial cells, whilst higher flow rates can be used for samples with lower cell density (Gasol and Del Giorgio, 2000; Shapiro, 2003). Typical flow rates used herein range from 21 µL min^{-1} to 63 µL min^{-1}, with minimum time periods for analysis of 400 µL ranging from 19:02 to 4:29 minutes. Whilst flow rate is a critical parameter influencing cell detection (Shapiro, 2003), Santibanez et al. (2016) report negligible variations in cell concentration estimates using a flow rates between 14 and 66 µL min^{-1}, presumably due to the low cell density of glacial cell samples.

From FCM measurement data, microbial cells were discriminated from clastic sediments using a multi-stage gating technique, designed to eliminate non-nucleic acid containing material from counts, and examine the degree of flocculation of cells and clasts. Firstly, experimental aliquots were examined for the presence of aggregates. Comparison of FSC-A and FSC-H on a linear-linear plot can identify clumping; non-clumped events demonstrate a linear correlation (BD

Biosciences, 2012) (Figure 4.4a). Samples which demonstrated significant clumping (≥ 5 % events) were re-vortexed and re-measured, which resolved the issue of excess aggregation in all cases. Secondly, to discriminate microbial cells, gating was undertaken using the BSC and FL2 channels on a log-log axes using gates determined via the comparison of stained and unstained sample pairs (Figure 4.4b and c). By comparison of stained and unstained paired samples, non-nucleic acid containing material can be "gated out" and removed from the enumeration, reducing the possibility of overestimation of microbial cells (e.g. Irvine-Fynn et al., 2012)). Thirdly, events defined as being microbial cells were then analysed for size, using gates were determined using a non-fluorescent size calibration kit (Molecular Probes, USA) allowing the identification of microbial cells into seven size bins (≤ 1 μm, 1-2 μm, 2-4 μm, 4-10 μm, 10-15 μm and 15 ≤ μm). Beads were analysed as per the manufacturer's instructions, with discrimination in the FSC channel.

Cell concentrations in experimental aliquots were calculated as per Equation 4.1, and accuracy estimates as per Equation 4.2, where E_{cells} is the number of cell events, FR flow rate (mL min^{-1}), FD flow duration (min), and CC_{obs} and CC_{exp} are the concentrations of cells measured

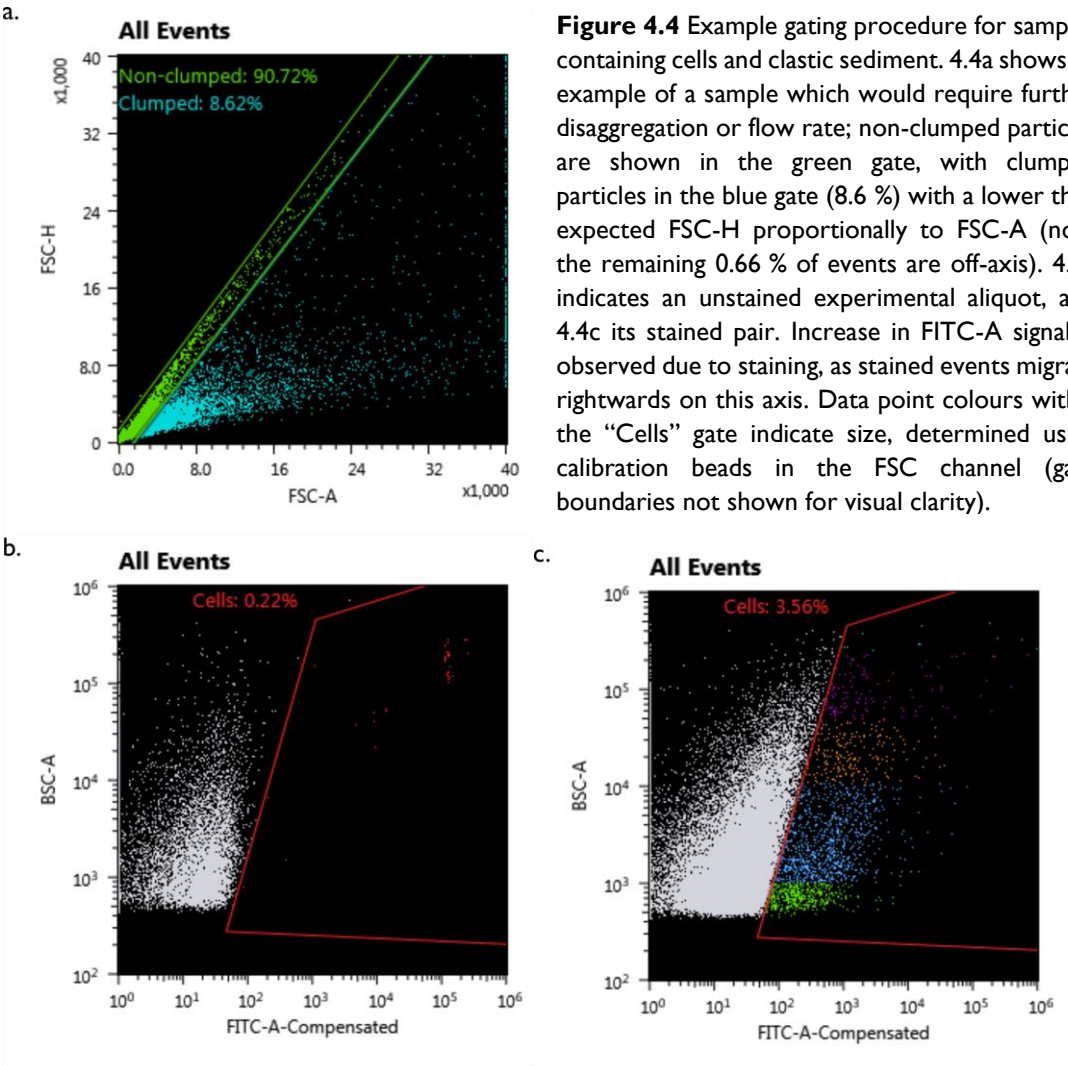

Figure 4.4 Example gating procedure for samples containing cells and clastic sediment. 4.4a shows an example of a sample which would require further disaggregation or flow rate; non-clumped particles are shown in the green gate, with clumped particles in the blue gate (8.6 %) with a lower than expected FSC-H proportionally to FSC-A (note the remaining 0.66 % of events are off-axis). 4.4b indicates an unstained experimental aliquot, and 4.4c its stained pair. Increase in FITC-A signal is observed due to staining, as stained events migrate rightwards on this axis. Data point colours within the "Cells" gate indicate size, determined using calibration beads in the FSC channel (gate boundaries not shown for visual clarity).

and expected to be contained within the sample respectively (mL^{-1}). Note that "accuracy", whilst reported as a percentage, is in fact a comparative value between cells expected and cells observed; and hence can exceed 100%. Mineral concentrations were not estimated via FCM; a multitude of sedimentary techniques exist for measurement of this variable if desired.

$$CC_{obs}\ (mL^{-1}) = \frac{E_{cells}}{FD \times FR} \quad \text{[Equation 4.1]}$$

$$\text{FCM accuracy } (\%) = \frac{CC_{obs}}{CC_{exp}} \times 100 \quad \text{[Equation 4.2]}$$

4.3 Results

4.3.1 Pilot study: effect of fixative on enumeration accuracy

The pilot study exploring fixatives did not show any discernible difference in final cell concentration accuracy (< 5 % variation), and two ANOVA tests revealed that for each cell genera, there was no significant different in enumeration accuracy when using different fixative ($p > 0.05$, $n = 40$ in both cases). Paraformaldehyde was used for the entire sample set due to its recommended use within the literature for similar sample types (see (Duhamel and Jacquet, 2006)). Whilst no fixative could have been used as the recommended protocol, this was discarded as a solution due to the desire for long-term storage (i.e. ≥ 12 months) of environmental samples; the suggested low temperature limits for cold-adapted organisms are -12 °C for reproduction and -20 °C for metabolism (Bakermans, 2008).

4.3.2 Enumeration accuracy

Mean cell concentration accuracy for the entire dataset was 160.0 ± 16.4 % ($n = 120$); with a mean relative standard deviation of 10.3% for each triplicate sample set. However, prominent variations are observed within this dataset, with accuracies covering a range of 29.6 to 486.3 %. *Janthinobacterium* bearing samples demonstrated a higher mean accuracy of 180.4 ± 15.7 % in contrast to *Polaromonas* bearing samples with a mean accuracy of 139.7 ± 16.5 %. To further evaluate the role of cell genera in accuracy estimates, a two-tailed independent t-test indicated that genera does not significantly influence accuracy of FCM in cell enumeration at the 5 % significance level ($p > 0.05$, $n = 120$). Furthermore, the type of clastic sediment in the sample does not significantly influence the accuracy of microbial enumeration using FCM for samples containing 10^{-1} and 10^{0} g L^{-1} of sediment, as demonstrated by a one-way ANOVA ($p = 0.928$, $n = 96$). Only

samples containing 10^{-1} or 10^{0} g L^{-1} of clastic particles were included to eliminate effects of sediment concentrations ≤ 10^{-2} g L^{-1}, for which only HACH clasts were used.

Clastic sediment concentration plays a key role in the determination of accuracy (Figure 4.5); samples with an abiotic particle concentration ≤ 10^{-2} g L^{-1} do not exceed the region of acceptable accuracy except in the one instance, whereas the highest overestimates of microbial concentration occur and sediment concentrations of 10^{-1} and 10^{0} g L^{-1}. This phenomenon is less apparent in the case of cell concentrations, for which there is no clear trend. However, large overestimations of cell numbers are most prevalent at lower cell concentrations, with a maximum overestimation of a factor of ~5 for samples with 5.9 x 10^{3} cells mL^{-1} of *Janthinobacterium*, highlighting the importance of the ratio between cell and sediment concentration in determining

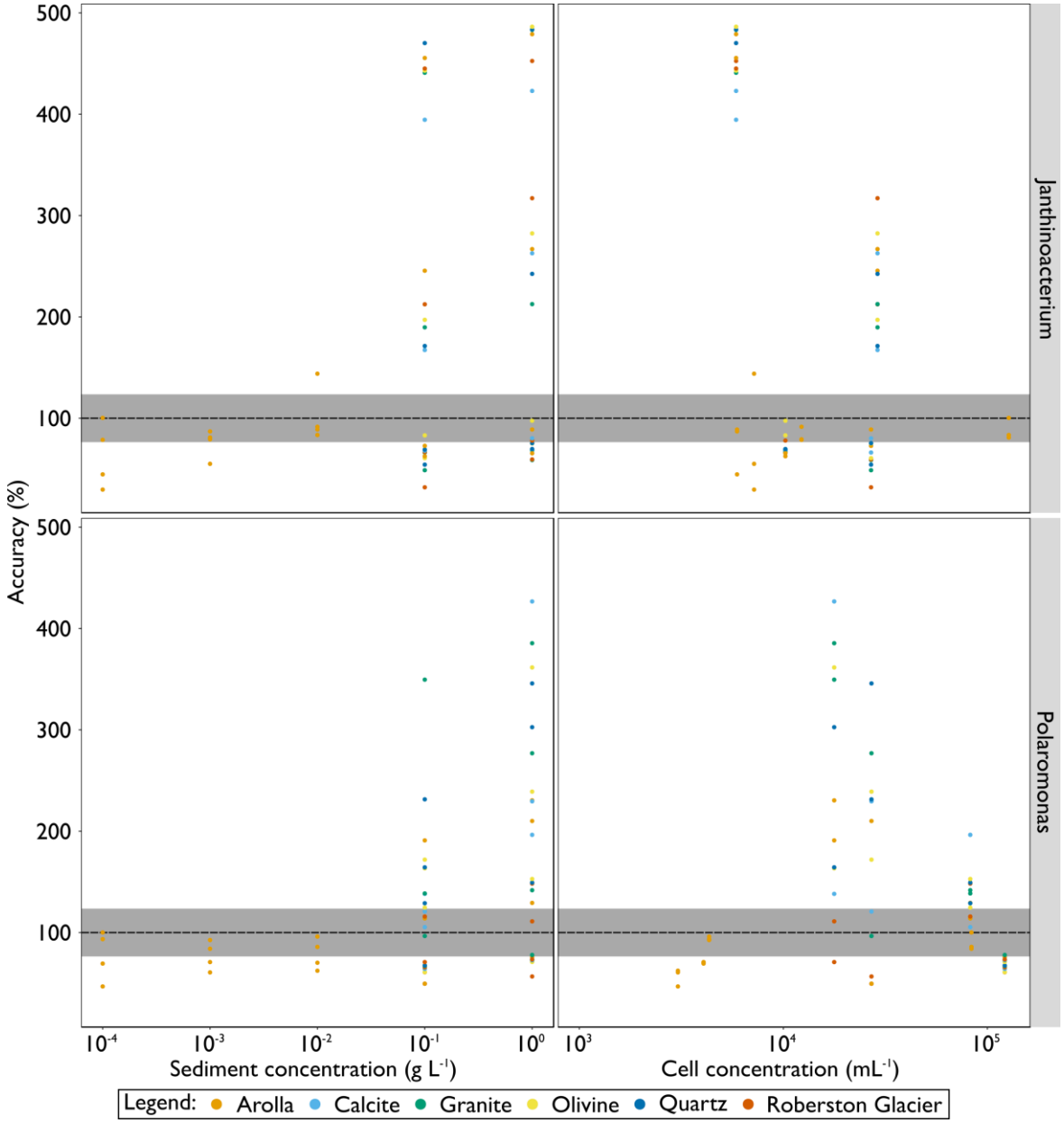

Figure 4.5 Accuracy scores (%) as a function of sediment and cell concentration, considering the role of cell and sediment type. The grey section of each plot indicates the 100 ± 25 % region of acceptable accuracy.

enumeration accuracy. This ratio, CC-APC (cells g^{-1}, Equation 4.3), also acts to determine the accuracy of samples (Figure 4.6); the majority of samples with a CC-APC > 500 demonstrate acceptable accuracy scores, however it should be noted that many samples with CC-APC values < 500 also fall within this window, typically those of lower sediment concentrations. These criteria are observed across both cell genera, with no clear pattern linked with sediment type.

$$\mathrm{CC-APC} = \frac{\text{Cell concentration (cells } mL^{-1})}{\text{Sediment concentration (g } mL^{-1})} \quad \text{[Equation 4.3]}$$

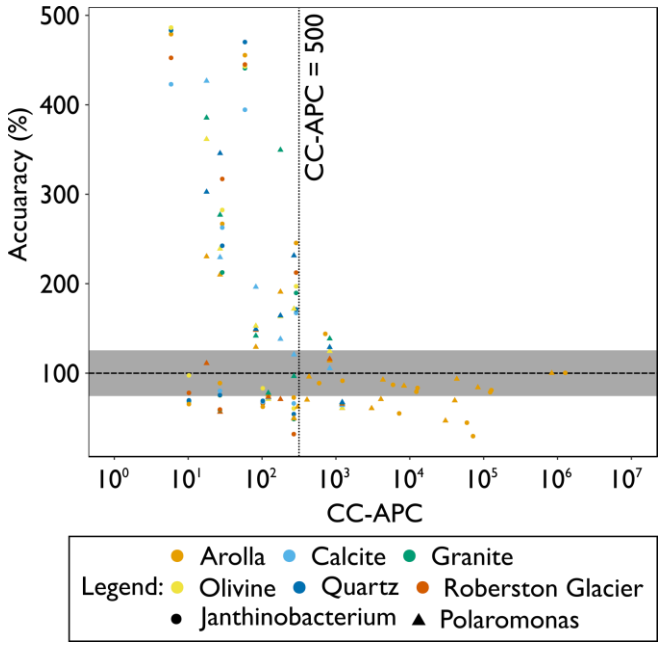

Figure 4.6 Accuracy scores as a function of CC-APC, highlighting the area of acceptable accuracy (100 ± 25 %, grey) and CC-APC enumeration threshold determined by this study.

4.3.3 Cell size distribution

Size distributions were successfully determined for all samples, alongside a series of cell-only control samples (n = 48) (Figure 4.7). The modal size class is a cell diameter of 1 to 2 µm, comprising over 50 % of events in all cases, with 10 µm to 15 µm the least common class. Typically, artificial samples containing both cells and clasts have a greater proportion of events in the 4 to 10 µm class, and fewer in the < 1 µm range than the cell only controls. Note that whilst present, these differences are within the range of one standard deviation.

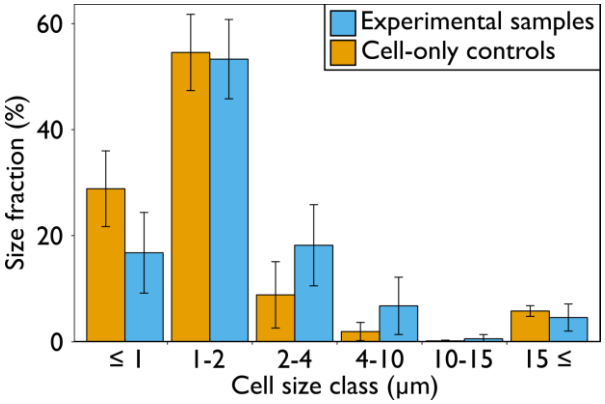

Figure 4.7 Mean size distributions for cell events for cell only control samples (n = 48) and mixed media experimental samples (n = 359). Error bars represent ± 1 standard deviation.

4.4 Interpretation and Discussion

4.4.1 Accuracy and precision

This study reports a mean cell enumeration accuracy exceeding 100 % for samples containing ≤ 10^{0} g L^{-1} of abiotic particles, with a relative standard deviation between triplicate repeats of ~10 %; however, when certain criteria are satisfied FCM can be applied to enumerate glacial samples to an acceptable degree of accuracy (and precision). Samples ≤ 10^{-2} g L^{-1} exhibit accuracies almost exclusively below 100 % (in contrast to samples which contain ≥ 10^{-2} g L^{-1} of sediment particles), implying that primarily cellular material is enumerated within the cell gate in these instances. At higher abiotic particle concentrations, samples with enumeration accuracies < 100% are observed, but higher accuracy values > 150 % are found exclusively at abiotic particle concentrations ≥ 10^{-1} g L^{-1} (Figure 4.5). Regarding the role of cell concentration upon accuracy scores, no clear trend is observed for either *Polaromonas* or *Janthinobacterium*. Samples with an acceptable level of accuracy and precision are observed throughout the range of cell concentrations. As such, this study demonstrates that FCM is an appropriately robust technique for the enumeration of glacial cells when abiotic particulate load is ≤ 10^{-2} g L^{-1}, regardless of cell concentration. At greater sediment loads, the technique should be applied with care and the following guidelines should be considered:

- the ratio of cells and clastic sediments (CC-APC) should be examined;
- utmost caution is required in gating strategy;
- and the concurrent application of alternative enumeration techniques may be advisable.

4.4.2 Environmental applicability

The cell concentrations tested herein align well with those of the supraglacial environment; contemporary observations suggesting 2×10^3 to 2×10^6 cells mL^{-1} in stream, cryoconite waters and surface ice in samples collected in Greenland, Svalbard, the European Alps and Antarctica (Amato et al., 2007; Anesio et al., 2010; Foreman et al., 2007; Hodson et al., 2013; Irvine-Fynn et al., 2012; Mindl et al., 2007; Santibanez et al., 2016; Säwström et al., 2002; Stibal et al., 2015). Note that this range of cell concentrations presented does not include the substrate found within cryoconite holes (which is included in Anesio et al. (2010)), only estimates from the water within the hole which is hydrologically connected to the weathering crust. Considering sediment concentrations, the methods presented herein are well suited to glacial surface environments, including supraglacial streams and glacier ice, with typical sediment concentrations of $\leq 10^{-2}$ g L^{-1} (Skidmore et al., 2000); but could also be applied with caution in subglacial environments ($\geq 10^{-1}$ g L^{-1}; Skidmore et al., 2000). Furthermore, under certain conditions of low sediment concentrations, FCM may also be suited to proglacial systems; for example, sediment concentrations as low as 2 and 5×10^{-2} g L^{-1} have been reported in Greenland (Bartholomew et al., 2011) and the European Alps (Collins, 1979) respectively. Glacier thermal regime will influence proglacial sediment loads due to differential erosion rates, with cold-based ice masses yielding lower sediment perennially (Hodson et al., 1997), whilst warm based glaciers exhibit greater, but seasonally variable sediment loads which correlate positively with discharge (e.g. Stott and Mount, 2007). Thus, caution should be applied with any potential study considering cell concentrations using FCM in proglacial streams, but the technique demonstrates for potential at cold-based glaciers and/or during periods of low proglacial suspended sediment load. Englacial samples also fall within this range of sediment concentration where FCM is suitable, with observed abiotic particle concentrations of $\leq 5 \times 10^3$ g L^{-1} in Greenland and Antarctica (Bøggild et al., 2010; Karl et al., 1999; Miteva et al., 2009; Priscu et al., 1999; Svensson et al., 2000).

This study highlights a minimum ratio between cell concentration and abiotic particle concentration (CC-APC; cells g^{-1}) for acceptable levels of cell enumeration accuracy using FCM. For cell enumeration accuracy to be satisfactory, CC-APC must ≥ 500. For the CC-APC criterion to be met, when sediment load is 10^{-2} g L^{-1}, cell concentration must $\geq 5 \times 10^3$ cells mL^{-1}, with cell concentration increasing with linear proportionality to sediment load. For example, a cell concentration $\geq 5 \times 10^4$ cells mL^{-1} is required when sediment load is 10^{-1} g L^{-1}, and so on. Paradoxically, CC-APC cannot be determined without knowledge of the cell and sediment concentration, although with measurements of the latter the minimum cell number required for a CC-APC ≥ 500 can be calculated and considered in comparison with existing environmental

estimates of microbial cells. Whilst FCM is not suited to the calculation of sediment loads due to differing sizes, shapes density clasts, which prevents conversion from the commonly used g L^{-1} unit to a particles mL^{-1} unit, a two-order of magnitude difference was observed in clast counts for samples with differing particle loads. Samples with abiotic particle concentrations of 10^{-1} g L^{-1} yielded a mean non-cell event count of $1.2 \times 10^6 \pm 2.2 \times 10^6$ mL^{-1} in contrast to $5.3 \times 10^4 \pm 1.5 \times 10^4$ mL^{-1} for samples with a sediment concentration 10^{-2} g L^{-1}. These non-cell event counts suggest that samples that may not meet the CC-APC criterion due to high sediment loads could be initially discerned via FCM and subsequently analysed for sediment concentration in an appropriate manner to ensure that the CC-APC criterion is met. It should be noted that whilst high confidence can be placed in FCM to accurately enumerate samples with a CC-APC ≥ 500, samples with CC-APC values beneath this threshold may be enumerated to a satisfactory level of accuracy when sediment concentrations are ≤ 10^{-2} g L^{-1}.

4.4.3 Comparison with prior cell enumeration evaluations

Throughput the entire range of samples examined herein, accuracy scores exceed those of other similar works by a factor of ~2 (e.g. (Stibal et al., 2015)), representing a development of FCM when applied to supraglacial environments and offering it as a reliable and advantageous alternative to the widespread EFM. However, an acceptable range of application for FCM to the supraglacial environment is suggested, that is for samples with an abiotic particulate load ≤ 10^{-2} g L^{-1} OR an APC-CC ≥ 5×10^5 (note that all samples with an abiotic particulate load of ≤ 10^{-2} g L^{-1} also satisfied the APC-CC criterion) for which accuracy scores are 83.6 ± 6.0 % (n = 36); an RSD of 7 %. This compares favourably to the work of (Stibal et al., 2015), who reported accuracies of 50 ± 16 % (RSD 32 %) for EFM, 18 ± 15 % (RSD 87 %) for FCM, and 32 ± 17 % (RSD 53 %) for qPCR for samples with concentrations equal to those examined herein. Note that the lower-end acceptable range of FCM, or 'practical minimum detection limit' is 10^2 cells mL^{-1} (Santibanez et al., 2016), lower than the minimum cell concentration tested herein.

Our accuracy scores with the determined acceptable range of application for FCM compare well with other environments, such as streambed (Amalfitano and Fazi, 2008), coastal (Lavergne et al., 2014) and lake (Duhamel and Jacquet, 2006; Tennant et al., 2013) sediments; sludge (Falcioni et al., 2006; Foladori et al., 2007; Frossard et al., 2016); and natural (Frossard et al., 2016) and agricultural (Bressan et al., 2015) soils, which report a range of cell yields (equivalent to our accuracy scores) of 83 – 93 % via FCM. In contrast, lower yields (64 %) were reported via plate counts (Bressan et al., 2015) and EFM (Duhamel and Jacquet, 2006; Lavergne et al., 2014); no figures

provided) than FCM. As such, this protocol falls within the window of an equivalent level of accuracy to other environments.

We report a mean RSD of 7 % between triplicate replicates within the range of application for FCM. Similar work with triplicate samples by (Hammes et al., 2008) suggest an RSD of 5 % for water samples analysed by FCM, in contrast to plating (Allen et al., 2004), imaging (Vital et al., 2007) (both > 10 %) and qPCR (2 – 10 %) (Boon et al., 2003; Wang et al., 2010). RSDs were > 10 % for EFM, FCM and qPCR when applied by (Stibal et al., 2015); hence the protocol we describe gives satisfactory levels of precision. This protocol offers greater accuracy for supraglacial samples than other methods applied in the cryosphere to-date, and an equivalent level of accuracy and precision to those in other environmental samples containing sediment. Considering reproducibility, this protocol compares favourably with techniques applied for drinking water examination.

4.4.4 Over- and underestimation of cell concentration

Overall, this study presents favourable accuracy figures for the application of FCM to the supraglacial environment. However, both over and underestimation of cell concentrations are observed (Figures 4.5 and 4.6). Factors which influence accuracy scores are a) pre-analysis cell lysis and/or replication; b) imprecise gating procedures resulting in the inclusion of abiotic particles in the cell gate; c) stain efficacy; and d) aggregation of cells with each other, abiotic particles, or both.

Replication is excluded as a mechanism for overestimation of cell populations due to the application of fixative to the samples. Formaldehyde is fast acting, preventing cell replication in substantially less than published population doubling times for cryospheric bacteria which are in the order of days (Anesio et al., 2010). Cell lysis, whilst common in cryospheric environments due to viral action (Anesio et al., 2007; Säwström et al., 2007) is not thought to play a key role in the outcome of this experiment. Firstly, cell fragments would be expected to be smaller than intact cells; conversely Figure 4.7 shows greater proportion in mixed samples of larger events than cell only controls, with ~12 % fewer events in the ≤ 1 μm size class, and ~2 % fewer events in the modal 1 μm – 2 μm class, implying that cell lysis has not occurred in the created of the artificial samples. Secondly, fragmented or degraded cells exhibit a unique FSC/BSC footprint (Irvine-Fynn et al., 2012) which was not observed. As such, cell lysis and replication can be excluded as a cause of over and underestimation estimation of cell populations.

Abiotic particles located with the cell gate are the most probable cause of cell population overestimation. Conventionally, cells are discriminated from electronic background noise and abiotic particles via the use of nucleic acid stains; this study uses SYBR Gold (Invitrogen, USA). Despite staining, and the clear discrimination of the stained cell population in comparison to unstained samples, there is an overlap in the maximum extent of gates for stained cell-only samples and abiotic particle only samples (Figure 4.8). However, the crossover region is located on the extremes of each gated region, including only rare events limiting this effect, with at most tens of thousands (from hundreds of thousands to millions) of abiotic particle events counted within the cell gate. Overestimation is most prevalent at higher (10^{0} and 10^{-1} g L^{-1}) abiotic particle loads, as would be expected for this hypothesis. Furthermore, some lipophilic dyes can stain abiotic particles (Müller and Nebe-von-Caron, 2010) which may contribute to this phenomenon. Further contribution is made by intrinsic autofluorescence of particles and non-specific binding of stain to clay particles (Klauth et al., 2004; Morono et al., 2009). In all these cases, the quantum yield of nucleic acid stains is lower than if bonded to a nucleic acid; however large, stained clastic particles appear to fluorescence at an intensity akin to small cells with limited DNA (Figure 4.8).

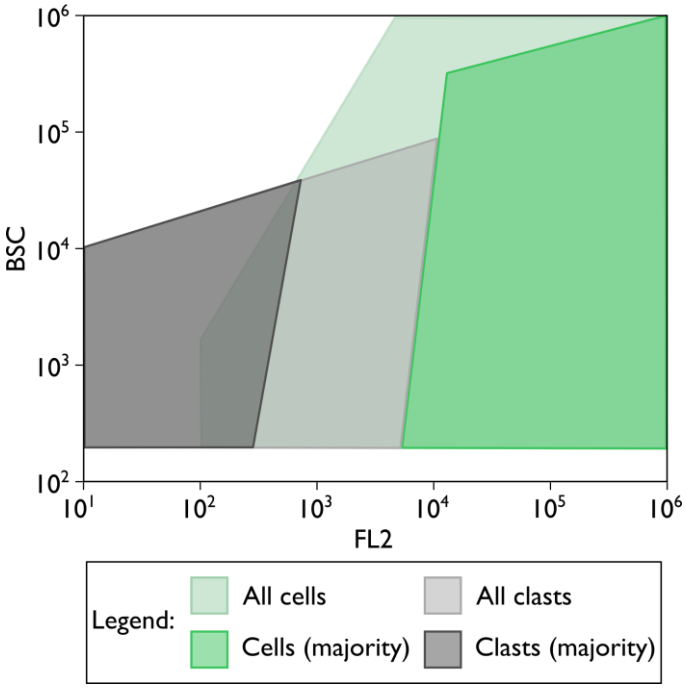

Figure 4.8 Crossover regions of typical gates for cells and clastic sediment. The potential for masking of rare cell events by rare clast events is demonstrated by the intersecting gates for population extremes, one cause of under- and overestimation of cell concentrations, demonstrating the importance of tight gate positioning.

The primary cause of underestimation of cell enumeration is the formation of aggregates of cells with each other and clastic particles; bacteria commonly grow in colonies and biofilms in nature with only a small element observed as planktonic cells (Nadell et al., 2009; Pamp et al., 2009). The result of the formation of these aggregates is the reduction in the apparent number of cell events, as multiple cells are recorded as a singular cell event. It would be hypothesised that this phenomenon may occur more readily for *Janthinobactium* than for *Polaromonas*, as, in liquid environments, the species *J. lividum* forms extended biofilms via the production of

exopolysaccharides (EPS) during periods of cell stress (Pantanella et al., 2007) which is likely their dominant condition in the cold, nutrient poor cryosphere (Irvine-Fynn et al., 2012). However, no statistically significant links were observed between cell genera or sediment type on accuracy, indicating that whilst microbe-mineral interactions may differ dependent upon the cell genera or substrate, this study does not provide evidence to this end.

Bacterial aggregate formation is also promoted by slow-acting -aldehyde fixation (e.g. glutaraldehyde), enabling cells to produce EPS, or other high molecular weight compounds, to protect themselves against such chemicals (Müller and Nebe-von-Caron, 2010). This phenomenon was, however, not apparent in the preliminary fixative study, with no difference in accuracy observed as a function of fixative type. Therefore, formaldehyde is identified as the preferred fixative; glutaraldehyde is prone to polymerisation, (Rasmussen and Albrechtsen, 1974) with a corresponding loss of antimicrobial activity (Gorman et al., 1980) and may not permeate all gram-negative cells (Bullock, 1984); and ethanol fixation can cause elution of lipids in the cell membrane, altering cell structure (Salton, 1963) and preventing reliable cell-size analyses. Long-term storage requirements mean that the application of no-fixative does not represent a viable solution, as cold-tolerant microbes may remain in a state of dormancy even at -80 °C.

Cell-cell and cell-particle aggregation is the implied cause of the < 100 % accuracy scores for samples within the acceptable application window. The larger proportion of events in the $2 - 4$ μm and $4 - 10$ μm size classes (Figure 4.7) indicates a presence of larger material than observed in the cell only samples; with a reduction of < 1 μm material indicating a net increase in size, hypothesised as the formation of aggregate material. As formaldehyde was added to both cell-only controls and mixed-media samples this cannot have directly caused this size disparity, even if the fixative acted to alter cell size. Hence, this study interprets this shift in particle size as the formation of aggregates, which has potential to be reduced via disaggregation procedures.

Disaggregation procedures are common in other environmental applications of FCM but are not without drawbacks. Techniques can be chemical or physical: sodium pyrophosphate (or other phosphate solutions (Riis et al., 1998)), polysorbate, Tween 80, Histodenz®, shaking, sonication (Boenigk, 2004; Buesing and Gessner, 2002) and centrifugation have been applied to isolate bacterial cells and virus-like particles from abiotic particles (Amalfitano and Fazi, 2008; Boenigk, 2004; Bressan et al., 2015; Duhamel and Jacquet, 2006; Falcioni et al., 2006; Foladori et al., 2007; Frossard et al., 2016; Lavergne et al., 2014; Tennant et al., 2013). Chelating agents such as sodium pyrophosphate weaken electrostatic and chemical forces attaching cells to particles and shaking and sonication releases cells entrapped in micropores (Müller and Nebe-von-Caron, 2010).

Whilst increasing cell yields, such detachment protocols can prove damaging to cells (Amalfitano and Fazi, 2008), and sonication has proven to cause disintegration of large proportions of *E.coli* cells (Foladori et al., 2007) as well as leading to the selective loss of filamentous organisms (Müller and Nebe-von-Caron, 2010) which are prevalent in cryoconite aggregates (e.g. (Langford et al., 2010)). Therefore, these procedures were not tested due to the requirement to assess cell size, for which cells must remain intact.

Stain efficacy is considered to play minimal role in this outcome of experiment. Primarily, a rightward-shift in events along the FITC (FL2) axis of the FCM output, covering the emission spectra of SYBR Gold (~525 nm), is clearly observed between stained and unstained samples containing both mixed media and cellular material exclusively. Secondly, SYBR Gold is considered more sensitive than many commonly used alternatives, such as ethidium bromide, DAPI and SYBR Green I and II for detecting DNA and RNA (Marie et al., 1997; Tuma et al., 1999), with previous successful application for bacterial and viral enumeration in marine environments (e.g. (Chen et al., 2001; Shibata et al., 2006)).

4.5 Conclusions

This chapter presents a protocol for the enumeration of cells within supraglacial meltwater samples with potential to expand to analysis of low-sediment proglacial systems. FCM is reliable and faster than alternative methods previously tested within this environment (i.e. EFM and qPCR), and its application is key to the expansion of current microbial abundance datasets in this rapidly-developing field and provides a fundamental basis for supraglacial microbiology studies. A key determinant of the accuracy of FCM for enumeration of these samples is the abiotic particulate concentration; the data herein indicates that this protocol is suitable for samples with a) abiotic particle concentration $\leq 10^{-2}$ g L^{-1}, regardless of cell concentration (providing the cell concentration is above the detection limit of the instrument used, typically 10^2 cells mL^{-1}) or b) the ratio of cells to clastic particles (CC-APC) is > 500 cells g^{-1}. When the CC-APC is below this threshold, large clasts and smaller cells overlap on the FSC/FL2 output plot and sedimentary material is observed with the cell gate which causes overestimation of cell numbers. These criteria correspond with expected clastic sediment and microbial cell concentrations in supraglacial environments. Cell genera and abiotic particle type do not appear to influence accuracy scores, and large particles (> 15 μm) are observed in all samples implying the formation of aggregates for all abiotic particle and cell mixes.

When the accuracy criteria are met, FCM presents a viable, accurate and reproducible method of quantifying water-suspended cells in supraglacial environments and can be further expanded to the proglacial environment under certain conditions, if pre-analysis of sample sediment concentration is undertaken. This protocol provides mean cell enumeration accuracy of 83.6 ± 6.0 %, comparing favourably with EFM and qPCR, in addition to previous trials of FCM (Figure 4.9). Therefore, the enumeration method presented is well suited to enumeration of cryospheric bacteria within surface samples allowing for the development of future research to examine microbial numbers and fluxes within the near surface of melting ice masses on a global scale.

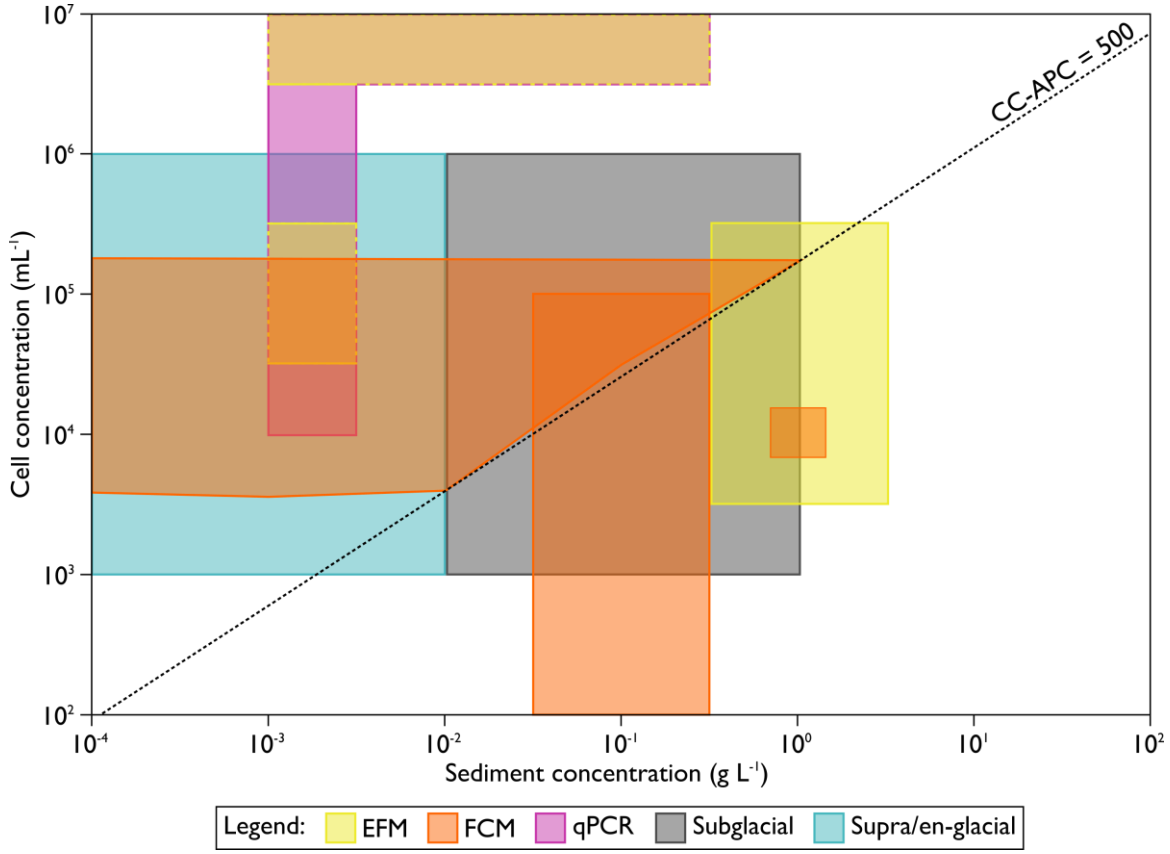

Figure 4.9 Ranges of cell and sediment concentrations for which EFM, FCM and qPCR exhibit acceptable accuracy (100 ± 25 %) and precision (≤ 20 % relative standard deviation) for the enumeration of glacial samples, considering the additions of this study (after Figure 4.1).

5. Microbial Abundance in Weathering Crust Meltwaters of Northern Hemisphere Glaciers

5.1 Introduction and study design

Meltwater is generated on glacier surfaces during the ablation season and is transported via the highly porous near-surface weathering crust ((Stevens et al., 2018; Chapter 3) before transfer to the supra-, en- and sub- glacial networks (Fountain and Walder, 1998) and subsequently downstream to aquatic and marine environments. Weathering crust meltwater provides an environment suitable for the support of active microbial communities (e.g. Hodson et al., 2015; Hodson et al., 2008). However, current cell enumeration estimates for supraglacial systems are based upon a limited number of samples in comparison with other ecosystems (e.g. Whitman et al., 1998). This chapter applies the FCM protocol developed in Chapter 4 to 11 glaciers located across the Northern Hemisphere, from the Greenland Ice Sheet to the European Alps to present enumerative estimates of cellular biomass in the weathering crust of ablating glaciers. Hydraulic conductivities, initially presented in Chapter 3, are considered as a potential control upon cell concentrations within the weathering crust. These cell concentrations are coupled with annual meltwater run-off modelling to 2099 (Bliss et al., 2014) to estimate cellular carbon, nitrogen and phosphorus flux from glacier surfaces to downstream environments; where such nutrients may seed ecosystem development in aquatic and marine environments into which glacial meltwaters drain (Battin et al., 2004; Bhatia et al., 2013; Hood et al., 2015; Milner et al., 2017; Musilova et al., 2017; Wilhelm et al., 2013).

This study was designed to expand upon the existing estimates of cell concentrations in near surface environments, utilising the high-throughput protocol tested in Chapter 4. Cell concentrations in the weathering crust are expected to be in the range 10^3 – 10^5 cells mL^{-1}, equivalent to previous studies in similar environments (Table 5.1).

By associating these measurements with the hydrological examination of the weathering crust (Chapter 3), the study also aimed to draw broad-scale links between hydraulic conductivity and cell concentrations across the depth-profile of the weathering crust. Based on groundwater studies and the conceptual model outlined in section 2.7, it would be expected that cell concentration would increase with hydraulic conductivity. However, in supraglacial streams, the opposite phenomenon has been observed; increased discharge is correlated inversely with cell concentrations (Irvine-Fynn et al., 2012).

Table 5.1 Microbial abundances observed in glacier environments.

Glacier	Country	Habitat	Cells mL^{-1}	Method	Source
Borup Fjord Pass	Canada	Surface meltwater	$1.3 \pm 0.2 \times 10^4$	qPCR	Trivedi et al., 2018
Austre Brøggerbreen	Svalbard	Cryoconite hole water	$5.4 \pm 1.6 \times 10^4$	EFM	Anesio et al., 2010
Midtre Lovénbreen	Svalbard	Cryoconite hole water	$2.9 \pm 0.8 \times 10^4$	EFM	Säwström et al., 2002
Midtre Lovénbreen	Svalbard	Cryoconite hole water	$3.4 \pm 1.2 \times 10^4$	EFM	Anesio et al., 2010
Midtre Lovénbreen	Svalbard	Supraglacial meltwater	$1.4 - 4.9 \times 10^4$	EFM	Mindl et al., 2007
Midtre Lovénbreen	Svalbard	Stream	$2.0 \pm 0.1 \times 10^4$	FCM	Irvine-Fynn et al., 2012
Midtre Lovénbreen	Svalbard	Shallow ice core	$5.7 \pm 0.3 \times 10^4$	FCM	Irvine-Fynn et al., 2012
Thule	Greenland	Shallow ice core	$3.7 \pm 0.3 \times 10^3$ $3.4 \pm 1.2 \times 10^4$	EFM	Stibal et al., 2015
A.P. Olsen Ice Cap	Greenland	Shallow ice core	$3.2 \pm 0.5 \times 10^5$ $4.7 \pm 1.0 \times 10^5$	EFM	Stibal et al., 2015
Kangerlussaq	Greenland	Shallow ice core	$3.9 \pm 0.6 \times 10^4$ $6.7 \pm 3.4 \times 10^4$	EFM	Stibal et al., 2015
Qasimiut	Greenland	Shallow ice core	$6.2 \pm 4.2 \times 10^4$ $4.3 \pm 1.5 \times 10^5$	EFM	Stibal et al., 2015
Tasiilaq	Greenland	Shallow ice core	$4.6 \pm 1.1 \times 10^4$ $1.2 \pm 0.5 \times 10^5$	EFM	Stibal et al., 2015
Matanuska Glacier	Alaska, USA	Weathering crust water	$200 - 8.3 \times 10^3$	EFM	Christner et al., 2018
Rotmoosferner	Austria	Cryoconite hole water	$4.1 \pm 3.8 \times 10^4$	EFM	Anesio et al., 2010
Stubacher Sonnblickkees	Austria	Cryoconite hole water	$3.7 \pm 1.4 \times 10^4$	EFM	Anesio et al., 2010
Patriot Hills	Antarctica	Cryoconite hole water	$1.3 \pm 0.8 \times 10^4$	EFM	Hodson et al., 2008
McMurdo Dry Valleys	Antarctica	Cryoconite hole water	$4.4 \pm 2.4 \times 10^4$	EFM	Hodson et al., 2008
McMurdo Dry Valleys	Antarctica	Cryoconite hole water	$4.6 \pm 2.1 \times 10^4$	EFM	Foreman et al., 2007
Vestfold Hills	Antarctica	Cryoconite hole water	260 ± 190	EFM	Hodson et al., 2008

Where two values are indicated, these are the maximum and minimum values observed by each study. Single values are means.
Uncertainties are indicated where available.

The explanation for this is that at low discharge, transport through the weathering crust is effective, whereas at high discharge, four process reduce cell transport rates:

1. As discharge rises, larger interstitial flowpaths within the weathering crust may effectively capture flow, thereby reducing water flow in other areas of the weathering crust decreasing the areas contributing to cell entrainment, in a manner analogous to englacial hydraulics (e.g. Röthlisberger, 1972).

2. At times of increased melt, the weathering crust becomes water-logged, and water pressures direct flow away from preferential flow paths reducing contributions from interstitial spaces to the meltwater which is transported to supraglacial streams. This pressure gradient is reversed at low melt, enhancing apparent particle transport through the porous media in a manner equivalent to the subglacial hydrological system (e.g. Hubbard et al., 199)).
3. The particles themselves may impede transport and clog interstitial spaces within the weathering crust (see Mader et al., 2006), reducing the effective porosity and the numbers of particles transported.
4. Nutrient starvation, linked with reduced hydraulic conductivity, has been demonstrated to enhance bacteria transport (Han et al., 2013). When nutrient starved, cell sizes are reduced (Cunningham et al., 2007; Sanin et al., 2003), increasing the transport potential (Mueller, 1996) as cells can move through smaller pores. Furthermore, starvation reduces the protein and polysaccharide content of extra-cellular polymeric substances (EPS) in *Bacillus* (Haznedaroglu et al., 2008), and may occur in other bacteria in the Firmicutes phylum (observed in the weathering crust, see Christner et al., 2018) and other phyla which may influence the ability of cells to form biofilms preventing their transport.

Therefore, if hydraulic conductivity and cell concentrations are positively correlated, such as is observed in the groundwater system, this will be indicative of a simple system where increased pore water velocity delivers more nutrients to cells and increased rates of cell advection. This trend may only be apparent when each glacier sampled is considered individually, due to potential differences in microbial cell delivery controlled by regional scale differences in dust delivery and cell concentration in snow (although it should be noted that consideration of inoculation rates is beyond the scope of this study).

If a negative correlation is apparent, it may be possible to elucidate if any of the four proposed mechanisms are occurring. In the case of 1, effective pathways will most likely be observed near the surface, where ice density is lowest and porosity and hydraulic conductivity greatest. The presence of effective flow near the surface can be identified using the height of the water table; the closer the water table to the surface, the greater efficiency of flow. As such, cell concentration would be expected to correlate negatively with water table height when considered for each glacier individually. In the case of 2 and 3, these phenomena cannot be observed using the piezometer method described in Chapter 3. However, the implication of mechanical filtering may be demonstrated if cell concentrations within

streams are lower than in weathering crust meltwaters. To assess 2, in-depth consideration of sub-metre scale flow direction and water pressure is required, and to fully assess 3 consideration of the flow paths of individual particles is needed. If cells are nutrient starved by reduction in hydraulic conductivity (4), this will be apparent when considering cell size distributions with hydraulic conductivity and/or permeability as the dependent variable; lower hydraulic conductivities would be associated with smaller cells and greater concentrations of planktonic cells in weathering crust meltwater.

5.2 Materials and methods

5.2.1 Field sites and sampling strategy

Weathering crust recharge and cell samples were collected at 11 sites across the northern hemisphere between 2014 and 2016, covering a range of latitudes and climatic settings (Table 5.2 Figure 3.4). At Haut Glacier d'Arolla, Vadrec del Forno (both Switzerland), and Fountain Glacier Bylot Island (HACH, VFCH and FGBI, respectively), holes were drilled at strategic locations along transects or semi-randomised grids within a defined supraglacial micro-catchment, whereas on the K-transect of western Greenland (GRDS), nine holes were distributed cross a 30 × 30 m grid. At other sites including those in Sweden (SGSE and RGSE), in Austria (RMOS and GBOS), at the Greenland Ice Sheet margin (GRKM), and in Svalbard (PBSV and FFSV) glacier-wide randomised grid sampling or short transects over smaller, hydrologically active areas were applied.

5.2.2 Hydrological data collection and processing

Stream discharge was also recorded for PBSV, FFSV, FGBI, SGSE HACH and VFCH, with cell samples collected throughout the study period at the measurement point. At VFCH, measurement of discharge was undertaken using a Druck pressure transducer and Campbell CR1000 logger to measure supraglacial stream stage. Discharge was measured using salt dilution gauging, following the protocol outlined by (Hudson and Fraser, 2005) using 10 g of table salt, and a stage-discharge relationship established for the stream. At all other sites (PBSV, FFSV, FGBI, SGSE and HACH), salt dilution gauging alone was used, with electrical conductivity (EC) measured in the field. The relationship between salt concentration and EC was established in a laboratory experiment prior to each field season, using Millipore water at a temperature of 1 °C as a substitute for glacial meltwater.

Table 5.2 Summary of glacier sites sampled within the study.

Glacier Name	Country	Fieldwork Period	Glacier Code	Latitude (°N)	Area (km^2)	Elevation (m asl)	Daylight hours (decimal)	Max daily solar zenith (°)	Climate and thermal regime	Further reference
Protektorbreen	Svalbard, Norway	13/08/15 to 17/08/15	PBSV	78.24	7.60	5 – 700	24	25.2 – 26.5	Polar maritime Cold	Hagen et al., 1993; Hodson and Irvine-Fynn, unpublished data
Foxfonna	Svalbard, Norway	08/08/15	FFSV	78.12	3.95	675 – 950	24	28.0	Polar maritime Cold	Hagen et al., 1993; Liestøl, 1967; Rutter et al., 2011
Fountain Glacier	Bylot Island, Canada	07/07/14 to 23/07/14	FGBI	72.95	72.0	330 – 1100	24	37.2 – 39.5	Polar continental Non-temperate polythermal	St. Germain and Moorman, 2016; Wainstein et al., 2014; Whitehead et al., 2013; Whitehead et al., 2014
Rabots Glaciär	Sweden	22/08/14	RGSE	67.91	3.70	1070 – 1640	16.4	33.8	Polar maritime Non-temperate polythermal	Björnsson, 1981; Brugger, 2007; Brugger et al., 2005
Storglaciären	Sweden	24/08/14	SGSE	67.90	3.10	1120 – 1730	16.1	33.1	Polar maritime Non-temperate polythermal	Björnsson, 1981; Brugger, 2007; Hock and Holmgren, 2005; Holmlund and Eriksson, 1989; Jansson, 1995
Greenland Ice Sheet (Point 660)	Greenland	06/08/14 to 07/08/14	GRKM	67.16	-	≈ 630	18.2 – 18.3	39.6 – 39.9	Polar maritime Non-temperate	Smith et al., 2015; van de Wal et al., 2008; van de Wal et al., 2005; Yang et al., 2016

Table 5.2 (continued).

Glacier Name	Country	Fieldwork Period	Glacier Code	Latitude (°N)	Area (km^2)	Elevation (m asl)	Daylight hours (decimal)	Max daily solar zenith (°)	Climate and thermal regime	Further reference
Greenland Ice Sheet (S6)	Greenland	22/07/14 to 29/07/14	GRDS	67.08	NA	≈ 1100	19.5 – 20.6	41.9 – 43.4	Polar maritime Non-temperate	Smith et al., 2015; van de Wal et al., 2008; van de Wal et al., 2005; Yang et al., 2016
Gaisbergferner	Austria	08/09/14	GBOS	46.83	1.03	2460 - 3390	12.9	48.8	Alpine continental Temperate	Abermann et al., 2009; Fischer, 2010
Rotmoosferner	Austria	11/09/14	RMOS	46.82	3.17	2450 - 3000	12.9	47.6	Alpine continental Temperate	Abermann et al., 2009; Anesio et al., 2010; Edwards et al., 2013
Vadrec del Forno	Switzerland	01/07/16 to 22/07/16	VFCH	46.31	8.20	2330 – 2850	15.2 – 15.5	64.1 – 66.7	Alpine continental Temperate	Huss et al. 2010; Jennings et al., 2014
Haut Glacier d'Arolla	Switzerland	19/07/15 to 28/07/15	HACH	45.98	6.30	2550 – 3500	14.9 – 15.3	63.0 – 64.5	Alpine continental Temperate	Brock et al., 2000; Mitchell et al., 2001; Pellicciotti et al., 2005; Willis et al., 2002

A concentration-conductivity curve was constructed using a range of known masses of salt, covering an EC range that would be expected in a supraglacial stream, ≤ 6 μS cm^{-1} (see Collins, 1979).

For calculation of hydraulic conductivity (*K*), 36 cm deep auger-holes of 5 cm dimeter were drilled using an ice auger (Kovacs Enterprise, USA) and a Makita 18V Combi Drill. Data collection and processing followed the protocol outlined in Chapter 3 (see Stevens et al., 2018). At PBSV, HACH and VFCH EC and temperature of borehole waters were measured using a combined Reed SD-4307 probe at a depth representing a mid-point between the auger-hole base and water table, post microbial sample collection to prevent cross-contamination of samples.

5.2.3 Meltwater sample collection and interrogation

Post-recharge measurement, meltwater from recharge holes was collected from a mid-depth in the filled auger-hole using a syringe and plastic tubing. Meltwater within the hole entered from all depths within the weathering crust and was perturbed and mixed by removal of the recharge probe, so robust depth-specific sample collection was not considered possible. Prior to sample collection, the tubing and syringe were pre-contaminated three times using water from the relevant auger-hole before collection of the sample which was transferred to a sterile, 15 mL falcon tube in most instances. For some glaciers (GRDS, GRKM and SGSE), 4 mL tubes were used due to logistical limitations regarding the transport of large volumes (and hence masses) of sample. Stream samples were collected directly, prior to salt dilution gauging where applied, and stored in an identical fashion. Whilst on the glacier, samples were stored in the dark in contact with the ice, ensuring that temperature remained low. At the end of each day, samples were fixed with glutaraldehyde (collection in 2014 and 2015) or paraformaldehyde (2016) (both 2 % w/v final concentration). Samples were kept dark and frozen at -80 °C upon return for the UK, a maximum of three weeks after collection.

Samples were defrosted at room temperature and cell enumeration undertaken via flow cytometry (FCM) using a Sony SH-800EC (Sony Biotechnology, Japan) following the protocol outlined in Chapter 4. Size gates where distinguished using a non-fluorescent Flow Cytometry Size Calibration Kit (Molecular Probes, UK) as per the manufacturer's instructions (see https://assets.thermofisher.com/TFS-Assets/LSG/manuals/mp13838.pdf for further information).

5.2.4 Carbon, nitrogen and phosphorus flux calculations

Using cell concentrations and size distributions of cells within the weathering crust, coupled with regional scale glacier-run off modelling, carbon, nitrogen and phosphorus fluxes from glacier surfaces are calculated for a) geographic regions and b) globally. Whilst previously undertaken by (Irvine-Fynn et al., 2012), this work substantially expands the geographic scope of these flux calculations Only cells from the weathering crust are considered to avoid double counting and subsequent over-estimation of nutrient flux, as cells observed in-streams are expected to have been transferred through the weathering crust. To convert microbe fluxes to nutrient biomass, constant values can be used (see Lee and Fuhrman, 1987), but to account for variations in microbe size, biomass can be approximated using biovolume ratio or allometric methods which consider biovolume and use domain-scale scaling factors (c and a; Equation 5.1) linking mass (m) and cell volume (V_{cell}). For bacteria, $c = 120$ and $a = 0.72$ (Norland, 1993) and for algae, $c = 109$ and $a = 0.991$ (Montagnes et al., 1994). However, this study does not aim to discern the types of cells sampled, even at the domain level, but based upon the conceptual model it is assumed that planktonic cells in weathering crust waters sampled are bacterial, and for simplicity a conversion factor of 5.6×10^{-13} g C μm^{-3} (Bratbak, 1985) was used. Cellular carbon concentration was used to additionally calculate cellular nitrogen and phosphorus concentrations using known ratios of 50:10:1 (C:N:P), defined for a range of genera of aquatic bacteria (Fagerbakke et al., 1996).

$$m = cV_{cell}^{a} \qquad \text{[Equation 5.1]}$$

When converting diameter of a single axis to cell volume, it is important to consider the cell shape; the two primary prokaryotic morphologies are cocci (spheres) and bacilli (rods), but budding, helical, corkscrew, spirochete and filamentous morphologies are also observed (Madigan et al., 2015). This study will consider cells as both cocci and bacilli, indicating the maximum and minimum potential nutrient mass. It is expected that cells within weathering crust meltwaters are a combination of these morphologies, and actual nutrient estimates will be somewhere within this range. However, without detailed knowledge of cell morphology, this is impossible to quantify. For spheres, cell volume is calculated using Equation 5.2, where V_{cell} is the volume of an individual cell of radius r, defined using the mid-point of the size class into which it falls. For rods, Equation 5.3 is used, where length, L, is defined as the size fraction mid-point and cell width (w) is modelled based on standard bacterial geometries (Equation 5.4; Saccà, 2017). Cell volume was initially calculated for an individual cell each

size class for each shape. Equation 5.5 was then used to calculate the total cell volume for each site for each cell shape; CC_{size} is the concentration of cells in a given size class. Total size class volume (μm^3 mL^{-1}) was calculated per-size class, which were added to obtain a total cell volume for each glacier using the mean cell concentration and size distribution. Cells in the ≥ 15 μm size class were considered to have radii of 7.5 μm.

$$V_{cell} = \frac{4}{3}\pi r_{cell}^{3} \quad \text{[Equation 5.2]}$$

$$V_{cell} = \frac{\pi}{4} w^2 \left(l - \frac{w}{3}\right) \quad \text{[Equation 5.3]}$$

$$w = 0.888l + 0.111 \quad \text{[Equation 5.4]}$$

$$\sum V_{cell} CC_{size} \quad \text{[Equation 5.5]}$$

Mean nutrient concentrations were subsequently upscaled to the glacier run-off scale using data from Bliss et al., 2014). This work presents modelled run-off under the RCP 4.5 emissions scenario (see IPCC, 2013), accounting for glacier size change, to 2099. This modelled discharge is proglacial; however, melting at the bed of glaciers is negligible in terms of contribution to mass balance (Cuffey and Paterson, 2010), so it is assumed that all proglacial melt is provided from surface melt. Data within this work is provided by region, and glaciers sampled by this study are associated with the relevant region. However, some regions include multiple glaciers within this study, in which instance a weighted mean of mean nutrient concentration, based on sample number at each glacier, is used to provide the input nutrient concentration data for the region. For the global (excluding Antarctica) nutrient flux, a weighted mean of nutrient concentration based on sample number was used across all sites. The calculation of extraglacial nutrient export from weathering crust cells was undertaken by multiplying mean nutrient concentration for each region (and globally) by the corresponding meltwater flux (mL a^{-1}). Note that this calculation excludes any modifications in the subglacial environment, and only considers the planktonic cells observed within a developed weathering crust as sampled within this study. It does not consider immobile cells which are attached to or incorporated within ice crystals, which may be advected from the glacier surface during synoptic conditions, such as extreme rainfall events, which degrade the weathering crust. As such, these calculations are likely to represent low-end or underestimates of bacterial nutrient flux from the supraglacial environment.

5.3. Results

5.3.1 Microbial cell enumerations

Total event counts were used to imply sediment loads, ensuring that the CC-APC criterion outlined in Chapter 4 was adhered to and suitable confidence could be applied to FCM cell enumerations. Sediment concentration was not directly measured. As outlined in Chapter 4, a sediment load of 10^{-1} g L was associated with a non-cell event count in the order of 10^{6} mL^{-1}. This was observed in eight instances (seven at GRDS, and one as SGSE), however CC-APC for each of these sites was $\geq 5 \times 10^{5}$ and hence confidence can be placed in the accuracy of these analyses. All other samples also met the CC-APC criterion; cells with the lowest cell concentrations (the order of 10^{3} cells mL^{-1}) exhibited low non-cell event counts in the order of 10^{3} mL^{-1}.

Mean microbial cell concentrations in the weathering crust across all sites were $2.2 \times 10^{4} \pm 5.5 \times 10^{4}$ cells mL^{-1} ($n = 763$), equal to in-stream cell concentrations which were $2.2 \times 10^{4} \pm 3.0 \times 10^{4}$ cells mL^{-1} ($n = 142$). Note that $\pm$ uncertainties are reported as standard deviation of a glacier-scale dataset and represent the inherent variability of the data rather than implying the negative cell concentrations are possible or indeed plausible. When considered on a glacier-by-glacier basis (Figure 5.1), cell concentrations in streams and the weathering crust can be seen to occupy the same range in almost all cases, aside from at RMOS where only one stream sample was collected.

Differences in cell concentrations between glaciers can be observed in the weathering crust (Figure 5.1; Table 5.3.), with a one-way ANOVA indicating a significant difference in mean cell concentrations between glaciers ($p < 0.05$, $n = 763$). Tukey's HSD post-hoc testing revealed significant pairwise differences between GRDS and HACH, RMOS, SGSE, and VFCH, with GRDS having higher cell concentrations than all four sub-arctic and alpine valley glaciers in this study (2.9, 3.9, 3.3 and 3.2×10^{4} cells mL^{-1} respectively; in contrast to mean cell concentration for GRDS which is $4.7 \times 10^{4} \pm 1.3 \times 10^{5}$ cells mL^{-1}).

The modal cell size class is 1 – 2 μm, containing 56 ± 9.1 % of cells enumerated ($n = 905$) (Figure 5.2). The second most common grouping is the ≤ 1μm group (≈ 19 %) followed by the 2 – 4 μm group (≈ 14 %). As such, ≈ 75 % of cells have a diameter ≤ 2 μm, and 89 % ≤ 4 μm. Samples from the weathering crust and supraglacial streams demonstrate similar cell size distributions, with overlap of uncertainties (± 1 standard deviation). Measurements with associated permeability data

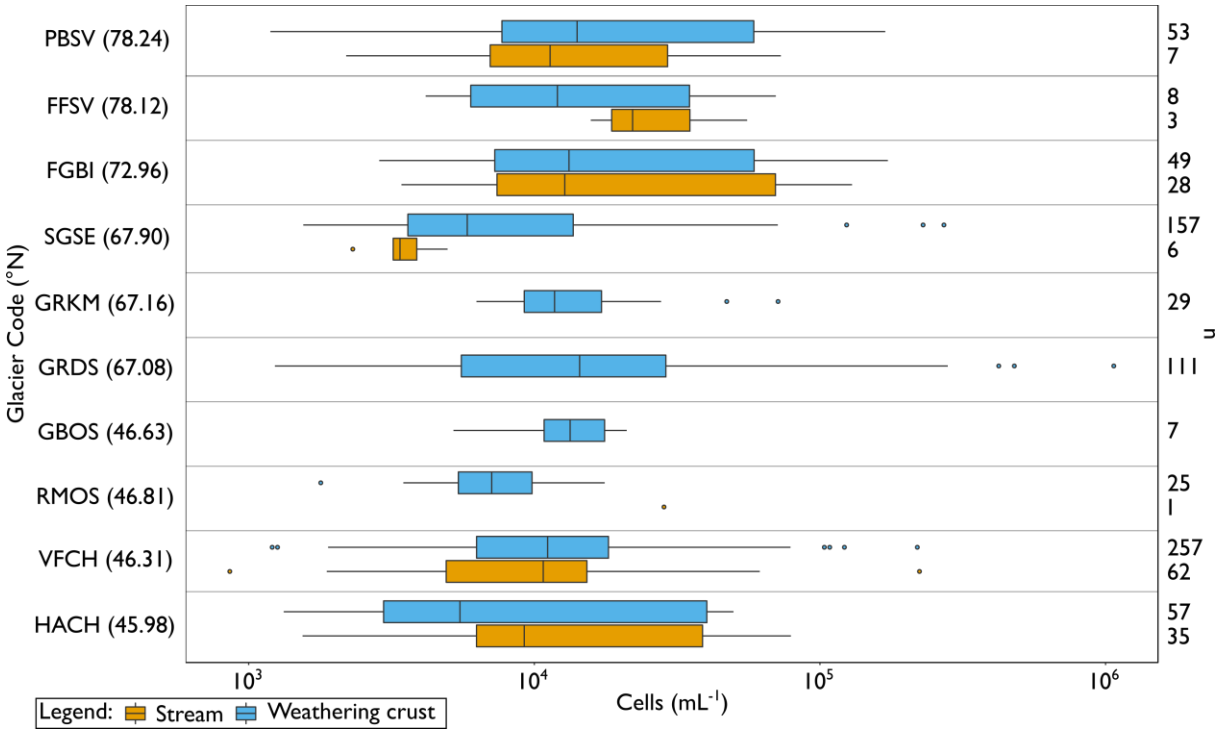

Figure 5.1 Cell concentrations in weathering crust (blue) and stream (orange) meltwaters for glaciers across the northern hemisphere (latitudes in brackets). Outliers are indicated with dots of corresponding colour, and sample numbers on the right align with the corresponding box. For GRKM, GRDS and GBOS, no stream samples were collected, and only one stream sample was collected at RMOS. Note that for all glaciers with ≥ 1 stream sample, interquartile ranges of cell concentrations in the weathering crust and stream samples overlap.

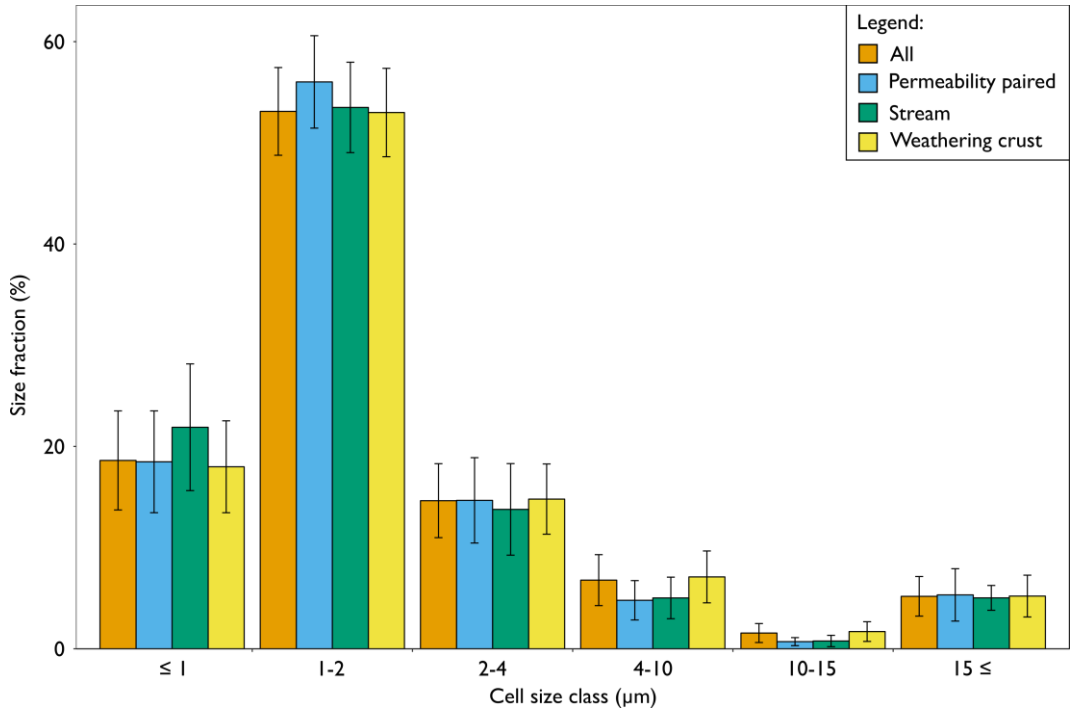

Figure 5.2 Cell size distributions for all samples and sub-samples including those with paired permeability measurements, and from weathering crust/stream meltwaters. Error bars show ± 1 standard deviation.

Table 5.3 Microbial abundances observed by this study.

Site	Country	Habitat	Mean Cells mL^{-1}
FFSV	Svalbard	Weathering crust water	$2.5 \pm 2.6 \times 10^4$
FGBI	Bylot Island, Canada	Weathering crust water	$3.3 \pm 4.1 \times 10^4$
GBOS	Austria	Weathering crust water	$1.4 \pm 0.6 \times 10^4$
GRDS	Greenland	Weathering crust water	$4.4 \pm 2.1 \times 10^4$
GRKM	Greenland	Weathering crust water	$1.6 \pm 1.3 \times 10^4$
HACH	Switzerland	Weathering crust water	$1.8 \pm 1.9 \times 10^4$
PBSV	Svalbard	Weathering crust water	$3.1 \pm 3.4 \times 10^4$
RMOS	Austria	Weathering crust water	$7.9 \pm 3.8 \times 10^3$
SGSE	Sweden	Weathering crust water	$1.4 \pm 3.1 \times 10^4$
VFCH	Switzerland	Weathering crust water	$1.5 \pm 2.0 \times 10^4$
FFSV[#]	Svalbard	Stream	$3.1 \pm 2.2 \times 10^4$
FGBI	Bylot Island, Canada	Stream	$3.6 \pm 4.0 \times 10^4$
HACH	Switzerland	Stream	$2.2 \pm 2.0 \times 10^4$
PBSV	Svalbard	Stream	$2.6 \pm 3.2 \times 10^4$
RMOS*	Austria	Stream	2.8×10^4
SGSE	Sweden	Stream	$3.5 \pm 0.9 \times 10^3$
VFCH	Switzerland	Stream	$1.5 \pm 2.8 \times 10^4$

Uncertainties stated are ± 1 standard deviation.
[#]whilst both datasets are collected from Foxfonna, the weathering crust sites are from the dome, whereas the stream samples are from the lower outlet.
*n = 1.

(n = 316), have similar cell size distributions to the entire dataset, and hence analysis of this sub-sample can be considered representative of the entire dataset when considering cell sizes.

5.3.2 Links between cell concentrations and hydrology

614 samples were successfully paired with matching hydrological data. This loss of data (n = 149) was attributed to incomplete record keeping and/or worn sample labels meaning microbial samples could not be paired confidently with hydrological data. When considered as an overall dataset (Figure 5.3), or on a glacier-by-glacier basis (Figure 5.4), no trend is apparent between hydraulic conductivity and cell concentration, or water table depth and cell concentration. No trends were observed between EC or temperature of weathering crust meltwater and cell counts for sites with available data (HACH, VFCH and PBSV; n = 316).

Permeability values were available from VFCH, HACH and PBSV, with 316 paired samples. No relationship is demonstrated between permeability and cell concentration (Figure 5.5); which is reflected when considered at each individual glacier. Furthermore, permeability does not appear to affect the size distribution of cells, with similar cell size distributions observed across the entire range of permeabilities recorded (Figure 5.6). Given the lack of variation in cell size distributions shown in Figure 5.6, cell size distributions were not considered on a glacier-by-glacier basis. Considering

comparisons between in-stream samples and the weathering crust, no statistically significant differences can be observed between size class distributions in the overall dataset or when the data is considered by glacier, but some enrichment of smaller size fractions in stream samples is observed (Figure 5.2).

For stream samples, 90 cell samples were successfully paired with discharge data. No correlations between discharge or cell concentration are apparent, either when considering the dataset as a whole, or on a glacier-by-glacier basis (Figure 5.7).

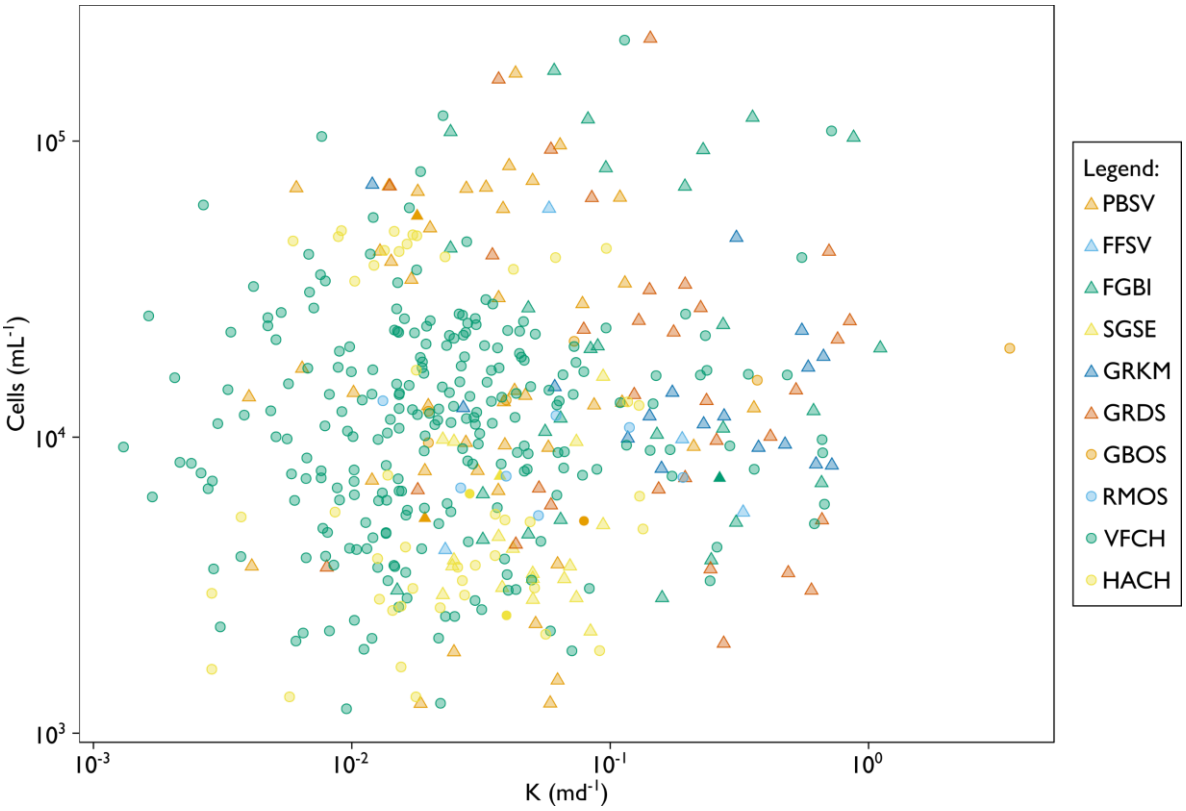

Figure 5.3 Cell concentration as a function of hydraulic conductivity at all sites, using a log-log scale. Glaciers are highlighted by colour, and the environment of sites (polar or alpine) is indicates using a triangles and circles respectively. No trends are apparent between these two variables across the dataset as a whole.

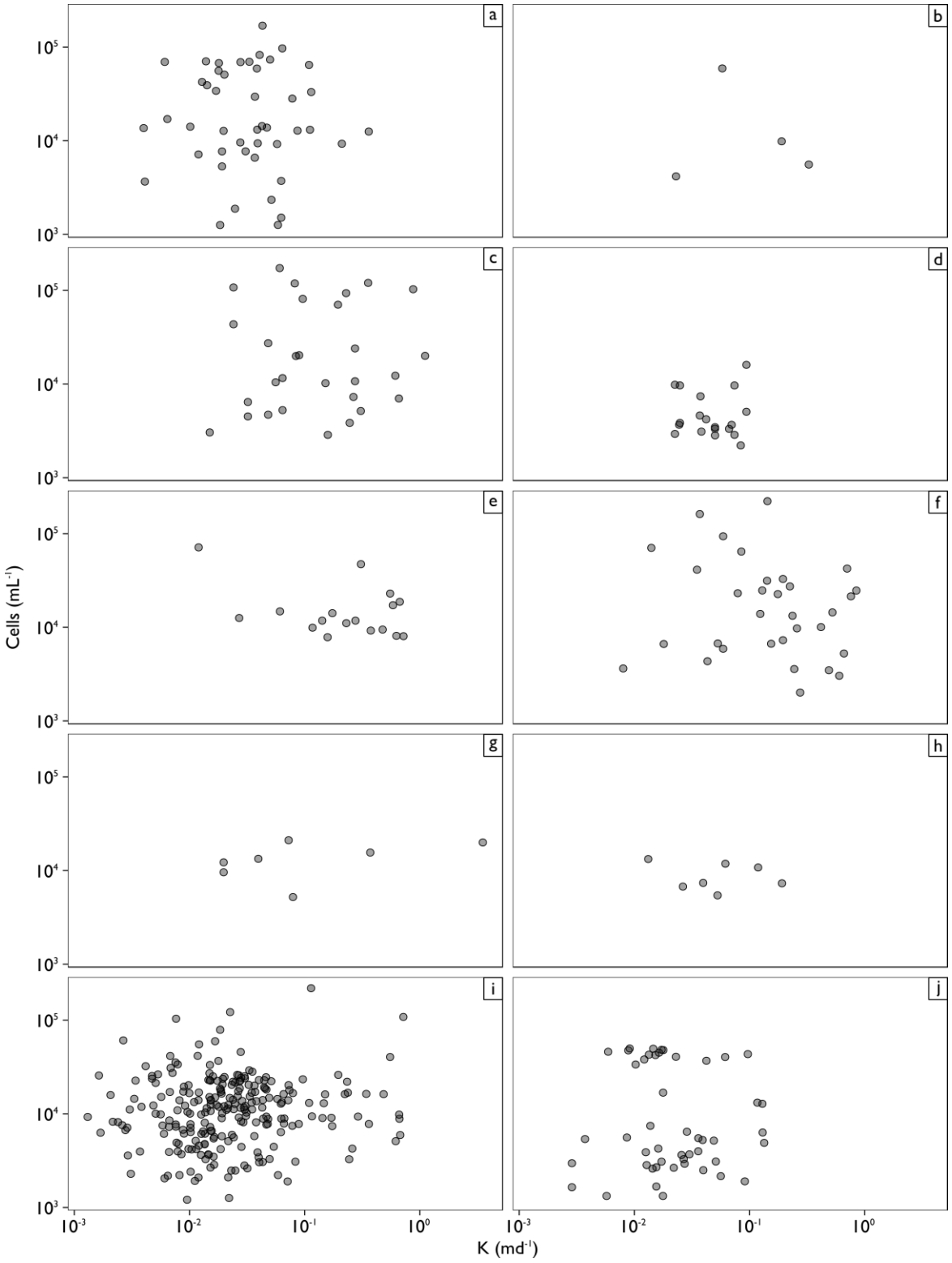

Figure 5.4 Cell concentrations as a function of hydraulic conductivity, with each sub-plot indicating a different glacier, as follows (n): a: PBSV (45); b: FFSV (4); c: FGBI (21); d: SGSE (19); e: GRKM (17); f: GRDS (32); g: GBOS (7); h: RMOS (7); i: VFCH (243); j: HACH (48).

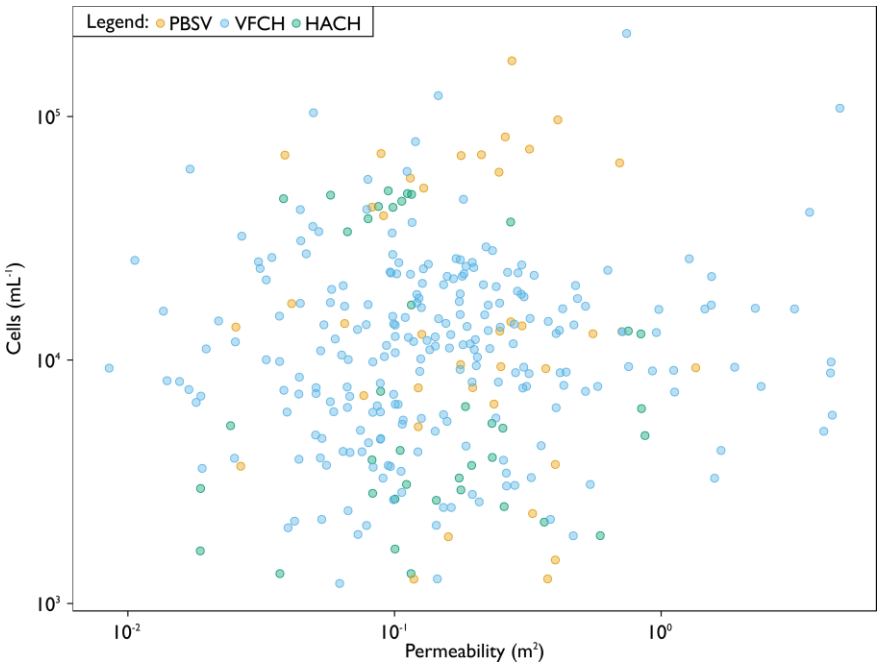

Figure 5.5 Cell concentration as a function of permeability at all sites, using a log-log scale. No trends are apparent across the entire dataset, or when considered on a glacier-by-glacier basis.

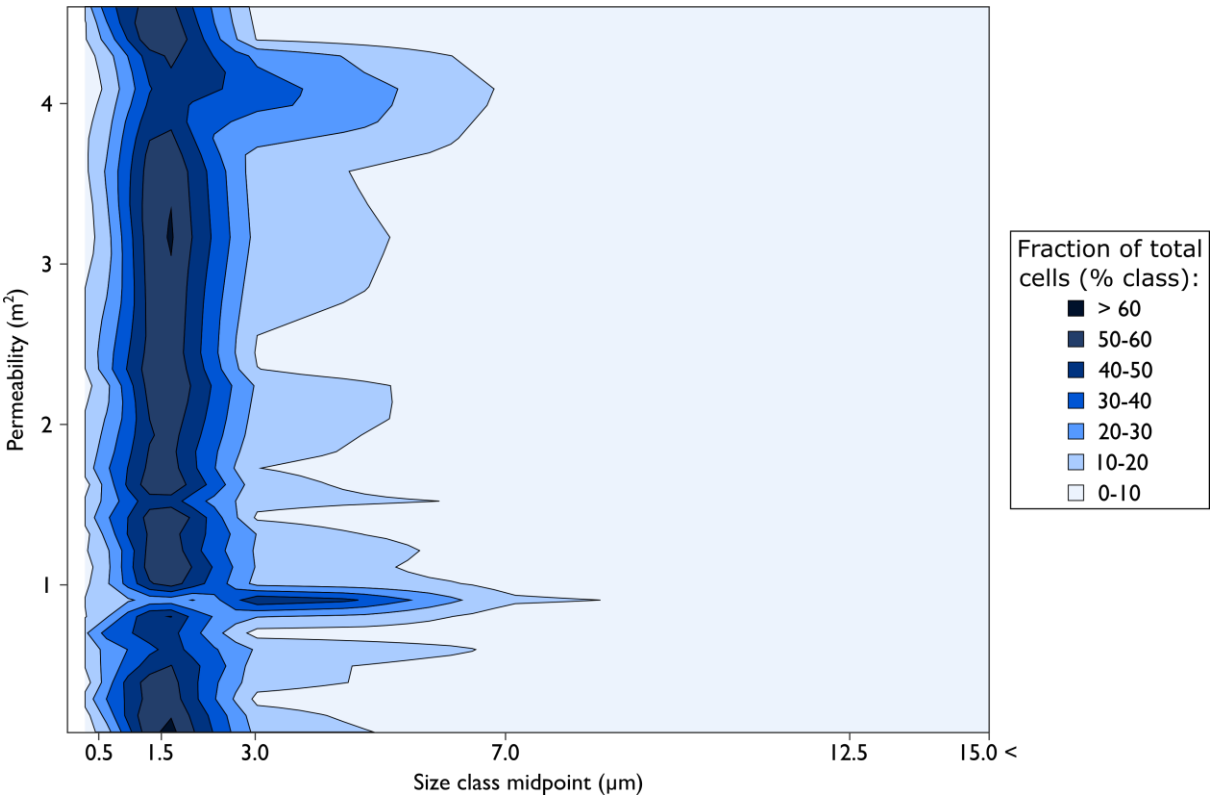

Figure 5.6 Cell size distributions using the mid-point of each size class as the diameter of the cells within it, note that the x axis breaks are defined by the sizes of calibration beads. The ≤ 1 µm class is attributed a diameter of 0.5 µm (as cells cannot have a diameter ≤ 0) and the > 15 µm class is attributed a nominal diameter of > 15 µm given the lack of upper-bound. A linear interpolation is applied to the point data to generate the contour surface, $r^2 = 0.998$.

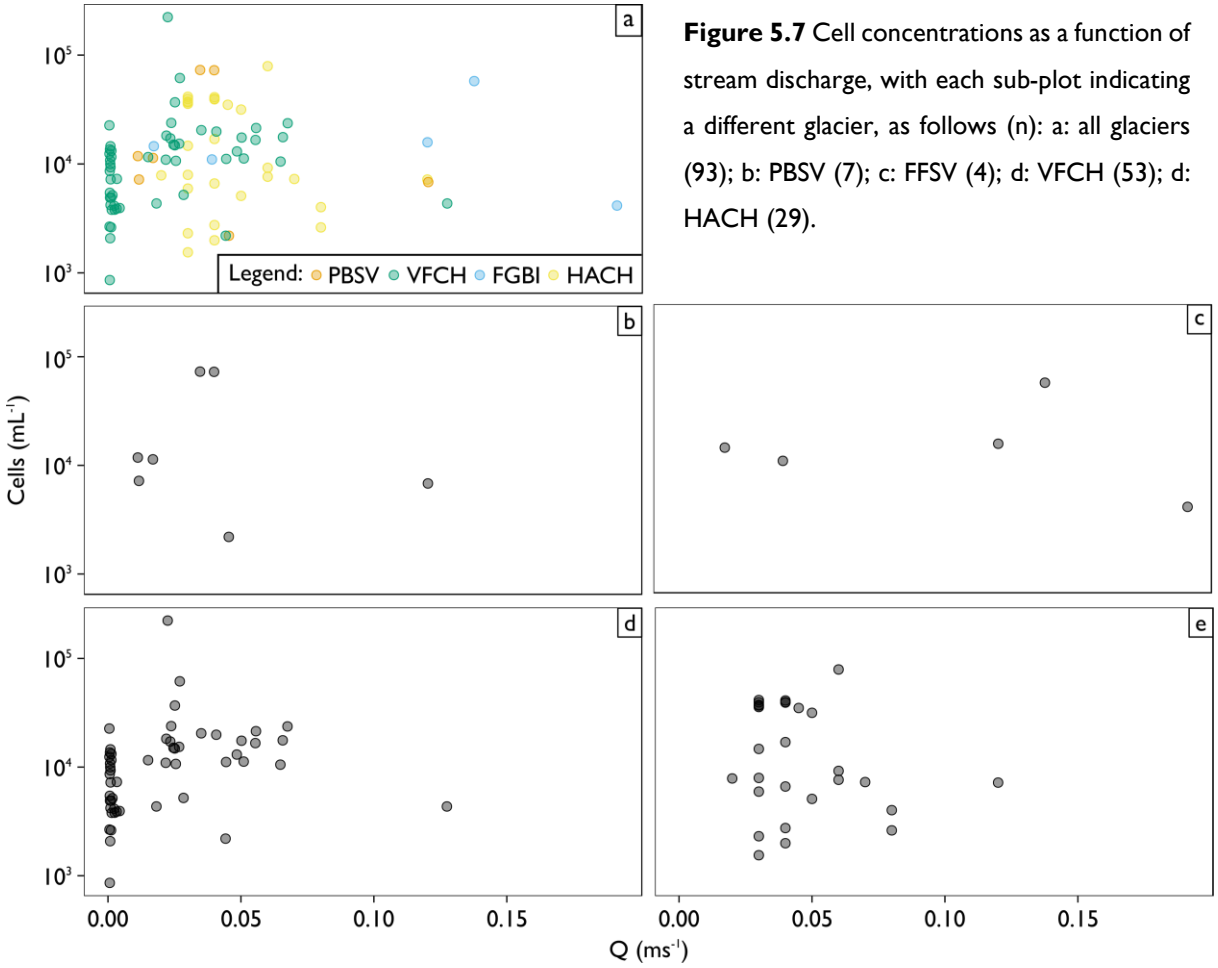

Figure 5.7 Cell concentrations as a function of stream discharge, with each sub-plot indicating a different glacier, as follows (n): a: all glaciers (93); b: PBSV (7); c: FFSV (4); d: VFCH (53); d: HACH (29).

5.3.3 Carbon, nitrogen and phosphorus fluxes

Between 2003 and 2099, annual cellular carbon flux from glacier surfaces in the five regions sampled in this study is between 3.4×10^8 kg a^{-1} and 1.1×10^9 kg a^{-1}, depending on the shape of bacterial cells. Rod-shaped bacteria yield lower nutrient fluxes, around one-third of those for spherical bacteria. Excluding Antarctica, the regions sampled represent ≈ 30 % of modelled global glacier runoff over the next century, and as such further upscaling to a global scale implies carbon fluxes of 1.1×10^9 kg a^{-1} and 3.6×10^9 kg a^{-1} from glacier surfaces. Detailed regional and temporal breakdown, and nitrogen and phosphorus fluxes can be seen in Tables 5.4 and 5.5, with trends linked with discharge fluctuations.

Table 5.4 Global total is calculated by comparison of run-off from regions as a proportion of total global runoff (excluding Antarctica) for spherical cells.

Region	C	N	P	C	N	P
	2003 – 2099 (kg a^{-1})			2003 – 2022 (kg a^{-1})		
Svalbard	1.7×10^8	3.5×10^7	3.5×10^6	1.6×10^8	3.2×10^7	3.2×10^6
Arctic Canada (N)	3.7×10^8	7.5×10^7	7.5×10^6	3.0×10^8	5.9×10^7	5.9×10^6
Greenland	5.3×10^8	1.1×10^8	1.1×10^7	5.0×10^8	1.0×10^8	1.0×10^7
Scandinavia	8.7×10^6	1.7×10^6	1.7×10^5	1.2×10^7	2.4×10^6	2.4×10^5
Central EU	5.6×10^6	1.1×10^6	1.1×10^5	8.4×10^6	1.7×10^6	1.7×10^5
Total	1.1×10^9	2.2×10^8	2.2×10^7	9.8×10^8	2.0×10^8	2.0×10^7
Global Total	3.6×10^9	7.3×10^8	7.3×10^7	3.8×10^9	7.7×10^8	7.6×10^7
Region	2041 – 2060 (kg a^{-1})			2080 – 2099 (kg a^{-1})		
Svalbard	2.0×10^8	4.1×10^7	4.1×10^6	1.4×10^8	2.9×10^7	2.9×10^6
Arctic Canada (N)	4.1×10^8	8.2×10^7	8.2×10^6	4.0×10^8	8.1×10^7	8.1×10^6
Greenland	5.5×10^8	1.1×10^8	1.1×10^7	5.1×10^8	1.0×10^8	1.0×10^7
Scandinavia	8.7×10^6	1.7×10^6	1.7×10^5	4.4×10^6	8.7×10^5	8.7×10^4
Central EU	4.7×10^6	9.3×10^5	9.3×10^4	2.8×10^6	5.6×10^5	5.6×10^4
Total	1.2×10^9	2.4×10^8	2.4×10^7	1.1×10^9	2.1×10^8	2.1×10^7
Global Total	3.2×10^9	7.7×10^8	7.7×10^7	3.2×10^9	6.3×10^8	6.3×10^7

Regions are split as follows: Svalbard: FFSV, PBSV; Arctic Canada: FGBI; Scandinavia: SGSE; Greenland: GRDS, GRKM; Central EU: GBOS, HACH, RMOS, VFCH.

Table 5.5 Global total is calculated by comparison of run-off from regions as a proportion of total global runoff (excluding Antarctica) for rod-shaped cells.

Region	C	N	P	C	N	P
	2003 – 2099 (kg a^{-1})			2003 – 2022 (kg a^{-1})		
Svalbard	5.2×10^7	1.0×10^7	1.6×10^6	4.8×10^7	9.6×10^6	9.6×10^5
Arctic Canada (N)	1.2×10^8	2.3×10^7	2.3×10^6	9.8×10^7	1.9×10^7	1.9×10^6
Greenland	1.7×10^8	3.3×10^7	3.3×10^6	1.6×10^8	3.2×10^7	3.2×10^6
Scandinavia	3.0×10^6	6.0×10^5	6.0×10^4	4.1×10^6	8.2×10^5	8.2×10^4
Central EU	1.8×10^6	3.6×10^5	3.6×10^4	2.7×10^6	5.3×10^5	5.3×10^4
Total	3.4×10^8	6.8×10^7	6.8×10^6	3.7×10^8	6.1×10^7	6.1×10^6
Global Total	1.1×10^9	2.3×10^8	2.3×10^7	1.2×10^9	2.4×10^8	2.4×10^7
Region	2041 – 2060 (kg a^{-1})			2080 – 2099 (kg a^{-1})		
Svalbard	6.1×10^7	1.2×10^7	1.2×10^6	4.3×10^7	8.7×10^6	8.7×10^5
Arctic Canada (N)	1.3×10^8	2.6×10^7	2.6×10^6	1.3×10^8	2.5×10^7	2.5×10^6
Greenland	1.7×10^8	3.5×10^7	3.5×10^6	1.6×10^8	3.2×10^7	3.2×10^6
Scandinavia	3.0×10^6	6.0×10^5	6.0×10^4	1.5×10^6	3.0×10^5	3.0×10^4
Central EU	1.5×10^6	3.0×10^5	3.0×10^4	8.9×10^5	1.8×10^5	1.8×10^4
Total	3.7×10^8	7.4×10^7	7.4×10^6	3.7×10^8	6.7×10^7	6.7×10^6
Global Total	1.2×10^9	2.4×10^8	2.4×10^7	9.9×10^8	2.0×10^8	2.0×10^7

Regions are split as follows: Svalbard: FFSV, PBSV; Arctic Canada: FGBI; Scandinavia: SGSE; Greenland: GRDS, GRKM; Central EU: GBOS, HACH, RMOS, VFCH.

5.4. Interpretation and discussion

5.4.1 Microbial cell enumeration and size distribution

This chapter presents a sample set of 907 microbial abundances within glacier surface meltwater, vastly expanding the number of samples and geographic scope of other work to date. The data herein likely represent an underestimation of microbial cells within the weathering crust due to the sampling strategy applied. Samples collected from auger-hole recharge waters only enable examination of mobilised microbes, and hence those that are stored within the weathering crust (either individually or as a component of large cell-particle agglomerations) (Irvine-Fynn et al., 2012), or bound to and within ice-crystals (via ice binding proteins; Dolev et al., 2016) which comprise the weathering crust cannot be sampled using the methods applied here. Bulk sampling would enable the collection of such microbiota if complete concentration quantification was desired, but the destructive nature of this would prevent examination of change over time at-a-point.

The mean microbial concentration presented herein (2.2×10^4 cells mL^{-1}) in both the weathering crust and streams compares well with existing estimates for glaciers worldwide in near-surface ice, surface meltwater and water within cryoconite holes (Tables 5.1 and 5.3). Interestingly, cell concentrations observed in the weathering crust at Rotmoosferner (Austria) are 80 % lower than those observed within cryoconite hole waters (Anesio et al., 2010), highlighting cell-enrichment in the water phase of cryoconite holes relative to the weathering crust. These cell concentrations are within the range observed for terrestrial aquifers (albeit at the lower end) of $10^2 – 10^8$ cells mL^{-1} (Madigan et al., 2015), and compare similarly to those found in snow, where cell concentrations range between 600 (e.g. Liu et al., 2009) and 2×10^5 cells mL^{-1} (e.g. Amato et al., 2007).

There is a statistically significant difference in mean microbial cell concentrations in the weathering crust at each glacier sampled in this study; with pairwise differences between GRDS and the Central European and Scandinavian glaciers, with more cells observed at GRDS. Given the lack of correlation between hydraulic conductivity, permeability, EC and temperature with cell concentrations, further work is required to ascertain the mechanism for this cell concentration differential. Inter-glacier scale variation in cell concentrations may be attributable to, a) nutrient input and bioavailability, b) cell replication rates, c) differential cell inoculation and d) frequency and intensity

of weathering crust degradation events. Exploration of these variables extend beyond the scope of this dataset, instead presenting avenues for further research.

The modal cell size of 1 - 2 μm observed is larger than reported by (Irvine-Fynn et al., 2012), who observed a modal size of ≤ 0.5 μm and interestingly describe a bimodal distribution for both ice-core and stream samples with a secondary size peak at 0.9 - 3.0 μm. The apparent lack of smaller particles herein may be a result of a) increased flocculation in these samples or b) lack of ability to resolve smaller sized particles. Flocculation is excluded the analysis protocol applied (see Chapter 4 for further detail). The Sony SH800-EC used for sample analysis offers scatter resolution of ≤ 0.5 μm and hence should prove capable of resolving smaller particles. For absolute counts, thresholding was undertaken based upon fluorescence, negating this issue and ensuring complete counting of even small cells. However, size fractions were estimated using FSC given the use of non-fluorescent beads; notably the ≥ 15 μm size fraction was calculated by elimination (i.e. containing all cells not included in another size gate). Hence it is possible that some particles exhibited fluorescence, and were counted as cells, but fell below the detection threshold for FSC due to their small size. Any cells exhibiting these characteristics would be counted as being ≥ 15 μm. Even if all cells classed in the ≥ 15 μm group where mis-categorised, the modal size group of this dataset would remain the 1 – 2 μm class (in this instance 23.8 % of cells would fall within the ≤ 1 μm group, still substantially below the ≤ 0.9 μm cell proportions reported by (Irvine-Fynn et al., 2012)). The size of cells moving through the weathering crust is dependent on two variables: a) the size of cells available for transfer, and b) the properties of the ice through which they are mobilised.

Without knowledge of the phylogenetic affiliation of cells, it cannot be determined whether cells are diminutive "dwarf" cells (because of nutrient limitations) or stable cells with a small size phenotype (Irvine-Fynn et al., 2012). This study does not have data to further elucidate this relationship, and a combined study would represent an important step forward in weathering crust cell transport. More recent work suggests a typical weathering crust phylum-level breakdown as follows: Proteobacteria (with OTUs observed for Alpha-, Beta- and Gamma- classes) (39%), Cyanobacteria (22%) and Bacteroidetes (18%), Actinobacteria (9%), Armatimonadetes (2%), Acidobacteria (1%) and Deinococcus-Thermus (1%) [Christner, 2018 #975}. However, this level of cell identification is unsuited to suggesting a "typical" cell size, even for the Proteobacteria that can be identified to a class level. For example, aquatic unicellular cyanobacteria have been demonstrated to range in size from 1 to 20 μm (Zehr et al., 2001). This highlights a clear research gap, more precise cell identification (for

example, to a genera level) is necessary to determine the community function of the cells within, and more pertinently, moving through the weathering crust and potential impact on downstream environments and biogeochemical cycling.

5.4.2 Weathering crust hydraulics and cell transport implications

The conceptual model of the weathering crust (section 2.7) and hypotheses outlined in section 5.1 outline two possible scenarios, for positive and negative correlations between hydraulic conductivity and cell concentrations within the weathering crust. However, no such relationship is observed, with no correlation apparent between hydraulic conductivity and cell concentration when considering the entire dataset or glacier-scale relationships. When considering this dataset and applying it to assess weathering crust mechanics, it is important to firstly consider the sampling strategy. Meltwater samples for which cells were enumerated were collected from water discharged from the weathering crust into auger-holes, and hence only mobile planktonic cells are considered. It should be noted that there are no direct measurements of either cells bound to ice crystals (either in biofilms or via mechanical means), or planktonic cells which are "trapped" in pores which have a smaller diameter than themselves or are disconnected. However, the data presented here do demonstrate that cells are mobilised within weathering crust meltwaters, as evidenced by the presence of cells within the sampled waters.

5.4.2.1 Cell transport

Previous work has argued that the weathering crust appears to represent somewhat of a logical paradox, with the accumulation of microbial biomass occurring during the process of ablation (Irvine-Fynn et al., 2012). One limitation of this study is that the cells enumerated only represent a component of those found on glacier surfaces, and hence only some elements of cell transport can be examined. Mader et al. (2006) report that in glacial ice, between 30 and 50 % of microbial cells are found in ice crystals, and the remaining 50 to 70 % are observed in interstitial melt water. At the near surface, (Irvine-Fynn et al., 2012) report reduced bacterial cell concentrations in supraglacial stream water when contrasted to near surface ice cores; stream concentrations are ≈ 15 % of ice core concentrations. The proposed mechanism for this reduction in cell concentrations through the transport pathway is that the weathering crust acts to remove cells from meltwaters via filtration or flow dynamics.

However, this apparent reduction in cell concentrations may in fact reflect the inclusion of cells bound to ice crystals in addition to those in interstitial meltwaters when measuring ice core concentrations, rather than the loss of cells to the weathering crust during transport. This is demonstrated by the data presented herein; the equivalent concentrations in weathering crust meltwaters and supraglacial streams implies that once entrained in weathering crust transport processes, cells are advected unhindered to supraglacial streams. Whilst there is no direct evidence of this occurring, the implied process is that cells within weathering crust meltwaters are efficiently advected through the medium without a change in concentration during this transport. To further examine this phenomenon and support this assertion, consideration of meltwater flowpaths and tracer-based examination of particles is required to further understand how individual particles move and/or are entrained within the weathering crust.

In the case of efficient advection, biological darkening of the near-surface throughout the melt season (Ryan et al., 2018; Tedstone et al., 2018; Tedstone et al., 2017), and biogeochemical cycling (e.g. Anesio et al., 2009) would be attributable to growth and replication of cells bound to ice-crystals in biofilms and filamentous cyanobacteria, with periodic removal of biologically darkened ice by synoptic-scale weathering crust degradation events. However, this negates the possibility of any cell reproduction of planktonic cells within the weathering crust, or viral cell lysis which has been observed to occur in the supraglacial microbial biome (Rassner et al., 2016; Säwström et al., 2007). Considering reproduction, it is possible that advected planktonic cells are dead, and therefore unable to reproduce, highlighting the need to examine this phenomenon, which could be undertaken using live-dead staining protocols (Boulos et al., 1999), despite their potential flaws (Davey and Hexley, 2011).

Alternatively, the rate of addition of cells to weathering crust meltwaters (increasing cell concentration) is equal their removal. Processes for removal including cells becoming stuck in pores (mechanical filtering; (Irvine-Fynn et al., 2012) or lysed by viruses. Addition of cells would occur via replication, as described above, the liberation of cells from ablating ice crystals (Dancer et al., 1997) and aeolian transport (e.g, Anesio et al., 2017). Clearly, this hypothesis recovers a range of mechanisms which require further investigation. Viral control rates require quantification, the occurrence and the potential for and proportion of mechanical filtering must be determined (via a tracer particle study) despite the implication of the results presented herein, and the delivery of cells to weathering crust melt waters from ice crystal melt and aeolian deposition must be examined in a detailed budgeting study at a single site. Doubling times of glacier surface microbes have been examined by (Anesio et al.,

2010) for Alpine surfaces, but require consideration in parallel with the residence times of planktonic cells within the weathering crust.

The nature of the hydraulic conductivity measurements undertaken here (i.e. and average across the depth profile) preclude detailed examination of flow dynamics. However, the presence of preferential flowpaths can be excluded. One mechanism to explain the apparent reduction in cell concentrations between near-surface ice and streams is that rising discharge is associated with the effective capture of flow by larger pathways. Given the depth-density relationship outlined in section 2.7, efficient pathways, associated with larger pores, would be found near the surface. With a rise in water table, these efficient pathways would become saturated capturing flow and hence a negative correlation between cells and water table level, where a water table close to the surface would be associated with reduced cell concentrations, would be expected. However, no correlation was observed between water table depth and cell concentrations, and as such this phenomenon seems unlikely to occur. However, this does not consider the role of fracture flow, which may also act as an efficient transport pathway, capturing flow.

5.4.2.2 Inter-crystal pore size

This dataset demonstrates that at all sites, cells (and therefore particles) with a diameter of ≤ 15 μm can pass through the weathering crust, implying the presence of pores of this size within the saturated layer of the weathering crust through which water flux is measured in this study. The dataset presented herein does not directly enable definitive identification of an upper size boundary for mobilised particles. The flow cytometer used, the Sony SH-800EC, can permit a maximal particle diameter of 100 μm through its fluidics system, and as no flow blockages occurred during sample analysis, it can be assumed that no particles ≥ 100 μm where present in the meltwaters collected. However, it is important to note that samples were intentionally disaggregated to enable accurate cell enumeration, so cell-cell and cell-particle aggregates ≥ 100 μm may have been present in the sample prior to pre-treatment. Therefore, these data indicate that pores of at least 15 μm must be present in the weathering crust but cannot elucidate a maximal pore size.

The pore size suggested is substantially smaller than the maximum inter-crystalline vein size of 10^{-3} m (1000 μm) suggested for "rotting" ice by Nye (1991). Considering the proposed formation mechanism for the weathering crust, a pore-size depth relationship would be expected, and larger pores may transport large particles may only be observed at close to the surface where crystal boundary melt

is greatest, in the unsampled unsaturated zone of the weathering crust. The sampling strategy applied here does not enable the consideration of depth variation of particle size transport capacity, as samples of cells were collected from meltwater obtained throughout the saturated depth profile of the weathering crust. In further assessing the transport capacity of the weathering crust, future studies should consider attempts to directly measure pore size throughout the depth profile of the weathering crust in both the saturated and unsaturated zones. Nuclear magnetic resonance imagery has been successfully applied to laboratory ice samples (Brox et al., 2015), but is logistically unfeasible to apply in a field setting, although appropriate ice exhumation techniques which maintain ice structure may enable this analysis to be carried out.

Pore size acts as a control upon porosity in groundwater settings (Schwartz and Zhang, 2004), but in such an environment there is no empirical relationship between the two as the density of pores, dependent on crystal size also acts as a control (Bear, 1972). However, considering the conceptual model presented in section 2.7, porosity in the weathering crust is the result of widening of interstitial spaces between crystals as they melt along their boundaries (Müller and Keeler, 1969) (Nye, 1991); and an increase in pore size implies and increase in weathering crust porosity. Porosity is not directly measured in this study due to the destructive nature of removing bulk samples, however permeability, itself a function of porosity is, and can be used to imply changes in pore size within the weathering crust. Permeability, and therefore porosity and pore size, appears to have no influence on planktonic weathering crust cell size distributions (Figure 5.7), with all cell sizes recorded mobilised at all measured permeabilities. The implication of this, coupled with considerations above, is that, to the 36 cm depth sampled, pore density acts as the control upon permeability and pore diameters exceed 15 μm, at least in part of the depth profile of the saturated zone. It should be noted that unweathered ice crystals are not a uniform size; structural features in glaciers, such as foliation, are defined largely by crystal size variation (Hudleston, 2015) and hence the influence of pre-weathering ice structure should be considered in future work regarding pore sizes and development in weathered ice.

The assertion that even large cells, exceeding 15 μm in diameter, are mobilised through the weathering crust appears to be in direct contrast to the proposed mechanical filtration (Irvine-Fynn et al., 2012) and associated darkening of glacier surfaces commonly observed throughout the ablation season in the northern hemisphere (e.g. Tedstone et al., 2017). As mentioned above, the sampling strategy applied is only suitable to capture planktonic cells which move through the weathering crust, not those retained within it. Large eukaryotic cells, such as algae, are known to be retained on the

surface of the Greenland Ice Sheet (Ryan et al., 2018; Stibal et al., 2017), and larger colloids, such as bacterial-particulate aggregates, such as the early stages of cryoconite formation (Langford et al., 2010) may also retained within the weathering crust; note that the data presented herein is unable to place an upper bound on weathering crust pore size. Darkening may also be attributable to cells bound to ice crystals either mechanically or in biofilms.

5.4.3 Supraglacial contribution to downstream nutrient fluxes

This dataset allows for a conservative estimate of nutrient fluxes in the form of bacterial cells (a key component of particulate organic carbon, POC), but it should be noted that these calculations involve an extensive degree of upscaling and are subject to a range of assumptions and limitations. Firstly, modelled run-off from Bliss et al. (2014) is considered for RCP 4.5 only, associated with a "more likely than not" temperature rise of 2 °C (IPCC, 2013). In contrast, the highest emission scenario, RCP 8.5, is associated with a temperature rise of up to 4.8 °C by 2100. As glacier melt rates over the next century are strongly linked with temperature (and thus emissions scenarios), so is runoff. Melt and runoff is the key control upon the number of cells liberated and exported from glacier surfaces, and therefore POC flux from glaciers, therefore there is clearly large variance in POC estimate dependent on the emissions scenario considered. Any uncertainties in the hydrological modelling will also be reflected when estimating POC and nutrient flux. Changes in community composition and cell concentration on the glacier surface may also occur throughout the next century and cannot be estimated without understanding of controls upon them, which are currently lacking for ice-surface environments; although increasing temperatures have been associated with increased microbial activity in Arctic Tundra soils (Mikan et al., 2002).

The upscaling exercise undertaken here is based upon 11 sites across the northern hemisphere. Whilst the glaciers studied incorporate a range of climates and thermal settings, surface characteristics are markedly different from other glaciers found globally, such as debris covered glaciers prevalent in the Himalaya (e.g. Nakawo et al., 1999), which are not thought to exhibit a weathering crust due to the presence of the surface debris layer. Furthermore, the potential for surface cover changes (for example, an increase in debris on European Alpine glaciers as surfaces lower and flatten in future due to mass loss) are not considered. The effect of this upscaling is best exemplified with sample volumes; converting < 1 L of cell samples to represent millions of litres will magnify any imprecision and uncertainty by vast amount. The robustness of this upscaling estimate could therefore be enhanced

with the collection of samples for unsampled environments, such as the Himalaya (or Patagonia or Alaska) and by increasing the number a volume of samples for which cells are enumerated.

The microbial cell concentrations presented herein exclude cells which are bound to ice crystals, which are possibly eluted from the glacier surface during weathering crust degradation events (such as rainfall). Without determination of the fate of such ice-bound cells, robust estimates of POC and nutrient flux cannot be made, however the values presented here, which exclude such cells, represent a minimum POC flux from glacier surfaces based on the assumption that the glacial discharges of (Bliss et al., 2014) occurs.

The final limitation related to these calculations is that of cell shape. When considering the two assumed shapes, rods and spheres, the smaller cell volume associated with the former result in fluxes ≈ one-third of the latter. To further refine this estimate, knowledge of the phylogenetic association of cells moving through the weathering crust, which would enable cell shape to be established, would enhance the reliability of these estimates. The limitations outlined above infer the calculated fluxes are likely to represent minimum estimates of carbon flux from glaciers over the next century, and as such the values calculated assuming rod shaped cells are used to reflect this. Therefore, the annual average estimate between 2003 – 2099 of extraglacial export of carbon is 1.1×10^9 kg C a^{-1} (1.1 Tg C a^{-1}), nitrogen 2.3×10^8 kg N a^{-1} and phosphorus 2.3×10^7 kg P a^{-1}.

Hood et al. (2015) report POC export rates for the Greenland Ice Sheet and mountain glaciers of 1.89 Tg a^{-1}, 1.7 times the POC export estimated herein. The carbon fluxes presented in this chapter are the equivalent of mobilising 0.05 - 0.11 % of the 1 – 2 Pg C stored within the aquatic biosphere per annum (Falkowski et al., 2000). The fluctuations in carbon export through the next century we report are attributable to changes in water flux, as constant cell concentrations are assumed. More pertinently, 44.6 % of this meltwater export is directly because of mass loss rather than annual cycling. This implies the liberation of long-term ice-archived nutrients from glaciers to downstream environments at a rate of 4.4×10^8 kg C a^{-1}, 1.5×10^8 kg N a^{-1}, and 1.5×10^7 kg P a^{-1}. Furthermore, as runoff reduces due to glacier retreat, this annual supply of nutrients to the aquatic and marine biosphere reduces at the end of the next century, marking a substantial change in the availability of both carbon and other macronutrients and molecules in downstream environments.

5.5. Conclusions

This chapter reports a mean weathering crust microbial cell concentration of $2.2 \times 10^4 \pm 5.5 \times 10^4$ cells mL^{-1} with a modal size of 1 – 2 μm from a dataset of 763 samples collected from 11 glaciers across the Northern Hemisphere. Cell abundances vary on a glacier scale, with the highest abundances being observed in Greenland, and the lowest in the Central European Alps and Scandinavia. Equal concentrations of cells are observed in streams and the weathering crust, albeit within large ranges, and cells (and inorganic particulates) in excess of 15 μm diameter are mobilised within the weathered near surface of ablating ice masses. Therefore, no evidence is presented that the weathering crust acts as a mechanical filter, darkening glacier surfaces, but that further investigation is needed involving a) an intensive, catchment-scale study on a single glacier for an extended period incorporating a range of synoptic conditions and b) the application of conservative particulate tracers to the weathering crust to ascertain links between transport of microbial cells through it and (potentially) into supraglacial streams. Under this model, surface darkening of glaciers can be attributed to growth of cellular communities which are not mobilised in weathering crust waters, such as those bound to ice-crystals, throughout the ablation season. These values enable an conservative estimation of carbon (in the form of POC), nitrogen and phosphorus export from the supraglacial environment, albeit with numerous limitations, of 1.1×10^9 kg C a^{-1} (1.1 Tg C a^{-1}), nitrogen 2.3×10^8 kg N a^{-1} and phosphorus 2.3×10^7 kg P a^{-1}, 1.7 times lower than existing estimates, but equivalent to the annual mobilisation of ≈ 0.08 % of carbon stored in the aquatic biosphere. Future evaluation of these fluxes should look to consider cells bound to weathering crust ice crystals, including their fate, and the morphologies of cells used to increase its robustness.

6. The Eco-Hydrology of the Weathering Crust in a Supraglacial Alpine Micro-Catchment

6.1 Introduction and study design

This chapter examines the supraglacial hydrology and ecology of a singular supraglacial micro-catchment, applying a strategy akin to Munro (2011) and Willis et al. (2002), and aiming to further develop the work undertaken in these studies. Chapter 3 revealed no regional-scale links between the hypothesised control of SWR receipt and hydraulic conductivity in the weathering crust. Chapter 5 revealed no links between hydraulic conductivity and cell concentration, but implied the presence of an efficient transport pathway, advecting planktonic weathering crust to streams. Therefore, this chapter aims to characterise links between energy balance, including sub-surface water and ice temperature, and weathering crust development over time, measured using the proxy of hydraulic conductivity, on a local scale, aiming to eliminate confounding variables such as unweathered ice crystal size. Density measurements are arguably a more applicable proxy measure of weathering crust development, as the process of near-surface weathering causes loss of ice mass without the loss of volume (section 2.7). However, undertaking density measurements of near-surface ice is a destructive process requiring the removal of a shallow core, precluding the repeat measurements to meet the other aims of this study. As such hydraulic conductivity, itself proportional to effective porosity which is empirically linked to density by Cooper et al. (2018), is used as a proxy measure for weathering crust development. To assess porosity, which is partially controlled by grain size in unconsolidated porous media (Schwartz and Zhang, 2004), ice crystal size measurements were attempted following completion of hydraulic conductivity measurements. It is hypothesised that hydraulic conductivity will increase with periods of high SWR receipt and reduce with periods of low SWR receipt when turbulent fluxes are more prominent. This is unlikely to present as a correlation on a simple scatter plot due to the hysteric nature of the relationship and relevance of preceding conditions, rather consideration of a time series is required (see Figure 2.4, p35 for a conceptual model of weathering crust development over time).

A catchment-scale study is also well suited to test the assertion that weathering crust meltwaters are advected laterally to supraglacial streams, transporting planktonic cells efficiently through the surface. Examination of the surface and water table will enable the consideration of flow paths from-a-point to the supraglacial stream network. Chapter 5 highlighted that planktonic weathering crust cells

are likely to be efficiently advected through the weathering crust once entrained within meltwater in the saturated layer, and as such the rate of transport can be described by the pore water velocity of the weathering crust. This study therefore is designed to couple cell concentrations with pore water velocities and transport pathways to establish residence time of planktonic cells within the saturated zone of the weathering crust. Calculation of pore water velocity requires knowledge of hydraulic conductivity, hydraulic gradient and effective porosity, which can be calculated using ice density. As ice density will not be measured directly for the reasons stated above, the modelling work of Schuster, (2001) will be used to calculate this variable. Concentration of cells bound to ice, mechanically or in biofilms, will not be considered. As for ice density, the sampling technique requires the removal of ice from the glacier surface, precluding repeat measurements and the assessment of the development of the system over time.

6.1.1 A micro-catchment approach?

Munro (2011) examined delays in supraglacial runoff from two microbasins of differing geometries on the Peyto Glacier (Canada), recording net radiation, wind speed, temperature, vapour pressure and supraglacial runoff on warm and sunny days. The study revealed a major difference in run-off time, a purposely delineated rhomboidal area demonstrated a delay time of 1 – 2 h, whilst in contrast a naturally delineated elongated area, aligned with microtopography, demonstrated delay time of 7.5 – 11.5 h. The hypothesised control upon drainage time was different flow connections in the weathering crust for the different shaped catchments, and the recommendation was made that the response time of the elongate catchment should be incorporated into hydrological glacier runoff models. A key point raised is that supraglacial microbasin work yields potentially useful results about the hydrological response of the ice surface to melt input and highlights the importance of measuring discharge at the stream outlet of the defined catchment, and to provide sufficient description of the weathering crust.

(Willis et al. (2002) consider the effects of up-glacier retreat of the snowline on the spatial and temporal patterns of meltwater routing across a 0.11 km^2 catchment on Haut Glacier d'Arolla (Switzerland) using a physically based model, considering catchment elevation, modelled melt rate and energy balance of radiative and turbulent fluxes. Melt was also directly measured using an ultrasonic depth gauge. Water was assumed to flow downslope to the catchment outlet, where discharge was measured using a Druck pressure transducer and a stage-discharge curve. These variables were assessed

over time with consideration of observing change associated with snowpack retreat, application of these techniques in the same fashion equally demonstrates the potential to examine weathering crust development.

6.1.2 Weathering crust density modelling

Schuster, (2001) examines weathering crust processes on ablating glacier ice. Of interest in this study, is the modelled depth-density profile of a developing weathering crust, simulated using energy balance parameters. A column of ice with a 1 m^2 surface area is divided into units of increasing thickness, such that each layer is twice as thick as the layer above it. As such, level one (L_1) is 1 cm thick, level 2 (L_2) is 2 cm thick (total depth 3 cm) and so on, with level 6 (L_6) being 32 cm thick, a total column depth of 63 cm. It is assumed that beneath L_6, a layer of ice of density 890 kg m^{-3} exists to infinite depth. The model uses five-minute energy inputs to determine melt and enable calculation of a depth-density profile. The required inputs include SWR_{in}, net LWR, and turbulent fluxes to model melt at each layer, which are used to calculate the density of each layer allowing for consideration of density at the previous timestep. The work also presents example non-linear depth-density curves for a developing and degrading weathering crust, as described in section 2.7.

6.2 Materials and methods

Data collection was undertaken between the 1st and 25th July 2016 (DOY 183 – 207) at Vadrec del Forno, Valais, Switzerland (Figure 6.1; Table 6.1), located at 46.31 °N, 9.70 °E. The glacier has an area of 8.2 km^2, and an elevational range of 2330 – 2850 m (Table 5.2). Detailed background regarding the geological setting and ice structure of the glacier can be seen in the work of (Jennings et al. (2014). All auger-hole sites are referred to as VFx herein, with x corresponding to the auger-hole number identified in Figure 6.1, whilst the stream gauging station is referred to as VDS. A suite of metrics was recorded from a micro-catchment on the eastern side of the glacier relating to stream and weathering crust hydrology, samples for microbial analysis, meteorological data, orthoimagery, near-surface ice temperature, and ice crystal imagery. Two main sampling strategies were applied throughout the study period, both collecting hydrological data and microbiological samples:

1. to examine spatial changes of these variables across the entire micro-catchment (DOY 187, 188, 199, 200 and 202) (all VFRs)
2. to examine temporal changes along a transect of VFR 1-4 (DOY 191 and 201).

Opportunistic sampling was applied on days with poor weather and logistical requirements that prevented a full day of fieldwork, to supplement the structured dataset. This includes data collected on DOY 198 (VFR 1, 2, 5 and 6) where slow recharge prevented more than two measurements being undertaken at each hole and samples collected at VFR14 (n = 1) and VFR22 (n = 2).

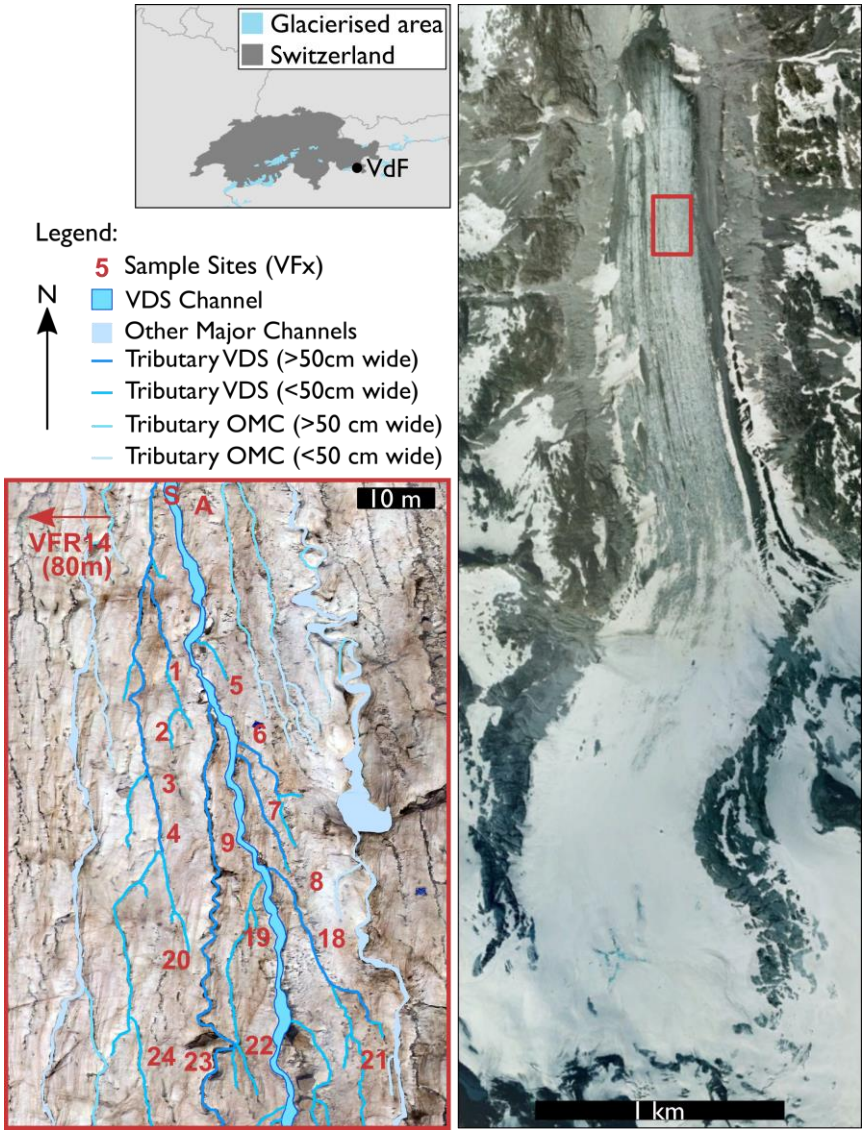

Figure 6.1 Map showing the location of Vadrec del Forno within Switzerland, and location of study site on the glacier. The location of recharge holes, stream gauging point (S) and water table array (A) in the context of immediate streams and rills are shown. Further information is given about each auger-hole in Table 6.1.

Table 6.1 Auger-hole site information.

Site	Location (CH 1903)	Elevation (m asl)	Distance from stream (m)	Surface slope (°)	Notes
VFS	774230 E 133302 N	2556*	-	-	Stream gauging site.
VFR1	774235 E 133275 N	2557.8	2.7	6.9	
VFR2	774234 E 133267N	2558.4	5.9	4.7	
VFR3	774231 E 133260 N	2558.8	11.7	5.6	
VFR4	774232 E 133254 N	2559.2	6.6	5.0	
VFR5	774237 E 133267 N	2557.7	3.1	5.6	
VFR6	774241 E 133259 N	2558.0	3.2	4.1	
VFR7	774245 E 133251 N	2558.6	2.7	4.6	
VFR8	774247 E 133247 N	2559.4	4.0	6.4	
VFR9	774230 E 133261 N	2558.8	1.7	7.6	
VFR14	774178 E 133303 N	2555*	-	-	Not in VDS catchment.
VFR18	774222 E 133214 N	2559.8	4.1	6.5	Coarse, clear ice in vicinity.
VFR19	774229 E 133240 N	2559.6	4.2	5.2	Distributed surface debris in vicinity.
VFR20	774232 E 133236 N	2560.2	2.4	10.3	
VFR21	774254 E 133224 N	2560.7	9.6	3.7	
VFR22	774242 E 133247 N	2560.4	4.6	4.1	
VFR23	774239 E 133229 N	2560.9	3.9	9.8	
VFR24	774232 E 133228 N	2561.1	5.6	7.0	

n.b. VFR10-13 and 15-17 abandoned due to lack of recharge.
Elevations are from the DEM (Figure 6.2) unless indicated as thus (*), where data is from a handheld GPS.

6.2.1 Meteorological conditions and ice temperature

A HOBO automated weather station (AWS) was installed on the glacier surface, measuring air temperature (2 m above the surface), average wind speed and direction, wind gust speed, relative humidity and precipitation (via a tipping bucket) at 15-minute intervals throughout the study period. This record is, however, incomplete, with gaps in the dataset from 18:15 on DOY 193 to 9:45 on DOY 197, and 11:45 on DOY 204 to 9:30 on DOY 205. These breaks in the dataset are due to high

winds toppling the AWS and were identified in the record using periods of high windspeed which rapidly (i.e. within one measurement period) fell to 0 m s^{-1}, coupled with anecdotal field observations.

Maximum potential shortwave incident radiation (SWR_{in}) was modelled as described by (Irvine-Fynn et al. (2014) using a cloud cover correction (see Greuell et al., 1997). Cloud cover was recorded at least thrice-daily during daylight hours, typically at 8:00, 12:00 and 16:00. Hourly averages of these data were used to model hourly melt rate using the model described by Brock and Arnold (2000), developed for Haut Glacier d'Arolla, also in the Swiss Alps and a similar size and geometry to Vadrec del Forno. For the melt model, albedo was set at a universal value of 0.29, typical of "slightly dirty ice" (Paterson, 1994). Roughness was set to the default value, 0.04 m, typical of an ablating alpine glacier surface. Proportional contribution to melt of SWR receipt at the surface and other fluxes (net LWR and the turbulent fluxes) were calculated from model output, as were cumulative SWR energy flux and cumulative melt throughout the study period.

Surface ice temperature was recorded in proximity to VDS and VFA at nominal depths of 10, 20, 30 and 40 cm using a Measurement Computing 5104 logger and TMC6-HD temperature sensors (calibrated by the manufacturer), logging at 10-second intervals. Probes were installed in 1 cm diameter holes drilled into the ice. Due to surface melting, temperature probes were periodically re-installed at depth between installation (DOY 198) and the end of the study period (DOY 207), often "melting out" onto the surface.

6.2.2 Orthomosaic and DEM generation

The orthomosaic was constructed using a DJI Phantom 3 quadcopter to capture aerial imagery in August 2016, using the in-built camera at a flight altitude of 30 m. Images were recorded every 2 s at a 12-megapixel resolution with a 20 mm (35 mm equivalent) focal length and an aperture of *f*2.8 Attempts to fly an alternate UAV, a 3DR X8 equipped with a Canon EOS M3 (24.2-megapixel, *f*3.5, 18 mm/29 mm equivalent focal length), in July were unsuccessful due to a series of mechanical failures. Agisoft Photoscan was used to generate an Orthomosaic with a pixel size of 0.02 m, geo-located using a Leica dGPS and a series of ground control points. Image overlap was not adequate for the generation of a DEM using these data. Supraglacial channels were identified and mapped using ArcMap 10.5 at a 1:100 scale.

A DEM (0.05 m pixel size) was generated in July 2017, using imagery collected by a fixed-wing Skywalker X-8, equipped with a Sony A500 20.1-megapixel resolution camera at a 16 mm focal length (24 mm equivalent). The DEM was constructed using structure-from-motion in Agisoft Photoscan, and initially georeferenced using Sentinel Imagery and feature-matching. To account for displacement of the DEM relative to the orthomosaic due to glacier flow, the geolocation of the DEM was adjusted to align with the orthomosaic collected 2016, using distinctive features thought to remain static on the glacier surface including large boulders (< 2 m) and distinctive stream features. The resultant DEM and stream network are shown in Figure 6.2.

Attempts were made to collect data relating to ice crystal size by bulk-sampling of the weathering crust once the final bail-recharge experiment was complete. The adze of an ice axe was used to gently exhume intact crystals from the ice surface, which were then placed on a dark sheet for photographing using a Canon EOS 7Dmkii (20.2-megapixels, *f*5.6, 22 mm actual/35 mm effective focal length). Post-processing was undertaken using ImageJ via the "Analyze Particles" tool and a set scale established from including a ruler in the original photo. Final images had a resolution of ~3700 px m^{-1}. However, smaller ice crystals melted preferentially, resulting in data bias, and these data were not included in the final analyses.

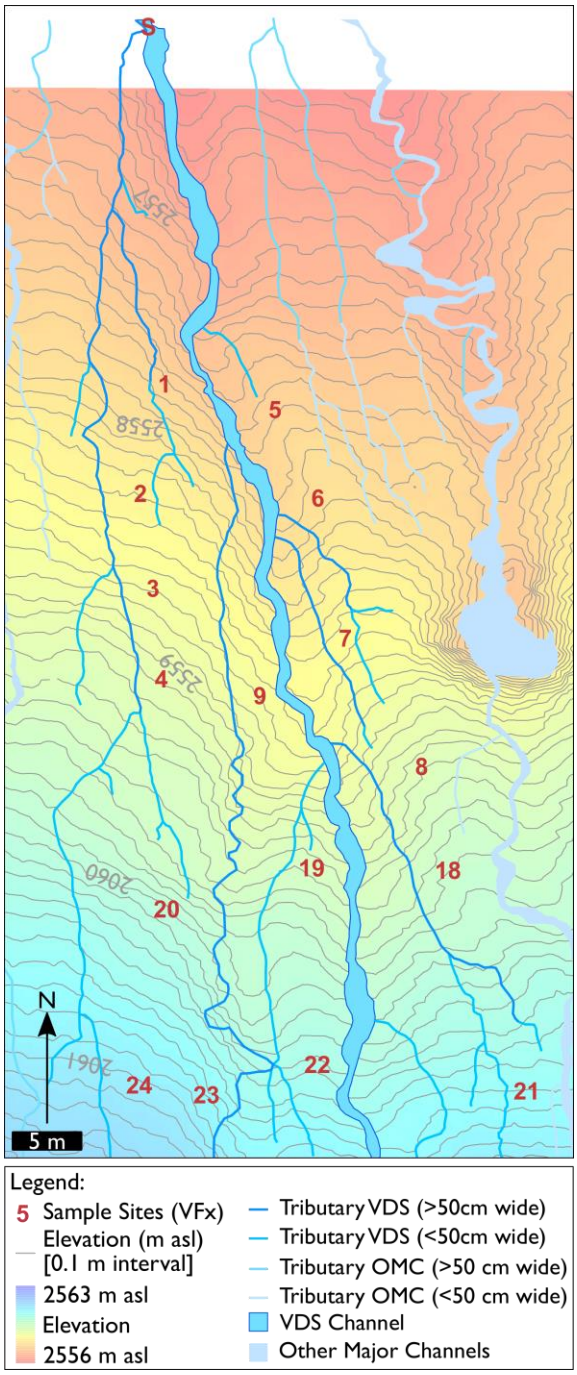

Figure 6.2 Digital elevation model (DEM) constructed for the VDS micro-catchment in July 2017. Channels were mapped using the orthoimage generated in 2016; the VDS stream and its tributaries are mapped, as are the two adjacent major channels (OMC) and their corresponding tributaries. Note that some channel migration (< 5 m) is demonstrated between the mapped channels (August 2016) and implied channel locations from the DEM (July 2017).

6.2.3 Hydrological data collection

For calculation of hydraulic conductivity, 36 cm deep auger-holes of 5 cm dimeter were drilled using an ice auger (Kovacs Enterprise, USA) and a Makita 18V Combi Drill. Data collection and processing followed the protocol outlined in Chapter 3 (see Stevens et al., 2018). Holes were reutilised throughout the study period and were re-drilled to a depth of 36 cm at the start of each day to minimise the effects of surface melting. Electrical conductivity (EC) and temperature of borehole waters were measured using a combined Reed SD-4307 probe at a depth representing a mid-point between the auger-hole base and water table, following microbial sample collection.

Stream discharge was measured at VDS using the protocol described in Chapter 5 (section 5.2.2). VDS was selected as a location into which water from the VFx sites was expected to drain into based on a field assessment. EC and temperature were recorded at 2 second intervals between 9:30 and 17:30 on the 6th July (DOY 188; note 2016 is a leap year) using a Reed SD-4307 logging conductivity meter (± 0.2 °C and 0.2 μS cm^{-1}).

To measure water table depths, an array of 10 modified piezometers (as described in Chapter 3; Stevens et al., 2018) were installed in a 5 × 1 m grid adjacent to VDS (VFA; Figure 6.1). Piezometers were modified to be powered by and output to the Campbell CR1000 used for logging at VDS. Voltage output was recorded every 10 minutes and subsequently converted to water table depth using a laboratory determined calibration curve. VDA probes were initially installed to a depth of 50 cm and were periodically reinstalled due to melt-out throughout the study period.

6.2.4 Microbial sample collection and analysis

Each hydraulic conductivity measurement was associated with a sample for microbial analysis. These samples were collected using a syringe and plastic tubing which were pre-contaminated by rinsing three times using recharge water before sample collection. Samples were collected from the meltwater collected in the recharge hole from a mid-point depth between the water table surface and auger-hole base. Periodic samples were collected directly from the stream gauging point (VDQ). Samples were stored in 15 mL Falcon tubes and fixed with Formaldehyde (2% w/v final) within eight hours of collection and stored in the dark and were frozen at – 80 °C upon return to the UK. Samples were defrosted gently at 4 °C, with the defrosting process finalised at room temperature whilst stored

in the dark throughout. Microbial cell concentrations and sizes examined using flow cytometry using the optimised protocol described in Chapter 4.

6.2.5 Data processing

6.2.5.1 Pore water velocities and water transport pathways

Equation 6.1 (Schwartz and Zhang, 2004) was used to examine pore water velocity, v, to assess the transport rate of impurities in the weathering crust, assuming that impurities entrained within weathering crust meltwaters are advected. K is hydraulic conductivity, i hydraulic gradient, and n_e effective porosity.

$$v = \frac{Ki}{n_e} \quad \text{[Equation 6.1]}$$

Hydraulic gradient was calculated using the water table elevation above sea level, the length of the drainage pathway established via the DEM (measured to the nearest 0.1 m) and the elevation of the channel at the terminus of the drainage pathway. Drainage pathways were determined to be orthogonal to surface slope, terminating at their confluence with a mapped surface channel.

Effective porosity (n_e) was calculated using Equation 6.2 (after (Cooper et al., 2018)) using weathering crust ice densities, ρ_{ice}. Ice density was not directly measured. As such, a weathering crust depth-density profile obtained for a weathering crust undergoing formation using figures available in the work of Schuster (2001). Density was calculated for saturated weathering crust ice for each auger hole. The level of the water table for each hydraulic conductivity measurement was used to determine the depth of the saturated zone from the surface, at depth d. The aquiclude was considered to be at 63 cm depth after Schuster (2001). Bulk density for the weathering crust between d and 63 cm depth was calculated the depth-density profile of Schuster (2001). For example, for a water table 10 cm beneath the surface, the mean density of ice from 10 cm to 63 cm deep was determined, and this was subsequently to calculate effective porosity for each auger-hole measurement.

$$n_e = -0.97\rho_{ice} + 0.89 \quad \text{[Equation 6.2]}$$

However, calculation of porosity involved a degree of assumption which cannot be quantified without further experimental work. This process only considers total primary weathering crust

porosity, which is defined by the ice matrix, and does not consider secondary porosity (in the form of fractures, regardless of formation mechanism, which could include cracking linked with thermal expansion and contraction (e.g. (Sanderson, 1978)), insolation driven pathway opening and, in the case of terrestrial systems, solution weathering and erosion) which has been observed in the weathering crust (Cook et al., 2015).

6.2.5.2 Heat map creation

Hydrological measurements and samples collected for spatial analysis were attributed a "time-slice", based on the time of day collected, to enable partial elimination of temporal variation. The time taken to collect measurements from 12 auger-holes took around three hours and could be repeated a maximum of three times daily. As such, three sessions are used: morning (AM; before 13:00), afternoon (PM; between 13:00 and 15:30) and evening (EVE; after 15:30). Heat maps of water table elevation, hydraulic conductivity, EC, weathering crust water temperature and cell concentration were created for DOY 187 (AM only), 188, 199, 200 and 202 using ArcMap 10.5 (ESRI). Failure of piezometers

Water table depth from the ice surface, recorded via piezometer, was subtracted from the elevation of each auger-hole at the surface (Table 6.1) to generate a point-based weathering crust water table relative to sea level. These point data, along with the digitised stream network, were used generate a water table for the catchment via interpolation of point values from auger-holes using the hydrologically correct "topo-to-raster" tool, configured for spot data, included in the 3D Analyst package of ESRI ArcGIS 10.5.

Inverse distance weighting (IDW), with streams and rills set as boundaries was used to interpolate weathering crust hydraulic conductivity, EC and temperature in space for each time-slice from point-data collected using recharge probes and the combined EC/Temperature meter. A power of one was used for the IDW calculation, deemed most suited to interpolation of soil properties (Robinson and Metternicht, 2006). IDW was deemed to produce a superior output to kriging over decimetre scales for nutrient content in soils by Mueller et al. (2004) and hence was considered the most appropriate interpolation method.

6.3. Results

6.3.1 Meteorological conditions and ice temperature

Throughout the field campaign, prevailing meteorological conditions were as expected for a summer alpine period, with conditions generally clear and sunny with some development of afternoon cloud. Maximal daily temperatures were 10 – 15 °C, and daily minima 3 – 7 °C. However, this pattern was disrupted by the progression of a cold frontal system between DOY 194 and 197 which caused snowfall across the entire glacier surface to a depth of 15 cm from the evening of DOY 195 to midday on DOY 196. It should be noted that no AWS data was collected during this period. Ablation rates followed a typical diurnal pattern, with peak daily melt (10.2 mm we hr^{-1}) occurring between 13:00 and 16:00, depending on sky conditions. Lowest melt rates (< 1 mm we hr^{-1}) are observed in the early morning, prior to sunrise, but do not reach zero due to turbulent fluxes. Meteorological data are summarised in Figure 6.3 (a-d).

Near-surface ice temperature within the weathering crust was not successfully recorded. Probes were installed to depths of ≤ 50 cm between DOY 201 and 208 but were prone to melt out, and partial incursion of meltwater. Due to melt out, temperatures equal to, or exceeding air temperature were recorded and as such the data were deemed unreliable.

6.3.2 Weathering crust and stream hydrology

Hydraulic conductivity was successfully measured on 237 occasions at 15 auger-holes throughout the study period. On multiple occasions, recharge was insufficient to allow for the calculation of hydraulic conductivity. This occurred at VFR1-4 on DOY 197, VFR6 on DOY 198 at 16:30, and VFR22 on DOY188 at 13:43 and 16:20. It is important to note that recharge was incalculable at these holes for differing reasons: at VFR6 the water table was too low (i.e. < 6cm from the hole base) to allow for recharge measurement given the limitations of the probes (Chapter 3). VFR22 did not receive any water flow during either attempt to measure recharge; it is important to consider the location of the site on a topographic high near two channels (< 2 m; Figure 6.1). All 237 hydraulic conductivity values are associated with microbial enumerations, and 232 are associated with electrical conductivity (EC) and auger-hole water temperature measurements. As per Chapter 5, no significant correlation is observed (i.e. $p > 0.05$) between cells and hydraulic conductivity ($n = 237$),

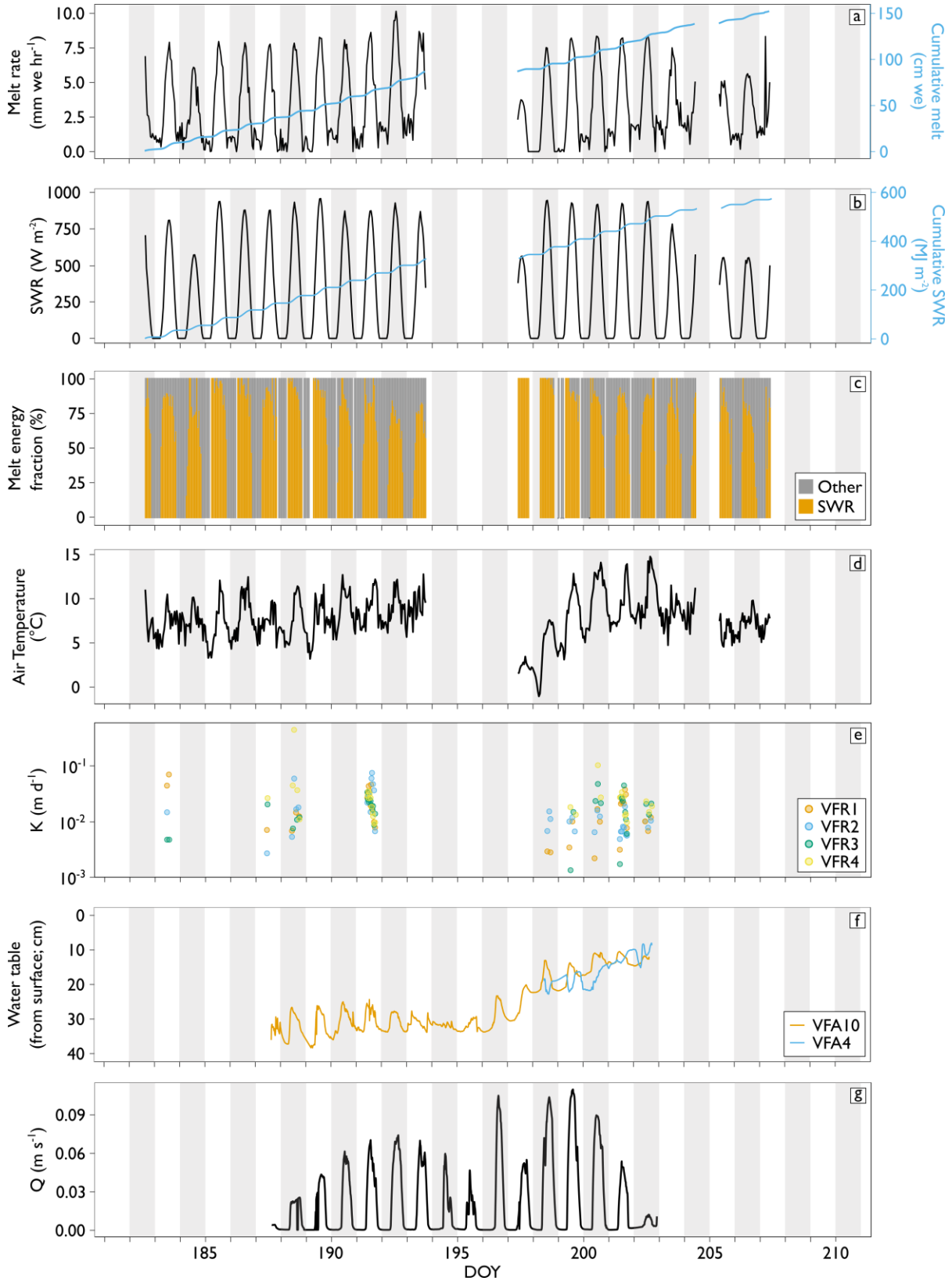

Figure 6.3 Time-series of a) modelled ablation rate and cumulative ablation, b) Hourly-averaged modelled SWR and cumulative energy receipt from SWR, c) proportional contribution to melt of SWR and all other energy fluxes; d) air temperature; e) auger-hole hydraulic conductivity for VFR 1-4; f) water table level at VFA and g) stream discharge at VDS. Trends are described in the main text.

permeability, EC, temperature (all n = 232). Furthermore, when considered on a per-hole basis, no significant correlations between microbial cell abundance and the hypothesised independent variables (hydraulic conductivity, permeability, EC and temperature) are apparent. No clear links are apparent between hydraulic conductivity, melt rate, the proportion of melt energy or stream discharge are observed in Figure 6.3, however low hydraulic conductivities on DOY 198 and 199 are associated with low air temperatures, including those which are < 0 °C overnight.

As the snowfall event was associated with cloud cover and low temperatures, degradation of the weathering crust would be expected to occur, with associated reduction in hydraulic conductivity. Figure 6.3e indicates a reduction in hydraulic conductivity at VFR 1-4 following the snowfall event; it should be noted that measurements of hydraulic conductivity were attempted on DOY 197 but it was not possible to take measurements as the water level in the auger-holes did not reach the 6 cm minimum threshold within ≈ 5 hours. Hydraulic conductivity is statistically compared before and after the snowfall event using an independent t-test. Levene's test for equality of variances demonstrated a statistically significant difference in variances between the before (n = 95) and after (n = 141) groups ($p < 0.05$). Hence, an unequal variances t-test was used, which showed that before the snowfall, hydraulic conductivity was statistically significantly lower (0.033 m d^{-1}) than after the snowfall event (0.056 m d^{-1}) (n = 236, adjusted df = 218, $p < 0.05$). Despite this broad trend, hydraulic conductivity on DOY 198 and 199, immediately following the snow is notably lower than on other days for VFR1-4.

A diurnal pattern is exhibited in the water table within the weathering crust at VFA10 (Figure 6.3f), but variability is reduced from DOY 194 - 196, corresponding with the snowfall period. This pattern is less clear at VFA4. On days when a peak in water table occurs, the peak is observed between 10:30 and 18:00, preceding peak melt on 9 out of 11 days by a mean of 119 minutes; and peak discharge by a mean of 164 minutes (n = 9), skewed by a value exceeding 7 h on DOY 188. On the two days where the water table peak follows peak melt and peak Q, it does so by a mid-point of 264 and 154 minutes respectively (both n = 2). It should be noted that the second of these mid-points (the time difference between peak Q and the water table maxima) is comprised of two highly spread values, 20 minutes and 288 minutes. In addition to the diurnal pattern, water table levels in the weathering crust at VFA4 and VFA10 exhibit a positive trend after DOY 196, indicating an upward movement of the water table. This trend is initiated following the snowfall event.

Stream discharge at VDS ranged from 0.0004 to 0.1098 $m^3 s^{-1}$ throughout the measurement period (Figure 6.3g). Peak discharge was observed between 11:30 and 17:40, a mean of 47 minutes after the peak melt rate (n = 12). As Figure 6.3g indicates, the highest discharge measured was on DOY 197, one day after cessation of snowfall. Unfortunately, meteorological data are lacking for this day due to AWS failure, but it should be noted that field observations the glacier surface was virtually clear of snow by the afternoon of DOY 197, and as such this high discharge can be linked with snowmelt. It should also be noted that discharge above the overnight baseline values was recorded during the snowfall event, implying the occurrence of melt processes. No correlation was observed between stream discharge and cell concentration (n = 53)

Stream EC and temperature was recorded on DOY 188 between 9:28 and 17:33 at two second intervals (Figure 6.4). EC ranged from 0 to 1.2 μS cm^{-1}, decreasing from 10:00 to 12:00, to > 0.6 μS cm^{-1} and further reducing to a stable 0.3 μS cm^{-1} from 15:00 until the removal of the sensor. Temperature variation was minimal, between 0.1 and - 0.1 °C with the lowest temperatures observed between 11:45 and 16:15. EC and temperature values from the weathering crust were also recorded and are compared with those in the stream. When considering EC, instrumental measurement uncertainties of ± 0.2 μS cm^{-1} mean that it cannot be concluded with certainty that auger hole EC and stream EC is different for all holes excluding VFR8. EC was statistically significantly lower after the snowfall event (0.5 μS cm^{-1}) (n = 231, adjusted df = 156, $p < 0.05$) higher (0.7 μS cm^{-1}), as revealed by an unequal variances t-test. This test was selected as Levene's test for equality of variances indicated a statistically significant difference in variances between the pre- (n = 95) and post- snowfall (n = 136) event groups ($p < 0.05$).

Mean, minimum and maximum storage times of water in the weathering crust were calculated for VFR 1-9 and 18-20 (i.e. all holes with more than two measurements). It was assumed that water flowed downslope, orthogonal to contour lines (Figure 6.2) into VDS or one of its connecting rills. Mean velocity (n = 224) was 0.24 ± 0.49 m d^{-1}, with a range of 0.01 – 3.35 m d^{-1}. Mean effective porosity of the saturated zone of the weathering crust (estimated *post hoc* using modelled data from Schuster (2001) and Cooper et al. (2018) was 9.6 ± 0.6 %, equivalent to that of a sandstone (Freeze and Cherry, 1979). Mean transfer time of a parcel of water from an auger hole into a stream via the assumed flowpaths was 61.1 ± 225.6 days, but values were highly variable ranging from 0.5 to 2144.7 days. Note that ± errors are given as ± 1 standard deviation, and despite implication of negative values these are clearly implausible.

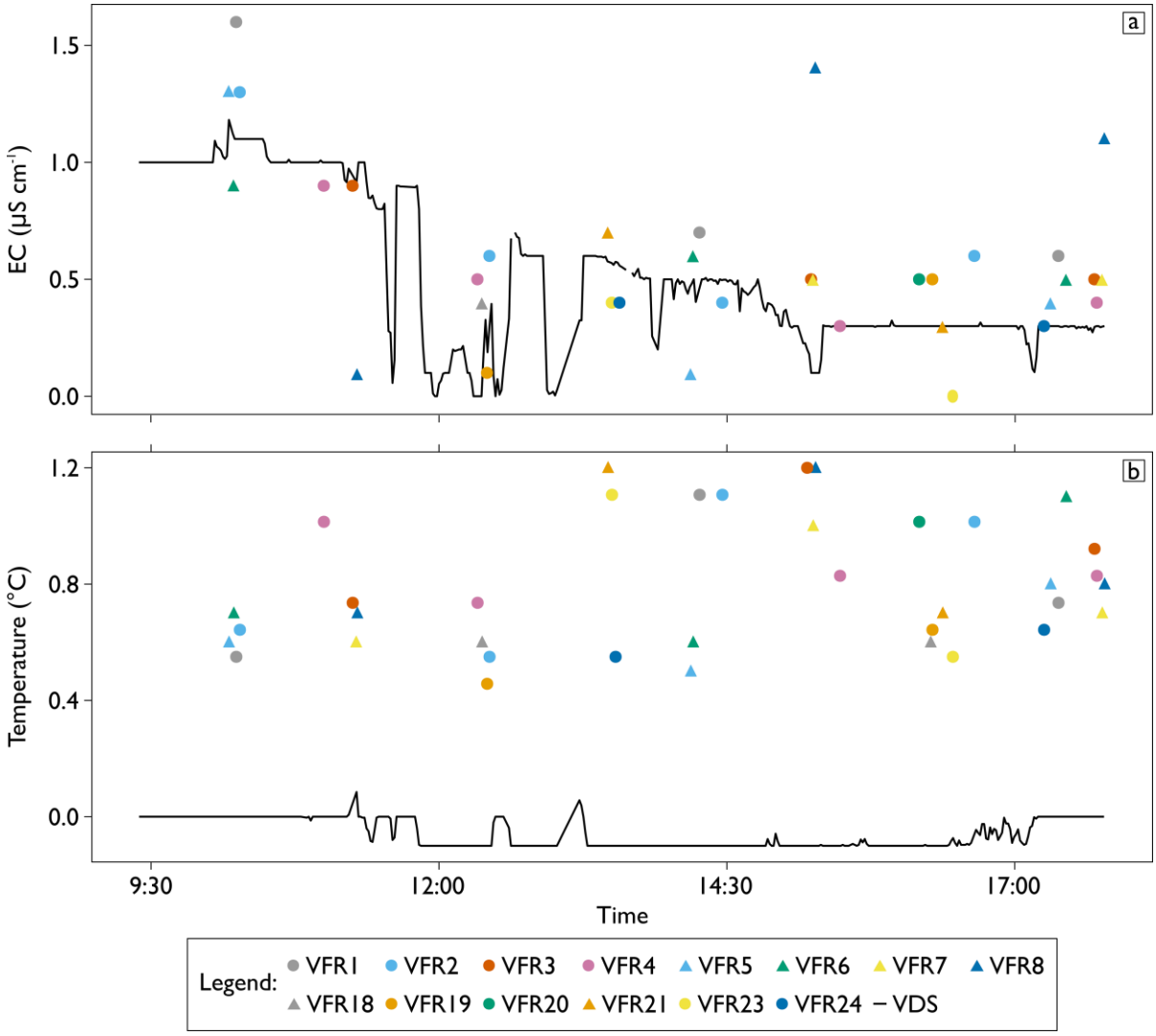

Figure 6.4 1-minute averages of a) EC and b) temperature at VDS and in the auger-holes on DOY 188. Auger holes on the east of VDS are indicated with a circle, and those on the west with a triangle. Instrumental uncertainty is ± 0.2 µS cm^{-1} and 0.1 °C for all measurements, error bars are not included for visual clarity. Therefore, it should be noted that the uncertainties associated with stream and EC measurements overlap for all holes aside from VFR8, for which uncertainties do not overlap with stream uncertainties for any of the three data points. For temperature, no uncertainty ranges for the stream and auger-holes overlap.

6.3.3 Microbial concentration and size distribution

Mean microbial abundance in the weathering crust was $1.5 \pm 2.2 \times 10^4$ cells mL^{-1}, ranging from 1.2×10^3 to 2.2×10^5 cells mL^{-1}, whilst mean cell concentration in the VDS channel was $1.5 \pm 2.1 \times 10^4$ cells mL^{-1}, ranging from 8.6×10^2 to 2.2×10^5 cells mL^{-1} (Figure 5.1). Note that ± errors are given as 1 standard deviation and represent variability of cell concentrations rather than

implying that a negative cell concentration is possible. As highlighted in Chapter 5, all samples meet the CC-APC criteria established in Chapter 4. To examine contrasts in microbial cell concentration due to the snowfall event, a t-test was used. Levene's test for equality of variances did not demonstrate a statistically significant difference in variances between the pre- ($n = 102$) and post-snowfall ($n = 149$) event groups ($p > 0.05$). The t-test showed that before the snowfall, cell concentrations were statistically significantly higher ($2.0 \pm 1.5 \times 10^4$ cells mL^{-1}) than after the snowfall event ($1.2 \pm 2.12 \times 10^4$ cells mL^{-1}) ($n = 235$, $df = 249$, $p < 0.05$).

The modal cell size group for all samples was a diameter of 1 – 2 µm (Figure 6.5a and b). As in Chapter 5, no significant difference in size distribution was observed between the weathering crust and the stream. To further explore the effects of the snowfall event on hydraulic conductivity, cell size distribution before and after the event was contrasted in both the weathering crust and the stream. The hypothesis was that the degradation of the weathering crust, due to a drop in SWR receipt and refreezing of interstitial meltwater would reduce pore sizes and may prevent mobilisation of larger cells. However, no significant change in size distribution was observed as a result of the snowfall event.

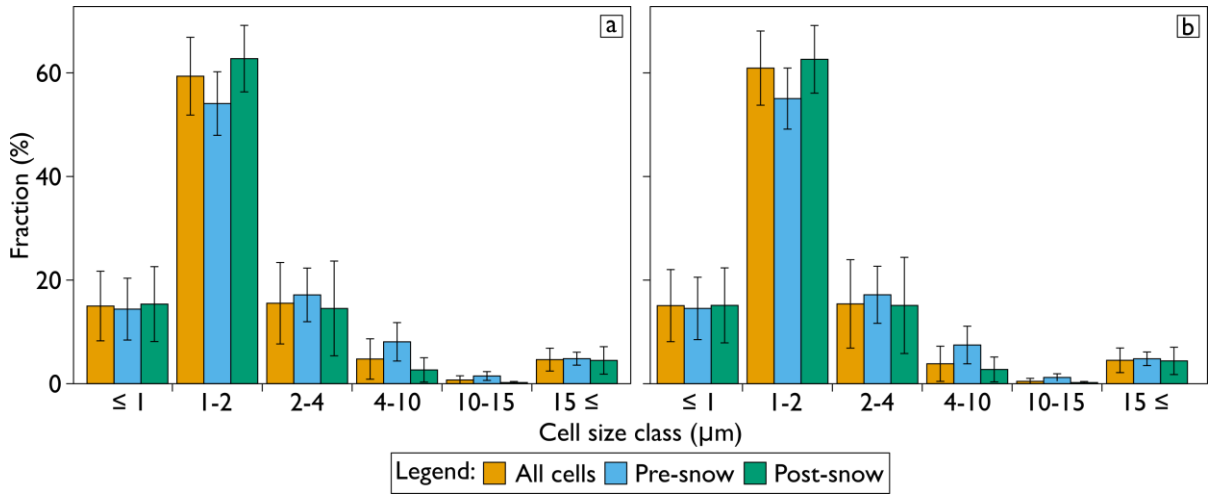

Figure 6.5 Cell size distributions in a) the weathering crust and b) at VDS, highlighting change before and after the snowfall event. Error bars are ± 1 standard deviation.

6.3.4 Spatial and temporal variation

6.3.4.1 Diurnal-scale trends

On DOY 191 and 201, a sampling strategy designed to examine temporal change across a transect was applied to auger-holes VFR1-4, which were examined at 13 and eight intervals

respectively. These data are summarised in Figure 6.6. It is assumed that all sites drain into the VDS stream above the gauging site, and do not drain into each other, using the downslope flowline construction described above (see Figure 6.2).

During DOY 191 and 201, all four auger-holes follow a similar pattern with regard in hydraulic conductivity, peaking in the afternoon between 14:00 and 16:00 (Figure 6.6). An equivalent pattern is observed in weathering crust permeability (Figure 6.7b). Notably, this pattern is not replicated in the discharge of the main channel. As per the spatial dataset, the location of each auger-hole (and hence its elevation) is the main factor in determination of relative water table with respect to all auger-holes. No clear trend is observed in EC. Considering changes in temperature, all four holes appear to respond in an identical fashion, with broadly similar temperatures which peak between 12:00 (noon) and 14:00. Microbial cell abundances do not exhibit any universal trend across the four auger-holes and channel on either of the temporal study days. On DOY 191, microbial cell abundances are of a similar magnitude at all sites. On DOY 201, VFR1 exhibits lower cell abundances than the other four sites.

6.3.4.2 Spatial analyses

Spatial variation of the water table (Figure 6.7), hydraulic conductivity (Figure 6.8), EC (Figure 6.9), temperature and cell concentration were examined on DOY 187, 188, 199, 200 and 202. The position of the water table remained relatively constant throughout the study period, notably being primarily defined by the surface micro-topography of the glacier. Elevation differences between each auger-hole was in the order of metres, whilst water table depth within each hole varied on a scale of decimetres, hence micro-topography was the primary determinant of spatial variation in absolute water table height (above sea level). Water table elevation reduces from south-west to north-east, at a generalised dip direction of 343 °.A constant depth is presumed for porous weathering crust (Schuster, 2001) crust (given equal melt across the 100 × 40 m sample area, which was equally unshaded), and as such can consider this water table surface as the hydraulic head surface and therefore flow direction of water within the weathering crust. Considering changes in time, which can be inferred from this data despite not being the focus of study design, an increase in water table elevation can be observed throughout all days with three time-slices (i.e. 188, 199, 200, 201) as demonstrated by the down-glacier shift of the red region containing the upper one-third of values.

The highest hydraulic conductivities were observed at VFR9 (0.3 – 0.68 m d^{-1}) which is usually the site with the highest hydraulic conductivity (aside from DOY188 AM and DOY 200 AM). This

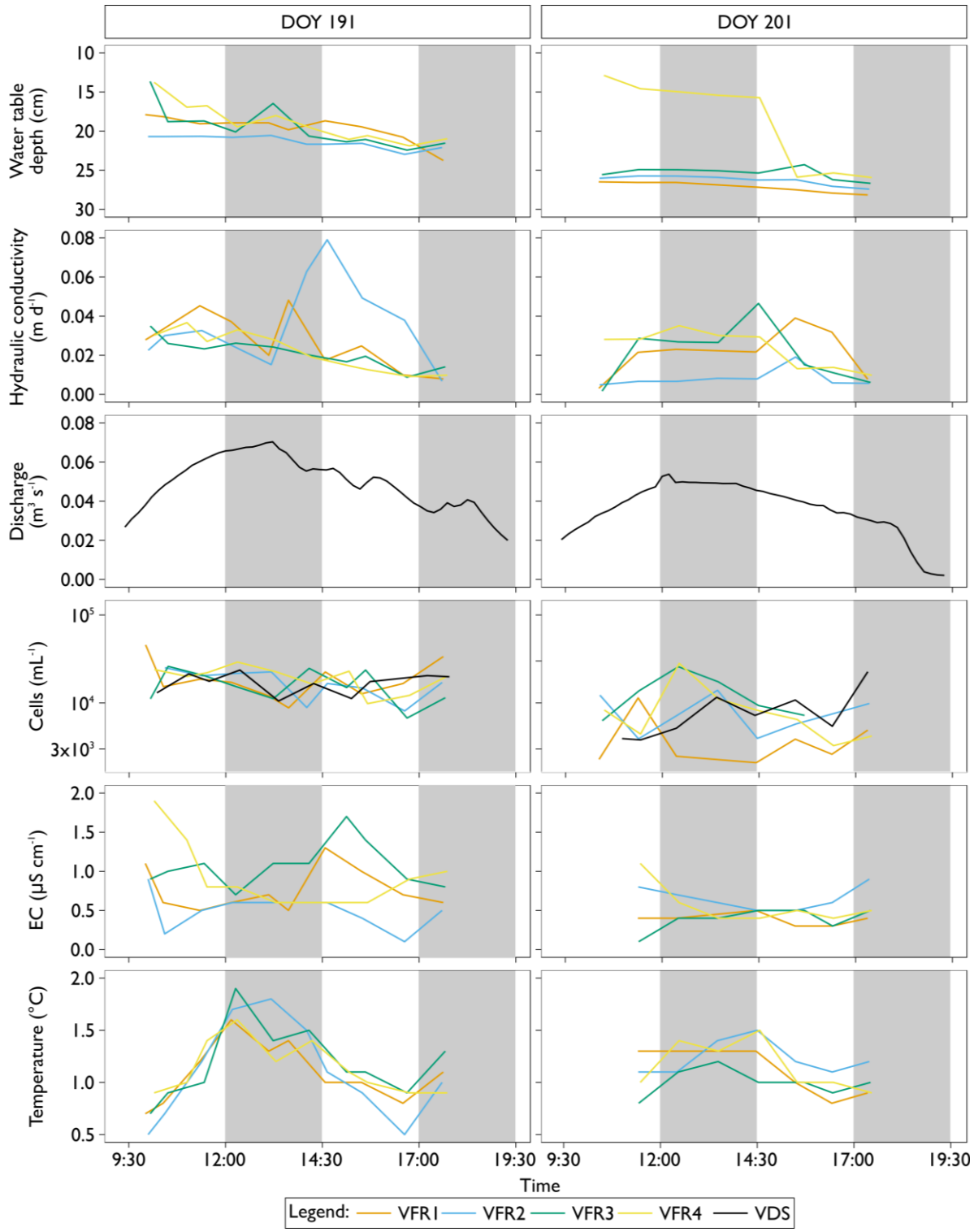

Figure 6.6 Hourly-scale fluctuation in water table depth, hydraulic conductivity, stream discharge, cell concentration, EC and auger-hole water temperature on DOY 191 and 201.

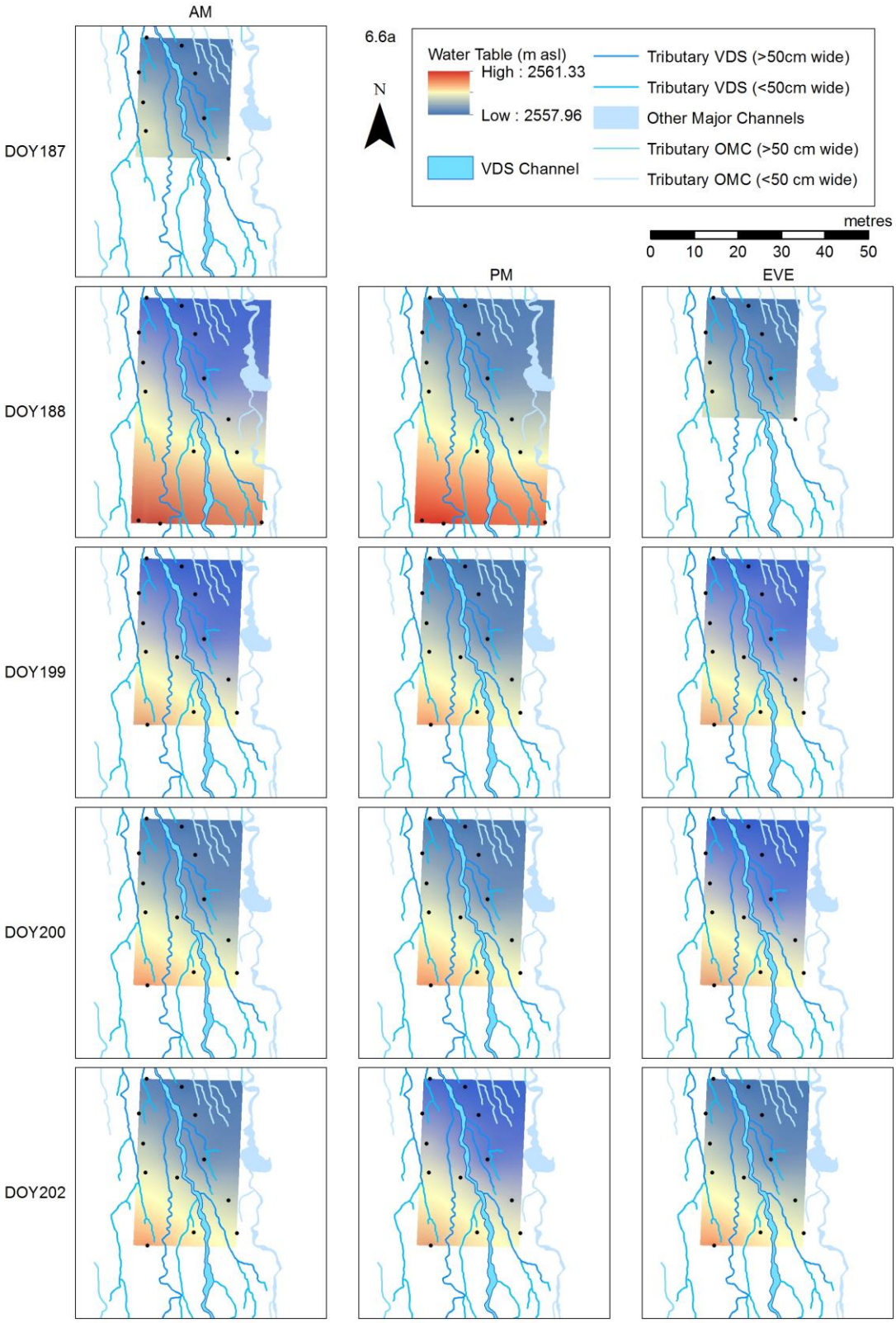

Figure 6.7 IDW interpolation of water table elevation in the weathering crust across the VFCH micro-catchment on DOY 187, 188, 199, 200 and 202.

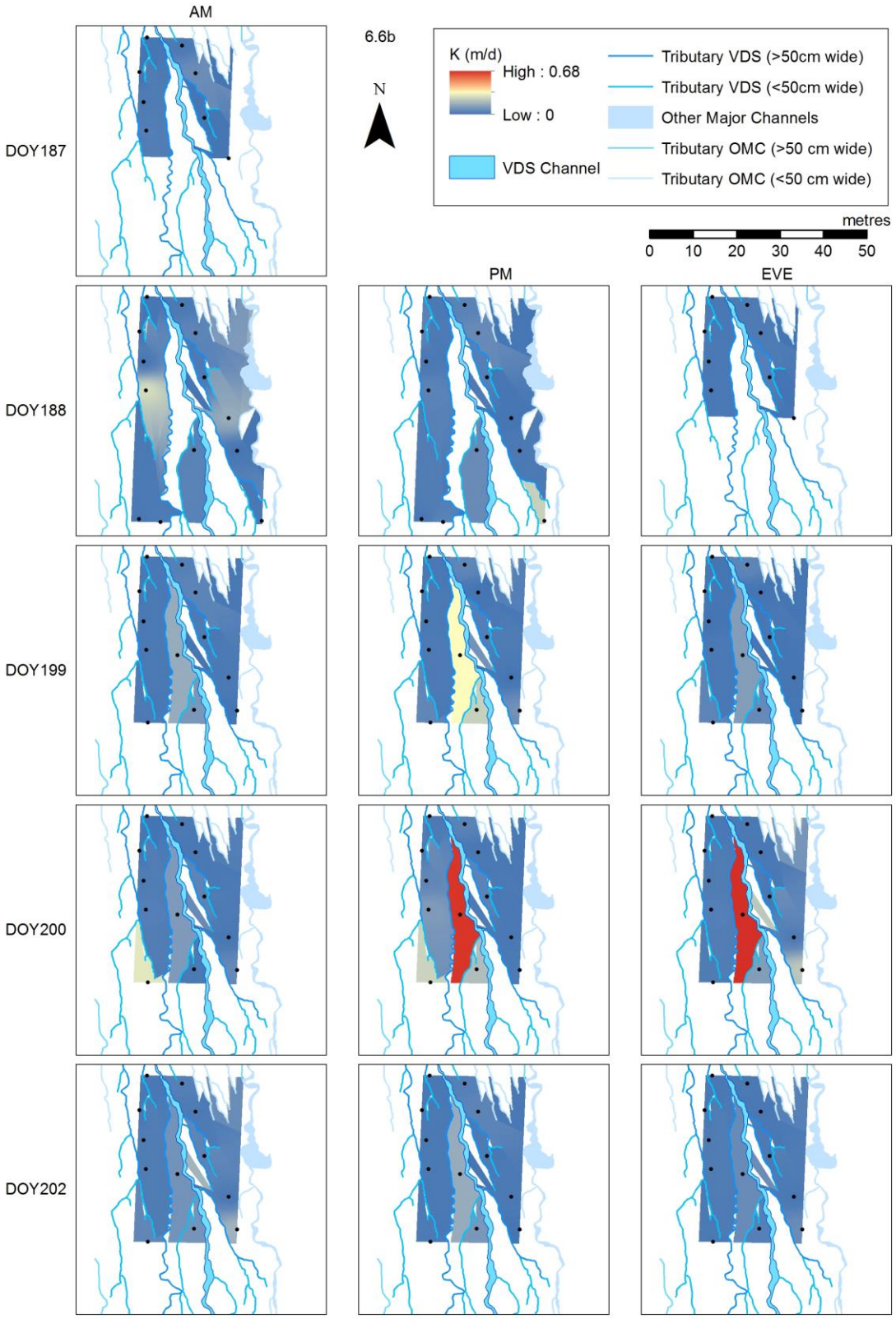

Figure 6.8 IDW interpolation of hydraulic conductivity in the weathering crust across the VFCH micro-catchment on DOY 187, 188, 199, 200 and 202.

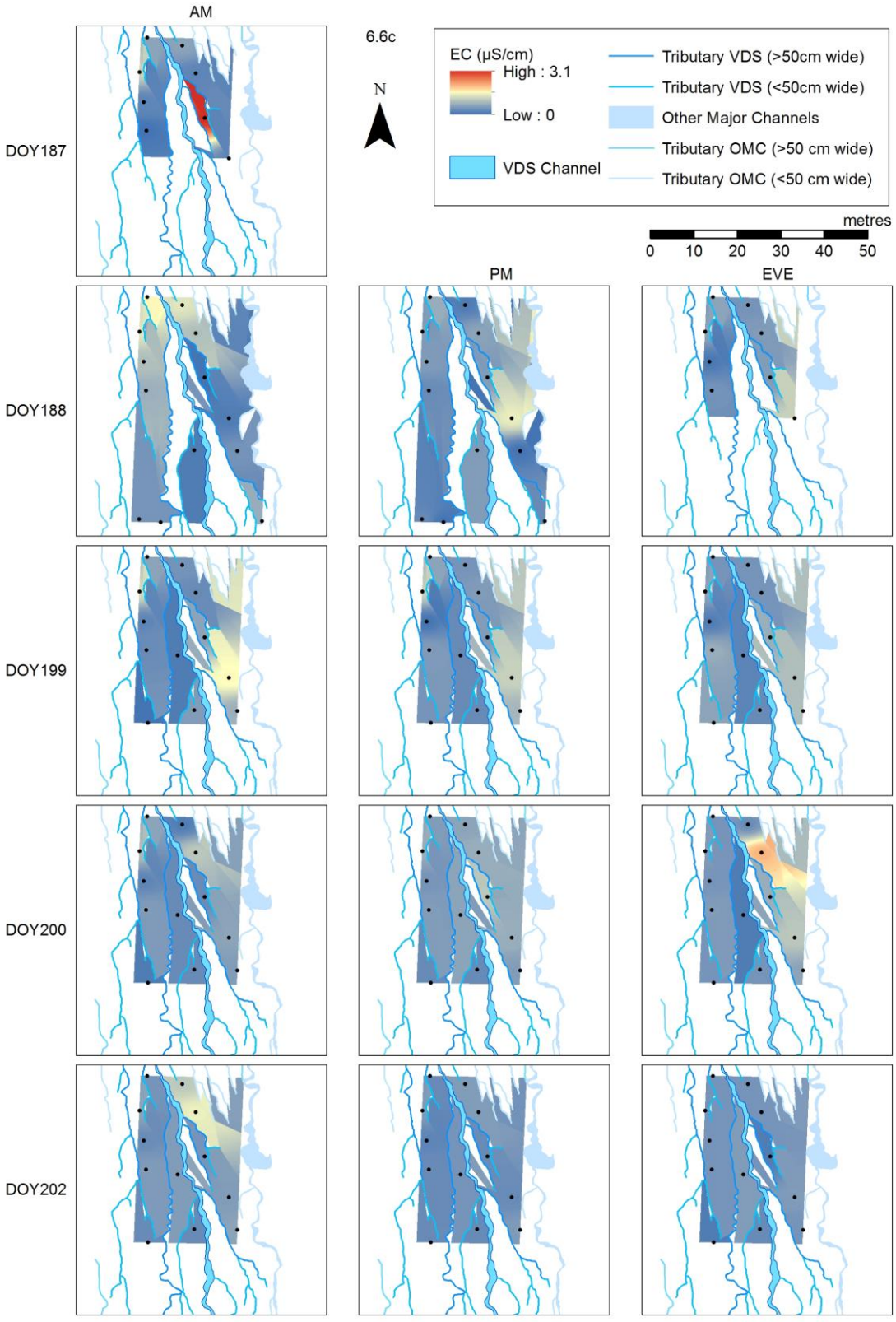

Figure 6.9 IDW interpolation of EC in the weathering crust across the VFCH micro-catchment on DOY 187, 188, 199, 200 and 202.

difference is increasingly exaggerated during the afternoon. At most sites during most time slices, hydraulic conductivity is commonly at the lower end of the observed range and increases from this are observed primarily on the western bank of the main channel.

Weathering crust EC ranges from 0 – 3.1 μS cm^{-1} during the study period, with highest values observed on the eastern side of the main channel. When EC spikes are recorded (e.g. DOY 199 AM) they tend to persist and are observed, albeit in a weakened fashion, into the next time slice. Above average EC values are often observed at VFR 6 and 8, which do not appear to be hydrologically connected as indicated by the assumed flowpaths, orthogonal to the surface. No discernible spatial trends were observed for temperature or cell concentration of weathering crust meltwaters, which ranged from 0 – 1.8 °C. This highpoint was observed throughout the catchment during the study period.

6.4. Interpretation and discussion

6.4.1 Meteorological conditions, weathering crust formation and sub-surface ice temperature

Throughout the study period, meteorological conditions were typical of a European Alpine summer, with peak melting observed between 13:00 and 16:00, and falling overnight in parallel with a drop in solar radiation receipt. However, this "typical" weather pattern (e.g. Brock et al., 2010; Senese et al., 2012) was broken by a period of snowfall, covering the ablation area, enabling consideration of the effect of a summer snowfall event upon microbial transfer through the weathering crust.

SWR_{in} is proposed in the conceptual model (section 2.7) as the driving mechanism for the formation of the weathering crust (e.g. Müller and Keeler, 1969), providing a substantial (i.e. > 70 % of melt energy for European Alpine Glaciers) energy source to the glacier surface (Willis et al., 2002). Throughout the study period, SWR_{in} provided 71.8 % of melt energy. However, a direct link between SWR receipt and weathering crust formation, measured using the proxy of hydraulic conductivity, is unclear (Figure 6.3 a-c, e). However, the role of subsurface SWR_{in} penetration is well established (e.g. Irvine-Fynn and Edwards, 2014; Munro, 1990; Shumskii, 1964), as is its role in weathering crust formation (e.g. Müller and Keeler, 1969; Schuster, 2001). Therefore, it is proposed that the weathering crust at Vadrec del Forno has reached a quasi-steady state equilibrium (see Figure 2.4) throughout

DOY 183 (when the study began) to DOY 192, and from DOY 200 to DOY 203 (when the study ended). Considering the period DOY 182-192, at the start of this period the surface of the lower half of Vadrec del Forno had been snow-free for c. 1 month (personal communication from Fornohütte guardian) allowing for receipt of SWR, weathering the ice surface. Therefore, it is feasible that the weathering crust had reached a state of quasi-equilibrium by DOY 182 following the onset of the ablation season. Following the snowfall event on DOY 195/196, a marked reduction in hydraulic conductivity was observed in the VFR1-4 auger holes on DOY 197, 198 and 199 (Figure 6.3e), with hydraulic conductivities unmeasurable on DOY 197 due to a lack of auger-hole recharge. During this period, clear skies and low air temperatures (Figure 6.3d) resulted in almost 100 % of melt energy being provided by SWR. Following this period, hydraulic conductivities returned to their pre-snowfall levels, hence this interval is interpreted as a time of weathering crust formation, driven by SWR receipt. The implication of this is that development of the weathering crust on an ablating ice surface is rapid, occurring over timescale in the order of several days.

The use of the hydraulic conductivity measurements presented herein do however not provide an entire overview of weathering crust development, as they only relate to the saturated zone of the weathering crust. On DOYs 197 to 200, this was $\geq$ 15 cm below the ice surface. Arguably, the unsaturated zone of the weathering crust, closer to the surface, is a critical element to consider in an exploration of formation processes of the weathering crust, as density change in this area is greater than at depth in the saturated zone (see Figure 2.3). Whilst the data presented here allow for the implication of SWR driving weathering crust formation in $\leq$ 5 days, future work should directly measure ice density-depth profiles during weathering crust formation to better constrain this mechanism.

Due to frequent melt out of probes, sub-surface ice temperature was not reliably measured. If future work aims to elucidate a depth-temperature relationship within the weathering crust, temperature probes should be installed prior to the melt season and frozen within near surface ice. However, surface ablation will still result in probes melting out of the surface, at which point measurement should be ceased rather than attempting to reinstall the probes as this will generate flawed data as observed herein. To monitor the rate of melt out and hence probe depth within the near surface, surface lowering should be recorded, ideally using an ultrasonic depth gauge to provide a complete record (e.g. Willis et al., 2002).

6.4.2 Stream and weathering crust hydrology

This chapter reports hydraulic conductivity at 237 sites within the micro-catchment. Additionally, "unsuccessful" attempts at measuring hydraulic conductivity occurred at VFR 1-4 on DOY 197 VFR6 on DOY 198 and VFR22 on DOY 188. On DOY 198, all recharge experiments undertaken took over 3 h to complete and mean hydraulic conductivity for all sites on this day was less than half the mean value observed (0.020 m d^{-1} contrasted with 0.047 m d^{-1}). For VFR22, no water at all was observed in the auger-hole on either attempted measurement, despite average recharge throughout the day at all other sites recorded being broadly comparable with the average for the entire study (0.046 m d^{-1}). VFR22 was located on a high point near (< 2 m) to two rills, implying that water did not drain through the hole and/or water table level was deeper than 36 cm from the ice surface. It should be noted that mean hydraulic conductivity is a quarter of the northern hemisphere average observed in Chapter 3 (0.185 m d^{-1}) but compares well with the other temperate European alpine glaciers (see Figure 3.7).

Water table elevation was continuously recorded at auger-hole throughout the study period at VFA10, with additional data recorded for four days at a second auger-hole during DOY 198 – DOY 202 at VFA4. Water table height at these sites varies with melt, with a reduction in kurtosis during the snowfall period. Unfortunately, there is a paucity of meteorological data during this period, however this reduction in water table variation implies a reduction in melt, as would be expected. After the snowfall event, the water table increases linearly (excluding diurnal variation). Such a change in the water table can be attributed to two potential factors, both linked with an increase in water storage within the weathering crust: a) an increase in water input to the aquifer, and/or b) a decrease in hydraulic conductivity, reducing the drainage of water. Paradoxically, there is no evidence for a decrease in hydraulic conductivity, alternatively the opposite situation prevails, and hydraulic conductivity demonstrates a statistically significant increase after the snowfall event. However, as demonstrated in (Figure 6.3e) and by the unsuccessful recharge experiments at VFR 1-4 on DOY 197 and VFR6 on DOY 198, hydraulic conductivity was initially very low following the snowfall event before establishment of higher hydraulic conductivities leading to this statistically significant difference.

An increase in water input to the weathering crust, associated with the melting of surface snow, would appear to present a key element in the increase in the water table height preceding the snowfall

event. Modelled melt does not consider the presence of the snow layer, which melted over a period of 3 days adding water into the supraglacial hydrological system. The increase in water input (and transfer) is evidenced by the increase in stream discharge in the main channel from a peak of ~0.06 m s^{-1} to > 0.10 m^3 s^{-1} in the days following the snowfall event (Figure 6.3g). This water input must exceed the maximal output potential of the weathering crust, causing the water table to rise in an identical fashion to a storm event in a terrestrial environment (e.g. Lu and Godt, 2013).

Mean pore water velocity in the weathering crust was 0.24 ± 0.49 m d^{-1}, with a range of 0.01 – 3.35 m d^{-1}. This aligns with the lower end estimates of 0.052 to 60.5 m d^{-1} previously established at Medenhall Glacier (AK, USA) (Wakahama, 1978), but notably is slower. When coupled with the assumed drainage pathways derived from surface slope, mean transfer time of a parcel of water from an auger hole into a stream via the assumed flowpaths was 61.1 ± 225.6 days, but values were highly variable ranging from 0.5 to 2144.7, implying multiday storage of water within the weathering crust. Clearly, transport times in the order of thousands of days are unfeasible due to the period of the ablation season (typically 3 months, or ≈ 100 days for European Alpine glaciers; (e.g. Sicart et al., 2008), which highlights the need to further examine the fate of particles subject to advective transport in such meltwaters.

6.4.3 Hydraulic connectivity of the weathering crust and supraglacial streams

Mean transfer time of a parcel of water from an auger hole into a stream via the assumed flowpaths was 61.1 ± 225.6 days, but values were highly variable ranging from 0.5 to 2144.7 days. These values imply that during the study period (26 days), water measured in each auger hole is not transported to the VDS stream in all cases. This value is double the minimum storage time of 34 hours suggested in Chapter 3 (Stevens et al., 2018), based upon stream spacing in the order of ≤ 10^1 m. However, these values are highly variable, and paradoxically other evidence suggests a link between the waters sampled in auger holes and the stream.

The EC values recorded on DOY 188 (Figure 6.4a) indicate that, once instrumental uncertainty is considered, a difference in EC cannot be distinguished in the auger holes and the VDS stream, aside from for VFR8. This implies that water in the VDS channel has equivalent ionic concentrations to the water in the weathering crust, which coupled with the lack of other water sources implies that stream

water originates from the weathering crust, validating the assumption that water from auger holes VFR1-7, 18-21, 23 and 24 does flow into the VDS channel . However, this does not allow for implication of drainage time. The lack of spatial variation in EC (Figure 6.9) enables consideration of displacement flow, commonly observed in terrestrial environments (e.g. Lu and Godt, 2013). That is, the addition of water (via melt) may drive the transfer of water stored in the weathering crust further along the flowpath between a point and the stream, i.e. water added to the weathering crust is not immediately discharged from it, rather it replaces water which is simultaneously discharged. Given that EC shows little spatial variation, "old" waters discharged into streams can be expected to have ECs within the same uncertainty bounds as that observed in the auger holes. The close alignment of planktonic cell concentrations and size distributions in the stream and the weathering crust, and lack of spatial variation across the catchment, is further indicative of the same process.

Further evidence for displacement flow is provided by the delay of 47 minutes which was observed between peak Q and peak melt. This value compares favourably with the 1 – 2 h delay observed on the Peyto Glacier (Canada; (Munro, 2011)), and ≤ 1 hr response observed at Haut Glacier d'Arolla (Willis et al., 2002). When coupled with the multiday estimates of the transfer of weathering crust water to the stream network, it is clear that 47 minutes does not provide ample time for most at-a-point melt to reach the supraglacial stream network. As such, the implication is that "old" water stored within the weathering crust is responsible for the response of the stream to melting. Therefore, this 47-minute delay is interpreted as the time required for the weathering crust system to respond to meltwater addition. Considering the conceptual model (section 2.7), to provoke a response in the water transport system of the weathering crust, meltwater must infiltrate the unsaturated zone to reach the water table. This will then cause the water table to rise with an associated increase in hydraulic conductivity, driving interstitial water flow along the flowpath from a point (i.e. an auger hole) to a stream ((Stevens et al., 2018); Chapter 3). For a water table 10 cm below the surface, water velocity through the unsaturated zone is 12.8 cm hr^{-1}, or 5.3×10^{-3} m d^{-1}, lower than pore water velocities in the saturated zone of the weathering crust. This would be expected, supporting the validity of the above conclusions, as unsaturated hydraulic conductivities (and therefore pore water velocities) are lower than those in the saturated zone in terrestrial systems (see (Schwartz and Zhang, 2004), section 2.4).

Water temperatures within the weathering crust demonstrate no patterns in space or time and show no correlation with stream water temperatures (Figure 6.4b). There are no patterns observed in

space indicating that transfer of heat through the weathering crust does not occur due to the movement of plumes of warm water, and rather water stored within the weathering crust is heated and cooled by atmospheric changes with all auger-holes demonstrating equivalent temperature trends (Figure 6.4b and Figure 6.7). Notably, on DOY 188, water temperature within the weathering crust (< 1 °C) is substantially higher than in the main channel which never exceeds 0.1 °C (Figure 6.4b). The proposed mechanism for this is a difference in water velocity; within the weathering crust velocities are low (0.24 ± 0.49 m d^{-1}) in contrast to supraglacial streams with velocities in the order of 10^{-1} m s^{-1} (e.g. Nienow et al., 1996). This relatively higher velocity of turbulent stream water results in conductive energy loss with the channel walls, evidenced by thermal incision (e.g. Karlstrom et al., 2013; Karlstrom and Yang, 2016). In contrast, the slow flow rates within the weathering crust mean that water is almost resident *in-situ*, with energy provided from incoming radiative and turbulent fluxes, and lost via outgoing longwave and turbulent fluxes, depending on surface meteorological conditions.

The proposed water storage within the weathering crust presents a habitat for supraglacial microbes, with storage times providing a suitable residence duration for replication. Doubling times range from < 1 to 5 days in water on Alpine glacier surfaces (median 1.8 days) (Anesio et al., 2010), indicating that it could be expected for microbial abundances in the weathering crust of Vadrec del Forno to increase when advected through the weathering crust. Paradoxically, this contrasts with observations, with in-stream and weathering crust abundances being equal and spatial variation in cell concentration being non-existent. Therefore, this indicates the presence of an alternative limiting factor preventing microbial replication in the weathering crust; low EC values observed indicate a lack of ionic solutes, which includes key biological nutrients such as phosphate, potassium, magnesium and calcium. Alternatively, viral control has been observed in Arctic glaciers (Rassner et al., 2016) and may represent a biotic control upon weathering crust cell concentrations. It is also possible that planktonic weathering crust cells are dead, and therefore unable to replicate. To establish the occurrence of these process, further examination of specific nutrient concentrations, bacteriophage viral loads and the status of planktonic cells within the weathering crust is required.

6.4.4 Other spatial and temporal trends

Hydraulic conductivity is generally highest at VFR9. Assuming equal SWR_{in} across the catchment (given minimal change in decimetre-scale slope, equal shading and similar debris cover), relatively increased pore size and density because of differential melt can be excluded as a mechanism

for this. Excessive water table elevation, also linked with increased hydraulic conductivity (Stevens et al., 2018); Chapter 3) is not observed, the water table relative to the surface at this site is equivalent to the mean value for the catchment. Alternatively, ice structure is deemed responsible for this spatial variation. Attempts were made to empirically measure ice crystal size with the aim of using this data to infer pore sizes, but the method applied was unsuccessful preventing the production of experimental data. However, observation of the ice structure in the field indicated that the ice at this location consisted of coarser crystals (see Jennings et al., 2014) than the other sites, which were poorly interlocking, and it is to this variation in ice-structure that above-average *K* values are attributed to, highlighting the importance of local-scale ice structure on hydraulic conductivity of the weathering crust. Water transfer through VFR9 is an order of magnitude greater than the catchment-wide average, which indicates that small areas of high hydraulic conductivity may represent a vital contribution the transfer of water through the weathering crust.

6.5. Conclusions

This chapter presents the weathering crust hydrology and microbial concentrations of a supraglacial Alpine micro-catchment on Vadrec del Forno, Switzerland. Evidence demonstrates that weathering crust development to a quasi-equilibrium state occurs within 5 days, measured by the proxy of hydraulic conductivity in the saturated zone. However, this study does not examine the development of the unsaturated zone, where most mass is lost, and density reductions are greatest. Future study needs to consider the development of the unsaturated zone following a "resetting" event, with the use of coupled depth-density measurements and meteorological data.

Hydraulic connectivity of the weathering crust and channelised drainage system are evidenced, with support for a mechanism of displacement flow, where meltwater introduced to the weathering crust displaces stored water which is discharged to the channelised stream network. A 47-minute delay between peak melt and peak stream discharge is inferred as the time taken for meltwater to infiltrate through the unsaturated zone of the weathering crust before reaching the saturated zone and driving displacement flow.

Mean water storage times in the weathering crust of 61.1 ± 225.6 days are reported but values were highly variable ranging from 0.5 to 2144.7 days, implying the potential for multi-season water storage in the weathering crust, with interstitial water refreezing during the accumulation season. This storage period provides ample time for planktonic cells to replicate, however observations do not

provide evidence of this occurring; it is unclear whether planktonic cells are nutrient starved, preventing replication, subject to bacteriophage control, or simply dead. Future work should look to establish the controls upon cell concentration within the weathering crust and apply multi-season tracer studies to better examine the storage and transport of cells, particulate impurities and solutes through the weathering crust.

7. Synopsis, Limitations and Recommendations for Future Study

This thesis develops hydrological and microbiological methods and provides data from eleven sites across the northern hemisphere to examine the eco-hydrology of glacier surfaces; predominantly water flow and cell transport through the near-surface weathering crust. Hydraulic conductivity values, pore water velocities are measured and storage periods of water implied in this hitherto unstudied porous medium, with consideration given to the transport, storage and export of cells from the surface. However, many questions remain unanswered, presenting opportunities for future research.

7.1 Review of study objectives

As outlined in section 2.7, the research gaps investigated by this study were as follows:

1. Whilst there are estimates of weathering crust hydraulic conductivities, little is known regarding the controls upon this beyond the theorised principles of radiation receipt as a driver for intercrystalline melt, density reduction and an associated increase in porosity and hydraulic conductivity. Furthermore, investigation needs to be undertaken to determine if the use of Darcy's Law is the most appropriate technique in which to examine this layer.
2. It is hypothesised and seems reasonable that the hydraulic conductivity of the weathering crust is highly variable in both time and space. However, no studies have yet aimed to characterise the spatio-temporal variability of this layer.
3. Transport of cells, particulate impurities, and solutes through the weathering crust from allo- and autochthonous sources remains poorly understood. Within the context of global climatic change and associated predicted melt rate increases of global glaciers, many contaminants archived within glacial ice are expected to "melt out" and become mobile. Understanding the transport mechanisms of these impurities is critical to ascertain their potential influence upon a) glacial biogeochemical cycles and microbial ecology and b) downstream interactions with proglacial and oceanic environments.

7.2 Objectives 1 and 2: Quantification of and controls upon hydraulic conductivity

This thesis has developed and tested a simple electronic logging piezometer for application in the supraglacial environment. The limited power requirements, low cost and robust design and demonstrate the potential for application in other remote environments in which high-resolution, repeatable water monitoring is required. However, the probe and methodology described herein (see Chapter 3 for full details) are only suited to the measurement of hydraulic conductivity in the saturated zone of porous media, and this limitation prevents the exploration of hydraulic conductivity and water transfer through the vadose zone of such media. Furthermore, the method is reliant on the assumption that flow is not captured by efficient pathways, such as fractures, and as presented is not able to examine heterogeneities in hydraulic conductivity across a depth profile. As such, future studies aiming to examine weathering crust development and controls upon it should look to directly measure mass lost in the near surface through density measurements paired with a full suite of meteorological data.

Data collected from a spatially extensive suite of field sites allows examination of weathering crust hydraulic conductivity, and this thesis quantifies a mean hydraulic conductivity for the weathering crust of 0.122 m d^{-1} across eleven northern hemisphere glaciers from 517 auger holes. Note that this figure differs from the one presented in Chapter 3, incorporating the 237 measurements collected as Vadrec del Forno in 2016. This is an equivalent value to sandstone and firn, and as such the weathering crust can be considered a poor aquifer and demonstrates the potential of the weathering crust to modulate supra-, en-, sub- and proglacial stream discharge.

The conceptual model (section 2.7) outlined the potential of SWR receipt as a fundamental control on weathering crust hydraulic conductivity, via the increase of interstitial pore size resulting from subsurface melt on ice crystal boundaries. However, no evidence is produced by this thesis to support this hypothesis; Chapter 3 indicated no correlation between SWR receipt and hydraulic conductivity following periods of energy balance dominated by turbulent fluxes or sub-zero air temperatures. One reason for this is that such events described in Chapter 3 may not have been of a suitable magnitude to fully "reset" the weathering crust, those attributed to resetting were limited to a period of hours (as opposed to days) where turbulent fluxes dominated the energy balance. Scenarios where air temperature was below 0 °C may not have acted to reset the weathering crust at all, and concurrent SWR receipt and the internal ice greenhouse effect (Hoffman et al., 2014) could have prevented refreezing at depth. In Chapter 6, a 2.5-day period of cold, cloudy weather

and snowfall demonstrates evidence of weathering crust reset, both by hydraulic conductivity values and observation of removal of weathered ice from the glacier surface (see Figure 2.1 for exemplar ice surfaces). In the proceeding days, energy input to the surface was almost entirely in the form of SWR an increase in hydraulic conductivity of auger holes was observed, with hydraulic conductivities returning to their pre-reset values within 5 days. As such, this is considered to represent a return to a quasi-equilibrium state (see Figures 2.2 and 2.4). However, due to the piezometer design, it is important to note that this only shows consideration of the saturated zone, and as such a study considering density change as a function of meteorological variability may demonstrate an alternative return period depending on processes in the unsaturated zone in which mass losses and density reduction via weathering is greater.

The clearest control on hydraulic conductivity of the weathering crust was water table, as exemplified in Chapter 3. As the water table rises (recharge from melt exceeds discharge to streams), the saturated zone is extended upwards to incorporate ice nearer the surface, which is of a lower density and therefore has greater pore space and is less resistant to water flow.

However, despite this analysis, it is clear that the precise nature of the controls that drive the hydrological characteristics of the weathering crust are clearly complex and multi-faceted. This study shows little to no consideration of ice structure, which may act as an important precondition to weathering crust development and hence hydraulic conductivity. Therefore, investigation of the role of hyper-local ice structure and crystallography upon near surface ice hydraulics likely represents a fruitful avenue for further investigation.

7.3: Objective 3: Enumeration and transport of cells within the weathering crust

Chapter 4 presents a protocol suited for application to the collection and enumeration of cells within weathering crust meltwater and supraglacial streams, with potential to expand to analysis of low-sediment proglacial systems. A key determinant of the accuracy of FCM for enumeration of these samples is the abiotic particulate concentration, and Chapter 4 indicates that this protocol is suitable for samples with a) abiotic particle concentration $\leq 10^{-2}$ g L^{-1}, regardless of cell concentration (providing the cell concentration is above the detection limit of the instrument used) or b) the ratio of cells to abiotic particles (CC-APC) is $> 5 \times 10^5$ cells g·abioticparticles^{-1}. Below this threshold, cell numbers are typically overestimated.

This method is applied to 763 samples from 11 glaciers across the northern hemisphere, revealing mean planktonic cell concentrations of $2.2 \times 10^4 \pm 5.5 \times 10^4$ cells mL^{-1} with a modal size of 1 – 2 μm. Planktonic cell concentrations vary on a glacier scale, with the highest concentrations being observed in Greenland, and the lowest in the European Alps and Scandinavia.

Coupled with proglacial discharge modelling, these planktonic cell concentrations enable a conservative estimation of carbon (in the form of POC), nitrogen and phosphorus export from the supraglacial environment, albeit with numerous limitations, of 1.1×10^9 kg C a^{-1} (1.1 Tg C a^{-1}), nitrogen 2.3×10^8 kg N a^{-1} and phosphorus 2.3×10^7 kg P a^{-1}, 1.7 times lower than existing estimates, but equivalent to the annual mobilisation of ≈ 0.08 % of carbon stored in the aquatic biosphere. Future evaluation of these fluxes should look to consider cells bound to weathering crust ice crystals, which may be liberated from glacier surfaces during non-refreezing weathering crust degradation events and subsequently contribute to downstream nutrient fluxes. The morphologies of exported cells should also be considered, which is a fundamental assumption made in these calculations.

The drivers behind this difference in cell concentrations remains unclear; it is apparent that weathering crust hydraulics measured herein are not a deterministic factor in the cell concentrations found within the weathering crust. It is notable that the highest microbial cell concentration observed in Greenland were observed near to the so-called "dark zone" (Tedstone et al., 2017), which plays host to photosynthetic, pigmented algae, in addition to dust and black carbon (Ryan et al., 2018). This area may act as a direct supply of planktonic cells and nutrients to the weathering crust and highlights that future studies should consider factors such as inoculation rates and nutrient concentrations as drivers of glacial scale variability of microbial concentrations.

No evidence is presented that the weathering crust acts as a mechanical filter, darkening glacier surfaces. Equal concentrations of cells are observed in streams and the weathering crust, albeit within large ranges, and cells (and inorganic particulates) in excess of 15 μm diameter are mobilised within the weathered near surface of ablating ice masses. Under this model, surface darkening of glaciers can be attributed to growth of cellular communities which are not mobilised in weathering crust waters, such as those bound to ice-crystals, throughout the ablation season.

Hydraulic conductivity values presented in Chapter 3 indicate that the weathering crust is a hydrologically poor, impervious aquifer that can delay water transfer to the supraglacial stream network acting as a transient, multi-day storage reservoir within this system. Further evidence is indicated for this in Chapter 6, which reports average, highly variable, water storage times in the

weathering crust of 61.1 ± 225.6 days, transferring meltwater from the point of melt to supraglacial streams via displacement flow. This storage period implies the potential for both multi-day and multi-season water storage in the weathering crust, with interstitial waters potentially refreezing during the accumulation season. This role as a regulator of meltwater egress has the potential to impact upon supraglacial sediment, impurity and biological budgets and associated basin-scale exports at a range of spatial and temporal scales. This storage period provides ample time for planktonic cells to replicate, however observations do not provide evidence of this occurring; it is unclear whether planktonic cells are nutrient starved, preventing replication, subject to bacteriophage control, or simply dead.

Future work should look to establish the controls upon cell concentration within the weathering crust and apply multi-season tracer studies to better examine the storage and transport of cells, particulate impurities and solutes through the weathering crust. Live-dead staining protocols many reveal reasons for the apparent lack of replication of planktonic cells within the weathering crust. Consideration of biotic controls such as viral control, common in Arctic environments (Säwstrom et al., 2007a, 2007b) should be incorporated into such a study. Further investigation involving the application of conservative particulate fluorescence tagged microbial cells to the weathering crust in an intensive, catchment-scale study across multiple melt seasons may further reveal transport mechanisms, pathways and controls of cells, particulate impurities and solutes though the glacier near-surface.

7.4 Summary

This thesis advances techniques for the exploration of weathering crust eco-hydrology. It develops a novel logging piezometer which is used to calculate mean weathering crust hydraulic conductivity of 0.122 m d^{-1}, equivalent to sandstone. Flow cytometry is presented as a fast, reliable and accurate tool for the quantification of supraglacial microbial cells, and herein is recommended as the "gold standard" for cell counting in supraglacial environments. These techniques were applied to characterise the eco-hydrology of the weathering crust, a hydrologically poor aquifer, which stores water at the surface for tens of days providing an ideal medium for biogeochemical cycling and replication for the ≈ 10^4 planktonic cells mL^{-1} that are transported through it by advection. However, this study provides no evidence of replication or biogeochemical cycling being carried out by these microbes. This active environment contributes 1.1 Tg of cellular carbon per year to downstream freshwater and marine environments. Given changing global climate and its impact upon glaciers (IPCC, 2013), controls upon the export of these nutrients from glacier

surfaces merit extensive further study. Despite retreating glacier termini, ablation areas are increasing in size enhancing the importance of the role of the eco-hydrology of glacier surfaces.

Reference List

Abermann, J., Lambrecht, A., Fischer, A., and Kuhn, M.: Quantifying changes and trends in glacier area and volume in the Austrian Ötztal Alps (1969-1997-2006), The Cryosphere, 3, 205-215, 2009.

Adhikary, S., Nakawo, M., and Seko, K.: Dust influence on melting process of glacier ice: experimental results from Lirung Glacier, Nepal Himalayas, Debris Covered Glaciers, IAHS 264, 2000.

Albert, M. R. and Perron, F. E.: Ice layer and surface crust permeability in a seasonal snow pack, Hydrological Processes, 14, 3207-3214, 2000.

Aldén, L., Demoling, F., and Bååth, E.: Rapid method of determining factors limiting bacterial growth in soil, Applied and environmental microbiology, 67, 1830-1838, 2001.

Alfreider, A., Pernthaler, J., Amann, R., Sattler, B., Glockner, F., Wille, A., and Psenner, R.: Community analysis of the bacterial assemblages in the winter cover and pelagic layers of a high mountain lake by in situ hybridization, Applied and Environmental Microbiology, 62, 2138-2144, 1996.

Allen, M. J., Edberg, S. C., and Reasoner, D. J.: Heterotrophic plate count bacteria—what is their significance in drinking water?, International Journal of Food Microbiology, 92, 265-274, 2004.

Amalfitano, S. and Fazi, S.: Recovery and quantification of bacterial cells associated with streambed sediments, Journal of Microbiological Methods, 75, 237-243, 2008.

Amato, P., Hennebelle, R., Magand, O., Sancelme, M., Delort, A.-M., Barbante, C., Boutron, C., and Ferrari, C.: Bacterial characterization of the snow cover at Spitzberg, Svalbard, FEMS Microbiology Ecology, 59, 255-264, 2007.

Ambrosini, R., Musitelli, F., Navarra, F., Tagliaferri, I., Gandolfi, I., Bestetti, G., Mayer, C., Minora, U., Azzoni, R. S., Diolaiuti, G., Smiraglia, C., and Franzetti, A.: Diversity and Assembling Processes of Bacterial Communities in Cryoconite Holes of a Karakoram Glacier, Microb Ecol, doi: 10.1007/s00248-016-0914-6, 2016. 1-11, 2016.

Amoozegar, A. and Warrick, A. W.: Hydraulic conductivity of saturated soils: field methods. In: Methods of soil analysis part I: physical and mineralogical methods, Klute, A. (Ed.), Soil Science Society of America, Wisconsin, USA, 1986.

Amoroso, A., Domine, F., Esposito, G., Morin, S., Savarino, J., Nardino, M., Montagnoli, M., Bonneville, J. M., Clement, J. C., Ianniello, A., and Beine, H. J.: Microorganisms in Dry Polar Snow Are Involved in the Exchanges of Reactive Nitrogen Species with the Atmosphere, Environmental Science & Technology, 44, 714-719, 2009.

Anesio, A. M., Hodson, A. J., Fritz, A., Psenner, R., and Sattler, B.: High microbial activity on glaciers: importance to the global carbon cycle, Global Change Biology, 15, 955-960, 2009.

Anesio, A. M. and Laybourn-Parry, J.: Glaciers and ice sheets as a biome, Trends in Ecology & Evolution, 27, 219-225, 2012.

Anesio, A. M., Lutz, S., Chrismas, N. A. M., and Benning, L. G.: The microbiome of glaciers and ice sheets, npj Biofilms and Microbiomes, 3, 10, 2017.

Anesio, A. M., Mindl, B., Laybourn-Parry, J., Hodson, A. J., and Sattler, B.: Viral dynamics in cryoconite holes on a high Arctic glacier (Svalbard), Journal of Geophysical Research: Biogeosciences, 112, G04S31, 2007.

Anesio, A. M., Sattler, B., Foreman, C., Telling, J., Hodson, A., Tranter, M., and Psenner, R.: Carbon fluxes through bacterial communities on glacier surfaces, Annals of Glaciology, 51, 32-40, 2010.

Azzoni, R. S., Senese, A., Zerboni, A., Maugeri, M., Smiraglia, C., and Diolaiuti, G. A.: Estimating ice albedo from fine debris cover quantified by a semi-automatic method: the case study of Forni Glacier, Italian Alps, The Cryosphere, 10, 665-679, 2016.

Baccolo, G., Di Mauro, B., Massabò, D., Clemenza, M., Nastasi, M., Delmonte, B., Prata, M., Prati, P., Previtali, E., and Maggi, V.: Cryoconite as a temporary sink for anthropogenic species stored in glaciers, Scientific Reports, 7, 9623, 2017.

Bagshaw, E. A., Tranter, M., Fountain, A. G., Welch, K., Basagic, H. J., and Lyons, W. B.: Do Cryoconite Holes have the Potential to be Significant Sources of C, N, and P to Downstream Depauperate Ecosystems of Taylor Valley, Antarctica?, Arctic, Antarctic, and Alpine Research, 45, 440-454, 2013.

Bakermans, C.: Limits for Microbial Life st Subzero Temperatures. In: Psychrophiles, Margesin, R., Schinner, F., Marx, J.-C., and Gerday, C. (Eds.), Springer, Berlin, 2008.

Bales, R. C. and Harrington, R. F.: Recent progress in snow hydrology, Reviews of Geophysics, 33, 1011-1020, 1995.

Barnett, M. J., Pawlett, M., Wadham, J. L., Jackson, M., and Cullen, D. C.: Demonstration of a multi-technique approach to assess glacial microbial populations in the field, Journal of Glaciology, 62, 348-358, 2016.

Barry, R. G.: Mountain weather and climate, Cambridge University Press, Cambridge, UK, 2008.

Bartholomew, I., Nienow, P., Sole, A., Mair, D., Cowton, T., Palmer, S., and Wadham, J.: Supraglacial forcing of subglacial drainage in the ablation zone of the Greenland ice sheet, Geophysical Research Letters, 38, 2011.

Battin, T. J., Besemer, K., Bengtsson, M. M., Romani, A. M., and Packmann, A. I.: The ecology and biogeochemistry of stream biofilms, Nature Reviews Microbiology, 14, 251, 2016.

Battin, T. J., Wille, A., Psenner, R., and Richter, A.: Large-scale environmental controls on microbial biofilms in high-alpine streams, Biogeosciences, 1, 2004.

Baxter, L. K.: Capacitive Sensors: Design and Applications, John Wiley & Sons, 1996.

Bear, J.: Dynamics of fluids in porous media, Elsevier, London, 1972.

Bellas, C., Anesio, A. M., Telling, J., Stibal, M., Tranter, M., and Davis, S.: Viral impacts on bacterial communities in Arctic cryoconite, Environ Res Lett, 8, 045021, 2013.

Benn, D. I. and Evans, D. J. A.: Glaciers and Glaciation, Hodder, Abingdon, 2010.

Benson, C. S.: Stratigraphic studies in the snow and firn of the Greenland ice sheet, SNOW ICE AND PERMAFROST RESEARCH ESTABLISHMENT WILMETTE IL, 1996.

Bettinetti, R., Quadroni, S., Boggio, E., and Galassi, S.: Recent DDT and PCB contamination in the sediment and biota of the Como Bay (Lake Como, Italy), Science of The Total Environment, 542, Part A, 404-410, 2016.

Bhatia, M. P., Das, S. B., Xu, L., Charette, M. A., Wadham, J. L., and Kujawinski, E. B.: Organic carbon export from the Greenland ice sheet, Geochimica et Cosmochimica Acta, 109, 329-344, 2013.

Biggs, B. J.: Patterns in benthic algae of streams, Algal ecology: freshwater benthic ecosystems, 1996. 31-56, 1996.

Biggs, B. J., Stevenson, R. J., and Lowe, R. L.: A habitat matrix conceptual model for stream periphyton, Archiv fur Hydrobiologie, 143, 21-56, 1998.

Biosciences, B.: http://static.bdbiosciences.com/documents/accuri/Accuri-TB-Guide-to-Absolute-Counting.pdf?_ga=2.41464610.1235145735.1551782391-2137533603.15517823912019.

Bizzotto, E. C., Villa, S., Vaj, C., and Vighi, M.: Comparison of glacial and non-glacial-fed streams to evaluate the loading of persistent organic pollutants through seasonal snow/ice melt, Chemosphere, 74, 924-930, 2009.

Björkman, M. P., Vega, C. P., Kühnel, R., Spataro, F., Ianniello, A., Esposito, G., Kaiser, J., Marca, A., Hodson, A., Isaksson, E., and Roberts, T. J.: Nitrate postdeposition processes in Svalbard surface snow, Journal of Geophysical Research: Atmospheres, 119, 12,953-912,976, 2014.

Björnsson, H.: Radio-Echo Sounding Maps of Storglaciaren, Isfallsglaciaren and Rabots Glaciar, Northern Sweden, Geografiska Annaler. Series A, Physical Geography, 63, 225-231, 1981.

Blatter, H. and Hutter, K.: Polythermal conditions in Arctic glaciers, Journal of Glaciology, 37, 261-269, 1991.

Bliss, A., Hock, R., and Radić, V.: Global response of glacier runoff to twenty-first century climate change, Journal of Geophysical Research: Earth Surface, 119, 717-730, 2014.

Boenigk, J.: A disintegration method for direct counting of bacteria in clay-dominated sediments: dissolving silicates and subsequent fluorescent staining of bacteria, Journal of Microbiological Methods, 56, 151-159, 2004.

Bogdal, C., Scheringer, M., Schmid, P., Bläuenstein, M., Kohler, M., and Hungerbühler, K.: Levels, fluxes and time trends of persistent organic pollutants in Lake Thun, Switzerland: Combining trace analysis and multimedia modeling, Science of The Total Environment, 408, 3654-3663, 2010.

Bogdal, C., Schmid, P., Zennegg, M., Anselmetti, F. S., Scheringer, M., and Hungerbühler, K.: Blast from the Past: Melting Glaciers as a Relevant Source for Persistent Organic Pollutants, Environmental Science & Technology, 43, 8173-8177, 2009.

Bøggild, C. E., Brandt, R. E., Brown, K. J., and Warren, S. G.: The ablation zone in northeast Greenland: ice types, albedos and impurities, Journal of Glaciology, 56, 101-113, 2010.

Boon, N., Top, E. M., Verstraete, W., and Siciliano, S. D.: Bioaugmentation as a Tool To Protect the Structure and Function of an Activated-Sludge Microbial Community against a 3-Chloroaniline Shock Load, Applied and Environmental Microbiology, 69, 1511-1520, 2003.

Bossio, D. A. and Scow, K.: Impacts of carbon and flooding on soil microbial communities: phospholipid fatty acid profiles and substrate utilization patterns, Microb Ecol, 35, 265-278, 1998.

Bougamont, M. and Bamber, J. L.: A surface mass balance model for the Greenland ice sheet, J Geophys Res-Earth, 110, 2005.

Boulos, L., Prévost, M., Barbeau, B., Coallier, J., and Desjardins, R.: LIVE/DEAD® BacLight™: application of a new rapid staining method for direct enumeration of viable and total bacteria in drinking water, Journal of Microbiological Methods, 37, 77-86, 1999.

Bouwer, H. and Rice, R. C.: A slug test determining hydraulic conductivity of unconfined aquifers with completely or partially pentrating wells, Water Resources Research, 12, 423-428, 1976.

Boyd, E. S., Lange, R. K., Mitchell, A. C., Havig, J. R., Hamilton, T. L., Lafrenière, M. J., Shock, E. L., Peters, J. W., and Skidmore, M.: Diversity, Abundance, and Potential Activity of Nitrifying and Nitrate-Reducing Microbial Assemblages in a Subglacial Ecosystem, Applied and Environmental Microbiology, 77, 4778-4787, 2011.

Bradley, J. A., Singarayer, J. S., and Anesio, A. M.: Microbial community dynamics in the forefield of glaciers, Proceedings of the Royal Society of London B: Biological Sciences, 281, 2014.

Brandt, R. E. and Warren, S. G.: Solar-heating rates and temperature profiles in Antarctic snow and ice, Journal of Glaciology, 39, 99-110, 1993.

Bratbak, G.: Bacterial Biovolume and Biomass Estimations, Applied and Environmental Microbiology, 49, 1488-1493, 1985.

Bressan, M., Trinsoutrot Gattin, I., Desaire, S., Castel, L., Gangneux, C., and Laval, K.: A rapid flow cytometry method to assess bacterial abundance in agricultural soil, Applied Soil Ecology, 88, 60-68, 2015.

Brock, B. W.: An Analysis of Short-Term Albedo Variations at Haut Glacier d'Arolla, Switzerland, Geografiska Annaler. Series A, Physical Geography, 86, 53-65, 2004.

Brock, B. W. and Arnold, N. S.: A spreadsheet-based (Microsoft Excel) point surface energy-balance model for glacier and snow melt studies, Earth Surface Processes and Landforms, 25, 649-658, 2000.

Brock, B. W., Mihalcea, C., Kirkbride, M. P., Diolaiuti, G., Cutler, M. E. J., and Smiraglia, C.: Meteorology and surface energy fluxes in the 2005–2007 ablation seasons at the Miage debris-covered glacier, Mont Blanc Massif, Italian Alps, Journal of Geophysical Research: Atmospheres, 115, 2010.

Brock, B. W., Willis, I. C., and Sharp, M. J.: Measurement and parameterization of albedo variations at Haut Glacier d'Arolla, Switzerland, Journal of Glaciology, 46, 675-688, 2000.

Brox, T. I., Skidmore, M. L., and Brown, J. R.: Characterizing the internal structure of laboratory ice samples with nuclear magnetic resonance, Journal of Glaciology, 61, 55-64, 2015.

Brugger, K. A.: The non-synchronous response of Rabots Glaciär and Storglaciären, northern Sweden, to recent climate change: a comparative study, Annals of Glaciology, 46, 275-282, 2007.

Brugger, K. A., Refsnider, K. A., and Whitehill, M. F.: Variation in glacier length and ice volume of Rabots Glaciär, Sweden, in response to climate change, 1910–2003, Annals of Glaciology, 42, 180-188, 2005.

Brun, F., Dumont, M., Wagnon, P., Berthier, E., Azam, M., Shea, J., Sirguey, P., Rabatel, A., and Ramanathan, A.: Seasonal changes in surface albedo of Himalayan glaciers from MODIS data and links with the annual mass balance, The Cryosphere, 9, 341-355, 2015.

Brutsaert, W.: Hydrology: an introduction, Cambridge University Press, 2005.

Buckingham, E.: Studies on the movement of soil moisture, 1907. 1907.

Buesing, N. and Gessner, M. O.: Comparison of detachment procedures for direct counts of bacteria associated with sediment particles, plant litter and epiphytic biofilms, Aquatic Microbial Ecology, 27, 29-36, 2002.

Bullock, G. R.: The current status of fixation for electron microscopy: A review, Journal of Microscopy, 133, 1-15, 1984.

Cahill, A. T. and Parlange, M. B.: On water vapor transport in field soils, Water Resources Research, 34, 731-739, 1998.

Cameron, K. A., Hodson, A. J., and Osborn, A. M.: Carbon and nitrogen biogeochemical cycling potentials of supraglacial cryoconite communities, Polar Biol, 35, 1375-1393, 2012a.

Cameron, K. A., Hodson, A. J., and Osborn, A. M.: Structure and diversity of bacterial, eukaryotic and archaeal communities in glacial cryoconite holes from the Arctic and the Antarctic, FEMS Microbiology Ecology, 82, 254-267, 2012b.

Cameron, K. A., Stibal, M., Hawkings, J. R., Mikkelsen, A. B., Telling, J., Kohler, T. J., Gözdereliler, E., Zarsky, J. D., Wadham, J. L., and Jacobsen, C. S.: Meltwater export of prokaryotic cells from the Greenland ice sheet, Environmental Microbiology, doi: 10.1111/1462-2920.13483, 2016. n/a-n/a, 2016.

Cameron, K. A., Stibal, M., Zarsky, J. D., Gözdereliler, E., Schostag, M., and Jacobsen, C. S.: Supraglacial bacterial community structures vary across the Greenland ice sheet, FEMS Microbiology Ecology, doi: 10.1093/femsec/fiv164, 2015. 2015.

Campbell, F. M. A., Nienow, P. W., and Purves, R. S.: Role of the supraglacial snowpack in mediating meltwater delivery to the glacier system as inferred from dye tracer investigations, Hydrological Processes, 20, 969-985, 2006.

Campbell, W. and Rasmussen, L.: The production, flow and distribution of meltwater in a glaicer treated as a porous medium, Cambridge1973, 11-27.

Carpenter, E. J., Lin, S., and Capone, D. G.: Bacterial activity in South Pole snow, Applied and environmental microbiology, 66, 4514-4517, 2000.

Chapin, F. S., Walker, L. R., Fastie, C. L., and Sharman, L. C.: Mechanisms of Primary Succession Following Deglaciation at Glacier Bay, Alaska, Ecological Monographs, 64, 149-175, 1994.

Chen, F., Lu, J.-r., Binder, B. J., Liu, Y.-c., and Hodson, R. E.: Application of Digital Image Analysis and Flow Cytometry To Enumerate Marine Viruses Stained with SYBR Gold, Applied and Environmental Microbiology, 67, 539-545, 2001.

Chikita, K., Jha, J., and Yamada, T.: Sedimentary effects on the expansion of a Himalayan supraglacial lake, Global Planet Change, 28, 23-34, 2001.

Christner, B. C., Lavender, H. F., Davis, C. L., Oliver, E. E., Neuhaus, S. U., Myers, K. F., Hagedorn, B., Tulaczyk, S. M., Doran, P. T., and Stone, W. C.: Microbial processes in the weathering crust aquifer of a temperate glacier, The Cryosphere, 12, 3653-3669, 2018a.

Christner, B. C., Lavender, H. F., Davis, C. L., Oliver, E. E., Neuhaus, S. U., Myers, K. F., Hagedorn, B., Tulaczyk, S. M., Doran, P. T., and Stone, W. C.: Microbial processes in the weathering crust aquifer of a temperate glacier, The Cryosphere Discuss., 2018, 1-34, 2018b.

Chuvochina, M. S., Alekhina, I. A., Normand, P., Petit, J. R., and Bulat, S. A.: Three events of Saharan dust deposition on the Mont Blanc glacier associated with different snow-colonizing bacterial phylotypes, Microbiology, 80, 125-131, 2011.

Collins, D. N.: Hydrochemistry of Meltwaters Draining from an Alpine Glacier, Arctic Alpine Res, 11, 307-324, 1979a.

Collins, D. N.: Sediment Concentration in Melt Waters as an Indicator of Erosion Processes Beneath an Alpine Glacier, Journal of Glaciology, 23, 247-257, 1979b.

Cook, J., Edwards, A., and Hubbard, A.: Biocryomorphology: Integrating Microbial Processes with Ice Surface Hydrology, Topography, and Roughness, Frontiers in Earth Science, 3, 2015a.

Cook, J., Edwards, A., Takeuchi, N., and Irvine-Fynn, T.: Cryoconite:The dark biological secret of the cryosphere, Progress in Physical Geography: Earth and Environment, 40, 66-111, 2016a.

Cook, J. M., Edwards, A., Bulling, M., Mur, L. A., Cook, S., Gokul, J. K., Cameron, K. A., Sweet, M., and Irvine-Fynn, T. D.: Metabolome-mediated biocryomorphic evolution promotes carbon fixation in G reenlandic cryoconite holes, Environmental microbiology, 18, 4674-4686, 2016b.

Cook, J. M., Edwards, A., Bulling, M., Mur, L. A. J., Cook, S., Gokul, J. K., Cameron, K. A., Sweet, M., and Irvine-Fynn, T. D. L.: Metabolome-mediated biocryomorphic evolution promotes carbon fixation in Greenlandic cryoconite holes, Environmental Microbiology, 18, 4674-4686, 2016c.

Cook, J. M., Hodson, A. J., Anesio, A. M., Hanna, E., Yallop, M., Stibal, M., Telling, J., and Huybrechts, P.: An improved estimate of microbially mediated carbon fluxes from the Greenland ice sheet, Journal of Glaciology, 58, 1098-1108, 2012.

Cook, J. M., Hodson, A. J., and Irvine-Fynn, T. D. L.: Supraglacial weathering crust dynamics inferred from cryoconite hole hydrology, Hydrological Processes, doi: 10.1002/hyp.10602, 2015b. n/a-n/a, 2015b.

Cook, J. M., Hodson, A. J., Taggart, A. J., Mernild, S. H., and Tranter, M.: A predictive model for the spectral "bioalbedo" of snow, Journal of Geophysical Research: Earth Surface, doi: 10.1002/2016JF003932, 2017. n/a-n/a, 2017.

Cook, J. M., Hodson, A. J., Telling, J., Anesio, A. M., Irvine-Fynn, T. D. L., and Bellas, C.: The mass-area relationship within cryoconite holes and is implications for primary production, Annals of Glaciology, 51, 106-110, 2010.

Cooper, M. G., Smith, L. C., Rennermalm, A. K., Miège, C., Pitcher, L. H., Ryan, J. C., Yang, K., and Cooley, S. W.: Meltwater storage in low-density near-surface bare ice in the Greenland ice sheet ablation zone, The Cryosphere, 12, 955-970, 2018.

Croff, A., Lomenick, T., Lowrie, R., and Stow, S.: Evaluation of Five Sedimentary Rocks Other Than Salt for High-Level Waste Repository Siting Purposes, Oak Ridge National Laboratory–Martin Marietta Report ORNL1CF-85/2, 3 volumes, 1985. 1985.

Cuffey, K. M. and Paterson, W. S. B.: The Physics of Glaciers, Butterworth-Heinemann, London, 2010.

Cunningham, A. B., Sharp, R. R., Caccavo, F., and Gerlach, R.: Effects of starvation on bacterial transport through porous media, Advances in Water Resources, 30, 1583-1592, 2007.

Cutler, P. M. and Munro, D. S.: Visible and near-infrared reflectivity during the ablation period on Peyto Glacier, Alberta, Canada, Journal of Glaciology, 42, 333-340, 1996.

Dancer, S. J., Shears, P., and Platt, D. J.: Isolation and characterization of coliforms from glacial ice and water in Canada's High Arctic, Journal of Applied Microbiology, 82, 597-609, 1997.

Darcy, H.: Les fontaines publiques de la ville de Dijon: exposition et application, Victor Dalmont, 1856.

Darcy, J. L., Lynch, R. C., King, A. J., Robeson, M. S., and Schmidt, S. K.: Global Distribution of *Polaromonas* Phylotypes - Evidence for a Highly Successful Dispersal Capacity, PLoS ONE, 6, e23742, 2011.

Das, S. B., Joughin, I., Behn, M. D., Howat, I. M., King, M. A., Lizarralde, D., and Bhatia, M. P.: Fracture propagation to the base of the Greenland Ice Sheet during supraglacial lake drainage, Science, 320, 778-781, 2008.

Davey, H. M. and Hexley, P.: Red but not dead? Membranes of stressed Saccharomyces cerevisiae are permeable to propidium iodide, Environmental Microbiology, 13, 163-171, 2011.

Delcourt, C., Van Liefferinge, B., Nolan, M., and Pattyn, F.: The climate memory of an Arctic polythermal glacier, Journal of Glaciology, 59, 1084-1092, 2013.

Derikx, L.: Glacier discharge simulation by ground-water analogue, Hydrology of Glaciers (IAHS), 1973a. 29-40, 1973a.

Derikx, L.: Glacier discharge simulation by groundwater analogue, Cambridge1973b, 29-40.

Dolev, M. B., Bernheim, R., Guo, S., Davies, P. L., and Braslavsky, I.: Putting life on ice: bacteria that bind to frozen water, Journal of The Royal Society Interface, 13, 20160210, 2016a.

Dolev, M. B., Braslavsky, I., and Davies, P. L.: Ice-Binding Proteins and Their Function, Annual Review of Biochemistry, 85, 515-542, 2016b.

Drenovsky, R. E., Vo, D., Graham, K. J., and Scow, K. M.: Soil Water Content and Organic Carbon Availability Are Major Determinants of Soil Microbial Community Composition, Microb Ecol, 48, 424-430, 2004.

Dubnick, A., Kazemi, S., Sharp, M., Wadham, J., Hawkings, J., Beaton, A., and Lanoil, B.: Hydrological controls on glacially-exported microbial assemblages, Journal of Geophysical Research: Biogeosciences, doi: 10.1002/2016JG003685, 2017. n/a-n/a, 2017.

Duhamel, S. and Jacquet, S.: Flow cytometric analysis of bacteria- and virus-like particles in lake sediments, Journal of Microbiological Methods, 64, 316-332, 2006.

Dumont, M., Brun, E., Picard, G., Michou, M., Libois, Q., Petit, J. R., Geyer, M., Morin, S., and Josse, B.: Contribution of light-absorbing impurities in snow to Greenland/'s darkening since 2009, Nature Geosci, 7, 509-512, 2014.

Dyurgerov, M. B. and Meier, M. F.: Twentieth century climate change: Evidence from small glaciers, Proceedings of the National Academy of Sciences, 97, 1406-1411, 2000.

Edwards, A.: Coming in from the cold: potential microbial threats from the terrestrial cryosphere, Frontiers in Earth Science, 3, 2015.

Edwards, A., Anesio, A. M., Rassner, S. M., Sattler, B., Hubbard, B., Perkins, W. T., Young, M., and Griffith, G. W.: Possible interactions between bacterial diversity, microbial activity and supraglacial hydrology of cryoconite holes in Svalbard, ISME J, 5, 150-160, 2011.

Edwards, A., Irvine-Fynn, T. D. L., Mitchell, A. C., and Rassner, S. M. E.: A germ theory for glacial systems?, WIREs: Water, 1, 331-340, 2014a.

Edwards, A., Mur, L. A., Girdwood, S. E., Anesio, A. M., Stibal, M., Rassner, S. M., Hell, K., Pachebat, J. A., Post, B., Bussell, J. S., Cameron, S. J., Griffith, G. W., Hodson, A. J., and Sattler, B.: Coupled cryoconite ecosystem structure-function relationships are revealed by comparing bacterial communities in alpine and Arctic glaciers, FEMS microbiology ecology, doi: 10.1111/1574-6941.12283, 2014b. 2014b.

Edwards, A., Pachebat, J. A., Swain, M., Hegarty, M., Hodson, A. J., Irvine-Fynn, T. D. L., Rassner, S. M. E., and Sattler, B.: A metagenomic snapshot of taxonomic and functional diversity in an alpine glacier cryoconite ecosystem, Environ Res Lett, 8, 035003, 2013a.

Edwards, A., Rassner, S. M. E., Anesio, A. M., Worgan, H. J., Irvine-Fynn, T. D. L., Wyn Williams, H., Sattler, B., and Wyn Griffith, G.: Contrasts between the cryoconite and ice-marginal bacterial communities of Svalbard glaciers, Polar Research, 32, 2013b.

Eicken, H., Krouse, H. R., Kadko, D., and Perovich, D. K.: Tracer studies of pathways and rates of meltwater transport through Arctic summer sea ice, Journal of Geophysical Research: Oceans, 107, SHE 22-21-SHE 22-20, 2002.

Fagerbakke, K. M., Heldal, M., and Norland, S.: Content of carbon, nitrogen, oxygen, sulfur and phosphorus in native aquatic and cultured bacteria, Aquatic Microbial Ecology, 10, 15-27, 1996.

Falcioni, T., Manti, A., Boi, P., Canonico, B., Balsamo, M., and Papa, S.: Comparison of disruption procedures for enumeration of activated sludge floc bacteria by flow cytometry, Cytometry Part B: Clinical Cytometry, 70B, 149-153, 2006.

Falkowski, P., Scholes, R. J., Boyle, E., Canadell, J., Canfield, D., Elser, J., Gruber, N., Hibbard, K., Högberg, P., Linder, S., Mackenzie, F. T., Moore III, B., Pedersen, T., Rosenthal, Y., Seitzinger, S., Smetacek, V., and Steffen, W.: The Global Carbon Cycle: A Test of Our Knowledge of Earth as a System, Science, 290, 291-296, 2000.

Falkowski, P. G., Fenchel, T., and Delong, E. F.: The microbial engines that drive Earth's biogeochemical cycles, Science, 320, 1034-1039, 2008.

Felip, M., Andreatta, S., Sommaruga, R., Straskrábová, V., and Catalan, J.: Suitability of flow cytometry for estimating bacterial biovolume in natural plankton samples: comparison with microscopy data, Appl. Environ. Microbiol., 73, 4508-4514, 2007.

Felip, M., Sattler, B., Psenner, R., and Catalan, J.: Highly active microbial communities in the ice and snow cover of high mountain lakes, Applied and environmental microbiology, 61, 2394-2401, 1995.

Ferguson, R. I.: Sinuosity of Supraglacial Streams, Geological Society of America Bulletin, 84, 251-256, 1973.

Finsterle, S., Kowalsky, M., and Pruess, K.: TOUGH: Model use, calibration, and validation, Transactions of the ASABE, 55, 1275-1290, 2012.

Fischer, A.: Klima und Gletscher in Obergurgl. In: Glaziale und periglaziale Lebensräume im Raum Obergurgl, Koch, E.-M. and Erschblamer, B. (Eds.), Innsbruck University Press, Innsbruck, 2010.

Fischer, H., Siggaard-Andersen, M. L., Ruth, U., Röthlisberger, R., and Wolff, E.: Glacial/interglacial changes in mineral dust and sea-salt records in polar ice cores: Sources, transport, and deposition, Reviews of Geophysics, 45, 2007.

Flanner, M. G., Zender, C. S., Hess, P. G., Mahowald, N. M., Painter, T. H., Ramanathan, V., and Rasch, P. J.: Springtime warming and reduced snow cover from carbonaceous particles, Atmos. Chem. Phys., 9, 2481-2497, 2009.

Foladori, P., Laura, B., Gianni, A., and Giuliano, Z.: Effects of sonication on bacteria viability in wastewater treatment plants evaluated by flow cytometry—Fecal indicators, wastewater and activated sludge, Water Research, 41, 235-243, 2007.

Foreman, C. M., Sattler, B., Mikucki, J. A., Porazinska, D. L., and Priscu, J. C.: Metabolic activity and diversity of cryoconites in the Taylor Valley, Antarctica, Journal of Geophysical Research: Biogeosciences, 112, G04S32, 2007.

Førland, E. J. and Hanssen-Bauer, I.: Increased precipitation in the Norwegian Arctic: true or false?, Climatic change, 46, 485-509, 2000.

Forster, R. R., Box, J. E., van den Broeke, M. R., Miege, C., Burgess, E. W., van Angelen, J. H., Lenaerts, J. T. M., Koenig, L. S., Paden, J., Lewis, C., Gogineni, S. P., Leuschen, C., and McConnell, J. R.: Extensive liquid meltwater storage in firn within the Greenland ice sheet, Nature Geoscience, 7, 95-98, 2014.

Fountain, A. G.: The storage of water in, and hydraulic characteristics of, the firn of South Cascade Glacier, Washington State, USA, Annals of Glaciology, 13, 69-75, 1989.

Fountain, A. G., Tranter, M., Nylen, T. H., Lewis, K. J., and Mueller, D. R.: Evolution of cryoconite holes and their contribution to meltwater runoff from glaciers in the McMurdo Dry Valleys, Antarctica, Journal of Glaciology, 50, 35-45, 2004.

Fountain, A. G. and Walder, J. S.: Water flow through temperate glaciers, Reviews of Geophysics, 36, 299-328, 1998.

Franco, B., Fettweis, X., and Erpicum, M.: Future projections of the Greenland ice sheet energy balance driving the surface melt, The Cryosphere, 7, 1-18, 2013.

Franzetti, A., Navarra, F., Tagliaferri, I., Gandolfi, I., Bestetti, G., Minora, U., Azzoni, R. S., Diolaiuti, G., Smiraglia, C., and Ambrosini, R.: Potential sources of bacteria colonizing the cryoconite of an Alpine glacier, PLOS ONE, 12, e0174786, 2017.

Franzetti, A., Tatangelo, V., Gandolfi, I., Bertolini, V., Bestetti, G., Diolaiuti, G., D'Agata, C., Mihalcea, C., Smiraglia, C., and Ambrosini, R.: Bacterial community structure on two alpine debris-covered glaciers and biogeography of Polaromonas phylotypes, ISME J, 7, 1483-1492, 2013.

Fredrickson, J., Garland, T., Hicks, R., Thomas, J., Li, S., and McFadden, K.: Lithotrophic and heterotrophic bacteria in deep subsurface sediments and their relation to sediment properties, Geomicrobiology Journal, 7, 53-66, 1989.

Fredrickson, J. K. and Balkwill, D. L.: Sampling and enumeration techniques. In: Techniques in microbial ecology, Burlage, R. S., Atlas, R., Stahl, D., Geesey, G., and Sayler, G. (Eds.), Oxford University Press, Oxford, 1998.

Freeze, R. A. and Cherry, J. A.: Groundwater, 1979.

Frossard, A., Hammes, F., and Gessner, M. O.: Flow Cytometric Assessment of Bacterial Abundance in Soils, Sediments and Sludge, Front Microbiol, 7, 903, 2016.

Fu, Q.: Radiation Transfer in the Atmosphere. In: Encyclopedia of Atmospheric Sciences (Second Edition), North, G. R., Pyle, J., and Zhang, F. (Eds.), Academic Press, Oxford, 2015.

Gasol, J. M. and Del Giorgio, P. A.: Using flow cytometry for counting natural planktonic bacteria and understanding the structure of planktonic bacterial communities, Sci Mar, 64, 197-224, 2000.

Georlette, D., Blaise, V., Collins, T., D'Amico, S., Gratia, E., Hoyoux, A., Marx, J. C., Sonan, G., Feller, G., and Gerday, C.: Some like it cold: biocatalysis at low temperatures, FEMS Microbiology Reviews, 28, 25-42, 2004.

Gerdel, R. W.: The transmission of water through snow, Eos, Transactions American Geophysical Union, 35, 475-485, 1954.

Ghiorse, W. C. and Wilson, J. T.: Microbial ecology of the terrestrial subsurface. In: Advances in applied microbiology, Elsevier, 1988.

Ginot, P., Dumont, M., Lim, S., Patris, N., Taupin, J.-D., Wagnon, P., Gilbert, A., Arnaud, Y., Marinoni, A., and Bonasoni, P.: A 10 year record of black carbon and dust from a Mera Peak ice core (Nepal): variability and potential impact on melting of Himalayan glaciers, The Cryosphere, 8, 1479-1496, 2014.

Gleason, C. J., Smith, L. C., Chu, V. W., Legleiter, C. J., Pitcher, L. H., Overstreet, B. T., Rennermalm, A. K., Forster, R. R., and Yang, K.: Characterizing supraglacial meltwater channel hydraulics on the Greenland Ice Sheet from in situ observations, Earth Surface Processes and Landforms, 2016. 2016.

Goordial, J., Lamarche-Gagnon, G., Lay, C.-Y., and Whyte, L.: Left out in the cold: life in cryoenvironments. In: Polyextremophiles, Springer, 2013.

Gorman, S. P., Scott, E. M., and Russell, A. D.: Antimicrobial Activity, Uses and Mechanism of Action of Glutaraldehyde, Journal of Applied Bacteriology, 48, 161-190, 1980.

Gowing, M.: Large viruses and infected microeukaryotes in Ross Sea summer pack ice habitats, Marine Biology, 142, 1029-1040, 2003.

Grannas, A., Bogdal, C., Hageman, K., Halsall, C., Harner, T., Hung, H., Kallenborn, R., Klán, P., Klánová, J., and Macdonald, R.: The role of the global cryosphere in the fate of organic contaminants, Atmos Chem Phys, 13, 3271-3305, 2013.

Gray, D., Toth, B., Zhao, L., Pomeroy, J., and Granger, R.: Estimating areal snowmelt infiltration into frozen soils, Hydrological Processes, 15, 3095-3111, 2001.

Greuell, W., Knap, W. H., and Smeets, P. C.: Elevational changes in meteorological variables along a midlatitude glacier during summer, Journal of Geophysical Research: Atmospheres, 102, 25941-25954, 1997.

Greuell, W. and Oerlemans, J.: Energy Balance Calculations on and near Hintereisferner (Austria) and an Estimate of the Effect of Greenhouse Warming on Ablation. In: Glacier Fluctuations and Climatic Change: Proceedings of the Symposium on Glacier Fluctuations and Climatic Change, held in Amsterdam, 1–5 June 1987, Oerlemans, J. (Ed.), Springer Netherlands, Dordrecht, 1989.

Gribbon, P.: Short Notes: Cryoconite Holes on Sermikavsak, West Greenland, Journal of Glaciology, 22, 177-181, 1979.

Hagen, J. O., Liestøl, O., Roland, E., and Jørgensen, T.: Glacier Atlas of Svalbard and Jan Mayen, Norsk Polarinstitutt, Oslo, 1993.

Hambrey, M. J., Alean, J., Alean, J., and Alean, J.: Glaciers, Cambridge University Press Cambridge, 2004.

Hambrey, M. J. and Lawson, W.: Structural styles and deformation fields in glaciers: a review, Geological Society, London, Special Publications, 176, 59-83, 2000.

Hamilton, T. L., Peters, J. W., Skidmore, M. L., and Boyd, E. S.: Molecular evidence for an active endogenous microbiome beneath glacial ice, ISME J, 7, 1402-1412, 2013.

Hammes, F., Berney, M., Wang, Y., Vital, M., Köster, O., and Egli, T.: Flow-cytometric total bacterial cell counts as a descriptive microbiological parameter for drinking water treatment processes, Water Research, 42, 269-277, 2008.

Han, P., Shen, X., Yang, H., Kim, H., and Tong, M.: Influence of nutrient conditions on the transport of bacteria in saturated porous media, Colloids and Surfaces B: Biointerfaces, 102, 752-758, 2013.

Hannah, D. M., Wood, P. J., and Sadler, J. P.: Ecohydrology and hydroecology: A 'new paradigm'?, Hydrological Processes, 18, 3439-3445, 2004.

Harding, T., Jungblut, A. D., Lovejoy, C., and Vincent, W. F.: Microbes in high arctic snow and implications for the cold biosphere, Appl. Environ. Microbiol., 77, 3234-3243, 2011.

Hartmann, A., Goldscheider, N., Wagener, T., Lange, J., and Weiler, M.: Karst water resources in a changing world: Review of hydrological modeling approaches, Reviews of Geophysics, 52, 218-242, 2014.

Haznedaroglu, B. Z., Bolster, C. H., and Walker, S. L.: The role of starvation on Escherichia coli adhesion and transport in saturated porous media, Water Research, 42, 1547-1554, 2008.

Healy, R. W.: Simulating water, solute, and heat transport in the subsurface with the VS2DI software package, Vadose Zone Journal, 7, 632-639, 2008.

Hock, R.: Reveiw of melt processes, Progress in Physical Geography, 29, 362-391, 2005.

Hock, R. and Holmgren, B.: A distributed surface energy-balance model for complex topography and its application to Storglaciären, Sweden, Journal of Glaciology, 51, 25-36, 2005.

Hock, R., Jansson, P., and Braun, L. N.: Modelling the Response of Mountain Glacier Discharge to Climate Warming. In: Global Change and Mountain Regions: An Overview of Current Knowledge, Huber, U. M., Bugmann, H. K. M., and Reasoner, M. A. (Eds.), Springer Netherlands, Dordrecht, 2005.

Hodgkins, R.: Glacier hydrology in Svalbard, Norwegian high arctic, Quaternary Science Reviews, 16, 957-973, 1997.

Hodgkins, R.: Seasonal evolution of meltwater generation, storage and discharge at a non-temperate glacier in Svalbard, Hydrological Processes, 15, 441-460, 2001.

Hodson, A., Brock, B., Pearce, D., Laybourn-Parry, J., and Tranter, M.: Cryospheric ecosystems: a synthesis of snowpack and glacial research, Environ Res Lett, 10, 110201, 2015.

Hodson, A. J.: Understanding the dynamics of black carbon and associated contaminants in glacial systems, Wiley Interdisciplinary Reviews: Water, 1, 141-149, 2014.

Hodson, A. J., Anesio, A. M., Ng, F., Watson, R., Quirk, J., Irvine-Fynn, T. D. L., Dye, A., Clark, C., McCloy, P., Kohler, J., and Sattler, B.: A glacier respires: Quantifying the distribution and respiration CO_2 flux of cryoconite across an entire Arctic supraglacial ecosystem, Journal of Geophysical Research, 112, 2007.

Hodson, A. J., Anesio, A. M., Tranter, M., Fountain, A. G., Osbourn, M., Priscu, J. C., Laybourn-Parry, J., and Sattler, B.: Glacial Ecosystems, Ecological Monographs, 78, 41-67, 2008.

Hodson, A. J., Mumford, P. N., Kohler, J., and Wynn, P. M.: The High Arctic glacial ecosystem: new insights from nutrient budgets, Biogeochemistry, 72, 233-256, 2005.

Hodson, A. J., Paterson, H., Westwood, K., Cameron, K., and Laybourn-Parry, J.: A blue-ice ecosystem on the margins of the East Antarctic ice sheet, Journal of Glaciology, 59, 255-268, 2013.

Hodson, A. J., Tranter, M., Dowdeswell, J. A., Gurnell, A. M., and Hagen, J. O.: Glacier thermal regime and suspended-sediment yield: a comparison of two high-Arctic glaciers, Annals of Glaciology, 24, 32-37, 1997.

Hoffman, F. M., Fountain, A. G., and Liston, G.: Distributed modeling of ablation (1996–2011) and climate sensitivity on the glaciers of Taylor Valley, Antarctica, Journal of Glaciology, doi: doi:10.1017/jog.2015.2, 2016. 1-15, 2016.

Hoffman, M. J., Fountain, A. G., and Liston, G. E.: Near-surface internal melting: a substantial mass loss on Antarctic Dry Valley glaciers, Journal of Glaciology, 60, 361-374, 2014.

Holmlund, P. and Eriksson, M.: The Cold Surface Layer on Storglaciaren, Geografiska Annaler. Series A, Physical Geography, 71, 241-244, 1989.

Hood, E., Battin, T. J., Fellman, J., O'Neel, S., and Spencer, R. G. M.: Storage and release of organic carbon from glaciers and ice sheets, Nature Geoscience, 8, 91-96, 2015.

Hood, E., Fellman, J., Spencer, R. G. M., Hernes, P. J., Edwards, R., D'Amore, D., and Scott, D.: Glaciers as a source of ancient and labile organic matter to the marine environment, Nature, 462, 1044-1047, 2009.

Horton, R. E.: The role of infiltration in the hydrologic cycle, Eos, Transactions American Geophysical Union, 14, 446-460, 1933.

Hotaling, S., Hood, E., and Hamilton, T. L.: Microbial ecology of mountain glacier ecosystems: Biodiversity, ecological connections, and implications of a warming climate, Environmental Microbiology, doi: 10.1111/1462-2920.13766, 2017. n/a-n/a, 2017.

Hubbard, B. and Nienow, P.: Alpine subglacial hydrology, Quaternary Science Reviews, 16, 939-955, 1997.

Hubbard, B. P., Sharp, M. J., Willis, I. C., Nielsen, M. K., and Smart, C. C.: Borehole water-level variations and the strucutre of the subglacial hydrological sysytem of Haut Glacier d'Arolla, Valais, Switzerland, Journal of Glaciology, 41, 572-583, 1995.

Hudleston, P. J.: Structures and fabrics in glacial ice: A review, Journal of Structural Geology, 81, 1-27, 2015.

Hudson, R. and Fraser, J.: The mass balance (or dry injection) method, Streamline Watershed Management Bulletin, 9, 6-12, 2005.

Huss, M., Usselmann, S., Farinotti, D., and Bauder, A.: Glacier mass balance in the south-eastern Swiss Alps since 1900 and perspectives for the future, Erdkunde, 2010. 119-140, 2010.

IPCC: Summary for Policymakers. In: Climate Change 2013: The Physical Science Basis. Contribution of Working Group I to the Fifth Assessment Report of the Intergovernmental Panel on Climate Change, Stocker, T. F., Qin, D., Plattner, G.-K., Tignor, M. M. B., Allen, S. K., Boschung, J., Nauels, A., Xia, Y., Bex, V., and Midgley, P. M. (Eds.), Cambridge University Press, Cambridge, UK, 2013.

Irvine-Fynn, T. D. L.: Modelling Runoff form the Maritime Arctic Cryosphere: Water storage and routing and Midtre Lovenbreen, Doctor of Philosophy, Department of Geography, University of Sheffield, 359 pp., 2008.

Irvine-Fynn, T. D. L., Barrand, N. E., Porter, P. R., Hodson, A. J., and Murray, T.: Recent High-Arctic glacial sediment redistribution: A process perspective using airborne lidar, Geomorphology, 125, 27-39, 2011a.

Irvine-Fynn, T. D. L., Bridge, J. W., and Hodson, A. J.: In situ quantification of supraglacial cryoconite morphodynamics using time-lapse imaging: an example from Svalbard, Journal of Glaciology, 57, 651-657, 2011b.

Irvine-Fynn, T. D. L. and Edwards, A.: A frozen asset: the potential of flow cytometry in constraining the glacial biome, Cytometry. Part A : the journal of the International Society for Analytical Cytology, 85, 3-7, 2014.

Irvine-Fynn, T. D. L., Edwards, A., Newton, S., Langford, H., Rassner, S. M., Telling, J., Anesio, A. M., and Hodson, A. J.: Microbial cell budgets of an Arctic glacier surface quantified using flow cytometry, Environmental Microbiology, 14, 2998-3012, 2012.

Irvine-Fynn, T. D. L., Hanna, E., Barrand, N. E., Porter, P. R., Kohler, J., and Hodson, A. J.: Examination of a physically based, high-resolution, distributed Arctic temperature-index melt model, on Midtre Lovenbreen, Svalbard, Hydrological Processes, 28, 134-149, 2014.

Irvine-Fynn, T. D. L., Hodson, A. J., Moorman, B. J., Vatne, G., and Hubbard, A. L.: Polythermal Glacier Hydrology: A Review, Reviews of Geophysics, 49, 2011c.

Irvine-Fynn, T. D. L., Moorman, B. J., Williams, J. L. M., and Walter, F. S. A.: Seasonal changes in ground-penetrating radar signature observed at a polythermal glacier, Bylot Island, Canada, Earth Surface Processes and Landforms, 31, 892-909, 2006.

Isenko, E., Naruse, R., and Mavlyudov, B.: Water temperature in englacial and supraglacial channels: Change along the flow and contribution to ice melting on the channel wall, Cold Regions Science and Technology, 42, 53-62, 2005.

Izumi, N. and Parker, G.: Inception of channelization and drainage basin formation: upstream-driven theory, Journal of Fluid Mechanics, 283, 341-363, 1995.

Jansson, P.: Water pressure and basal sliding on Storglaciären, northern Sweden, Journal of Glaciology, 41, 232-240, 1995.

Jansson, P., Hock, R., and Schneider, T.: The concept of glacier storage: a review, Journal of Hydrology, 282, 116-129, 2003.

Jennings, S. J. A., Hambrey, M. J., and Glasser, N. F.: Ice flow-unit influence on glacier structure, debris entrainment and transport, Earth Surface Processes and Landforms, 39, 1279-1292, 2014.

Jepsen, S. M., Adams, E. E., and Priscu, J. C.: Fuel movement along grain boundaries in ice, Cold Regions Science and Technology, 45, 158-165, 2006.

Jepsen, S. M., Adams, E. E., and Priscu, J. C.: Sediment melt-migration dynamics in perennial Antarctic lake ice, Arctic, Antarctic, and Alpine Research, 42, 57-66, 2010.

Jones, H. G., Pomeroy, J., Walker, D., and Hoham, R.: Snow ecology: an interdisciplinary examination of snow-covered ecosystems, Cambridge University Press, 2001.

Jones, J.: Studies on freshwater bacteria: factors which influence the population and its activity, The Journal of Ecology, 1971. 593-613, 1971.

Jordan, R. E. and Stark, J. A.: Capillary tension in rotting ice layers, DTIC DocumentNo. ERDC/CRREL-TR-01-13, 2001.

Jung, Y., Pau, G. S. H., Finsterle, S., and Pollyea, R. M.: TOUGH3: A new efficient version of the TOUGH suite of multiphase flow and transport simulators, Computers & Geosciences, 108, 2-7, 2017.

Karl, D. M., Bird, D. F., Björkman, K., Houlihan, T., Shackelford, R., and Tupas, L.: Microorganisms in the Accreted Ice of Lake Vostok, Antarctica, Science, 286, 2144-2147, 1999.

Karlstrom, L., Gajjar, P., and Manga, M.: Meander formation in supraglacial streams, Journal of Geophysical Research: Earth Surface, 118, 1897-1907, 2013.

Karlstrom, L. and Yang, K.: Fluvial supraglacial landscape evolution on the Greenland Ice Sheet, Geophysical Research Letters, 43, 2683-2692, 2016.

Karlstrom, L., Zok, A., and Manga, M.: Near-surface permeability in a supraglacial drainage basin on the Llewellyn Glacier, Juneau Icefield, British Columbia, The Cryosphere, 8, 537-546, 2014.

Kazumi, J. and Capone, D.: Heterotrophic microbial activity in shallow aquifer sediments of Long Island, New York, Microb Ecol, 28, 19-37, 1994.

Kelly, F. X., Dapsis, K. J., and Lauffenburger, D. A.: Effect of bacterial chemotaxis on dynamics of microbial competition, Microb Ecol, 16, 115-131, 1988.

Kestin, J., Sokolov, M., and Wakeham, W. A.: Viscosity of liquid water in the range− 8 C to 150 C, Journal of Physical and Chemical Reference Data, 7, 941-948, 1978.

Klauth, P., Wilhelm, R., Klumpp, E., Poschen, L., and Groeneweg, J.: Enumeration of soil bacteria with the green fluorescent nucleic acid dye Sytox green in the presence of soil particles, Journal of Microbiological Methods, 59, 189-198, 2004.

Klok, E. J. L., Greuell, W., and Oerlemans, J.: Temporal and spatial variation of the surface albedo of Morteratschgletscher, Switzerland, as derived from 12 Landsat images, Journal of Glaciology, 49, 491-502, 2003.

Knighton, A. D.: Channel form Adjustment in Supraglacial Streams, Austre Okstindbreen, Norway, Arctic Alpine Res, 17, 451-466, 1985.

Knighton, A. D.: Channel Form and Flow Characteristics of Supraglacial Streams, Austre-Okstindbreen, Norway, Arctic Alpine Res, 13, 295-306, 1981.

Koch, D. and Hansen, J.: Distant origins of Arctic black carbon: a Goddard Institute for Space Studies ModelE experiment, Journal of Geophysical Research: Atmospheres, 110, 2005.

Koenig, L. S., Lampkin, D. J., Montgomery, L. N., Hamilton, S. L., Turrin, J. B., Joseph, C. A., Moutsafa, S. E., Panzer, B., Casey, K. A., Paden, J. D., Leuschen, C., and Gogineni, P.: Wintertime storage of water in buried supraglacial lakes across the Greenland Ice Sheet, The Cryosphere Discussions, 8, 3999-4031, 2014.

Koizumi, K. and Naruse, R.: Experiments on formation of water channels in a glacier, Journal of the Japanese Society of Snow and Ice, 56, 137-144, 1994.

Kostrzewski, A. and Zwolinski, Z.: Hydraulic geometry of a supraglacial stream, Ragnarbreen, Spitsbergen, Quaestiones Geographicae. Zeszyt Specjalny, 4, 1995.

Koziol, K. A., Moggridge, H. L., Cook, J. M., and Hodson, A. J.: Organic carbon fluxes of a glacier surface: a case study of Foxfonna, a small Arctic glacier, Earth Surface Processes and Landforms, 0, 2018.

Krembs, C., Gradinger, R., and Spindler, M.: Implications of brine channel geometry and surface area for the interaction of sympagic organisms in Arctic sea ice, Journal of Experimental Marine Biology and Ecology, 243, 55-80, 2000.

LaChapelle, E.: Errors in ablation measurements from settlement and sub-surface melting, Journal of Glaciology, 3, 458-467, 1959.

Langford, H., Hodson, A. J., Banwart, S., and Bøggild, C.: The microstructure and biogeochemistry of Arctic cryoconite granules, Annals of Glaciology, 51, 87-94, 2010.

Larose, C., Berger, S., Ferrari, C., Navarro, E., Dommergue, A., Schneider, D., and Vogel, T. M.: Microbial sequences retrieved from environmental samples from seasonal Arctic snow and meltwater from Svalbard, Norway, Extremophiles, 14, 205-212, 2010.

Larose, C., Dommergue, A., and Vogel, T.: The dynamic arctic snow pack: an unexplored environment for microbial diversity and activity, Biology, 2, 317-330, 2013a.

Larose, C., Dommergue, A., and Vogel, T. M.: Microbial nitrogen cycling in Arctic snowpacks, Environ Res Lett, 8, 035004, 2013b.

Larson, G. J.: Internal drainage of stagnant ice: Burroughs Glacier, southeast Alaska, Institute of Polar Studies, Ohio State University, 1977.

Larson, G. J.: Meltwater storage in a temperate glacier: Burroughs Glacier, Southeast Alaska, Institute of Polar Studies, Ohio State University, 1978.

Laurion, I., Demers, S., and Vezina, A. F.: The microbial food web associated with the ice algal assemblage: biomass and bacterivory of nanoflagellate protozoans in Resolute Passage (High Canadian Arctic), Marine ecology progress series. Oldendorf, 120, 77-87, 1995.

Lavergne, C., Beaugeard, L., Dupuy, C., Courties, C., and Agogué, H.: An efficient and rapid method for the enumeration of heterotrophic prokaryotes in coastal sediments by flow cytometry, Journal of Microbiological Methods, 105, 31-38, 2014.

Lawson, E. C., Wadham, J. L., Tranter, M., Stibal, M., Lis, G. P., Butler, C. E. H., Laybourn-Parry, J., Nienow, P., Chandler, D., and Dewsbury, P.: Greenland Ice Sheet exports labile organic carbon to the Arctic oceans, Biogeosciences, 11, 4015-4028, 2014.

Laybourn-Parry, J., Tranter, M., and Hodson, A. J.: The Ecology of Snow and Ice Environments, Oxford University Press, Oxford, 2012.

Lee, S. and Fuhrman, J. A.: Relationships between Biovolume and Biomass of Naturally Derived Marine Bacterioplankton, Applied and Environmental Microbiology, 53, 1298-1303, 1987.

Lehmann, S., Gajek, G., Chmiel, S., and Polkowska, Ż.: Do morphometric parameters and geological conditions determine chemistry of glacier surface ice? Spatial distribution of contaminants present in the surface ice of Spitsbergen glaciers (European Arctic), Environmental Science and Pollution Research, 23, 23385-23405, 2016.

Levine, S. and Ghiorse, W.: Environmental factors affecting distribution and abundance of bacteria, fungi and protozoa in subsurface sediments of the Upper Atlantic Coastal Plain, USA, Cornell Univ., Ithaca, NY (United States). Dept. of Microbiology, 1990.

Liestøl, O.: Storbreen glacier in Jotunheimen, Norway, 1967. 1967.

Liston, G. E., Winther, J. G., Bruland, O., Elvehoy, H., and Sand, K.: Below-surface ice melt on the coastal Antarctic ice sheet, Journal of Glaciology, 45, 273-285, 1999.

Liu, Y., Yao, T., Jiao, N., Kang, S., Xu, B., Zeng, Y., Huang, S., and Liu, X.: Bacterial diversity in the snow over Tibetan Plateau Glaciers, Extremophiles, 13, 411-423, 2009.

Liu, Y., Yao, T., Kang, S., Jiao, N., Zeng, Y., Shi, Y., Luo, T., Jing, Z., and Huang, S.: Seasonal variation of snow microbial community structure in the East Rongbuk glacier, Mt. Everest, Chinese Science Bulletin, 51, 1476-1486, 2006.

Lliboutry, L.: Permeability, brine content and temperature of temperate ice, Journal of Glaciology, 10, 15-29, 1971.

Lliboutry, L.: Temperate ice permeability, stability of water veins and percolation of internal meltwater, Journal of Glaciology, 42, 1996.

Łokas, E., Zaborska, A., Kolicka, M., Różycki, M., and Zawierucha, K.: Accumulation of atmospheric radionuclides and heavy metals in cryoconite holes on an Arctic glacier, Chemosphere, 160, 162-172, 2016.

Łokas, E., Zawierucha, K., Cwanek, A., Szufa, K., Gaca, P., Mietelski, J. W., and Tomankiewicz, E.: The sources of high airborne radioactivity in cryoconite holes from the Caucasus (Georgia), Scientific Reports, 8, 10802, 2018.

Lu, N. and Godt, J. W.: Hillslope hydrology and stability, Cambridge University Press, 2013.

Lu, N., Kaya, B. S., and Godt, J. W.: Direction of unsaturated flow in a homogeneous and isotropic hillslope, Water Resources Research, 47, 2011.

Lu, N. and Likos, W.: Rate of capillary rise in soil, Journal of geotechnical and Geoenvironmental engineering, 130, 646-650, 2004.

Lu, S., Molz, F. J., Fogg, G. E., and Castle, J. W.: Combining stochastic facies and fractal models for representing natural heterogeneity, Hydrogeology Journal, 10, 475-482, 2002.

Lutz, S., Anesio, A. M., Jorge Villar, S. E., and Benning, L. G.: Variations of algal communities cause darkening of a Greenland glacier, FEMS Microbiology Ecology, 89, 402-414, 2014.

Lutz, S., Anesio, A. M., Raiswell, R., Edwards, A., Newton, R. J., Gill, F., and Benning, L. G.: The biogeography of red snow microbiomes and their role in melting arctic glaciers, Nat Commun, 7, 2016.

Maccario, L., Sanguino, L., Vogel, T. M., and Larose, C.: Snow and ice ecosystems: not so extreme, Research in microbiology, 166, 782-795, 2015.

MacDonell, S. and Fitzsimons, S.: The formation and hydrological significance of cryoconite holes, Progress in Physical Geography, 32, 595-610, 2008.

MacDonell, S. and Fitzsimons, S.: Observations of cryocnoite hole system processes on an Antarctic glacier, Revista Chilena de Historia Natural, 85, 393-407, 2012.

MacDonell, S., Sharp, M., and Fitzsimons, S.: Cryoconite hole connectivity on the Wright Lower Glacier, McMurdo Dry Valleys, Antarctica, Journal of Glaciology, FirstView, 1-11, 2016.

Mader, H. M.: Observations of the Water-Vein System in Polycrystalline Ice, Journal of Glaciology, 38, 333-347, 1992.

Mader, H. M., Pettitt, M. E., Wadham, J. L., Wolff, E. W., and Parkes, R. J.: Subsurface ice as a microbial habitat, Geology, 34, 169-172, 2006.

Madigan, M., Martinko, J., Bender, K., Buckley, D., and Stahl, D.: Brock Biology of Microorganisms, Pearson, London, 2015.

Mantelli, E., Camporeale, C., and Ridolfi, L.: Supraglacial channel inception: Modeling and processes, Water Resources Research, 51, 7044-7063, 2015.

Margesin, R., Spröer, C., Zhang, D.-C., and Busse, H.-J.: *Polaromonas glacialis* sp. nov. and *Polaromonas cryoconiti* sp. nov., isolated from alpine glacier cryoconite, International Journal of Systematic and Evolutionary Microbiology, 62, 2662-2668, 2012.

Marie, D., Partensky, F., Jacquet, S., and Vaulot, D.: Enumeration and cell cycle analysis of natural populations of marine picoplankton by flow cytometry using the nucleic acid stain SYBR Green I, Applied and Environmental Microbiology, 63, 186-193, 1997.

Marsh, P. and Woo, M. K.: Wetting front advance and freezing of meltwater within a snow cover: 1. Observations in the Canadian Arctic, Water Resources Research, 20, 1853-1864, 1984.

Marston, R. A.: Supraglacial Stream Dynamics on the Juneau Icefield, Ann Assoc Am Geogr, 73, 597-608, 1983.

McCormick, P. V. and Stevenson, R. J.: Mechanisms of benthic algal succession in lotic environments, Ecology, 72, 1835-1848, 1991.

McGrath, D., Colgan, W., Steffen, K., Lauffenburger, P., and Balog, J.: Assessing the summer water budget of a moulin basin in the Sermeq Avannarleq ablation region, Greenland ice sheet, Journal of Glaciology, 57, 954-964, 2011.

McIntyre, N. F.: Cryoconite hole thermodynamics, Canadian Journal of Earth Sciences, 21, 152-156, 1984.

McMinn, A., Ryan, K., Ralph, P., and Pankowski, A.: Spring sea ice photosynthesis, primary productivity and biomass distribution in eastern Antarctica, 2002–2004, Marine Biology, 151, 985-995, 2007.

Menzel, D. W. and Ryther, J. H.: Distribution and cycling of organic matter in the oceans, 1970. 1970.

Mikan, C. J., Schimel, J. P., and Doyle, A. P.: Temperature controls of microbial respiration in arctic tundra soils above and below freezing, Soil Biology and Biochemistry, 34, 1785-1795, 2002.

Miller, O. L., Solomon, D. K., Miège, C., Koenig, L. S., Forster, R. R., Montgomery, L. N., Schmerr, N., Ligtenberg, S. R., Legchenko, A., and Brucker, L.: Hydraulic conductivity of a firn aquifer in southeast Greenland, Frontiers in Earth Science, 5, 38, 2017.

Miller, R. J. and Low, P. F.: Threshold Gradient for Water Flow in Clay Systems, Soil Science Society of America Journal, 27, 605-609, 1963.

Milly, P. C. D.: A Simulation Analysis of Thermal Effects on Evaporation From Soil, Water Resources Research, 20, 1087-1098, 1984.

Milner, A. M., Khamis, K., Battin, T. J., Brittain, J. E., Barrand, N. E., Füreder, L., Cauvy-Fraunié, S., Gíslason, G. M., Jacobsen, D., Hannah, D. M., Hodson, A. J., Hood, E., Lencioni, V., Ólafsson, J. S., Robinson, C. T., Tranter, M., and Brown, L. E.: Glacier shrinkage driving global changes in downstream systems, Proceedings of the National Academy of Sciences, 114, 9770-9778, 2017.

Mindl, B., Anesio, A. M., Meirer, K., Hodson, A. J., Laybourn-Parry, J., Sommaruga, R., and Sattler, B.: Factors influencing bacterial dynamics along a transect from supraglacial runoff to proglacial lakes of a high Arctic glacieri, FEMS Microbiology Ecology, 59, 307-317, 2007.

Ming, J., Du, Z. C., Xiao, C. D., Xu, X. B., and Zhang, D. Q.: Darkening of the mid-Himalaya glaciers since 2000 and the potential causes, Environ Res Lett, 7, 2012.

Mitchell, A., Brown, G. H., and Fuge, R.: Minor and trace element export from a glacierized Alpine headwater catchment (Haut Glacier d'Arolla, Switzerland), Hydrological Processes, 15, 3499-3524, 2001.

Mitchell, A. C., Lafreniere, M. J., Skidmore, M. L., and Boyd, E. S.: Influence of bedrock mineral composition on microbial diversity in a subglacial environment, Geology, 41, 855-858, 2013.

Miteva, V.: Bacteria in Snow and Glacier Ice. In: Psychrophiles, Margesin, R., Schinner, F., Marx, J.-C., and Gerday, C. (Eds.), Springer, Berlin, 2008.

Miteva, V., Teacher, C., Sowers, T., and Brenchley, J.: Comparison of the microbial diversity at different depths of the GISP2 Greenland ice core in relationship to deposition climates, Environmental Microbiology, 11, 640-656, 2009.

Miteva, V. I. and Brenchley, J. E.: Detection and Isolation of Ultrasmall Microorganisms from a 120,000-Year-Old Greenland Glacier Ice Core, Applied and Environmental Microbiology, 71, 7806-7818, 2005.

Miteva, V. I., Sheridan, P. P., and Brenchley, J. E.: Phylogenetic and Physiological Diversity of Microorganisms Isolated from a Deep Greenland Glacier Ice Core, Applied and Environmental Microbiology, 70, 202-213, 2004.

Montagnes, D. J. S., Berges, J. A., Harrison, P. J., and Taylor, F. J. R.: Estimating carbon, nitrogen, protein, and chlorophyll a from volume in marine phytoplankton, Limnol Oceanogr, 39, 1044-1060, 1994.

Mook, D. H. and Hoskin, C. M.: Organic determinations by ignition: Caution advised, Estuarine, Coastal and Shelf Science, 15, 697-699, 1982.

Moore, J. C., Pälli, A., Ludwig, F., Blatter, H., Jania, J., Gadek, B., Glowacki, P., Mochnacki, D., and Isaksson, E.: High-resolution hydrothermal structure of Hansbreen, Spitsbergen, mapped by ground-penetrating radar, Journal of Glaciology, 45, 524-532, 1999.

Moore, J. E.: Field hydrogeology: a guide for site investigatioins and report preparation, Lewis Publsihers, New York, 2002.

Morita, R. Y.: Bacteria in oligotrophic environments: starvation-survival lifestyle, Chapman & Hall New York, 1997.

Morono, Y., Terada, T., Masui, N., and Inagaki, F.: Discriminative detection and enumeration of microbial life in marine subsurface sediments, The ISME journal, 3, 503, 2009.

Mortimer, C. A. and Sharp, M.: Spatiotemporal variability of Canadian High Arctic glacier surface albedo from MODIS data, 2001-2016, Cryosphere, 12, 2018.

Mueller, R. F.: Bacterial transport and colonization in low nutrient environments, Water Research, 30, 2681-2690, 1996.

Mueller, T. G., Pusuluri, N. B., Mathias, K. K., Cornelius, P. L., Barnhisel, R. I., and Shearer, S. A.: Map Quality for Ordinary Kriging and Inverse Distance Weighted Interpolation, Soil Science Society of America Journal, 68, 2042-2047, 2004.

Mullaney, P., Van Dilla, M., Coulter, J., and Dean, P.: Cell sizing: a light scattering photometer for rapid volume determination, Review of Scientific Instruments, 40, 1029-1032, 1969.

Müller, F.: Zonation in the accumulation area of the glaciers of Axel Heiberg Island, NWT, Canada, Journal of Glaciology, 4, 302-311, 1962.

Müller, F. and Keeler, C. M.: Errors in short term ablation measurement on melting ice surfaces, Journal of Glaciology, 8, 91-105, 1969.

Müller, S. and Nebe-von-Caron, G.: Functional single-cell analyses: flow cytometry and cell sorting of microbial populations and communities, FEMS Microbiology Reviews, 34, 554-587, 2010.

Munro, D. S.: Comparison of Melt Energy Computations and Ablatometer Measurements on Melting Ice and Snow, Arctic Alpine Res, 22, 153-162, 1990.

Munro, D. S.: Delays of supraglacial runoff from differently defined microbasin areas on the Peyto Glacier, Hydrological Processes, doi: 10.1002/hyp.8124, 2011. 2983-2994, 2011.

Musilova, M., Tranter, M., Bamber, J. L., Takeuchi, N., and Anesio, A.: Experimental evidence that microbial activity lowers the albedo of glaciers, Geochemical Perspectives Letters, 2, 106-116, 2016.

Musilova, M., Tranter, M., Bennett, S. A., Wadham, J., and Anesio, A. M.: Stable microbial community composition on the Greenland Ice Sheet, Front Microbiol, 6, 2015.

Musilova, M., Tranter, M., Wadham, J., Telling, J., Tedstone, A., and Anesio, A. M.: Microbially driven export of labile organic carbon from the Greenland ice sheet, Nature Geosci, 10, 360-365, 2017.

Nadell, C. D., Xavier, J. B., and Foster, K. R.: The sociobiology of biofilms, FEMS Microbiology Reviews, 33, 206-224, 2009.

Naegeli, K., Huss, M., and Hoelzle, M.: Change detection of bare-ice albedo in the Swiss Alps, The Cryosphere, 13, 397-412, 2019.

Nakawo, M., Yabuki, H., and Sakai, A.: Characteristics of Khumbu Glacier, Nepal Himalaya: recent change in the debris-covered area, Annals of Glaciology, 28, 118-122, 1999.

Nebe-von-Caron, G.: Standardization in microbial cytometry, Cytometry Part A, 75A, 86-89, 2009.

Nienow, P. W., Sharp, M., and Willis, I. C.: Velocity–discharge relationships derived from dye tracer experiments in glacial meltwaters: implications for subglacial flow conditions, Hydrological Processes, 10, 1411-1426, 1996.

Norland, S.: The relationship between biomass and volume of bacteria. In: Handbook of Methods in Aquatic Microbial Ecology, Kemp, P. F., Shedd, B. F., Sherr, E. B., and Cole, J. J. (Eds.), Lawrence Erlbaum, New Jersey, 1993.

Nye, F. and Frank, F. C.: Hydrology of the intergranular veins in a temperate glacier, Cambridge1973, 157-161.

Nye, J. F.: Comment on 'Temperate ice permeability, stability of water veins and percolation of internal meltwater' by L.Lliboutry, Journal of Glaciology, 43, 372, 1997.

Nye, J. F.: The Geometry of Water Veins and Nodes in Polycrystalline Ice, Journal of Glaciology, 35, 17-22, 1989.

Nye, J. F.: The rotting of temperate ice, J Cryst Growth, 113, 465-476, 1991.

Oerlemans, J., Giesen, R. H., and Van den Broeke, M. R.: Retreating alpine glaciers: increased melt rates due to accumulation of dust (Vadret da Morteratsch, Switzerland), Journal of Glaciology, 55, 729-736, 2009.

Oke, T. R.: Boundary Layer Climates, Routledge, London, 1987.

Painter, T. H., Flanner, M. G., Kaser, G., Marzeion, B., VanCuren, R. A., and Abdalati, W.: End of the Little Ice Age in the Alps forced by industrial black carbon, Proceedings of the National Academy of Sciences, 110, 15216-15221, 2013.

Pamp, S. J., Sternberg, C., and Tolker-Nielsen, T.: Insight into the microbial multicellular lifestyle via flow-cell technology and confocal microscopy, Cytometry Part A, 75A, 90-103, 2009.

Pantanella, F., Berlutti, F., Passariello, C., Sarli, S., Morea, C., and Schippa, S.: Violacein and biofilm production in Janthinobacterium lividum, Journal of Applied Microbiology, 102, 992-999, 2007.

Paterson, W. S. B.: The Physics of Glaciers, Pergammon, Oxford, UK, 1994.

Paul, F. and Kääb, A.: Perspectives on the production of a glacier inventory from multispectral satellite data in Arctic Canada: Cumberland Peninsula, Baffin Island, Annals of Glaciology, 42, 59-66, 2005.

Paul, F., Kääb, A., and Haeberli, W.: Recent glacier changes in the Alps observed by satellite: Consequences for future monitoring strategies, Global Planet Change, 56, 111-122, 2007.

Paul, F., Machguth, H., and Kääb, A.: On the impact of glacier albedo under conditions of extreme glacier melt: the summer of 2003 in the Alps, EARSeL eProceedings, 4, 139-149, 2005.

Pellicciotti, F., Brock, B., Strasser, U., Burlando, P., Funk, M., and Corripio, J.: An enhanced temperature-index glacier melt model including the shortwave radiation balance: development and testing for Haut Glacier d'Arolla, Switzerland, Journal of Glaciology, 51, 573-587, 2005.

Peterson, D. M. and Wilson, J. L.: Field study of ephemeral stream infiltration and recharge, New Mexico State University, New Mexico288, 1988.

Pettersson, R., Jansson, P., and Blatter, H.: Spatial variability in water content at the cold-temperate transition surface of the polythermal Storglaciären, Sweden, Journal of Geophysical Research: Earth Surface, 109, F02009, 2004.

Pinhassi, J. and Berman, T.: Differential Growth Response of Colony-Forming α- and γ-Proteobacteria in Dilution Culture and Nutrient Addition Experiments from Lake Kinneret (Israel), the Eastern Mediterranean Sea, and the Gulf of Eilat, Applied and Environmental Microbiology, 69, 199-211, 2003.

Porter, P. R., Vatne, G., Ng, F., and Irvine-fynn, T. D.: Ice-marginal sediment delivery to the surface of a high-Arctic glacier: Austre Brøggerbreen, Svalbard, Geografiska Annaler: Series A, Physical Geography, 92, 437-449, 2010.

Price, P. B.: Microbial life in glacial ice and implications for a cold origin of life, Fems Microbiology Ecology, 59, 217-231, 2007.

Priscu, J. C., Adams, E. E., Lyons, W. B., Voytek, M. A., Mogk, D. W., Brown, R. L., McKay, C. P., Takacs, C. D., Welch, K. A., Wolf, C. F., Kirshtein, J. D., and Avci, R.: Geomicrobiology of subglacial ice above Lake Vostok, Antarctica, Science, 286, 2141-2144, 1999.

Priscu, J. C. and Christner, B. C.: Earth's icy biosphere. In: Microbial diversity and bioprospecting, American Society of Microbiology, 2004.

Radić, V., Bliss, A., Beedlow, A. C., Hock, R., Miles, E., and Cogley, J. G.: Regional and global projections of twenty-first century glacier mass changes in response to climate scenarios from global climate models, Climate Dynamics, 42, 37-58, 2014.

Rafiq, M., Hayat, M., Anesio, A. M., Jamil, S. U. U., Hassan, N., Shah, A. A., and Hasan, F.: Recovery of metallo-tolerant and antibiotic resistant psychrophilic bacteria from Siachen glacier, Pakistan, PLOS ONE, 12, e0178180, 2017.

Rasmussen, K. E. and Albrechtsen, J.: Glutaraldehyde. The influence of pH, temperature, and buffering on the polymerization rate, Histochemistry, 38, 19-26, 1974.

Rassner, S. M. E., Anesio, A. M., Girdwood, S. E., Hell, K., Gokul, J. K., Whitworth, D. E., and Edwards, A.: Can the Bacterial Community of a High Arctic Glacier Surface Escape Viral Control?, Front Microbiol, 7, 2016.

Raymond, C. and Harrison, W.: Some observations on the behavior of the liquid and gas phases in temperate glacier ice, Journal of Glaciology, 14, 213-233, 1975.

Reasoner, D. J. and Geldreich, E. E.: A new medium for the enumeration and subculture of bacteria from potable water, Applied and Environmental Microbiology, 49, 1-7, 1985.

Rennermalm, A. K., Smith, L. C., Chu, V., Box, J., Forster, R. R., Van den Broeke, M., Van As, D., and Moustafa, S. E.: Evidence of meltwater retention within the Greenland ice sheet, The Cryosphere, 7, 1433-1445, 2013.

Reverter, F., Li, X., and Meijer, G. C.: Liquid-level measurement system based on a remote grounded capacitive sensor, Sensors and Actuators A: Physical, 138, 1-8, 2007.

Richards, L. A.: Capillary conduction of liquids through porous mediums, Physics, 1, 318-333, 1931.

Rignot, E., Velicogna, I., Broeke, M. R. v. d., Monaghan, A., and Lenaerts, J. T. M.: Acceleration of the contribution of the Greenland and Antarctic ice sheets to sea level rise, Geophysical Research Letters, 38, 2011.

Riis, V., Lorbeer, H., and Babel, W.: Extraction of microorganisms from soil: evaluation of the efficiency by counting methods and activity measurements, Soil Biology and Biochemistry, 30, 1573-1581, 1998.

Rinke, C., Schwientek, P., Sczyrba, A., Ivanova, N. N., Anderson, I. J., Cheng, J. F., Darling, A., Malfatti, S., Swan, B. K., Gies, E. A., Dodsworth, J. A., Hedlund, B. P., Tsiamis, G., Sievert, S. M., Liu, W. T., Eisen, J. A., Hallam, S. J., Kyrpides, N. C., Stepanauskas, R., Rubin, E. M., Hugenholtz, P., and Woyke, T.: Insights into the phylogeny and coding potential of microbial dark matter, Nature, 499, 431-437, 2013.

Rippin, D. M., Pomfret, A., and King, N.: High resolution mapping of supraglacial drainage pathways reveals link between micro-channel drainage density, surface roughness and surface reflectance, Earth Surface Processes and Landforms, doi: 10.1002/esp.3719, 2015. n/a-n/a, 2015.

Robinson, T. P. and Metternicht, G.: Testing the performance of spatial interpolation techniques for mapping soil properties, Computers and Electronics in Agriculture, 50, 97-108, 2006.

Rogers, S. O., Starmer, W. T., and Castello, J. D.: Recycling of pathogenic microbes through survival in ice, Medical Hypotheses, 63, 773-777, 2004.

Romm, E.: Flow characteristics of fractured rocks, Nedra, Moscow, 283, 1966.

Ross, P.: A water-level sensor using a capacitance to frequency converter, Journal of Physics E: Scientific Instruments, 16, 827, 1983.

Roth, B. L., Poot, M., Yue, S. T., and Millard, P. J.: Bacterial viability and antibiotic susceptibility testing with SYTOX green nucleic acid stain, Applied and environmental microbiology, 63, 2421-2431, 1997.

Röthlisberger, H.: Water pressure in intra-and subglacial channels, Journal of Glaciology, 11, 177-203, 1972.

Rudolph, J. V., Friedrich, K., and Germann, U.: Relationship between radar-estimated precipitation and synoptic weather patterns in the European Alps, Journal of Applied Meteorology and Climatology, 50, 944-957, 2011.

Ruth, U., Wagenbach, D., Steffensen, J. P., and Bigler, M.: Continuous record of microparticle concentration and size distribution in the central Greenland NGRIP ice core during the last glacial period, Journal of Geophysical Research: Atmospheres, 108, 2003.

Rutter, N., Hodson, A., Irvine-Fynn, T., and Solås, M. K.: Hydrology and hydrochemistry of a deglaciating high-Arctic catchment, Svalbard, Journal of Hydrology, 410, 39-50, 2011.

Ryan, J. C., Hubbard, A., Stibal, M., Irvine-Fynn, T. D., Cook, J., Smith, L. C., Cameron, K., and Box, J.: Dark zone of the Greenland Ice Sheet controlled by distributed biologically-active impurities, Nature Communications, 9, 1065, 2018.

Saccà, A.: Methods for the estimation of the biovolume of microorganisms: A critical review, Limnology and Oceanography: Methods, 15, 337-348, 2017.

Salton, M. R. J.: The Relationship Between the Nature of the Cell Wall and the Gram Stain, Microbiology, 30, 223-235, 1963.

Salzman, G., Crowell, J., Martin, J., Trujillo, T., Romero, A., Mullaney, P., and LaBauve, P.: Cell classification by laser light scattering: identification and separation of unstained leukocytes, Acta cytologica, 19, 374-377, 1975.

Sanderson, T.: Thermal stresses near the surface of a glacier, Journal of Glaciology, 20, 257-283, 1978.

Sanin, S. L., Sanin, F. D., and Bryers, J. D.: Effect of starvation on the adhesive properties of xenobiotic degrading bacteria, Process Biochemistry, 38, 909-914, 2003.

Santibanez, P. A., McConnell, J. R., and Priscu, J. C.: A flow cytometric method to measure prokaryotic records in ice cores: an example from the West Antarctic Ice Sheet Divide drilling site, Journal of Glaciology, 62, 655-673, 2016.

Šantl-Temkiv, T., Gosewinkel, U., Starnawski, P., Lever, M., and Finster, K.: Aeolian dispersal of bacteria in southwest Greenland: their sources, abundance, diversity and physiological states, FEMS Microbiology Ecology, 94, fiy031-fiy031, 2018.

Säwström, C., Graneli, W., Laybourn-Parry, J., and Anesio, A. M.: High viral infection rates in Antarctic and Arctic bacterioplankton, Environmental Microbiology, 9, 250-255, 2007a.

Säwström, C., Laybourn-Parry, J., Granéli, W., and Anesio, A. M.: Heterotrophic bacterial and viral dynamics in Arctic freshwaters: results from a field study and nutrient-temperature manipulation experiments, Polar Biol, 30, 1407-1415, 2007b.

Säwström, C., Mumford, P., Marshall, W., Hodson, A., and Laybourn-Parry, J.: The microbial communities and primary productivity of cryoconite holes in an Arctic glacier (Svalbard 79°N), Polar Biol, 25, 591-596, 2002.

Schimel, J.: Ecosystem consequences of microbial diversity and community structure. In: Arctic and alpine biodiversity: patterns, causes and ecosystem consequences, Springer, 1995.

Schneider, T.: Hydrological processes in firn on Storglaciaren, Sweden, PhD, Department of Physical Geogrpahy and Quaternary Geology, Stockholm University, 2001.

Schneider, T.: Water movement in the firn of Storglaciären, Sweden, Journal of Glaciology, 45, 286-294, 1999.

Schneider, T. and Jansson, P.: Internal accumulation in firn and its significance for the mass balance of Storglaciären, Sweden, Journal of Glaciology, 50, 25-34, 2004.

Schuster, C. J.: Weathering crust processes on melting glacier ices (Alberta, Canada), PhD, Wilfred Laurier University, 134 pp., 2001.

Schutte, U. M. E., Abdo, Z., Bent, S. J., Williams, C. J., Schneider, G. M., Solheim, B., and Forney, L. J.: Bacterial succession in a glacier foreland of the High Arctic, ISME J, 3, 1258-1268, 2009.

Schwartz, F. and Zhang, H.: Fundamentals of ground water, Environ. Geol, 45, 1037-1038, 2004.

Scott, D., Hood, E., and Nassry, M.: In-stream uptake and retention of C, N and P in a supraglacial stream, Annals of Glaciology, 51, 80-86, 2010.

Seckbach, J.: Extremophilies as Models for Extraterrestrial Life, 2000.

Segawa, T., Ishii, S., Ohte, N., Akiyoshi, A., Yamada, A., Maruyama, F., Li, Z., Hongoh, Y., and Takeuchi, N.: The nitrogen cycle in cryoconites: naturally occurring nitrification-denitrification granules on a glacier, Environmental Microbiology, 16, 3250-3262, 2014.

Segawa, T., Takeuchi, N., Rivera, A., Yamada, A., Yoshimura, Y., Barcaza, G., Shinbori, K., Motoyama, H., Kohshima, S., and Ushida, K.: Distribution of antibiotic resistance genes in glacier environments, Environmental Microbiology Reports, 5, 127-134, 2013.

Seki, K., Miyazaki, T., and Nakano, M.: Effects of microorganisms on hydraulic conductivity decrease in infiltration, European Journal of Soil Science, 49, 231-236, 1998.

Senese, A., Diolaiuti, G., Mihalcea, C., and Smiraglia, C.: Energy and Mass Balance of Forni Glacier (Stelvio National Park, Italian Alps) from a Four-Year Meteorological Data Record, Arctic, Antarctic, and Alpine Research, 44, 122-134, 2012.

Shapiro, H. M.: Practical flow cytometry, John Wiley & Sons, 2003.

Sharp, M., Richards, K. S., and Tranter, M.: Glacier hydrology and hydrochemistry, Wiley, 1998.

Shea, J. M., Anslow, F. S., and Marshall, S. J.: Hydrometeorological relationships on Haig Glacier, Alberta, Canada, Annals of Glaciology, 40, 52-60, 2005.

Shibata, A., Goto, Y., Saito, H., Kikuchi, T., Toda, T., and Taguchi, S.: Comparison of SYBR Green I and SYBR Gold stains for enumerating bacteria and viruses by epifluorescence microscopy, Aquatic Microbial Ecology, 43, 223-231, 2006.

Shivaji, S., Ray, M. K., Kumar, G. S., Reddy, G. S. N., Saisree, L., and Wynn-Williams, D. D.: Identification of Janthinobacterium lividum from the soils of the islands of Scotia Ridge and from Antarctic peninsula, Polar Biol, 11, 267-271, 1991.

Shreve, R.: Movement of water in glaciers, Journal of Glaciology, 11, 205-214, 1972.

Shumskii, P.: Ground (subsurface) ice, 1964. 1964.

Sicart, J. E., Hock, R., and Six, D.: Glacier melt, air temperature, and energy balance in different climates: The Bolivian Tropics, the French Alps, and northern Sweden, Journal of Geophysical Research: Atmospheres, 113, 2008.

Sigee, D.: Freshwater microbiology: biodiversity and dynamic interactions of microorganisms in the aquatic environment, John Wiley & Sons, 2005.

Šimůnek, J., Šejna, M., Van Genuchten, M. T., Jacques, D., Mallants, D., Saito, H., and Sakai, M.: HYDRUS-1D, Simulating the one-dimensional movement of water, heat, and multiple solutes in variably-saturated media, version, 2, 1998.

Šimůnek, J., van Genuchten, M. T., and Šejna, M.: Development and applications of the HYDRUS and STANMOD software packages and related codes, Vadose Zone Journal, 7, 587-600, 2008.

Sinai, G. and Dirksen, C.: Experimental evidence of lateral flow in unsaturated homogeneous isotropic sloping soil due to rainfall, Water resources research, 42, 2006.

Singer, G. A., Fasching, C., Wilhelm, L., Niggemann, J., Steier, P., Dittmar, T., and Battin, T. J.: Biogeochemically diverse organic matter in Alpine glaciers and its downstream fate, Nature Geoscience, 5, 710-714, 2012.

Skidmore, M. L., Foght, J. M., and Sharp, M. J.: Microbial life beneath a high Arctic glacier, Applied and Environmental Microbiology, 66, 3214-3220, 2000.

Smart, P. and Laidlaw, I.: An evaluation of some fluorescent dyes for water tracing, Water Resources Research, 13, 15-33, 1977.

Smith, H. J., Foster, R. A., McKnight, D. M., Lisle, J. T., Littmann, S., Kuypers, M. M. M., and Foreman, C. M.: Microbial formation of labile organic carbon in Antarctic glacial environments, Nature Geoscience, 10, 356, 2017a.

Smith, L. C., Chu, V. W., Yang, K., Gleason, C. J., Pitcher, L. H., Rennermalm, A. K., Legleiter, C. J., Behar, A. E., Overstreet, B. T., Moustafa, S. E., Tedesco, M., Forster, R. R., LeWinter, A. L., Finnegan, D. C., Sheng, Y., and Balog, J.: Efficient meltwater drainage through supraglacial streams and rivers on the southwest Greenland ice sheet, Proceedings of the National Academy of Sciences, 112, 1001-1006, 2015.

Smith, L. C., Yang, K., Pitcher, L. H., Overstreet, B. T., Chu, V. W., Rennermalm, Å. K., Ryan, J. C., Cooper, M. G., Gleason, C. J., Tedesco, M., Jeyaratnam, J., van As, D., van den Broeke, M. R., van de Berg, W. J., Noël, B., Langen, P. L., Cullather, R. I., Zhao, B., Willis, M. J., Hubbard, A., Box, J. E., Jenner, B. A., and Behar, A. E.: Direct measurements of meltwater runoff on the Greenland ice sheet surface, Proceedings of the National Academy of Sciences, 114, E10622-E10631, 2017b.

Sobota, I.: The near-surface ice thermal structure of the Waldemarbreen, Svalbard, Pol Polar Res, 30, 317-338, 2009.

St. Germain, S. L. and Moorman, B. J.: The development of a pulsating supraglacial stream, Annals of Glaciology, 57, 31-38, 2016.

Stevens, I. T., Irvine-Fynn, T. D. L., Porter, P. R., Cook, J. M., Edwards, A., Smart, M., Moorman, B. J., Hodson, A. J., and Mitchell, A. C.: Near-surface hydraulic conductivity of northern hemisphere glaciers, Hydrological Processes, 32, 850-865, 2018.

Stibal, M., Box, J. E., Cameron, K. A., Langen, P. L., Yallop, M. L., Mottram, R. H., Khan, A. L., Molotch, N. P., Chrismas, N. A. M., Calì Quaglia, F., Remias, D., Smeets, C. J. P. P., van den Broeke, M. R., Ryan, J. C., Hubbard, A., Tranter, M., van As, D., and Ahlstrøm, A. P.: Algae Drive Enhanced Darkening of Bare Ice on the Greenland Ice Sheet, Geophysical Research Letters, doi: 10.1002/2017GL075958, 2017. n/a-n/a, 2017.

Stibal, M., Gözdereliler, E., Cameron, K. A., Box, J. E., Stevens, I. T., Gokul, J. K., Schostag, M., Zarsky, J. D., Edwards, A., Irvine-Fynn, T. D. L., and Jacobsen, C. S.: Microbial abundance in surface ice on the Greenland Ice Sheet, Front Microbiol, 6, 2015.

Stibal, M., Lawson, E. C., Lis, G. P., Mak, K. M., Wadham, J. L., and Anesio, A. M.: Organic matter content and quality in supraglacial debris across the ablation zone of the Greenland ice sheet, Annals of Glaciology, 51, 1-8, 2010.

Stibal, M., Sabacka, M., and Zarsky, J.: Biological processes on glacier and ice sheet surfaces, Nature Geoscience, 5, 771-774, 2012a.

Stibal, M., Telling, J., Cook, J., Mak, K. M., Hodson, A., and Anesio, A. M.: Environmental Controls on Microbial Abundance and Activity on the Greenland Ice Sheet: A Multivariate Analysis Approach, Microb Ecol, 63, 74-84, 2012b.

Stott, T. and Mount, N.: Alpine proglacial suspended sediment dynamics in warm and cool ablation seasons: Implications for global warming, Journal of Hydrology, 332, 259-270, 2007.

Svensson, A., Biscaye, P. E., and Grousset, F. E.: Characterization of late glacial continental dust in the Greenland Ice Core Project ice core, Journal of Geophysical Research: Atmospheres, 105, 4637-4656, 2000.

Swartzendruber, D.: The Applicability of Darcy's Law, Soil Science Society of America Journal, 32, 11-18, 1968.

Sylvia, D. M., Fuhrmann, J. J., Hartel, P. G., and Zuberer, D. A.: Principles and applications of soil microbiology, Pearson Prentice Hall Upper Saddle River, NJ:, 2005.

Takeuchi, N.: Seasonal and altitudinal variations in snow algal communities on an Alaskan glacier (Gulkana glacier in the Alaska range), Environ Res Lett, 8, 035002, 2013.

Takeuchi, N., Fujisawa, Y., Kadota, T., Tanaka, S., Miyairi, M., Shirakawa, T., Kusaka, R., Fedorov, A. N., Konstantinov, P., and Ohata, T.: The effect of impurities on the surface melt of a glacier in the Suntar Khayata Mountain Range, Russian Siberia, Frontiers in Earth Science, 3, 2015.

Takeuchi, N., Kohshima, S., and Seko, K.: Structure, Formation, and Darkening Process of Albedo-Reducing Material (Cryoconite) on a Himalayan Glacier: A Granular Algal Mat Growing on the Glacier, Arctic, Antarctic, and Alpine Research, 33, 115-122, 2001a.

Takeuchi, N., Kohshima, S., Shiraiwa, T., and Kubota, K.: Characteristics of cryoconite (surface dust on glaciers) and surface albedo of a Patagonian glacier, Tyndall Glacier, Southern Patagonia Icefield, Bulletin of Glaciological Research, 18, 2001b.

Takeuchi, N., Kohshima, S., Yoshimura, Y., Seko, K., and Fujita, K.: Characterstics of cryoconite holes on a Himalayan glacier, Yala Glacier, Central Nepal, Bulletin of Glacier Research, 17, 51-59, 2000.

Tao, H., Shunlin, L., Yunyue, Y., Dongdong, W., Feng, G., and Qiang, L.: Greenland surface albedo changes in July 1981–2012 from satellite observations, Environ Res Lett, 8, 044043, 2013.

Tedesco, M., Doherty, S., Fettweis, X., Alexander, P., Jeyaratnam, J., and Stroeve, J.: The darkening of the Greenland ice sheet: trends, drivers, and projections (1981–2100), The Cryosphere, 10, 477-496, 2016.

Tedstone, A., Cook, J., Williamson, C., McCutcheon, J., Fettweis, X., Flanner, M., Bamber, J., and Tranter, M.: Assessing the impact of bio-albedo upon Greenland Ice Sheet melting, 2018, 4998.

Tedstone, A. J., Bamber, J. L., Cook, J. M., Williamson, C. J., Fettweis, X., Hodson, A. J., and Tranter, M.: Dark ice dynamics of the south-west Greenland Ice Sheet, The Cryosphere, 11, 2491-2506, 2017.

Telling, J., Anesio, A. M., Hawkings, J., Tranter, M., Wadham, J. L., Hodson, A. J., Irvine-Fynn, T., and Yallop, M. L.: Measuring rates of gross photosynthesis and net community production in cryoconite holes: a comparison of field methods, Annals of Glaciology, 51, 153-162, 2010.

Telling, J., Anesio, A. M., Tranter, M., Irvine-Fynn, T., Hodson, A., Butler, C., and Wadham, J.: Nitrogen fixation on Arctic glaciers, Svalbard, J Geophys Res-Biogeo, 116, 2011.

Telling, J., Anesio, A. M., Tranter, M., Stibal, M., Hawkings, J., Irvine-Fynn, T. D. L., Hodson, A. J., Butler, C., Yallop, M., and Wadham, J.: Controls on the autochthonous production and respiration of organic matter in cryoconite holes on high Arctic glaciers, Journal of Geophysical Research: Biogeosciences, 117, G01017, 2012a.

Telling, J., Stibal, M., Anesio, A. M., Tranter, M., Nias, I., Cook, J., Bellas, C., Lis, G., Wadham, J. L., Sole, A., Nienow, P., and Hodson, A.: Microbial nitrogen cycling on the Greenland Ice Sheet, Biogeosciences, 9, 2431-2442, 2012b.

Tennant, R. K., Jones, R. T., Love, J., and Lee, R.: A new flow cytometry method enabling rapid purification of diatoms from silica-rich lacustrine sediments, J Paleolimnol, 49, 305-309, 2013.

Tetens, O.: Uber einige meteorologische Begriffe, Z. geophys, 6, 297-309, 1930.

Theakstone, W. H. and Knudsen, N. T.: Dye tracer tests of water movement at the glacier Austre Okstindbreen, Norway, Norsk Geografisk Tidsskrift - Norwegian Journal of Geography, 35, 21-28, 1981.

Thompson, S. S., Kulessa, B., Essery, R. L. H., and Lüthi, M. P.: Bulk meltwater flow and liquid water content of snowpacks mapped using the electrical self-potential (SP) method, The Cryosphere, 10, 433-444, 2016.

Torsvik, V., Goksøyr, J., and Daae, F. L.: High diversity in DNA of soil bacteria, Applied and environmental microbiology, 56, 782-787, 1990.

Tranter, M., Fountain, A. G., Lyons, W. B., Nylen, T. H., and Welch, K. A.: The chemical composition of runoff from Canada Glacier, Antarctica: implications for glacier hydrology during a cool summer, Annals of Glaciology, 40, 15-19, 2005.

Trivedi, C. B., Lau, G. E., Grasby, S. E., Templeton, A. S., and Spear, J. R.: Low-temperature sulfidic-ice microbial communities, Borup Fiord Pass, Canadian high Arctic, Front Microbiol, 9, 2018.

Tuma, R. S., Beaudet, M. P., Jin, X., Jones, L. J., Cheung, C.-Y., Yue, S., and Singer, V. L.: Characterization of SYBR Gold Nucleic Acid Gel Stain: A Dye Optimized for Use with 300-nm Ultraviolet Transilluminators, Analytical Biochemistry, 268, 278-288, 1999.

Uetake, J., Naganuma, T., Hebsgaard, M. B., Kanda, H., and Kohshima, S.: Communities of algae and cyanobacteria on glaciers in west Greenland, Polar Science, 4, 71-80, 2010.

van de Wal, R. S. W., Boot, W., van den Broeke, M. R., Smeets, C. J. P. P., Reijmer, C. H., Donker, J. J. A., and Oerlemans, J.: Large and Rapid Melt-Induced Velocity Changes in the Ablation Zone of the Greenland Ice Sheet, Science, 321, 111-113, 2008.

van de Wal, R. S. W., Greuell, W., van den Broeke, M. R., Reijmer, C. H., and Oerlemans, J.: Surface mass-balance observations and automatic weather station data along a transect near Kangerlussuaq, West Greenland, Annals of Glaciology, 42, 311-316, 2005.

Vaughan, D. G., Comiso, J. C., Allison, I., Carrasco, J., Kaser, G., Kwok, R., Mote, P., Murray, T., Paul, F., Ren, J., E. Rignot, Solomina, O., Steffen, K., and Zhang, T.: Observations: Cryosphere. In: Climate Change 2013: The Physical Science Basis. Contribution of Working Group I to the Fifth Assessment Report of the Intergovernmental Panel on Climate Change, T.F. Stocker, T. F., Qin, D., Plattner, G.-K., Tignor, M., Allen, S. K., Boschung, J., Nauels, A., Xia, Y., Bex, V., and Midgley, P. M. (Eds.), Cambridge University Press, Cambridge, UK, 2013.

Vital, M., Füchslin, H. P., Hammes, F., and Egli, T.: Growth of Vibrio cholerae O1 Ogawa Eltor in freshwater, Microbiology, 153, 1993-2001, 2007.

Vogel, T., Huang, K., Zhang, R., and Van Genuchten, M. T.: The HYDRUS code for simulating one-dimensional water flow, solute transport, and heat movement in variably-saturated media, Riverside: US Salinity Laboratory, 1996. 1996.

Wadham, J. L., De'ath, R., Monteiro, F. M., Tranter, M., Ridgwell, A., Raiswell, R., and Tulaczyk, S.: The potential role of the Antarctic Ice Sheet in global biogeochemical cycles, Earth and Environmental Science Transactions of the Royal Society of Edinburgh, 104, 55-67, 2013.

Wadham, J. L., Hawkings, J., Telling, J., Chandler, D., Alcock, J., O'Donnell, E., Kaur, P., Bagshaw, E., Tranter, M., Tedstone, A., and Nienow, P.: Sources, cycling and export of nitrogen on the Greenland Ice Sheet, Biogeosciences, 13, 6339-6352, 2016.

Wadham, J. L. and Nuttall, A.-M.: Multiphase formation of superimposed ice during a mass-balance year at a maritime high-Arctic glacier, Journal of Glaciology, 48, 545-551, 2002.

Wainstein, P., Moorman, B., and Whitehead, K.: Glacial conditions that contribute to the regeneration of Fountain Glacier proglacial icing, Bylot Island, Canada, Hydrological Processes, 28, 2749-2760, 2014.

Wakahama, G.: Observations of the melt-water permeation in the near-surface ice layers of the Mendenhall Glacier, south-east Alaska, Mater. Glyatsiologicheskogo Issled. Khronika Obsuzhdeniya, 33, 175-178, 1978.

Wakahama, G., Kuroiwa, D., Kobayashi, D., Tanuma, K., Endo, Y., Mizuno, Y., and Kobayashi, S.: Observations of permeating water through a glacier body, Low Temperature Science A, 31, 217-219, 1973.

Waldrop, M., Balser, T., and Firestone, M.: Linking microbial community composition to function in a tropical soil, Soil biology and biochemistry, 32, 1837-1846, 2000.

Wang, Y., Hammes, F., De Roy, K., Verstraete, W., and Boon, N.: Past, present and future applications of flow cytometry in aquatic microbiology, Trends in Biotechnology, 28, 416-424, 2010.

Wharton, R. A., McKay, C. P., Simmons Jr, G. M., and Parker, B. C.: Cryoconite holes on glaciers, BioScience, 1985. 499-503, 1985.

Whitehead, K., Moorman, B. J., and Wainstein, P.: Measuring daily surface elevation and velocity variations across a polythermal arctic glacier using ground-based photogrammetry Journal of Glaciology, 60, 1208-1220, 2014.

Whitehead, R.: Groundwater Atlas of the United States, Montana, North Dakota, South Dakota, Wyoming, US Geological Survey Publication HA, 1996. 1996.

Whitman, W. B., Coleman, D. C., and Wiebe, W. J.: Prokaryotes: The unseen majority, Proceedings of the National Academy of Sciences, 95, 6578-6583, 1998.

Wientjes, I. G. M., Van de Wal, R. S. W., Reichart, G. J., Sluijs, A., and Oerlemans, J.: Dust from the dark region in the western ablation zone of the Greenland ice sheet, Cryosphere, 5, 589-601, 2011.

Wientjes, I. G. M., Van De Wal, R. S. W., Schwikowski, M., Zapf, A., Fahrni, S., and Wacker, L.: Carbonaceous particles reveal that Late Holocene dust causes the dark region in the western ablation zone of the Greenland ice sheet, Journal of Glaciology, 58, 787-794, 2017.

Wilhelm, L., Singer, G. A., Fasching, C., Battin, T. J., and Besemer, K.: Microbial biodiversity in glacier-fed streams, ISME J, 7, 1651-1660, 2013.

Willey, J. M., Sherwood, L., and Woolverton, C. J.: Prescott, Harley, and Klein's microbiology, McGraw-Hill Higher Education New York, 2008.

Williamson, C. J., Cameron, K. A., Cook, J. M., Zarsky, J. D., Stibal, M., and Edwards, A.: Glacier Algae: A Dark Past and a Darker Future, Front Microbiol, 10, 2019.

Willis, I. C., Arnold, N. S., and Brock, B. W.: Effect of snowpack removal on energy balance, melt and runoff in a small supraglacial catchment, Hydrological Processes, 16, 2721-2749, 2002.

Wilner, L. B.: Variable capacitance liquid level sensors, Review of Scientific Instruments, 31, 501-507, 1960.

Winter, T. C.: Relation of streams, lakes, and wetlands to groundwater flow systems, Hydrogeology Journal, 7, 28-45, 1999.

Yallop, M. L., Anesio, A. M., Perkins, R. G., Cook, J. M., Telling, J., Fagan, D., MacFarlane, J., Stibal, M., Barker, G., Bellas, C., Hodson, A. J., Tranter, M., Wadham, J., and Roberts, N. W.:

Photophysiology and albedo-changing potential of the ice algal community on the surface of the Greenland ice sheet, ISME J, 6, 2302-2313, 2012.

Yang, K., Karlstrom, L., Smith, L. C., and Li, M.: Automated High-Resolution Satellite Image Registration Using Supraglacial Rivers on the Greenland Ice Sheet, IEEE Journal of Selected Topics in Applied Earth Observations and Remote Sensing, 2016. 2016.

Yang, K. and Smith, L. C.: Supraglacial streams on the Greenland Ice Sheet delineated from combined spectral–shape information in high-resolution satellite imagery, IEEE Geoscience and Remote Sensing Letters, 10, 801-805, 2013.

Yang, K., Smith, L. C., Karlstrom, L., Cooper, M. G., Tedesco, M., van As, D., Cheng, X., Chen, Z., and Li, M.: A new surface meltwater routing model for use on the Greenland Ice Sheet surface, The Cryosphere, 12, 3791-3811, 2018a.

Yang, K., Smith, L. C., Karlstrom, L., Cooper, M. G., Tedesco, M., van As, D., Cheng, X., Chen, Z., and Li, M.: Supraglacial meltwater routing through internally drained catchments on the Greenland Ice Sheet surface, The Cryosphere Discuss., 2018, 1-32, 2018b.

Yao, T., Liu, Y., Kang, S., Jiao, N., Zeng, Y., Liu, X., and Zhang, Y.: Bacteria variabilities in a Tibetan ice core and their relations with climate change, Global Biogeochemical Cycles, 22, GB4017, 2008.

Yasunari, T. J., Bonasoni, P., Laj, P., Fujita, K., Vuillermoz, E., Marinoni, A., Cristofanelli, P., Duchi, R., Tartari, G., and Lau, K. M.: Estimated impact of black carbon deposition during pre-monsoon season from Nepal Climate Observatory – Pyramid data and snow albedo changes over Himalayan glaciers, Atmos. Chem. Phys., 10, 6603-6615, 2010.

Younger, P. L.: Groundwater in the environment: an introduction, John Wiley & Sons, 2009.

Zappa, M. and Kan, C.: Extreme heat and runoff extremes in the Swiss Alps, Natural Hazards and Earth System Science, 7, 375-389, 2007.

Zarsky, J. D., Stibal, M., Hodson, A., Sattler, B., Schostag, M., Hansen, L. H., Jacobsen, C. S., and Psenner, R.: Large cryoconite aggregates on a Svalbard glacier support a diverse microbial community including ammonia-oxidizing archaea, Environ Res Lett, 8, 2013.

Zeglin, L. H.: Stream microbial diversity in response to environmental changes: review and synthesis of existing research, Front Microbiol, 6, 2015.

Zehr, J. P., Waterbury, J. B., Turner, P. J., Montoya, J. P., Omoregie, E., Steward, G. F., Hansen, A., and Karl, D. M.: Unicellular cyanobacteria fix N2 in the subtropical North Pacific Ocean, Nature, 412, 635, 2001.

Zeng, Q., Cao, M., Feng, X., Liang, F., Chen, X., and Sheng, W.: A study of spectral reflection characteristics for snow, ice and water in the north of China, Hydrological applications of remote sensing and remote data transmission, 145, 451-462, 1984.

Zumsteg, A., Luster, J., Göransson, H., Smittenberg, R. H., Brunner, I., Bernasconi, S. M., Zeyer, J., and Frey, B.: Bacterial, Archaeal and Fungal Succession in the Forefield of a Receding Glacier, Microb Ecol, 63, 552-564, 2011.

Appendix 1: Supplementary Material

This appendix present eight exemplar recharge curves, selected at random, of hydraulic conductivity. Note that because of this selection method, not all sites are represented.

VFR3
11:51
17/07/16
K = 0.001

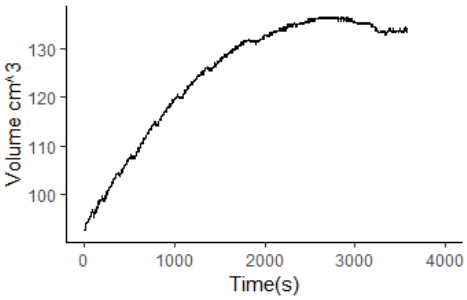

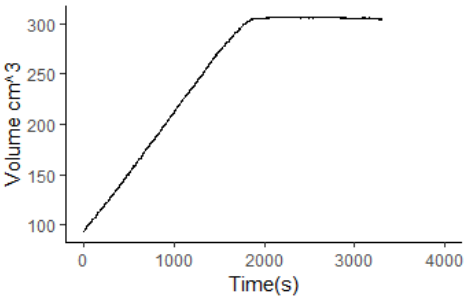

HAR19
12:33
25/07/15
K = 0.012

VFR6
13:36
06/07/16
K = 0.044

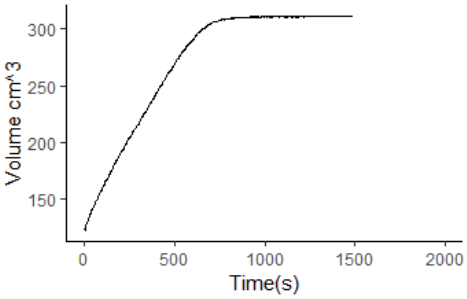

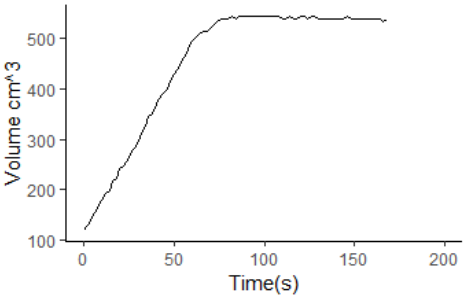

GBR1
15:01
08/09/14
K = 3.519

VFR9
13:54
18/07/16
K = 0.665

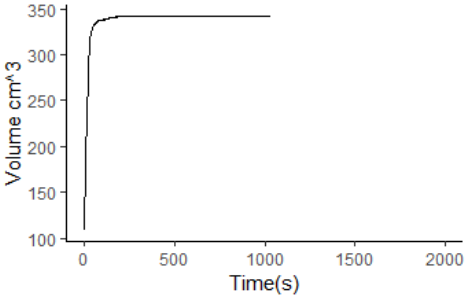

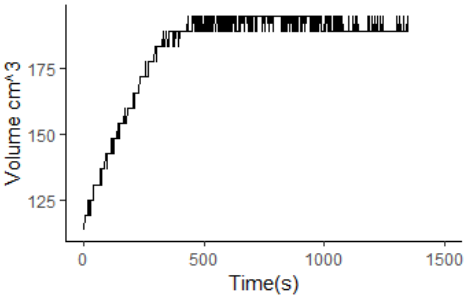

FGR10
11:40
09/07/14
K = 0.116

PBR20
14:12
17/08
K = 0.013

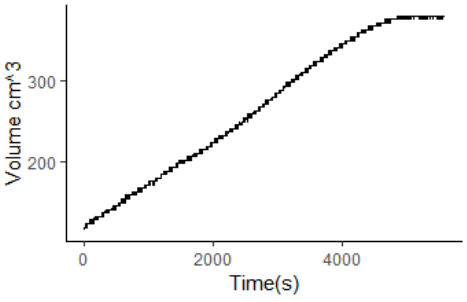

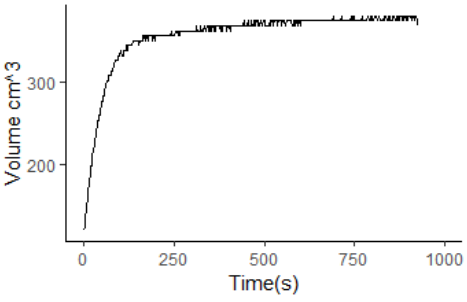

SGR1
10:33
27/08/14
K = 0.069

Appendix 2: Microbial Abundance in Surface Ice on the Greenland Ice Sheet

The following manuscript was published in Frontiers in Earth Science in 2015. It represents a pre-cursor to Chapter 3, evaluating cell enumeration techniques and examining microbe concentrations in the near surface.

frontiers in Microbiology

ORIGINAL RESEARCH
published: 24 March 2015
doi: 10.3389/fmicb.2015.00225

Microbial abundance in surface ice on the Greenland Ice Sheet

Marek Stibal[1,2,3]*, *Erkin Gözdereliler*[1,2], *Karen A. Cameron*[1,2], *Jason E. Box*[1], *Ian T. Stevens*[4], *Jarishma K. Gokul*[4], *Morten Schostag*[2], *Jakub D. Zarsky*[3,5], *Arwyn Edwards*[4], *Tristram D. L. Irvine-Fynn*[4] and *Carsten S. Jacobsen*[1,2,6]

[1] Geological Survey of Denmark and Greenland, Copenhagen, Denmark, [2] Center for Permafrost, University of Copenhagen, Copenhagen, Denmark, [3] Department of Ecology, Charles University in Prague, Prague, Czech Republic, [4] Centre for Glaciology, Aberystwyth University, Aberystwyth, UK, [5] Centre for Polar Ecology, University of South Bohemia, České Budějovice, Czech Republic, [6] Department of Plant and Environmental Sciences, University of Copenhagen, Copenhagen, Denmark

Measuring microbial abundance in glacier ice and identifying its controls is essential for a better understanding and quantification of biogeochemical processes in glacial ecosystems. However, cell enumeration of glacier ice samples is challenging due to typically low cell numbers and the presence of interfering mineral particles. We quantified for the first time the abundance of microbial cells in surface ice from geographically distinct sites on the Greenland Ice Sheet (GrIS), using three enumeration methods: epifluorescence microscopy (EFM), flow cytometry (FCM), and quantitative polymerase chain reaction (qPCR). In addition, we reviewed published data on microbial abundance in glacier ice and tested the three methods on artificial ice samples of realistic cell (10^2–10^7 cells ml^{-1}) and mineral particle (0.1–100 mg ml^{-1}) concentrations, simulating a range of glacial ice types, from clean subsurface ice to surface ice to sediment-laden basal ice. We then used multivariate statistical analysis to identify factors responsible for the variation in microbial abundance on the ice sheet. EFM gave the most accurate and reproducible results of the tested methodologies, and was therefore selected as the most suitable technique for cell enumeration of ice containing dust. Cell numbers in surface ice samples, determined by EFM, ranged from $\sim 2 \times 10^3$ to $\sim 2 \times 10^6$ cells ml^{-1} while dust concentrations ranged from 0.01 to 2 mg ml^{-1}. The lowest abundances were found in ice sampled from the accumulation area of the ice sheet and in samples affected by fresh snow; these samples may be considered as a reference point of the cell abundance of precipitants that are deposited on the ice sheet surface. Dust content was the most significant variable to explain the variation in the abundance data, which suggests a direct association between deposited dust particles and cells and/or by their provision of limited nutrients to microbial communities on the GrIS.

Keywords: glacier ice, microbial abundance, Greenland Ice Sheet, epifluorescence microscopy, flow cytometry, quantitative PCR, multivariate analysis

OPEN ACCESS

Edited by:
Catherine Larose, University of Lyon, France

Reviewed by:
Marc Gregory Dumont, Max-Planck-Institute for Terrestrial Microbiology, Germany
Steffen Kolb, University of Bayreuth, Germany

***Correspondence:**
Marek Stibal, Department of Geochemistry, Geological Survey of Denmark and Greenland, Øster Voldgade 10, 1350 Copenhagen, Denmark
msti@geus.dk

Specialty section:
This article was submitted to Terrestrial Microbiology, a section of the journal Frontiers in Microbiology

Received: *11 January 2015*
Paper pending published: *09 February 2015*
Accepted: *06 March 2015*
Published: *24 March 2015*

Citation:
Stibal M, Gözdereliler E, Cameron KA, Box JE, Stevens IT, Gokul JK, Schostag M, Zarsky JD, Edwards A, Irvine-Fynn TDL and Jacobsen CS (2015) Microbial abundance in surface ice on the Greenland Ice Sheet. Front. Microbiol. 6:225. doi: 10.3389/fmicb.2015.00225

Introduction

Glaciers and ice sheets cover 10% of Earth's land area and contain distinct microbe-dominated ecosystems that are highly sensitive to climate warming (see Hodson et al., 2008; Anesio and Laybourn-Parry, 2012, for reviews). Microbes in glacial ecosystems play important roles in local

and regional biogeochemical cycling processes (e.g., Foreman et al., 2007; Hodson et al., 2007; Stibal et al., 2008a; Anesio et al., 2010; Telling et al., 2012) and may contribute to glacier ice melting (Takeuchi et al., 2001; Yallop et al., 2012). Measuring microbial abundance in glacier ice and researching its spatiotemporal variability and its controls is necessary to estimate microbial growth and activity, as well as to estimate carbon stocks and flows in glacial ecosystems, and future extrapolations of these measurements are essential for the prediction of microbial responses to changes in climate and anthropogenic influences in the cryosphere (Stibal et al., 2012a).

Our knowledge of microbial abundance in glacier ecosystems is, however, sketchy in comparison with other ecosystems (Whitman et al., 1998), since it is based on a low number of samples from accessible glacier sites. As a result, our understanding of the factors controlling microbial abundance in the ice is limited and current large-scale estimates of microbial biomass in glacier ice are empirical and span many orders of magnitude. For example, a recent study offered a first-order estimate of between 10^{25} and 10^{29} microbial cells entombed in glacier ice world-wide, and emphasized that elevated biomass is associated with glacier surfaces and beds (Irvine-Fynn and Edwards, 2014). Moreover, glacier ice tends to have a low microbial abundance, and the microbial cells are typically mixed with or attached to mineral particles. This poses a challenge for the cell enumeration of most glacier samples, including cryoconite (surface debris), which is a conglomerate of mineral particles, microbial cells and organic matter (Hodson et al., 2010b; Langford et al., 2010), and sediment-laden basal ice (Foght et al., 2004; Yde et al., 2010; Montross et al., 2014).

Traditionally, epifluorescence microscopy (EFM) has been used to enumerate microbial cells in aqueous and sediment samples, including glacier ice, and sediments (Karl et al., 1999; Priscu et al., 1999; Abyzov et al., 2001; Säwström et al., 2002). This method is labor-intensive and slow compared to flow cytometry (FCM), which has previously been used for glacier ice microbial abundance analysis (Karl et al., 1999; Yao et al., 2008; Miteva et al., 2009; An et al., 2010; Irvine-Fynn et al., 2012). However, FCM is sensitive to higher particulate loads, which may result in instrumentation blockages (Vesey et al., 1994) and underestimations due to cell adhesion to abiotic particles (Amalfitano and Fazi, 2008). Recently, quantitative PCR (qPCR) has gained popularity in glacier ecology studies as it allows for a combined analysis of microbial abundance and diversity from the same nucleic acid extract (Hamilton et al., 2013; Zarsky et al., 2013; Stibal et al., 2015). However, due to differing numbers of gene copies in each microbial species (Klappenbach et al., 2001), and the efficacy of nucleic acid extraction (Krsek and Wellington, 1999) and amplification techniques (Lindberg et al., 2007; Albers et al., 2013), caution must be exercised when converting qPCR results into cell numbers.

The Greenland Ice Sheet (GrIS) is the largest ice body in the northern hemisphere and hosts Earth's largest seasonally melting glacier surface ice ecosystem (>200,000 km^2 and expanding; Hodson et al., 2010a; Fettweis et al., 2011). Microbial abundance, diversity, and activity in snow and cryoconite in some portions on the GrIS have been found to vary with distance from ice-free land. This variability has been attributed to differences in environmental disturbances, sources of microbial inocula and nutrients, and melt season duration (Hodson et al., 2010a; Stibal et al., 2010, 2012b, 2015; Telling et al., 2012; Cameron et al., 2015). However, there are currently no data on microbial abundance in bare ice, the dominant supraglacial environment in terms of volume and area, and the factors that control it.

The aim of this paper is to quantify for the first time the abundance of microbial cells in surface ice from geographically distinct sites on the GrIS and to identify factors responsible for its variation. In order to obtain robust cell numbers, we tested all three common methods of microbial enumeration (EFM, FCM, qPCR) on artificial ice samples of known, and realistic, cell and mineral particle concentrations prior to analysis of our samples. We then used multivariate statistical analysis to test the significance of environmental characteristics and reviewed the published data on microbial abundance in glacier ice in order to put our results into context.

Materials and Methods

Sample Collection

Samples of Greenland surface ice were collected from the ice sheet and an isolated ice cap between May and September 2013 from 14 sites at 7 geographically distinct locations (**Table 1**, **Figure 1**). Most sites were in the vicinity of an established meteorological station of the PROMICE network (http://promice.org) and were named after the nearest settlement or geographical feature (THU, Thule; KAN, Kangerlussuaq; QAS, Qasimiut; TAS, Tasiilaq; APO, A. P. Olsen ice cap). Additional samples of surface ice were taken at "Dark Site" (DS), one of the darkest 5 km pixels in optical satellite imagery after Box et al. (2012), and at a site situated in the accumulation area near the topographical divide of the southern ice sheet (Saddle). The sites were characterized by their geographical position (the N and W coordinates) and altitude which were measured by a hand-held GPS, surface type (bare ice vs. multi year snow a.k.a. firn), and distance from the nearest ice-free land determined in Google Earth using the distance tool with a precision of 0.5 km. The regional climate model HIRHAM5 was used to obtain additional climate data for each site. This model provides realistic simulations of the climate over Greenland, which are validated against observations from meteorological stations at the coast and on the ice sheet (Lucas-Picher et al., 2012). The data obtained from the model included the number of days with a positive surface air temperature and a positive surface energy balance ("melt days") from the beginning of the year until the day of sampling, and the time elapsed from the last snowfall event at the moment of sampling (**Table 1**).

Ten surface ice cores (∼15 cm long) were extracted at each site, except Saddle, using a small handheld drill and custom-built stainless steel corers (∼20 cm^2 surface area). The corers were autoclaved and kept sterile in polypropylene bags prior to use. The ice cores were transferred to sterile 750 ml WhirlPak bags (Nasco, USA). At Saddle, samples were obtained using a 9 cm diameter Kovacs coring drill, using sterile autoclaved corers. A deeper (220 cm) surface ice core was extracted at Saddle and cut into sections 10–30 cm long. Saddle samples were taken in order

TABLE 1 | Description of 2013 sampling sites at the surface of the GrIS.

Site name	Position	Distance to ice-free land (km)	Altitude (m)	Surface type	Date (DOY)	Days of T_S > 0°C in 2013	Melt days in 2013	Days since snow
THU_L	76°23.991′N 68°15.921′W	1.5	570	ice	12 Aug (224)	46	n.a.	11
THU_U	76°25.181′N 68°8.706′W	3	770	firn	13 Aug (225)	40	134	11
DS	69°28.56′N 49°34.838′W	18	956	ice	25 Jun (176)	15	n.a.	2
KAN_L	67°5.798′N 49°56.303′W	5	680	ice**	19 Sept (262)	90	189	7
KAN_M	67°3.964′N 48°49.356′W	42	1270	ice**	19 Sept (262)	38	158	2
KAN_U	67°0.014′N 47°1.162′W	112	1850	firn**	22 Sept (265)	9	190	5
QAS_L	61°1.873′N 46°50.91′W	1.5	310	ice	20 Aug (232)	124	164	47
QAS_U	61°10.653′N 46°49.042′W	12	890	ice**	20 Aug (232)	65	182	41
TAS_L	65°38.46′N 38°53.895′W	1.5	270	ice	27 Aug (239)	108	165	62
TAS_U	65°41.975′N 38°51.995′W	5	580	ice	29 Aug (241)	88	184	1
TAS_A	65°46.864′N 38°54.193′W	10	891	firn**	27 Aug (239)	68	n.a.	1
APO_L	74°37.471′N 21°22.507′W	0.5	644	ice***	1 May (121)	0	n.a.	1
APO_M	74°38.634′N 21°28.110′W	0.5	874	ice***	1 May (121)	0	n.a.	1
SADDLE	66°0.033′N 44°30.083′W	180/230*	2460	firn	8 Jul (189)	0	n.a.	1

DOY, day of year 2013; T_S, surface air temperature; n.a., data not available.
**Site is ca 180 km from the eastern edge and 230 km from the western edge of the ice sheet.*
***Samples may have been affected by fresh snow due to high wind during sampling.*
****Samples may have been contaminated due to breakdown of drilling equipment and additional handling.*

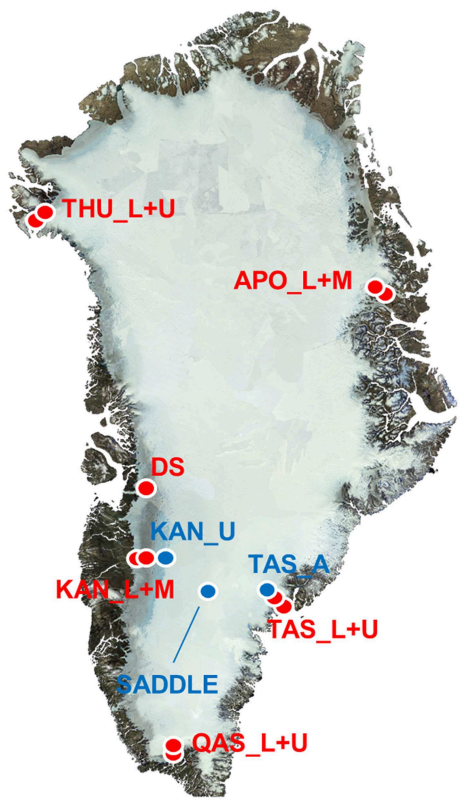

FIGURE 1 | Map of sampling sites on the GrIS. Red dots represent sites in the ablation area and blue dots in the accumulation area of the ice sheet. The background clear sky end of melt season mosaic is by J. E. Box using MODIS data from year 2011.

to compare microbial cell numbers of winter snow layers, from 2012 to 2013, with the summer 2012 refrozen melt layer (Nghiem et al., 2012). All samples were kept frozen in insulated boxes until transportation to Copenhagen where samples were stored at −20°C until analysis.

Cell Count Method Testing

Artificial ice samples were prepared using deionized water, quartz dust, and a culture of *Delftia acidovorans* in order to simulate glacier ice containing different amounts of debris and microbial cells. *Delftia* is a genus of Betaproteobacteria often found in glacial environments including surface ice (Zeng et al., 2013), cryoconite (Stibal et al., 2015), and basal ice (Skidmore et al., 2005). The water used (MilliQ, Millipore, USA) was checked for microbial cells using EFM (see below). Quartz dust (2600 mg ml^{-1}, particle size <63 µm; Sigma-Aldrich, Germany) was furnaced at 550°C for 5 h prior to use. The cell abundance of the *D. acidovorans* culture used was determined by EFM immediately before preparing the artificial ice samples. The dust concentrations used were from 0.1 to 100 mg ml^{-1}, and the cell concentrations used ranged from 10^2 to 10^7 cells ml^{-1}, resulting in cell:dust ratios between 1 and 10^8 cells mg^{-1}, roughly equivalent to 0.2–20,000,000 cells per dust particle. Samples containing no cells and/or no dust were tested in parallel.

Accuracy A was quantified as

$$A = 1 - \left(\frac{\left| \overline{X_m} - X_e \right|}{X_e} \right) \quad (1)$$

where X_e is the expected abundance and X_m the measured value. A can range between 1 (100% accuracy) and 0 (no cells or twice

as many as expected), and it can assume negative values when the measured abundance is more than twice as high as the expected value; however, for better plot clarity negative *A* values were manually corrected to 0. Standard deviations of triplicate measurements, representing the reproducibility of the analyses, were calculated and expressed as percentage of mean; values >100% were manually corrected to 100% for better clarity in the contour plots.

Greenland Ice Sample Analysis

Prior to analysis, ice samples from each location were pooled together and placed in a pre-furnaced (550°C for 5 h), foil-covered beaker and allowed to melt at 4°C. After melting, subsamples for EFM (150 ml) and FCM (15 ml) were taken. EFM enumerations were conducted immediately after subsampling, whereas samples for FCM were fixed with paraformaldehyde (final concentration 2%) and stored at 5°C until analysis. From the remaining sample, 300 ml was filtered through Sterivex GP 0.22 μm polyethersulfone filters (Millipore, USA) into acid washed Duran bottles. The filters were subsequently used for DNA extraction, while the filtered water was used for physico–chemical analysis. pH and electrical conductivity (EC) were measured using a Multi 3430 multimeter with a SenTix 940 pH electrode and a TetraCon 925 conductivity cell (WTW, Germany). Dissolved organic carbon (DOC) and total dissolved nitrogen (TDN) were measured on a TOC-V_{CPH} analyzer with a TNM-1 nitrogen unit (Shimadzu, Japan). Nitrate (NO_3^-) and phosphate (PO_4^{3-}) were analyzed by ion chromatography (IC) using an IonPac AS 14 column (Dionex, USA). Ammonium (NH_4^+) was determined on a Fiastar 5000 analyzer (Gerber Instruments, Switzerland). The detection limits, calculated as 3 standard deviations of procedural blanks, were 1.17 mg l^{-1} for DOC, 0.20 mg l^{-1} for TDN, and 4.4 μg l^{-1} for NH_4^+. No NO_3^- or PO_4^{3-} were detected in the procedural blanks and so 0.05 and 0.025 mg l^{-1} were assumed to be the detection limits for nitrate and phosphate, respectively, determined by previous testing. The remainder of the sample was filtered through a pre-weighed GF/F 0.7 μm glass fiber filter (Whatman, UK) in order to determine the dust load. The filter papers were then dried at 105°C for 5 h and re-weighed, and the amount of dust normalized to filtrate volume.

Samples were analyzed by EFM after staining with the DNA stain acridine orange (AO). 10 ml of sample was filtered onto a sterile 0.2 μm MontaMil black polycarbonate filter (Frisenette, Denmark). Dried filters were placed in a Petri dish containing AO (0.04% final concentration; Fluka, Switzerland) for 2 min, then in deionized water for another 2 min, dried and mounted on microscopic slides with immersion oil. More than 300 AO-stained cells were enumerated on each slide with an Olympus BX50 epifluorescence microscope (Olympus Optical, Japan) using the filter block U-N31001 (Chroma Technology, USA). Blanks with no cells were counted in parallel.

For FCM, samples were analyzed using a SH-800-EC cell sorter (Sony Biotechnology, Japan) according to protocols optimized for supraglacial meltwater. All samples were vortexed on a Vortex-Genie 2 (Cambio, UK) for 30 s before each stage of processing. Field samples and most artificial ice samples were analyzed undiluted while artificial ice samples with dust concentrations of 10 and 100 mg ml^{-1} were diluted 10- and 100-fold with 0.1 μm filtered deionized water, respectively, to prevent potential blockage of the cell sorter sample tubing. To control for autofluorescence and dust background, stained and unstained aliquots were processed in parallel. For stained samples, 2 μl of 10,000× SYBR Gold (in DMSO; Life Technologies, UK) stock solution was diluted to 1 ml in phosphate buffered saline (pH 7.4), and 1 μl of this solution was used to stain 2 ml of sample for 30 min at room temperature (∼23°C) prior to analysis. The cell sorter was operated with samples interrogated at a

TABLE 2 | Physico–chemical characteristics of surface ice sampled on the GrIS.

Site	Dust		EC μS cm^{-1}	pH	Nutrient concentrations		
	g l^{-1}	10^3 particles ml^{-1}			DOC mg l^{-1}	NO_3^- mg l^{-1}	NH_4^+ μg l^{-1}
THU_L	0.10	70 ± 3.4	4.0 ± 0.38	5.97 ± 0.09	3.0 ± 1.4	0.05 ± 0.05	25 ± 0.93
THU_U	0.29	81 ± 13	2.5 ± 0.25	5.64 ± 0.20	1.6 ± 0.55	b.d.	23 ± 32
DS	0.51	146 ± 38	2.8 ± 0.06	5.78 ± 0.09	1.1 ± 0.39*	0.02 ± 0.04*	18 ± 16
KAN_L	0.03	67 ± 34	2.0 ± 0.12	5.83 ± 0.03	b.d.	0.07 ± 0.02	b.d.
KAN_M	0.08	47 ± 10	2.0 ± 0.15	5.62 ± 0.08	0.36 ± 0.32*	0.06 ± 0.00	6.5 ± 5.7
KAN_U	0.01	39 ± 5.7	1.9 ± 0.10	5.40 ± 0.04	b.d.	0.09 ± 0.03	b.d.
QAS_L	0.93	425 ± 154	2.0 ± 0.10	5.82 ± 0.05	2.7 ± 0.51	b.d.	b.d.
QAS_U	0.20	62 ± 42	2.0 ± 0.15	5.65 ± 0.04	2.3 ± 1.1	b.d.	7.9 ± 3.3
TAS_L	0.35	122 ± 50	1.9 ± 0.30	5.59 ± 0.19	b.d.	b.d.	7.7 ± 13
TAS_U	0.18	62 ± 17	1.7 ± 0.06	5.63 ± 0.03	b.d.	b.d.	4.7 ± 4.5
TAS_A	0.20	46 ± 11	2.4 ± 0.06	5.69 ± 0.08	b.d.	b.d.	23 ± 13
APO_L	0.36	474 ± 103	4.0 ± 0.12	5.73 ± 0.05	1.2 ± 0.72	b.d.	4.7 ± 8.1
APO_M	1.87	317 ± 53	4.1 ± 0.46	5.53 ± 0.01	1.3 ± 0.74	b.d.	3.7 ± 6.4*

Mean ± st.dev.; n = 3, except dust weight (n = 1); b.d., below detection limit.

**Values below detection limit were treated as zeroes so the mean values shown can be below the respective detection limits.*

flow rate of 21 μl min^{-1} for 30 s with 488 nm laser excitation and fluorescence emissions in the 520–550 nm channel measured along with forward and back scatter. Populations were gated manually.

DNA was extracted from the Sterivex filters using the PowerWater Sterivex DNA Isolation Kit (MO BIO Laboratories, USA), following the manufacturer's protocol. An unused Sterivex filter was extracted alongside the samples as a procedural control. Quantitative PCR of 16S rRNA genes was performed using a CFX96 Touch system (Bio-Rad, USA). Reaction mixtures (20 μl total) consisted of 1 μl of template DNA, 10 μl of SYBR Premix DimerEraser (TaKaRa, Japan), and 0.6 μl of forward and reverse primers (10 pmol μl^{-1}). The primers used were 341F (5′-CCTACGGGAGGCAGCAG-3′) and 518R (5′-ATTACCGCGGCTGCTGG-3′). The cycle program was 95°C for 30 s followed by 50 cycles of 95°C for 30 s, 55°C for 30 s, and 72°C for 30 s. The reaction was completed by a final 72°C elongation step for 6 min and followed by high-resolution melt curve analysis in 0.5°C increments from 72 to 98°C. All qPCR reactions were performed in triplicate and were prepared under DNA free conditions in a pressurized clean-lab with a HEPA filtered air inlet and nightly UV-irradiation. Standards of bacterial 16S rRNA genes were prepared by extracting DNA from a serially diluted culture of *E. coli*. The gene copy number of the highest standard was 1.12×10^7 μl^{-1}. The detection limits were 1.6×10^2 and 1.7×10^3 gene copies per μl of reaction volume for the artificial ice samples and the Greenland ice samples, respectively. Due to the much diluted nature of our samples, potential inhibition due to humic acid or other inhibitory compounds was considered unlikely and was not evaluated.

Statistical Analysis

Multivariate statistical analysis was used to explain the variation in the data, as described previously (Stibal et al., 2012b). All nutrient concentration and microbial abundance data were log transformed prior to analysis and all data were standardized and centered. Data below detection limit (b.d.) were treated as zeroes. Redundancy analysis (RDA) with interactive forward selection and 999 Monte Carlo permutations in an unrestricted mode was used to explain the variation in the data. The *p*-values were corrected for multiple testing using false discovery rate. All the analyses were performed in the multivariate data analysis software Canoco 5 (ter Braak and Šmilauer, 2012).

Results and Discussion

Microbial Cell Enumeration Testing

Accurate enumeration of microbial cells in glacial samples with high debris contents is notoriously difficult due to the problems associated with masking by debris and the difficulty in obtaining adequate sample volumes (Foght et al., 2004; Langford et al., 2010; Hodson et al., 2013). The results of our artificial ice abundance measurements are illustrated in **Supplementary Figure S1**. EFM gave the highest accuracies of the three methods tested (up to 0.97), as well as the best reproducibility (standard deviation down to 1.2% of mean). However, the accuracy values within the realistic ranges of cell and dust concentrations were still low (between 0.15 and 0.23), and were only higher (>0.75) in the samples with more than 10^4 cells ml^{-1} and without dust addition. In contrast, both FCM and qPCR performed poorly, with all accuracy values below 0.7, even in samples with no dust added, and poor reproducibility (**Supplementary Figure S1**). No significant correlations between the FCM and qPCR data, expressed as the percentage of the respective EFM values and dust concentrations, were found (data not shown). We acknowledge a potential bias in favor of EFM since the expected values (X_e in Equation 1) were determined by this method; however, this bias is probably small due to the high

TABLE 3 | Microbial cell/16S rRNA gene copy abundances in the surface ice samples from the GrIS determined by epifluorescence microscopy (EFM), flow cytometry (FCM), and quantitative PCR (qPCR).

Site	Microbial abundance		
	EFM (10^3 cells ml^{-1})	FCM (10^3 cells ml^{-1})	qPCR (10^5 copies ml^{-1})
THU_L	34 ± 12	22 ± 7.9	4.5 ± 1.3
THU_U	3.7 ± 0.29	15 ± 16	0.46 ± 0.39
DS	370 ± 38	5.8 ± 3.9	200 ± 8.7
KAN_L	3.1 ± 0.74	0.60 ± 0.40	0.24 ± 0.11
KAN_M	28 ± 5.2	b.d.	8.8 ± 3.0
KAN_U	1.9 ± 1.2	0.19 ± 0.44	0.29 ± 0.14
QAS_L	1300 ± 82	26 ± 22	260 ± 120
QAS_U	110 ± 1.8	1.8 ± 0.07	22 ± 6.2
TAS_L	260 ± 83	5.3 ± 2.1	140 ± 5.3
TAS_U	74 ± 8.1	13 ± 12	63 ± 43
TAS_A	16 ± 2.5	1.2 ± 0.58	17 ± 2.2
APO_L	560 ± 39	71 ± 77	110 ± 24
APO_M	1900 ± 350	28 ± 17	240 ± 78

Mean ± st.dev.; n = 3; b.d., below detection limit.

reproducibility of cell enumeration by EFM in a high-abundance and dust-free bacterial culture.

FCM has a good history of application to glacier samples (Karl et al., 1999; Yao et al., 2008; Miteva et al., 2009; An et al., 2010; Irvine-Fynn et al., 2012); however, in this study its performance was suboptimal relative to EFM. Three factors may account for this. First, interference from dust particles is prominent. While concurrent analysis of unstained samples has been sufficient to mitigate against dust interference in supraglacial meltwater (Irvine-Fynn et al., 2012), the higher sediment loads which may be found in glacier ice may complicate analyses and result in enumeration of undesirable "noise" particles, adsorption of cells to dust particles or spurious abiotic autofluorescence. Second, the number of cells analyzed per sample under the typical flow rates and parameters used is small. This may compromise the accuracy of counts. Third, the cell sorter used is unable to measure side scatter, the preferred metric for the identification of individual cell "events" (Irvine-Fynn et al., 2012). Use of forward and back scatter may explain the underestimation of cell counts in this study (**Table 3**), as cells adsorbed to dust particles or other cells are only recorded as a single event. However, the inter-replicate reproducibility of FCM was relatively good. It is clear that to realize the potential of FCM in high-throughput robust enumeration of cells against higher backgrounds of dust levels in glacier ice (Irvine-Fynn and Edwards, 2014), further work to optimally deconvolve dust and cell populations is necessary. Detaching cells from mineral particles may be required prior to analysis, even though these techniques may only yield 80–90% efficiency (Amalfitano and Fazi, 2008).

While PCR is a useful tool in diversity studies, its suitability for accurate quantification of cells in natural microbial communities is limited by various biases. The fact that no correlation was found between the qPCR/EFM abundance ratios and the concentration of dust, the most likely source of potentially inhibitory compounds, suggests that inhibition of PCR polymerases (Lindberg et al., 2007; Albers et al., 2013) was not a significant bias in the analysis of our ice samples. However, other biases may have been at play, such as differential extraction efficiencies for different microbial groups (Krsek and Wellington, 1999) and different numbers of the ribosomal RNA operon copies per cell (Klappenbach et al., 2001). Therefore, based on our results, traditional EFM is recommended when accurate numbers of microbial cells in ice samples containing dust particles are required, despite its laboriousness. Caution must still be exercised not to overinterpret differences in abundance within an order of magnitude.

Physico–Chemical Characteristics of Greenland Surface Ice

Physico–chemical characteristics of the melted ice from the surface of the GrIS are shown in **Table 2**. The dust load measured by the filtration method was variable (0.01–1.9 g dust per liter of melted ice, mean ± sd: 0.39 ± 0.51 g l^{-1}), and consistent with particle concentrations measured by FCM (39–474 particles per ml; 150 ± 152 ml^{-1}), with two exceptions (QAS_L, APO_L; **Table 2**). The highest dust load was detected in samples from DS, QAS_L, and APO_M while samples from the Kangerlussuaq transect (KAN_L/M/U) were lowest in dust. Electrical conductivity ranged between 1.7 and 4.1 μS cm^{-1} and pH ranged between 5.40 and 5.97, with no obvious trends in the samples. DOC ranged from <1.17 to 3 mg l^{-1} while TDN was below the detection limit of 0.2 mg l^{-1} in all the samples. Ammonium concentrations were between <4.4 and 25 μg l^{-1}, while those of nitrate ranged between <0.05 and 0.09 mg l^{-1}. Phosphate concentrations were below the detection limit of 0.025 mg l^{-1} in all the samples measured. The nutrient concentrations were similar to those previously measured in surface ice on the GrIS (Telling et al., 2012) and within the range reported from other glaciers (Tranter et al., 2004; Bagshaw et al., 2007; Hodson et al., 2013).

Microbial Abundance in Greenland Surface Ice

Microbial abundances in the surface ice samples from the GrIS were measured by the three methodologies (**Table 3**). Cell numbers within ice samples, determined by EFM, spanned three orders of magnitude (from ~ 2×10^3 to ~ 2×10^6 cells ml^{-1}). The FCM analysis resulted in lower cell numbers (1.5 – 65% EFM) in all cases except one (THU_U; 400%). The 16S rRNA gene copy numbers determined by qPCR produced values of the same order of magnitude as those measured by EFM, assuming 5–10 copies per cell, except for the DS and TAS samples where the qPCR values were an order of magnitude higher than those determined by EFM (**Table 3**). The highest cell numbers were determined in samples from QAS_L, TAS_L, DS, and APO. Unlike in the first three samples, the high abundances in the APO samples were unexpected due to the early sampling date and the fact that no liquid water was present in the surface ice during sampling. Two possible explanations for this result are, first, contamination due to a breakdown of the drilling equipment and the necessity to handle the ice samples in a non-sterile way, and second, the high dust content (**Table 2**).

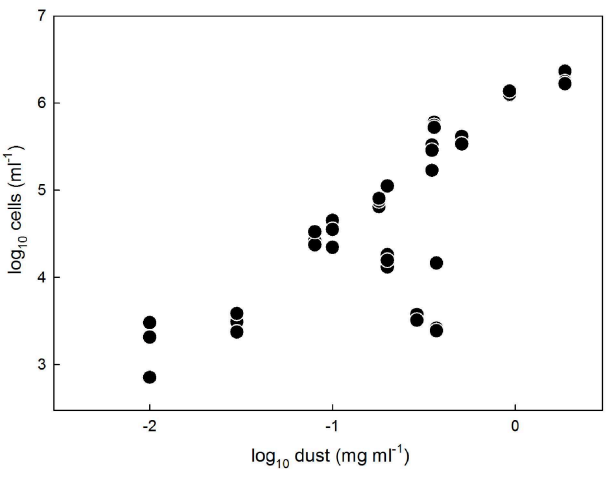

FIGURE 2 | Microbial cell abundances in surface ice samples from the GrIS determined by EFM plotted against the respective dust concentrations in the samples. Note the logarithmic scales on both axes.

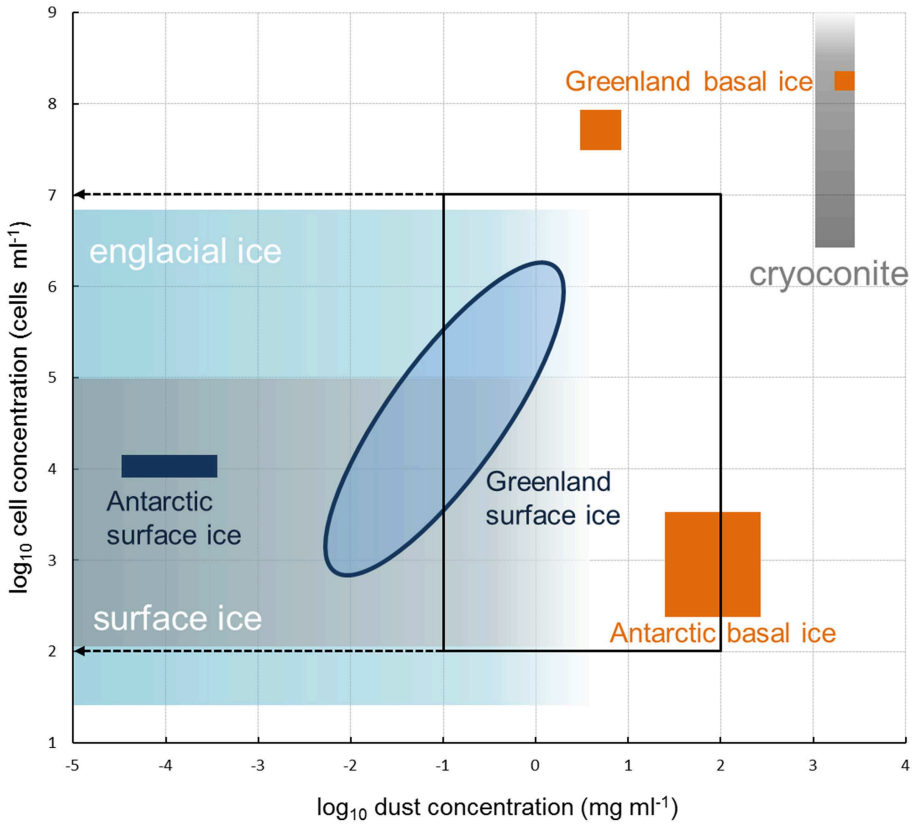

FIGURE 3 | Microbial cell abundances and dust concentrations in glacier ice samples. Blue oval represents samples collected in this study and measured by EFM (see **Figure 2**); the remainder of the data was compiled from the literature (see **Table 4**). Black frame represents the ranges used for method testing in this study. Note that due to logarithmic scales on both axes zeroes cannot be shown.

The abundances (10^3–10^6 cells per ml of melted ice) and dust concentrations (0.01–2 mg ml^{-1}) determined in surface ice samples in this study (**Tables 2, 3**; **Figure 2**) fit within the ranges reported for glacier ice samples from around the globe (**Figure 3**). **Table 4** shows an overview of the published data of cell abundances and dust concentrations in various glacier samples, including glacier snow and clean englacial ice with little dust and few cells, microbe-rich surface ice and debris slurries, and debris-laden basal ice with widely ranging cell abundances. These differences suggest a role of particulates for microbial abundance, which is further supported by the rich microbial community associated with cryoconite, where microbial abundance may reach 10^6–10^9 cells g^{-1}, as determined by EFM (Stibal et al., 2008a, 2010, 2012b; Anesio et al., 2010; Hodson et al., 2010a; Langford et al., 2010) and qPCR (Hamilton et al., 2013; Zarsky et al., 2013; Stibal et al., 2015).

Figure 4 illustrates microbial abundances measured by EFM in five sections of the 2.2 m deep Saddle firn core, representing winter snow from 2013 (18–42, 105–123, 130–147 cm) and 2012 (157–180 cm) and the 2012 summer melt layer between them at 147–157 cm depth. The abundance of cells in the 2012 summer melt layer (14,000 cells ml^{-1}) was an order of magnitude higher than the other analyzed core samples, especially in comparison with the immediately underlying and overlying snow layers (2400 and 3300 cells ml^{-1}, respectively). It should be noted however that, due to the small amount of sample volume available for analysis and the expected low cell concentrations, few replicates were measured and the differences are thus not significant. The abundances fall in the range reported from snow on glaciers on the Tibetan Plateau (0.7–700 $\times$ 10^3 cells ml^{-1}; Liu et al., 2009) and on the Antarctic ice sheet (200–5000 cells ml^{-1}; Carpenter et al., 2000), and are somewhat lower that those found in Svalbard glacier snow (10–40 $\times$ 10^3 cells ml^{-1}; Amato et al., 2007; **Table 4**). They are also similar to cell abundances determined by EFM in snow over sea ice in NE Greenland (0.8–3 $\times$ 10^3 cells ml^{-1}; Møller et al., 2013). The elevated abundance detected in the 2012 melt layer (**Figure 4**) may be a result of microbial growth during the short melt event in July 2012 (Nghiem et al., 2012), as suggested by Hell et al. (2013), and could represent a glimpse into the warmer future of the ice sheet; however, more data are needed to test this hypothesis.

Controls of Microbial Abundance in Surface Ice on the GrIS

In order to explain the variation in the microbial abundance data, a RDA was performed with physico-chemical data (position

along the N-S transect expressed as the N coordinate, altitude, distance from the margin, surface type, days with positive surface air temperature, days since last snowfall, and day of sampling from **Table 1**; dust content, EC, pH, and nutrient concentrations from **Table 2**) as the explanatory variables, and microbial abundance data (**Table 3**) as the explained variables. Several analyses were performed; first, with all the data available, and, subsequently, with some data removed due to their suspected lower accuracy. The APO sample data were removed due to their potential contamination, and the FCM abundance data were removed due to the low accuracy and reproducibility shown in the artificial ice experiments (**Supplementary Figure S1**). Data from the Saddle ice core could not be used due to the absence of the qPCR and FCM data and most physico–chemical data. The removal of the FCM abundance data and APO samples from the analysis resulted in a higher amount of total variability explained (data not shown).

Analysis that ignored FCM data and APO samples explained 97.3% of the total variation in the data. Dust content was the most significant variable, explaining 55.9% of the variation (pseudo$F = 36.7$; $p = 0.006$), followed by surface type (ice vs. firn; 14.6% explained, pseudo$F = 13.9$, $p = 0.012$), nitrate concentration (6.7% explained, pseudo$F = 7.9$, $p = 0.027$), and days since last snowfall (5.2% explained, pseudo$F = 37.3$, $p = 0.006$). Although the day of sampling was not a significant factor in this analysis (pseudo$F = 2.7$, $p = 0.20$), it is essentially an artifact of the sampling design, and, therefore, another RDA was conducted with this parameter as a covariate, thus showing only the results for the ecologically meaningful variables. This analysis explained 96.2% of the total variation; dust content explained 41.8% of the variation (pseudo$F = 20.1$; $p = 0.004$), followed by surface type (20.1% explained, pseudo$F = 13.4$, $p = 0.007$), the N-position (10.8% explained, pseudo$F = 10.1$, $p = 0.019$), and days since last snowfall (7.5% explained, pseudo$F = 37.3$,

TABLE 4 | Microbial cell abundances and dust concentrations in glacier snow, ice, and ice/debris mixture samples.

Sample type	Location	Cell count method	Cell abundance (10^3 ml^{-1})	Dust/debris concentration (mg ml^{-1})	References
Supraglacial snow	Greenland	EFM	2.4–15*	0.37*	This study
	Antarctica	EFM	0.2–5	n.d.	Carpenter et al., 2000
	Svalbard	EFM	0.03–40	n.d.	Amato et al., 2007; Björkman et al., 2014
	Central Asia	FCM	0.68–720	n.d.	Liu et al., 2009
Surface ice	Greenland	EFM FCM qPCR	1.9–1900 0–71 2.4–2600**	0.01–1.87	This study
	Svalbard	EFM FCM	200 57	n.d. n.d.	Amato et al., 2007 Irvine-Fynn et al., 2012
Englacial ice	Greenland	FCM	20–7000	0–0.005	Svensson et al., 2000; Tung et al., 2005; Miteva et al., 2009
	Antarctica	EFM	0.2–36	0–0.005	Karl et al., 1999; Priscu et al., 1999; Abyzov et al., 2001; Antony et al., 2012
	Central Asia	EFM FCM	0.02–170 3.2–830	n.d. n.d.	Zhang et al., 2008a,b Yao et al., 2008; An et al., 2010
Cryoconite hole ice/water	Antarctica	EFM	0.26–79	n.d.	Foreman et al., 2007; Hodson et al., 2013
	Svalbard	EFM	4.5–100	n.d.	Säwström et al., 2002; Mindl et al., 2007; Anesio et al., 2010
Cryoconite slurry	Antarctica	EFM	40–3800	n.d.	Foreman et al., 2007; Hodson et al., 2013
Basal ice	Greenland	EFM	6–30 × 10^4	up to ∼1600	Sheridan et al., 2003; Yde et al., 2010
	Antarctica	EFM	0.1–4.2	20–280	Montross et al., 2014

n.d., not determined.

**Data from the Saddle ice core 2013 winter snow layer (18–42 cm depth). **Assuming 10 16S rRNA gene copies per cell.*

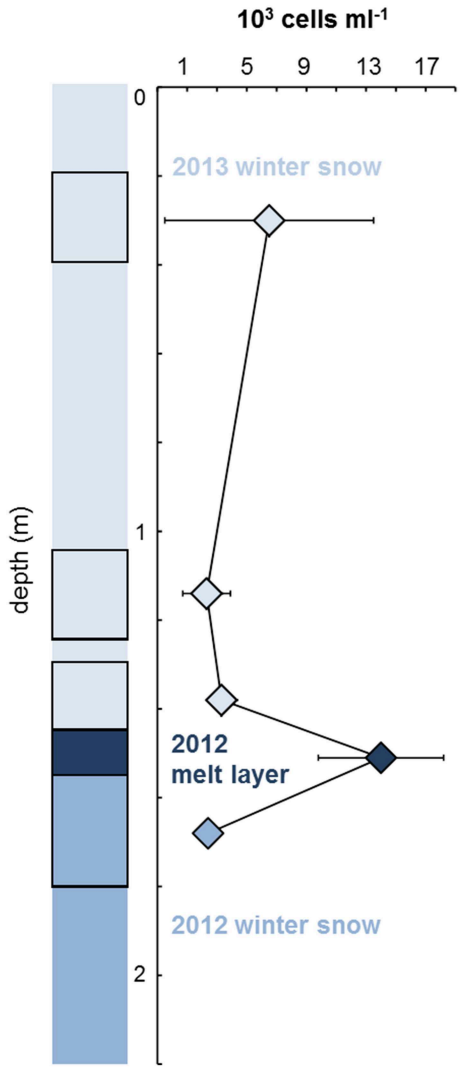

FIGURE 4 | Cell abundance measured by EFM in the Saddle ice core. The five sections used for enumeration are depicted by black frames. Values are means ± st.devs. of three measurements (2013 winter snow top layer, 2012 melt layer) or two measurements (remaining samples).

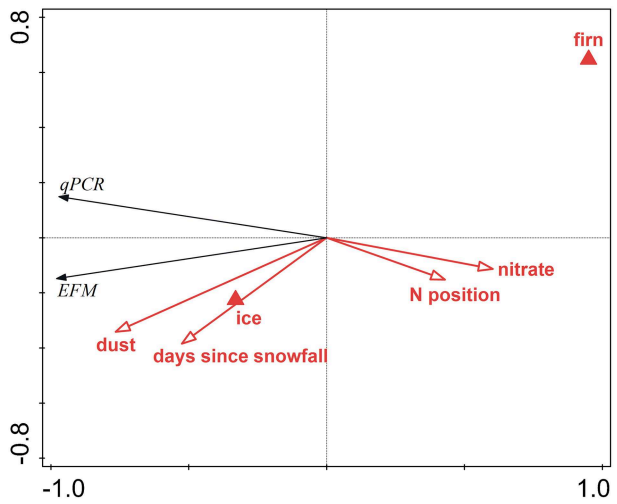

FIGURE 5 | Redundancy analysis biplot visualizing the effects of environmental variables on the microbial abundance in surface ice on the GrIS. Red arrows denote significant quantitative physical variables, red triangles the surface type, and black arrows the abundances determined by EFM and qPCR.

$p = 0.006$). **Figure 5** is an RDA biplot that illustrates the positive correlations of microbial abundance and dust contents and days since last snowfall, the negative correlation between cell numbers and the N-coordinate, and the preference of microbial cells for ice compared with firn. The relationship between dust content and cell numbers in surface ice on the GrIS is also illustrated in **Figure 2** in which the EFM abundance data are plotted against dust contents in all samples including those from APO and Saddle, showing a positive correlation between dust and cell numbers ($R^2 = 0.89$ with all data used; $R^2 = 0.81$ with APO samples removed).

The variation in microbial abundance in the surface ice samples collected on the GrIS reflects the differences between the sites and the important effect of local conditions on biological processes in the supraglacial ecosystem. The lowest abundances in our study ($\sim 10^3$ cells ml^{-1}) were found in samples from the accumulation area of the ice sheet (KAN_U, Saddle) or in those affected by fresh snow (KAN_L), and are similar to abundances found in atmospheric waters (Sattler et al., 2001; Bowers et al., 2012). Since microbial cells may act as ice nuclei (Christner et al., 2008; Delort et al., 2010), the lowest abundances found in surface ice may represent a "baseline" cell concentration, which is a result of deposition of snow already containing microbial cells.

Dust deposition is another possible source of microbial cells to the ice sheet (Xiang et al., 2009). Simultaneous analysis of dust and cell concentrations from glacial ice samples is scarce (e.g., Antony et al., 2012), and some studies suggest that microbial abundance in glacial ice cores is not always associated with dust deposition (Zhang et al., 2008a; Xiang et al., 2009). However, the results of the statistical analysis of our data show for the first time a significant association between dust and cell abundance in Greenland surface ice (**Figures 2**, **5**). This strong correlation may be explained in two ways: first, microbial cells may be deposited onto the GrIS in association with dust particles, and second, dust may provide a source of nutrients to stimulate the growth of microbes in the vicinity. Phosphorus, a rock-bound nutrient, is likely the limiting macronutrient in the supraglacial environment (Stibal et al., 2008b, 2009) and has been detected in surface debris on the southwestern GrIS (Wientjes et al., 2011), which supports this hypothesis.

Microbial abundance was also shown to be correlated to surface type (with ice showing higher cell numbers than firn) and the number of days since the last snowfall (**Figure 5**). We suggest that these controls are related to the process of cell retention at the glacier surface. This process begins in melting snow (Hell et al., 2013; Björkman et al., 2014) and continues in surface

ice, which potentially acts as a filter (Irvine-Fynn et al., 2012). Therefore, the bare ice surface is expected to accumulate more microbial cells over time compared with firn, unless their abundance is "diluted" by fresh snow. The preference of ice over firn can also be explained by the longer melt period at the sites with ice compared to those with firn, which is further supported by the significant effect of the N-S position, and is also likely related to the length of the melt season. Difference in the amount of solar radiation is another possible explanation of the significance of the N-S position. The significant negative correlation between microbial abundance and nitrate concentration could be interpreted as a result of microbial uptake of nitrate (Telling et al., 2012) and thus a sign of an active microbial community in surface ice on the ice sheet.

Conclusions

We quantified for the first time the abundance of microbial cells in surface ice from geographically distinct sites on the GrIS, including ablation and accumulation areas, using three different methods (EFM, FCM, and qPCR). EFM generated the most accurate and reproducible results of the three methods, and is therefore recommended for the cell enumeration of glacier ice. Cell abundance of surface ice samples, determined by EFM, ranged from $\sim 2 \times 10^3$ to $\sim 2 \times 10^6$ cells ml^{-1}, while the dust concentrations were found to be between 0.01 and 2 mg ml^{-1}. Dust content was the most significant factor explaining the variation in abundance data. Surface type (ice vs. firn), number of days since last snowfall, N-S position and nitrate concentration were also identified as significant controls. We suggest that the surface of the Greenland Ice Sheet receives a "baseline" cell supply via deposition of atmospheric waters, and that wind-borne dust deposited on the ice sheet likely contains additional cells and may provide limiting nutrients for microbial growth. Ablation areas with high dust concentrations and longer melt seasons are therefore expected to contain higher numbers of active microbes compared to the accumulation area and those portions of the ablation area that contain little dust and are primarily seeded with atmospheric waters.

Author Contributions

MS conceived and designed the study with inputs from JB, EG and CJ; MS, MS, JZ and JB collected samples; EG prepared the artificial ice samples and performed microscopy and qPCR assisted by MS, KC and CJ; AE, IS, JG and TI did flow cytometry analyses; JB provided glaciological and climate data for sampling sites; all authors contributed to the discussion of the results; MS wrote the paper with inputs from EG, KC, JB, IS, AE, TI, and CJ.

Acknowledgments

This research was funded by Villum Young Investigator Programme grant VKR 023121 to MS and Danish Research Council grant FNU 10-085274 to CJ, and supported by the Dark Snow Project (http://darksnowproject.org/). Flow cytometric analyses at Aberystwyth were supported by Royal Society grant RG130314 to AE. JZ was supported by Czech Ministry of Education grant LM2010009. We thank Pernille Stockmarr and Christina Rosenberg Lynge for technical assistance and Michele Citterio, Martin Veicherts, and McKenzie Skiles for field assistance.

Supplementary Material

The Supplementary Material for this article can be found online at: http://www.frontiersin.org/journal/10.3389/fmicb.2015.00225/abstract

Supplementary Figure S1 | Accuracies and standard deviations of cell abundance measurements of artificial ice samples by epifluorescence microscopy (EFM), flow cytometry (FCM) and quantitative PCR (qPCR). Note the logarithmic scales and differences in color scaling between plots.

References

Abyzov, S. S., Mitskevich, I. N., Poglazova, M. N., Barkov, N. I., Lipenkov, V. Y., Bobin, N. E., et al. (2001). Microflora of the basal strata at Antarctic ice core above the Vostok Lake. *Adv. Space Sci.* 28, 701–706. doi: 10.1016/S0273-1177(01)00318-0

Albers, C. N., Bælum, J., Jensen, A., and Jacobsen, C. S. (2013). Inhibition of DNA polymerases used in Q-PCR by structurally different soil-derived humic substances. *Geomicrobiol. J.* 30, 675–681. doi: 10.1080/01490451.2012.758193

Amalfitano, S., and Fazi, S. (2008). Recovery and quantification of bacterial cells associated with streambed sediments. *J. Microbiol. Meth.* 75, 237–243. doi: 10.1016/j.mimet.2008.06.004

Amato, P., Hennebelle, R., Magand, O., Sancelme, M., Delort, A.-M., Barbante, C., et al. (2007). Bacterial characterization of the snow cover at Spitzberg, Svalbard. *FEMS Microbiol. Ecol.* 59, 255–264. doi: 10.1111/j.1574-6941.2006.00198.x

An, L. Z., Chen, Y., Xiang, S.-R., Shang, T.-C., and Tian, L.-D. (2010). Differences in community composition of bacteria in four glaciers in western China. *Biogeosciences* 7, 1937–1952. doi: 10.5194/bg-7-1937-2010

Anesio, A. M., and Laybourn-Parry, J. (2012). Glaciers and ice sheets as a biome. *Trends Ecol. Evol.* 27, 219–225. doi: 10.1016/j.tree.2011.09.012

Anesio, A. M., Sattler, B., Foreman, C., Telling, J., Hodson, A., Tranter, M., et al. (2010). Carbon fluxes through bacterial communities on glacier surfaces. *Ann. Glaciol.* 51, 32–40. doi: 10.3189/172756411795932092

Antony, R., Krishnan, K. P., Laluraj, C. M., Thamban, M., Dhakephalkar, P. K., Engineer, A. S., et al. (2012). Diversity and physiology of culturable bacteria associated with a coastal Antarctic ice core. *Microbiol. Res.* 167, 372–380. doi: 10.1016/j.micres.2012.03.003

Bagshaw, E. A., Tranter, M., Fountain, A. G., Welch, K. A., Basagic, H., and Lyons, W. B. (2007). Biogeochemical evolution of cryoconite holes on Canada Glacier, Taylor Valley, Antarctica. *J. Geophys. Res.* 112, G04S35. doi: 10.1029/2007JG000442

Björkman, M. P., Zarsky, J. D., Kühnel, R., Hodson, A., Sattler, B., and Psenner, R. (2014). Microbial cell retention in a melting High Arctic snowpack, Svalbard. *Arct. Antarct. Alp. Res.* 46, 471–482. doi: 10.1657/1938-4246-46.2.471

Bowers, R. M., McCubbin, I. B., Hallar, A. G., and Fierer, N. (2012). Seasonal variability in airborne bacterial communities at a high-elevation site. *Atmos. Environ.* 50, 41–49. doi: 10.1016/j.atmosenv.2012.01.005

Box, J. E., Fettweis, X., Stroeve, J. C., Tedesco, M., Hall, D. K., and Steffen, K. (2012). Greenland ice sheet albedo feedback: thermodynamics and atmospheric drivers. *Cryosphere* 6, 821–839. doi: 10.5194/tc-6-821-2012

ter Braak, C. J. F., and Šmilauer, P. (2012). *Canoco Reference Manual and User's Guide: Software for Ordination (Version 5.0)*. Ithaca, NY: Microcomputer Power.

Cameron, K. A., Hagedorn, B., Dieser, M., Christner, B. C., Choquette, K., Sletten, R., et al. (2015). Diversity and potential sources of microbiota associated with snow on western portions of the Greenland Ice Sheet. *Environ. Microbiol.* 17, 594–609. doi: 10.1111/1462-2920.12446

Carpenter, E. J., Lin, S., and Capone, D. G. (2000). Bacterial activity in South Pole snow. *Appl. Environ. Microbiol.* 66, 4514–4517. doi: 10.1128/AEM.66.10.4514-4517.2000

Christner, B. C., Morris, C., Foreman, C. M., Cai, R., and Sands, D. C. (2008). Ubiquity of biological ice nucleators in snowfall. *Science* 319, 1214. doi: 10.1126/science.1149757

Delort, A.-M., Vaïtilingom, M., Amato, P., Sancelme, M., Parazols, M., Mailhot, G., et al. (2010). A short overview of the microbial population in clouds: potential roles in atmospheric chemistry and nucleation processes. *Atmos. Res.* 98, 249–260. doi: 10.1016/j.atmosres.2010.07.004

Fettweis, X., Tedesco, M., van den Broeke, M., and Ettema, J. (2011). Melting trends over the Greenland ice sheet (1958–2009) from spaceborne microwave data and regional climate models. *Cryosphere* 5, 359–375. doi: 10.5194/tc-5-359-2011

Foght, J. M., Aislabie, J., Turner, S., Brown, C. E., Ryburn, J., Saul, D. J., et al. (2004). Culturable bacteria in subglacial sediments and ice from two southern hemisphere glaciers. *Microb. Ecol.* 47, 329–340. doi: 10.1007/s00248-003-1036-5

Foreman, C. M., Sattler, B., Mikucki, D. L., Porazinska, D. L., and Priscu, J. C. (2007). Metabolic activity and diversity of cryoconites in the Taylor Valley, Antarctica. *J. Geophys. Res.* 112, G04S32. doi: 10.1029/2006JG000358

Hamilton, T. L., Peters, J. W., Skidmore, M. L., and Boyd, E. S. (2013). Molecular evidence for an active endogenous microbiome beneath glacial ice. *ISME J.* 7, 1402–1412. doi: 10.1038/ismej.2013.31

Hell, K., Edwards, A., Zarsky, J., Podmirseg, S. M., Girdwood, S., Pachebat, J. A., et al. (2013). The dynamic bacterial communities of a melting High Arctic glacier snowpack. *ISME J.* 7, 1814–1826. doi: 10.1038/ismej.2013.51

Hodson, A., Anesio, A. M., Ng, F., Watson, R., Quirk, J., Irvine-Fynn, T., et al. (2007). A glacier respires: quantifying the distribution and respiration CO_2 flux of cryoconite across an entire Arctic supraglacial ecosystem. *J. Geophys. Res.* 112, G04S36. doi: 10.1029/2007JG000452

Hodson, A., Bøggild, C., Hanna, E., Huybrechts, P., Langford, H., Cameron, K., et al. (2010a). The cryoconite ecosystem on the Greenland ice sheet. *Ann. Glaciol.* 51, 123–129. doi: 10.3189/172756411795931985

Hodson, A., Cameron, K., Bøggild, C., Irvine-Fynn, T., Langford, H., Pearce, D., et al. (2010b). The structure, biological activity and biogeochemistry of cryoconite aggregates upon an Arctic valley glacier: Longyearbreen, Svalbard. *J. Glaciol.* 56, 349–362. doi: 10.3189/002214310791968403

Hodson, A., Paterson, H., Westwood, K., Cameron, K., and Laybourn-Parry, J. (2013). A blue-ice ecosystem on the margins of the East Antarctic ice sheet. *J. Glaciol.* 59, 255–268. doi: 10.3189/2013JoG12J052

Hodson, A. J., Anesio, A. M., Tranter, M., Fountain, A., Osborn, M., Priscu, J., et al. (2008). Glacial ecosystems. *Ecol. Monogr.* 78, 41–67. doi: 10.1890/07-0187.1

Irvine-Fynn, T. D. L., and Edwards, A. (2014). A frozen asset: the potential of flow cytometry in constraining the glacial biome. *Cytometry A.* 85, 3–7. doi: 10.1002/cyto.a.22411

Irvine-Fynn, T. D. L., Edwards, A., Newton, S., Langford, H., Rassner, S. M., Telling, J., et al. (2012). Microbial cell budgets of an Arctic glacier surface quantified using flow cytometry. *Environ. Microbiol.* 14, 2998–3012. doi: 10.1111/j.1462-2920.2012.02876.x

Karl, D. M., Bird, D. F., Björkman, K., Houlihan, T., Shackelford, R., and Tupas, L. (1999). Microorganisms in the accreted ice of Lake Vostok, Antarctica. *Science* 286, 2144–3147. doi: 10.1126/science.286.5447.2144

Klappenbach, J. A., Saxman, P. R., Cole, J. R., and Schmidt, T. M. (2001). rrndb: the ribosomal RNA operon copy number database. *Nucl. Acids Res.* 29, 181–184. doi: 10.1093/nar/29.1.181

Krsek, M., and Wellington, E. M. H. (1999). Comparison of different methods for the isolation and purification of total community DNA from soil. *J. Microbiol. Meth.* 39, 1–16. doi: 10.1016/S0167-7012(99)00093-7

Langford, H., Hodson, A., Banwart, S., and Bøggild, C. (2010). The microstructure and biogeochemistry of Arctic cryoconite granules. *Ann. Glaciol.* 51, 87–94. doi: 10.3189/172756411795932083

Lindberg, E., Albrechtsen, H. J., and Jacobsen, C. S. (2007). Inhibition of real-time PCR in DNA extracts from aquifer sediment. *Geomicrobiol. J.* 24, 343–352. doi: 10.1080/01490450701456701

Liu, Y., Yao, T., Jiao, N., Kang, S., Xu, B., Zeng, Y., et al. (2009). Bacterial diversity in the snow over Tibetan Plateau glaciers. *Extremophiles* 13, 411–423. doi: 10.1007/s00792-009-0227-5

Lucas-Picher, P., Wulff-Nielsen, M., Christensen, J. H., Aðalgeirsdóttir, G., Mottram, R., and Simonsen, S. B. (2012). Very high resolution regional climate model simulations over Greenland: identifying added value. *J. Geophys. Res.* 117, D02108. doi: 10.1029/2011JD016267

Mindl, B., Anesio, A. M., Meirer, K., Hodson, A. J., Laybourn-Parry, J., Sommaruga, R., et al. (2007). Factors influencing bacterial dynamics along a transect from supraglacial runoff to proglacial lakes of a high Arctic glacier. *FEMS Microbiol. Ecol.* 59, 307–317. doi: 10.1111/j.1574-6941.2006.00262.x

Miteva, V., Teacher, C., Sowers, T., and Brenchley, J. (2009). Comparison of the microbial diversity at different depths of the GISP2 Greenland ice core in relationship to deposition climates. *Environ. Microbiol.* 11, 640–656. doi: 10.1111/j.1462-2920.2008.01835.x

Møller, A. K., Søborg, D. A., Al-Soud, W. A., Sørensen, S. J., and Kroer, N. (2013). Bacterial community structure in High-Arctic snow and freshwater as revealed by pyrosequencing of 16S rRNA genes and cultivation. *Polar Res.* 32:17390. doi: 10.3402/polar.v32i0.17390

Montross, S., Skidmore, M., Christner, B., Samyn, D., Tison, J.-L., Lorrain, R., et al. (2014). Debris-rich basal ice as a microbial habitat, Taylor Glacier, Antarctica. *Geomicrobiol. J.* 31, 76–81. doi: 10.1080/01490451.2013.811316

Nghiem, S. V., Hall, D. K., Mote, T. L., Tedesco, M., Albert, M. R., Keegan, K., et al. (2012). The extreme melt across the Greenland ice sheet in 2012. *Geophys. Res. Lett.* 39, L20502. doi: 10.1029/2012GL053611

Priscu, J. C., Adams, E. E., Lyons, W. B., Voytek, M. A., Mogk, D. W., Brown, R. L., et al. (1999). Geomicrobiology of subglacial ice above lake Vostok, Antarctica. *Science* 286, 2141–2144. doi: 10.1126/science.286.5447.2141

Sattler, B., Puxbaum, H., and Psenner, R. (2001). Bacterial growth in supercooled cloud droplets. *Geophys. Res. Lett.* 28, 239–242. doi: 10.1029/2000GL011684

Säwström, C., Mumford, P., Marshall, W., Hodson, A., and Laybourn-Parry, J. (2002). The microbial communities and primary productivity of cryoconite holes in an Arctic glacier (Svalbard 79°N). *Polar Biol.* 25, 591–596. doi: 10.1007/s00300-002-0388-5

Sheridan, P. P., Miteva, V. I., and Brenchley, J. E. (2003). Phylogenetic analysis of anaerobic psychrophilic enrichment cultures obtained from a Greenland glacier ice core. *Appl. Environ. Microbiol.* 69, 2153–2160. doi: 10.1128/AEM.69.4.2153-2160.2003

Skidmore, M., Anderson, S. P., Sharp, M., Foght, J., and Lanoil, B. D. (2005). Comparison of microbial community composition in two subglacial environments reveals a possible role for microbes in chemical weathering processes. *Appl. Environ. Microbiol.* 71, 6986–6997. doi: 10.1128/AEM.71.11.6986-6997.2005

Stibal, M., Anesio, A. M., Blues, C. J. D., and Tranter, M. (2009). Phosphatase activity and organic phosphorus turnover on a high Arctic glacier. *Biogeosciences* 6, 913–922. doi: 10.5194/bg-6-913-2009

Stibal, M., Lawson, E. C., Lis, G. P., Mak, K. M., Wadham, J. L., and Anesio, A. M. (2010). Organic matter content and quality in supraglacial debris across the ablation zone of the Greenland ice sheet. *Ann. Glaciol.* 51, 1–8. doi: 10.3189/172756411795931958

Stibal, M., Šabacká, M., and Žárský, J. (2012a). Biological processes on glacier and ice sheet surfaces. *Nat. Geosci.* 5, 771–774. doi: 10.1038/ngeo1611

Stibal, M., Schostag, M., Cameron, K. A., Hansen, L. H., Chandler, D. M., Wadham, J. L., et al. (2015). Different bulk and active bacterial communities in cryoconite from the margin and interior of the Greenland ice sheet. *Environ. Microbiol. Rep.* 7, 293–300. doi: 10.1111/1758-2229.12246

Stibal, M., Telling, J., Cook, J., Mak, K. M., Hodson, A., and Anesio, A. M. (2012b). Environmental controls on microbial abundance and activity on the Greenland ice sheet: a multivariate analysis approach. *Microb. Ecol.* 63, 74–84. doi: 10.1007/s00248-011-9935-3

Stibal, M., Tranter, M., Benning, L. G., and Řehák, J. (2008a). Microbial primary production on an Arctic glacier is insignificant in comparison with allochthonous organic carbon input. *Environ. Microbiol*. 10, 2172–2178. doi: 10.1111/j.1462-2920.2008.01620.x

Stibal, M., Tranter, M., Telling, J., and Benning, L. G. (2008b). Speciation, phase association and potential bioavailability of phosphorus on a Svalbard glacier. *Biogeochemistry* 90, 1–13. doi: 10.1007/s10533-008-9226-3

Svensson, A., Biscaye, P. E., and Grousset, F. E. (2000). Characterization of late glacial continental dust in the Greenland ice Sheet project ice core. *J. Geophys. Res*. 105, 4637–4656. doi: 10.1029/1999JD901093

Takeuchi, N., Kohshima, S., and Seko, K. (2001). Structure, formation, darkening process of albedo-reducing material (cryoconite) on a Himalayan glacier: a granular algal mat growing on the glacier. *Arct. Antarct. Alp. Res*. 33, 115–122. doi: 10.2307/1552211

Telling, J., Stibal, M., Anesio, A. M., Tranter, M., Nias, I., Cook, J., et al. (2012). Microbial nitrogen cycling on the Greenland ice sheet. *Biogeosciences* 9, 2431–2442. doi: 10.5194/bg-9-2431-2012

Tranter, M., Fountain, A. G., Fritsen, C. H., Lyons, W. B., Priscu, J. C., Statham, P., et al. (2004). Extreme hydrochemical conditions in natural microcosms entombed within Antarctic ice. *Hydrol. Process*. 18, 379– 387. doi: 10.1002/hyp.5217

Tung, H. C., Bramall, N. E., and Price, P. B. (2005). Microbial origin of excess of methane in glacial ice and implications for life on Mars. *Proc. Natl. Acad. Sci. U.S.A*. 102, 18292–18296. doi: 10.1073/pnas.0507601102

Vesey, G., Narai, J., Ashbolt, N., Williams, K., and Veal, D. (1994). Detection of specific microorganisms in environmental samples using flow cytometry. *Meth. Cell Biol*. 42, 489–522. doi: 10.1016/S0091-679X(08)61092-4

Whitman, W. B., Coleman, D. C., and Wiebe, W. J. (1998). Prokaryotes: the unseen majority. *Proc. Natl. Acad. Sci. U.S.A*. 95, 6578–6583. doi: 10.1073/pnas.95.12.6578

Wientjes, I. G. M., Van de Wal, R. S. W., Reichart, G. J., Sluijs, A., and Oerlemans, J. (2011). Dust from the dark region in the western ablation zone of the Greenland ice sheet. *Cryosphere* 5, 589–601. doi: 10.5194/tc-5-589-2011

Xiang, S.-R., Shang, T.-C., Chen, Y., and Yao, T.-D. (2009). Deposition and postdeposition mechanisms as possible drivers of microbial populationvariability in glacier ice. *FEMS Microbiol. Ecol*. 70, 165–176. doi: 10.1111/j.1574-6941.2009.00759.x

Yallop, M. L., Anesio, A. M., Perkins, R. G., Cook, J., Telling, J., Fagan, D., et al. (2012). Photophysiology and albedo-changing potential of the ice algae community on the surface of Greenland Ice Sheet. *ISME J*. 6, 2302–2313. doi: 10.1038/ismej.2012.107

Yao, T., Liu, Y., Kang, S., Jiao, N., Zeng, Y., Liu, X., et al. (2008). Bacteria variabilities in a Tibetan ice core and their relations with climate change. *Glob. Biogeochem. Cycl*. 22, GB4017. doi: 10.1029/2007GB003140

Yde, J. C., Finster, K. W., Raiswell, R., Steffensen, J. P., Heinemeier, J., Olsen, J., et al. (2010). Basal ice microbiology at the margin of the Greenland ice sheet. *Ann. Glaciol*. 51, 71–79. doi: 10.3189/172756411795931976

Zarsky, J. D., Stibal, M., Hodson, A., Sattler, B., Schostag, M., Hansen, L. H., et al. (2013). Large cryoconite aggregates on a Svalbard glacier support a diverse microbial community including ammonium oxidizing archaea. *Environ. Res. Lett*. 8:035044. doi: 10.1088/1748-9326/8/3/035044

Zeng, Y.-X., Yan, M., Yu, Y., Li, H.-R., He, J.-F., Sun, K., et al. (2013). Diversity of bacteria in surface ice of Austre Lovénbreen glacier, Svalbard. *Arch. Microbiol*. 195, 313–322. doi: 10.1007/s00203-013-0880-z

Zhang, S., Hou, S., Wu, Y., and Qin, D. (2008a). Bacteria in Himalayan glacial ice and its relationship to dust. *Biogeosciences* 5, 1741–1750. doi: 10.5194/bg-5-1741-2008

Zhang, X. F., Yao, T. D., Tian, L. D., Xu, S. J., and An, L. Z. (2008b). Phylogenetic and physiological diversity of bacteria isolated from Puruogangri ice core. *Microb. Ecol*. 55, 476–488. doi: 10.1007/s00248-007-9293-3

Conflict of Interest Statement: The authors declare that the research was conducted in the absence of any commercial or financial relationships that could be construed as a potential conflict of interest.